TRACTION ON SAND

José Manuel Nobre de Oliveira Peça

Mech. Eng., M.Sc.

Instituto Universitário de Évora, Portugal

Submitted for the Degree of Doctor of Philosophy

in the University of Newcastle upon Tyne

October 1982

ABSTRACT

The system for predicting tyre performance on sand, measuring sand strength with a cone penetrometer and using non-dimensional empirical curves developed by the Waterways Experiment Station (WES) of the U.S. Army was investigated. A series of tyre tests on dry Cresswell sand were carried out and the results were in complete disagreement with the WES system, in both its original and revised forms. It was therefore decided to try to discover the basic soil mechanics of such a system and modify it accordingly.

Critical State Soil Mechanics describes two types of soil behaviour, dilating and weakening or compacting and strengthening. It was found that the first of these processes occurred in most situations likely to be found naturally, compaction occurring only in the loosest states obtainable under laboratory conditions. Under dilating conditions sand strength is described by the density, γ, and the angle of internal friction, $\emptyset$. The angle of friction, for a single sand, was found to vary over a very wide range, depending on the state of compaction and the confining pressure. Density does not vary greatly.

The cone penetrometer gradient, G, was found to be related to $\emptyset$ at a low confining pressure, and the relationship was well described by the theory of Durgunoglu and Mitchell (1975). This lead to the idea that tractive performance would be dependent on $\emptyset$, which would be lower the higher the tyre contact pressure.

A series of tyre tests on a single tyre on two sands showed clearly that performance depended on both tyre pressure and tyre load. The WES numeric only contains pressure. It was therefore decided to include both parameters by expressing performance by several curves depending on the tyre deflection. Deflection being expressed as a ratio of tyre diameter rather than tyre section height. The new system was shown to describe all of the WES data better and more logically than their system.

The reason why the system cannot describe performance in Yuma and Mortar sands with the same single curve as for Leighton Buzzard and Cresswell remains a mystery.

ACKNOWLEDGEMENT

I would like to thank my supervisor Dr A R Reece and also Dr A D Trapp, Mr T W Grinsted and Mr Michael Foster for their advice and assistance throughout the course of this work.

The work described in this thesis was carried out during the tenure of a grant from the Instituto Nacional de Investigação Científica - Portugal.

C O N T E N T S

CONTENTS (cont.)

N O T A T I O N

b	Wheel width, m.
c	Soil cohesion, kPa.
CI	Cone index force on the cone divided by the cone base are, kPa.
CI_{av}	Average cone index over top 150mm of soil, kPa.
CI_{150}	Cone index at 150mm depth, kPa.
C_u	Coefficient of uniformity of the soil = d_{60}/d_{10}, dimensionless.
d	Wheel diameter; cone base diameter, m.
d_{50}	Soil grain diameter at 50% finer by weight; mean grain diameter of soil grains, mm.
D'	Compactability of the soil = $\frac{v_{max} - v_{min}}{v_{min} - 1} \times 100$, percent.
D_d	Relative density of the soil = $\frac{v_{max} - v}{v_{max} - v_{min}} \times 100$, percent
D_{de}	Turnage's effective relative density, percent.
e	Voids ratio = v - 1, dimensionless.
E_s	Energy wasted by the wheel in soil and tyre deformation, N x m.
G	Cone resistance gradient = $\frac{CI_{2v} - CI_{surf}}{\frac{1}{2} \text{ depth of interest}}$, MPa/m
G_e	Turnage's effective cone resistance gradient, MPa/m.
G_s	Specific gravity of soil grains, dimensionless.
h	Unloaded carcass section height, m.
i	Slip, dimensionless
i.p.	Inflation pressure, psi.
M	Stress ratio, q/p, at the critical state line, dimensionless.
N_c	WES clay number, dimensionless.
N_s	WES sand number, dimensionless.
N_{se}	Turnage's effective sand number, dimensionless.
p	Stress invariant = $\frac{1}{3}(\sigma_1 + \sigma_2 + \sigma_3)$.
PN	Power number, the energy supplied at the wheel axle per unit of vertical load, per unit of distance travelled forward, dimensionless.

N O T A T I O N (cont.)

P_t Towing force, N.

q Stress invariant = $\frac{1}{\sqrt{2}} \left[(\sigma_1 - \sigma_2)^2 + (\sigma_2 - \sigma_3)^2 + (\sigma_3 - \sigma_1)^2\right]^{\frac{1}{2}}$

r_r Rolling radius, m.

T Torque, N x m.

v Specific volume of the soil = $(G_s\ \gamma_w)/\gamma$, dimensionless.

v_{min} Specific volume at the soil densest state, dimensionless.

v_{max} Specific volume at the soil loosest state, dimensionless.

v_a Forward speed of the wheel, m/sec.

W Weight on the wheel axle, N.

z Wheel sinkage; depth of penetration, m.

z* Wheel sinkage relative to the rut surface of the previous pass.

z_i Initial wheel sinkage when the wheel tester is lowered onto the soil surface, m.

z_r Depth of the wheel rut, m.

γ Soil bulk density, kN/m^3.

γ_w Unit weight of water = 9.8 kN/m^3.

γ_{10} Soil bulk density at 10% relative density, kN/m^3.

ϕ Angle of internal friction at peak of stress, degrees.

ϕ_{cv} Angle of internal friction at constant volume deformation.

ϕ_{dil} Dilation component of ϕ, degrees.

ϕ_{70} ϕ at 70% relative density, degrees.

ϕ_μ Angle of interparticle friction, degrees.

ϕ_f Effective angle of friction in Rowe-Horne Stress Dilatancy theory, degrees.

$\varepsilon_1, \varepsilon_2, \varepsilon_3$ Principal strains, dimensionless.

ε_v Volumetric strains = $\varepsilon_1 + 2\varepsilon_3$, in triaxial test.

ε_a Axial strain in triaxial test = ε_1, dimensionless.

ε_s Energy wasted by the wheel per unit of distance travelled forward, (N x m)/m.

N O T A T I O N (cont.)

ω	Angular speed of the wheel, rad/sec.
δ	Tyre deflection on an unyielding surface, m.
η	Tractive efficiency, dimensionless.
τ	Shear stress in Mohr-Coulomb yield criterion, kPa.
σ	Normal stress in Mohr-Coulomb yield criterion, kPa.
$\sigma_1, \sigma_2, \sigma_3$	Principal stresses, kPa.

1. INTRODUCTION

1.1 An urgent requirement

This work started from the pratical requirement to decide on the optimum tyres to fit to a seabed vehicle, and then to recommend a suitable system of soil measurements which could economically predict its performance on a particular site. The seabed environment poses the following special problems:

a) It is known that seabed soils range from firm to very soft. The proportion of very soft soils is much higher than on dry land, because there are great areas where soil is still being laid down after a slow descent through the water coming to rest in a still environment with a minimum of compacting disturbance.

b) No practical experience of driving or even walking is available. Very high costs of mobilization and deployment preclude trials as part of the process of making a proposal for a particular job.

c) Site soil surveys are very expensive and difficult to perform so that limited and poor quality measurements are all that are available.

d) It seems possible that performance on a particular soil will be different when it is submerged.

In an effort to solve specific seabed mobility problems quickly the extensive literature on vehicle mobility, particularly in a military context, was reviewed. The Department of Agricultural Engineering at Newcastle has long been associated with the attempt to relate vehicle performance to fundamental soil mechanics parameters, pioneered by M.G. Bekker. It was therefore surprising to find that, confronted with a real problem, this approach was not very helpful.

The immediately applicable body of knowledge was the empirical system relating vehicle performance to cone penetrometer data developed by the Waterways Experiment Station of the Corps of Engineers of the U.S. army.

The W.E.S. system relates vehicle performance in saturated clay or dry sand to a single soil strength number obtained by driving a cone penetrometer into the soil. The results of a very large number of tests in the laboratory on tyres ranging in width from 1.6 to 16 inches and in diameter from 14 to 30 inches carrying a wide range of loads on sand and clay have been plotted in two sets of four curves reproduced in Fig. 1.1. The four curves plot four dimensionless performance ratios against a numeric containing a measure of soil strength. The ratios are $^{DP}/W$, the ratio of drawbar pull at 20% slip to the weight carried by the tyre, $^{T}/Wr_r$ the ratio of the applied torque to the weight carried times the rolling radius, $^{z}/d$ the ratio of sinkage at 20% slip to tyre diameter and $^{Pt}/W$ the ratio of the pull required by a free rolling wheel to the weight it carries.

The data has been reduced to fairly narrow bands by plotting the performance ratios against the two dimensionless mobility numbers.

$$\text{For clay } N_c = \frac{CIbd}{W}\left(\frac{\delta}{h}\right)^{\frac{1}{2}} \frac{1}{1 + b/2d}$$

$$\text{For sand } Ns = \frac{G(bd)^{3/2}}{W}\left(\frac{\delta}{h}\right)$$

These two dimensionless groups are of tremendous importance because for a given N number performance is the same and they therefore give a clear quantitative picture of the relative importance of the parameters. They show that the load carried is proportional to the tyre dimensions cubed for sand and squared for clay, and to G for sand and CI for clay.

Perhaps most important of all they show the relative merits of tyre proportions for the two most difficult soil types. This can perhaps be best illustrated by comparing the ratio of load W to soil strength CI or G for two possible tyre configurations i.e. dual 11 x 28 or single 48 x 25 Terratyre assuming the same ratio of $\delta/h = .25$ in each case.

In Clay

$$\text{Duals } \frac{N_c W}{CI} = 2 \times 11.2 \times 47 \times \tfrac{1}{2} \times \frac{1}{1 + 11/96} = 472$$

$$\text{Terratyre } \frac{N_c W}{CI} = 25 \times 48 \times \tfrac{1}{2} \times \frac{1}{1 + 25/96} = 476$$

The conclusion is that the performance is the same.

In Sand

$$\text{Duals } \frac{N_s W}{G} = 2 \times (11.2 \times 47.2)^{3/2} \, (\tfrac{1}{4}) = 6{,}080$$

$$\text{Single } \frac{N_s W}{G} = (25 \times 48)^{3/2} \, (\tfrac{1}{4}) = 10{,}400$$

$$\text{Triple } \frac{N_s W}{G} = 3 \times (11.2 \times 47.2)^{3/2} \, (\tfrac{1}{4}) = 9{,}120$$

The conclusion is quite different. In the sand the single wide tyre has a 70% greater carrying capacity than the duals. This is in accord with simple bearing capacity theory which shows that the pressure that can be carried in sand is proportional to width.

Furthermore the only soil test necessary, the pushing in of a cone, is the simplest conceivable, and is already commonly used on the seabed. This is evidently a very powerful system, it was siezed upon with enthusiasm and used to make confident proposals to trusting clients. These proposals were then checked by experiments on various tyres in sand and clay in the Soil Mechanics Laboratory at the University of Newcastle. The experiments in clay showed excellent agreement with the published W.E.S. results and have been described in the present Author's M.Sc. Thesis (Peca 1979) and Reece and Peca (1981). The results in sand provided no such agreement, as shown for example in Fig. 1.2. In the search for the reason for this, a comprehensive review of the latest developments in the W.E.S. system was undertaken.

1.2 Recent developments in the W.E.S. system

There are three separate W.E.S. systems according to the soil type, as follows: pure cohesive soils (wet clays), pure frictional soils (dry sands) and cohesive - frictional soils, mainly in the form of agricltural top soils. Herein is presented a summary of the development of the W.E.S. system for purely frictional soils only, which for the sake of simplicity will be called "the W.E.S. system in sand".

Information concerning the W.E.S. system in purely cohesive soils can be obtained from Freitag (1966), Turnage (1972b), Swanson (1973) and Reece and Peca (1981). Concerning the W.E.S. system in cohesive frictional soils information can be obtained from Wismer and Luth (1974) and Dwyer et al (1975).

Freitag (1968), as a result of a very large number of tests performed at 20% slip in air-dry Yuma sand, using four tyres (4.00-7, 2PR; 9.00-14, 2PR; 6.00-16, 2PR; 4.00-20, 2PR), reported that there is a good correlation when dimensionless performance coefficients are plotted against a dimensionless sand number which is based on information of soil strength, tyre geometry and normal load.

These performance numbers are:

$$\text{coefficient of traction} = \frac{DP}{W}$$

$$\text{torque number} = \frac{T}{Wd}$$

$$\text{sinkage number} = z/d$$

and the sand number in

$$N_s = \frac{G\,(bd)^{3/2}}{W} \times \delta/h$$

where:

G - Cone Resistance Gradient, averaged over the top 15cm of soil, obtained by pushing a standard W.E.S. cone penetrometer (A.S.A.E. Recommendation R 313.1) into the soil at 30mm/sec.

b - tyre width; d - tyre diameter
h - unloaded carcass section height
W - vertical load; δ - tyre deflection on unyielding surface.

All discussions and deformation are measured according to I.S.T.V.S. standards, Meyer (1977).

Turnage (1972 a and b) reported the extension of Freitag's results to virtually all the tyres tested by W.E.S. and presented in Fig. 1.3, with the exception of the tyre 9.00-20.

In Turnage (1972 a) the results (Fig. 1.1) are presented in graphic form showing curves representing the central line and the envelope in which 68% of the data is said to lie. In Turnage (1972 b) the information is more detailed, since there are well organized tables with the parameters and results for each wheel test. The W.E.S. curves are said to be a result for tests within the following limits:

$G = 0.6 - 7.5$ MPa/m

$W = 450 - 6000$ N

$\delta/h = 0.15;\ 0.25;\ 0.35$

$b/d = 0.15 - 0.88$

Using the results published by Turnage (1972 b), Fig. 1.4 was constructed with the intention of showing each individual tyre and also results per groups of soil density represented by relative density ^{D}d.

It was observed in the above reference that the tests were done in a variable slip mode, i.e., the wheel turning at constant speed and the carriage supporting the wheel decelerating along the soil tank. It is said that correction was made taking into account the inertia forces interfering with the measured pull, however, in some tables the corrected value was not produced. On the other hand tests were also done on a few tyres in a constant slip mode.

The results plotted in Fig. 1.4 are a mixture of the information of both constant and variable slip tests, with and without correction for inertia forces.

They show a remarkably well defined curve bearing in mind the diversity of tyre shapes and loads. It is however very striking to find that most of the shape of the curve is defined by the results of tests performed in very dense sand, and that the results of test performed in the less dense sands of practical importance are concentrated in the steep part of the curve where reading is easily affected by error, i.e. the $^{DP}/W$ ratio at $N_s = 30$ lies between .4 and .5 while at $N_s = 5$ it lies between -.1 and +.15.

Tests in a different sand (Mortar sand) are reported by Turnage and Green (1966) with a 9.00-14 tyre, by Patin (1971) with the set of "fat tyres" (16 x 6.50-8, 2PR; 16 x 11.50-6, 2PR; 16 x 15.00-6, 2PR; 26 x16.00-10, 4PR; 31 x 15.50-13, 4PR) and by Turnage (1976) with a 9.00-20 tyre. Detailed information concerning most of the tests may be found in Turnage (1972 b). Fig. 1.5 shows the results, and to facilitate comparison with Fig. 1.4 the envolope for tests in Yuma sand is also represented. Whenever available the corrected values for inertia forces were used. Leaving out, for the moment, the tests with the 9.00-20 tyre, the remaining tests are always below the envelope for the results in Yuma sand.

According to Patin (1971) the non-agreement between the results in two sands is due to the fact that in Mortar and Yuma sands the same value of cone resistance gradient (G) does not correspond to the same relative density (^{D}d). He then put forward the following hypothesis: two sands provide similar traction performance at the same relative density. If so, the curve representing the correlation in Mortar sand should collapse on the curve for Yuma sand when the value of G used in computing the sand number N_s would be the one obtained in Yuma sand at the same relative density. Such process, called "normalization to Yuma sand", was performed with success.

One of the intriguing results presented by Fig. 1.5 is that concerning the 9.00-20 tyres. It is noticeable that for one value of sand number it was possible to find two quite separate values of coefficient of traction. Turnage (1976) observed that the results with the 9.00-20 tyres show a pronounced separation by values of penetration resistance gradient, Fig. 1.6. It may be added that there is also a separation according to the values of deflection ($\delta/_h$) and, since these tests were done at one single value of vertical load, there is also a separation according to inflation pressure.

Turnage (1976) claims that the separation in Fig. 1.6a is caused by using an in-situ, pre-traffic value of G to compute the sand number N_s. He observed that the value of G (and therefore the soil strength) is different after traffic, typically as in Fig. 1.6b, which means that the value of G to be used in describing type performance for a given pass should be the value that predominated during that pass. He found that the separation in Fig. 1.6a disappears if the value of G is calculated by adding 25% of the pre-traffic value of G to 75% of the after pass value of G, that is, G should be weighed 3:1 towards its after-first-pass value.

So according to Turnage (1976) what matters is the range of sand mechanical properties over the whole range of densities between its in-situ condition and the condition after the loading by the wheel. The original W.E.S. system only included the initial conditions. This principle seems acceptable but not promising if a simple prediction system is required.

Turnage (1976) also observed that "the relation shown in Fig. 1.6b appears not to be strongly influenced by tyre conditions (size, shape, deflection, tread pattern, inherent stiffness) over a rather broad range". Furthermore "the mechanics by which sand strength changes with tyre traffic varies with tyre slip". The necessity for "normalization to Yuma sand" (Patin 1971), and the inclusion in the theory of a "prevailing soil strength" (Turnage 1976) was combined in a single method described by Turnage (1978).

The objective of this new method is to provide a more general correlation between dimensionless performance coefficients and a dimensionless sand number of the following form:

$$N_{se} = \frac{G_e\ (bd)^{3/2}\ \delta/_h}{W}$$

Where G_e "is the effective sand penetration resistance gradient, i.e., the value of G that predominated during a given tyre pass normalized to one type of frictional soil (selected as Yuma sand) no matter what frictional soil the tyre is operating in.".

The scheme for estimating G_e involves five steps described in appendix A of Turnage (1978) and also transcribed in Fig. 1.7a. The first three steps find the relevant G during the pass in question, allowing at the same time for the influence of tyre shape factor b/d. Steps 4 and 5 account for the normalization to Yuma sand.

The last two steps were found, however, to be insufficient to make the results in Yuma and Mortar sand collapse on the same curve, and the whole process had to be complemented by the use of the term tan ϕ_{70} affecting the performance coefficients, ϕ_{70} being the angle of soil internal friction at 70% relative density.

The two sets of curves representing the correlation found in Mortar and Yuma sand are shown in Fig. 1.7c and d.

The first observation that can be made about this method, from now on called Turnage's Method, is that it is no longer a quick method for a go-no-go evaluation. The original concept of a single simple measurement that could be made in the field by one operator is now lost. Furthermore it seems unreasonable to use the term tan ϕ_{70} associated with the dimensionless performance numbers instead of keeping the soil properties in

the sand number. Also ϕ_{70} is always a difficult value to evaluate let alone the fact that is not a single number even for one sand as it will be shown later. The most interesting aspect of the method is expressed by Fig. 1.7b where an attempt is made to relate the prevailing soil density during the wheel pass with the pre-traffic soil density and tyre basic geometry.

What is shown is that in dense sand a low shape factor tyre (narrow tyre) dilates the soil less than a tyre with a high shape factor (fat tyre). However in loose sand a higher compaction of the soil is achieved with a narrow tyre. Moreover there is a value of initial relative density which is kept unchanged after traffic. Such value depends on the value of shape factor and varies from D_d = 75% for b/d = 0.2 to D_d = 20% for b/d = 0.8.

Turnage (1978) admitted that the universality of the method had still to be tested. Different sand types should be used to test the method which, at least in Yuma and Mortar sand is able to make the results of a variety of tyres to collapse in narrow bands.

1.3 An appraisal of the new W.E.S. system

It is probably reasonable to describe the present picture presented by W.E.S. as follows:

> Sand is a very complex material and can only be adequately described by the following variables:

1) the compactability of the sand. This can be described by the ratio $D' = \frac{v_{max} - v_{min}}{v_{min} - 1}$, where v max and v min are the maximum and minimum specific volumes.

2) It's in-situ density or specific volume, v.

3) It's angle of internal friction, at its in-situ specific volume.

Scheme 1 and 2 are combined in the concept of relative density which is given by $D_d = \frac{v_{max} - v}{v_{max} - v_{min}}$

The measurement of relative density involves making in-situ cone penetrometer tests on the site and the recovery of a disturbed sample of about $0.1m^3$ weighing about 1.7 KN (400lb). The maximum and minimum densities are measured in a well equipped laboratory using standard procedures. The cone penetrometer is then calibrated by making a series of tests in carefully prepared molds 400mm in diameter by 250mm deep containing uniformly compact sand, with the series covering a wide range of compactions. This enables the in-situ penetrometer tests to be converted to a single figure of in-situ density (or specific volume).

The value of the angle of internal friction at the in-situ density is then measured by a series of shear box tests over a range of densities spanning the in-situ density.

It is clear then that the original concept of a single simple measurement that could be made in the field by one soldier has been replaced by the whole expensive geotechnical business of in-situ testing, sample acquisition and routine laboratory testing.

The system with its clear statements of the relative value of different tyre parameters and its elegant and symbolic measuring device has gone altogther. In its place is a great deal of experimental information and lots of useful ideas culminating in the general proposal that tyre performance in sand must be a function of a numeric N_s of the form

$$N_s = \left[\frac{D_d}{\tan\phi}\right]_{\text{soil}} \times \left[\frac{\gamma(bd)^{3/2}}{W}\right]_{\text{tyre load}} \times \left[f(D_d, {}^{b}/_{d})\right]_{\text{tyre shape}}$$

Despite the complexity of the new W.E.S. system it still seems feasible to use it in a seabed situation. All serious site investigations on the seabed involve the recovery of samples, and in-situ cone testing is quite usual. Once this has been paid for, any amount of laboratory testing on the samples costs a negligible extra amount.

It was therefore decided to carry out the full set of measurements required on one sand in a wide range of densities, and to test a single tyre size at three loads in the laboratory at these densities to see if the new system would correctly describe the wheel performance. At the same time the experiments would be repeated with the sand submerged. It was expected that once the new W.E.S. system could predict the performance in dry sand, effort could now be concentrated on adapting it to the submerged situation. The effect of submergence is described in Peca and Reece (1981). The basic comparison of the results obtained with the old and new W.E.S. system is shown in Fig. 1.2 a and b. It is plain that performance in Cresswell sand is much different to Yuma and Mortar sand and that the new system is no improvement on the old.

It was therefore decided that the object of the research would have to be changed, the interest in the effect of submergence being given up. It seemed quite certain that if the problem of tyre performance in sand could not be solved by a major laboratory, spending millions of dollars over 20 years then it would not be solved by one Ph.D. student.

1.4 The objectives of the research programme

It is clear that the W.E.S. system failed because it assumed that sand is a simple material that can be totally described, as far as mechanical behaviour is concerned by a single measurement (in remoulded clay this assumption proved acceptable). The recently observed fact is that two sands which offer te same resistance to penetration by a cone can have very different capacities to support traction. This fact has already driven W.E.S. to consider the properties of internal friction and density and their interrelation with each other. It seems certain that this interest in the basic mechanical properties of sand is the key to obtaining a system of performance prediction that really works.

There is only one possible variable in a dry sand and that is its state of packing. The key question then becomes: how does the strength of sand depend on its packing (or specific volume)? It should be noted that we are here limiting ourselves to uniform, isotropic sand as can with difficulty be prepared in a laboratory tank.

The second question is: how can we most simply measure the in-situ strength and/or specific volume of sand? If this is to be done with a cone penetrometer, then how are the results to be interpreted?

The third question is: does the performance of a wheel depend on the strength and specific volume of a sand?

The whole question of the way the strength of soil varies with specific volume has, in recent years, been put into a comprehensive framework with the development of the ideas of Critical State Soil Mechanics. This has been developed particularly in relation to saturated clays. A starting point is therefore a consideration of Critical State Soil Mechanics applied to dry sands.

The mechanical properties of sand have been the subject of an enormous amount of work in the main stream of soil mechanics. It is evidently necessary to review this, in the hope of presenting a short, clear picture of the relationships between angle of friction, specific volume and particle shape, mineralogy and particle size distribution. It was then planned to use this understanding to measure the properties of several sands, which were available in large enough quantities to use in soil tanks for wheel traction tests.

The crux of the problem of predicting vehicle performance in a particular sand is the measurement of its relevant in-situ mechanical properties. At present this can only be done by means of at least one in-situ measurement, together with extensive laboratory testing on a fairly large sample. The next stage, therefore, was to use a cone penetrometer in the same sands, and to find out how to interpret the results, in the light of the previously gained knowledge of mechanical properties. This forms Chapter 4 of this Thesis.

This preceding work made it then possible to test wheels in sands of very well known mechanical properties. This programme was planned from the idea that the W.E.S. system had failed because their emphasis was initially on the trye with the sand being assumed to be a simple material. It was hoped that by starting by concentrating on the sand, some new understanding could be arrived at.

2. CRITICAL STATE SOIL MECHANICS

Within the last 25 years a very substantial amount of literature concerned with the Cambridge theories of Critical State Soil Mechanics has been published. Perhaps the most recent complete account is given by Atkinson and Bransby (1978), used as a source in this work. Mention must also be made to the series of papers introducing Critical State Soil Mechanics to the general field of Soil Machine Mechanics; among others, Reece (1969), Kurtay and Reece (1970), Reece (1977) and Hettiaratchi and O'Callaghan (1980) are the most relevant.

The main idea of Critical State Soil Mechanics is that soil fails under load in one of two separate ways. In the first it fails by deforming and flowing plastically, growing more compact and stronger until this strengthening comes to an end and plastic flow then continues at constant stress and constant volume, the Critical State.

In the second mode the soil fails in a brittle manner along a single shear plane, with dilation along that plane. After this first and each subsequent failure, the loading may rearrange itself and other planes of a similar type may appear.

The first mode can be observed in results of triaxial compression tests in isotropically consolidated clay and are represented in the critical state space p; q; v, by the Roscoe surface, a curved surface joining the virgin compression line with the critical state line, Fig. 2.1.

The second mode can be observed doing similar experiments in overconsolidated clay. These tests, when performed drained, show the usual peak of stress and the development of the shear plane along which the deformation concentrates. It was observed that a surface, the Hvorslev surface, limits the peak values of stress in the critical state space. Since the deformation is concentrated in those elements of soil which have already failed in preference to the whole mass, then boundary measurements of force and displacement, to compute stress and strains in the most deforming regions of the sample, become highly inaccurate. For this reason it is only accepted as a working hypothesis that the ultimate states of individual elements of overconsolidated clay lie on the critical state line defined by the ultimate states on normally consolidated samples.

A complete state boundary surface, as shown in Fig. 2.2, emerges then as representing the whole picture of the deformation of saturated clays under load. It consists of the Roscoe and Hvorslev surfaces which meet at the critical state line, and serves for drained and undrained triaxial compression test on normally consolidated and overconsolidated samples of clay, as well as for special cases of the above tests like the isotropic and one-dimensional compression, hence unifying a wide range of behaviour. The soil is assumed rigid or elastic when the loading path is within the volume limited by the complete boundary surface and plastic when the loading path intersects and traverses the surface. Outside the surface the soil cannot exist.

Soil elements in field situations will be subjected to a wide range of stress paths and may well be very different from that imposed in a standard triaxial compression test, thus making it very important to consider what governs failure under general states of stress. Here research is limited by the difficulty of devising an apparatus which able to load a soil sample in a completely general manner. One of such apparatus is the true triaxial

test machine which applies to the sample three different principal stresses at the same time. The hollow cylinder test may be regarded as an example. Experimental evidence with true triaxial test machines show the effective stress paths for undrained tests on isotropically normally consolidated clay defining a smooth axisymmetric surface as sketched in Fig. 2.3, which may be assumed as the generalized Roscoe surface in the principal stress space.

For overconsolidated samples of clay, unfortunately, there is little or no experimental evidence available concerning with their behaviour in stress states other than those which can be imposed in the triaxial apparatus, and so the form of the generalized Hvorslev surface in the principal stress space is uncertain. The experimental evidence in triaxial compression and triaxial extension, making a complete section to the unknown surface, leads to the hypothesis that such surface might be the irregular hexagonal pyramid which represents the well known Mohr-Coulomb yield criterion $\tau = c + \sigma \tan \phi$.

According to the previous hypothesis, Fig. 2.4 shows what might be a generalized state boundary surface for clay at a particular density. It comprises an hexagonal pyramid whose apex lies on the space diagonal at a negative mean normal pressure, representing the Hvorslev surface, and a curved axisymmetric surface representing the Roscoe surface. Both surfaces should intersect in a line which should be called the generalized critical state line, the precise geometry of which has not been established experimentally due to reasons already explained.

Triaxial compression tests in sands revealed similarities between the behaviour of loose sand and that of normally consolidated clay, and between that of dense sand and that of overconsolidated clay, therefore suggesting that the behaviour of sand can be fitted into the same framework that serves for clay.

It is important to realize that only under unusually high confining pressures it is possible to find the strength hardening compacting behaviour in sands, as it was shown in the classic experiments by Vesic and Clough (1968), with the exception of situations of very loose packing. Under loads common in engineering practice, sands behave like overconsolidated clay, therefore dilating. In the field of Soil-Vehicle Mechanics that is certainly the experience, as shown by Turnage (1976) in Fig. 1.6b, and indeed our own as it will be discussed in Chapter 6. Therefore in sands the most relevant part of the state boundary surface is the Hvorslev surface, which, as seen before, is thought to be associated with the classic Mohr-Coulomb yield criterion. Again, as for over-consolidated clays, there are considerable experimental difficulties in achieving uniform stress and strain conditions in triaxial specimens at the large deformations that are required to take the states of the specimens to the critical state line. The use of other testing techniques like the simple shear test apparatus seems not to have overcome this problem.

So, however disappointing, the mathematical model for soil behaviour described by Critical State Soil Mechanics does not seem of much use to the present study. It was regretted that the chosen field of study was not the performance of a compaction plant or the traction of tyres in agricultural soils to which Critical State Soil Mechanics seems to offer a very accurate description of soil behaviour.

In the end the scope of the relevant soil mechanics become reduced to the question of the way the angle of internal friction varied with specific volume and the range of specific volume available to any particular sand.

3. THE ANGLE OF INTERNAL FRICTION OF SANDS

An extensive survey of the literature was carried out with the objective of analysing the present stat of knowledge concerning the frictional properties of granular material, particularly sands. The summary of the results was then tested against experimental evidence in available sands, two of which were to be use in the traction studies.

The frictional properties of soils is linked traditionally with the angle of internal friction introduced by Coulomb from simple extension of the same concept relating to friction of solids. However, one cannot ignore the fact that sand consists of individual grains forming a mass which changes volume during a shear process. This makes the phenomenon of friction in sand different from the basic principles of friction for non-deforming bodies.

While this is no new observation it still seems pertinent, within the purpose of this work, to emphasize it to obtain a deeper comprehension of the problem. In relation to this the theories put forward by Critical State Soil Mechanics have proved to be of the utmost value.

3.1 Angle of internal friction from triaxial tests

The triaxial apparatus is mainly used to evaluate soil strength by its two classic parameters: cohesion c and internal friction ϕ.

Fig. 3.1 shows the stress paths for a set of four drained triaxial tests required to evaluate the angle of friction of a sample of dense sand.

At the initial state the specific volume of the sample is v_1 and the four tests are done at cell pressures increasing from $\sigma_3 = p_1$ to $\sigma_3 = p_4$.

The soil dilates since it is initially dense and fails (at the peak of axial load) on the Hvorslev surface, points b_1; b_2; b_3. After the peak, the axial load as well as the rate of dilation starts to decrease. Also the deformation of the sample starts to concentrate on distinct failure of planes making inaccurate the measurement of stress and strains. As a result it is only admitted as an hypothesis that towards the end of the test the sample is reaching the critical state (points c_1; c_2; c_3 and c_4) where the sample, however distorting, does not change volume and the axial stress has reached a constant value.

Fig. 3.2 shows tests 1,2 and 4 on a Mohr's plane for values taken at the peak of stress, points b_1, b_2 and c_4 respectively. Any attempt to fit a tangent simultaneously to the three circles will be unrealistic and in fact shows an impossible value for cohesion.

The other alternative is shown in Fig. 3.2 which makes it evident that the angle of internal friction at the peak of stress for a dense sand is a function of the confining pressure at which the test is performed, decreasing for increasing values of p.

If it can be assumed that the ultimate state for each specimen is the critical state line then, at that stage, a single value of the angle of internal friction, ϕ_{cv}, should be expected for all the samples. This

friction angle is related with the critical state line by the equation

$$M = \frac{6 \sin\phi_{cv}}{3-\sin\phi_{cv}}$$

Where M is the slope of the critical state line on the p,q plane of the critical state space. As a result, at the critical state, the angle of internal friction is independent of the specific volume (v) and of the confining pressure (p), since it is only a function of M. The equivalent representation in the Mohr's plane is shown in Fig. 3.3. The Mohr's envelope, which was a curve in Fig. 3.2, becomes in Fig. 3.3 the classic straight line of the Mohr's-Coulomb yield criterion.

It is clear, when comparing soil strength at point b_1 and c_1 or b_2 and c_2 that, as a result of dilation (maximum rate at b_1 and b_2), the soil becomes stronger. There is a link between the stress ratio q/p and the rate of dilation $d\varepsilon_v/d\varepsilon_a$ of the sand. The highest value of q/p will be observed for samples which are dense, when they are tested drained at low stress levels since they will dilate strongly at failure.

It seems therefore acceptable to consider the angle of internal friction at the peak of stress as being the sum of an angle expressing the contribution of friction plus an angle expressing the contribution of dilation.

If the conditions of tests represented on Fig. 3.1 were repeated this time on loose sand, it is possible that the equivalent diagram for the loading path would be as shown in Fig. 3.4. The soil now becomes more compact and no clear peak of axial load is obtained, but instead a continuous increase until a steady maximum value. At this stage the sample, however deforming, does not change volume, indicating that the critical state has been reached. If it can be assumed that the same critical state line is common to both dense and loose samples, then the tests on the loose sample could also be represented in the Mohr's space by Fig. 3.3.

However the above statements are made based on the theories of Critical State Soil Mechanics, there seems to be some experimental evidence: Figures 3.5 to 3.7 were obtained respectively by Rowe (1962), Vesic and Clough (1968) and Lee (1967). They show that when soil is deforming on the Hvorslev side of the critical state boundary, exhibiting a peak of stress at the maximum dilation rate, the angle of friction at the peak is always higher than the angle of friction at the critical state. Also the angle of friction at the peak is variable depending on the initial density (or specific volume) of the sample and on the test confining pressure; these two parameters locating the sample relative to the critical state line and, therefore, reflecting the amount of dilation present when the sample is deforming.

3.2 The dilation component of the angle of internal friction

From the previous section it became apparent that the angle of internal friction, ϕ, may be separated into two different components: ϕ_{cv}, associated with the friction developed by groups of grains sliding on other groups, with no overall change in the volume, plus ϕ_{dil} representing the energy lost in the dilation process against the confining pressure applied by the apparatus.

In the present section ϕ_{dil} will be discussed, basically using the theoretical background of the Rowe-Horne stress dilatancy theory, which is probably the most notable stress-strain relationship for soils in the presence of dilation. A review, in a summarized form, of the Rowe-Horne stress-dilatancy theory is presented in Appendix 1. The basic idea is that there is a link between the stress ratio, σ_1/σ_3 (or q/p), and the rate of dilation, $d\varepsilon_v/d\varepsilon_a$, of the sand. According to Rowe (1969) that link is given by equation 1

$$\left(\frac{\sigma_1}{\sigma_3}\right)_{peak} = 2 \tan^2 (45 + \tfrac{1}{2} \phi_\mu) \qquad (1)$$

valid, at the peak of stress ratio, for a sample of granular material, at its maximum density, being tested in triaxial compression at low cell pressure. ϕ_μ is the true angle of friction between the mineral surfaces of the soil particles, called the angle of interparticle friction. It is expected to be dependent on grain features like mineralogy, shape, surface roughness and presence of water films or any other contamination. Due to the conditions of the test, the value of peak stress ratio given by equation 1 is expected to be the maximum value possible for a particular sand.

At the stage when the sample is deforming, with no change in volume (critical state), then, according to Rowe (1962), the stress ratio becomes:

$$\frac{\sigma_1}{\sigma_3} = \tan^2 (45 + \tfrac{1}{2} \phi_{cv}) \qquad (2)$$

It follows that for any particular sand there is a range of values for the angle of internal friction increasing from ϕ_{cv} given by equation 2 to ϕ max given by the following equation

$$\max\left(\frac{\sigma_1}{\sigma_3}\right)_{peak} = \tan^2 (45 + \tfrac{1}{2} \phi_{max}) \qquad (3)$$

where the peak of stress ratio on the left side is given by equation 1.

Fig. 3.8 shows a plot of ϕ_{max} versus ϕ_μ obtained from the combination of equations 1 and 3, and alongside, the relationship between ϕ_{cv} and ϕ_μ obtained theoretically by Horne (1969). It suggests that, at least for soils with $\phi_\mu \geq 20$ degrees ($\phi_{cv} \geq 27$ degrees), the value of max $\phi_{dil} = \phi_{max} - \phi_{cv}$ measured in triaxial cell test is a rather constant value of about 9 degrees. So it seems that the differences in strength revealed by different cohesionless soils when tested in triaxial compression, comes from the component ϕ_{cv} (soil deforming at constant volume) and not from the component representing soil dilation. This fact seems to be experimentally supported by results from tests (Rowe, 1969) in granular materials as different as crushed glass, medium to fine graded quartz sand and glass ballotini, which are also plotted in Fig. 3.8

There are, however, some other sources from where it is possible to reach some conclusions concerning ϕ_{dil} and its range in granular soils. These are the empirical relations between the angle of internal friction (a.i.f.) and soil density. Within the last 20 years a variety of relations have been published in an attempt to describe the a.i.f. as a function of soil density of cohesionless soils, particularly sands. The following equations

are probably better known:

$$\cot \phi = ae + b \qquad (4)$$

$$\cot \phi = \frac{1}{c} e \qquad (5)$$

$$\cot \phi = c_1 - c_2 D_d \qquad (6)$$

where ϕ is the a.i.f. measured at failure in a triaxial test, e is the initial voids ratio, D_d is the relative density and a, b, c, c_1 and c_2 are constants. Correlations were tried between a, b, and c and soil properties like grain size and grain size distribution but apparently without success. Equation 6, by Melzer (1973), was derived from equation 4 and was tested in 22 different sands showing a good agreement between the constant c_2 and soil compactability with c_1 not varying a great deal, 1.52 to 2.02.

Tests on different granular soils varying particle shape and particle size distribution indicate that granular soils at the same relative density may present drastically different engineering properties. So the validity of equation 6 is requiring that the constants are conveying all the information concerning particle shape and particle size distribution. Compactability may be thought as a combined information of those two properties.

Recalling that $\phi = \phi_{cv} + \phi_{dil}$ and that $\phi = \phi_{cv}$ in the case of a very loose soil, then:

$\cot \phi_{cv} = c_1$, which means, for the 22 different sands on which equation 6 was tested, the following limits:

$c_1 = 2.02 \Rightarrow \phi_{cv} = 26.3$ degrees

$c_1 = 1.52 \Rightarrow \phi_{cv} = 33.3$ degrees.

These values of ϕ_{cv} are within the possible limits of $\phi_{cv} = 24$ degrees for glass ballotini (Rowe 1962) and $\phi_{cv} = 43$ degrees for crushed glass (Parikh 1967).

The maximum value of ϕ_{dil}, max ϕ_{dil}, is according to equation 6:

$$\max \phi_{dil} = \phi_{max} - \phi_{cv} = \text{arc cot } (c_1 - c_2 \times 100) - \text{arc cot } c_1$$

and being a function of c_2 is dependent on the soil compactability. Based on data obtained from Melzer (1973), max ϕ_{dil} is plotted versus compactability in Fig. 3.9. It appears to suggest a well defined relation which is neither included nor even experimentally observed in the stress-dilitancy work by Rowe (1962).

It seems possible to conclude that there are specific features of the sand grains which, not only influence their basic frictional properties, as revealed by the concept of angle of interparticle friction, but also effect the range of possible states of packing, as revealed by the concept of compactability. In the following sections is presented a review of published work dealing with the effect of grain shape, grain size and grain size distribution on matters like the angle of internal friction and soil compactability.

3.3 The effect of particle shape

A recent account on the effect of particle shape on soil behaviour using the angle of interparticle friction, ϕ_μ, is given by Frossard (1979). He measured the values of ϕ_μ in eight soils as a function of the asperity index which is a measurement of particle shape, increasing with particle roundness.

Soils with calcareous grains and soils with quartz grains were used. The soils were also divided according to the shape of particles into very angular and rounded. In each of the lots two classes were formed according to size of particles: 2 to 1mm and 1 to 0.5mm.

The soils were tested in the dry state in triaxial compression, the results being presented in Fig. 3.10. It shows a higher angle of interparticle friction for lower asperity index, i.e. for increasingly distorted grains.

The results are consistant with the work by Koerner (1970b) who, performing triaxial tests in sands with the same particle size and particle size distribution, found that the angle of internal friction measured at the peak of stress ratio was always higher for sands with angular grains. Frossard's results are also in good agreement with the work by Koerner (1970a) and Procter and Barton (1974) in the sense that the angle ϕ_μ is higher for calcareous sands than for the sands with quartz grains.

Summarizing, Fig. 3.10 shows that grain minerology is a factor as important as particle shape in its effect on the angle of interparticle friction, and particle size, at least within the range of ungraded coarse sands tested, had little effect.

Furthermore, in limit density tests, Koerner (1970b) also found that v_{max}, v_{min}, $v_{max} - v_{min}$ as well as soil compactability increase going from sands with rounded grains to sands with angular grains.

A practical implication of the above is that to induce the same amount of strain in a compacting process (say in an one-dimensional compression test) a much higher value of stress is required in sands with rounded particles, assuming the same particle size and particle size distribution as well as the same initial relative density. Furthermore in conventional triaxial tests and presumably in a direct shear test much less deformation has to be achieved to mobilize full strength in sands with rounded particles.

Experimental confirmation of the above is shown by Holubec et al (1973), who also produced evidence of increasing strength with the angularity of the soil particles.

3.4 The effect of particle size

Figure 3.11 shows the results by Rowe (1962) concerning the effect of particle size on the angle of interparticle friction. Scarce information was given on the soils tested being quartz granular material tested saturated. No information on shape or gradation was available. By using the relationship between ϕ_{cv} and ϕ_μ of Fig. 3.8 the results may be re-plotted this time in a non-logarithmic scale as in Fig. 3.11b.

It seems that for coarser soils the effect of particle size is relatively unimportant. That is, in fact, in agreement with the results of Frossard (1979) discussed in the previous section.

Figure 3.12 shows the results by Koerner (1970b) from saturated drained triaxial compression tests in seven different granular soils from fine gravel to coarse silt. In a similar way to Fig. 3.11b it presents the angle of friction (after deducting the effect of dilation) versus particle size on a linear scale.

From the table on Fig. 3.12 it can be seen that going from gravel to silt there is an increase in v_{max}, v_{min}, $v_{max} - v_{min}$ and soil compactability. Also, from figures 3.11b and 3.12 it seems clear that the angle of friction at constant volume, ϕ_{cv}, increases for finer soils. The rate of increase is small from a fine gravel to a coarse sand but is high from a fine sand to a coarse silt.

It has been claimed, Youd (1973), that the above effects are associated with particle shape rather than size alone. As particles become smaller it is more difficult to assess their shape. This seems to be partially confirmed by tests done by Kirkpatrick (1965) in six different sieve aperture samples of the same sand (Leighton Buzzard), with mean grain size ranging from .39 to 1.85mm. No difference was found in the values of limit density.

Kolbuszewski (1963) also showed small differences in the limiting porosity of samples of glass ballotini, with mean diameter ranging from 0.15mm to 1.3mm, but a large variation on limiting porosity when comparing samples of crushed and uncrushed glass ballotini with the same mean diameter, emphasizing the relative importance of shape over size already seen in Frossard (1979).

It seems also pertinent to extend the same claim to the results of Fig. 3.11b and 3.12, saying that the increase in ϕ_{cv} in very fine granular soils may be attributed to an increase in angularity of the particles rather than to the single effect of size. The experimental results by Kirkpatrick (1965) in samples of Leighton Buzzard sand of different sieve aperture seem to confirm just that, despite the considerable scater, due probably to the method used in determining ϕ_{cv}.

3.5 The effect of particle size distribution

The sources of information concerning this subject are scarce and some of them inconclusive. From work done by Koerner (1970b) in three different sands with the same grain shape and the same value of d_{10} (grain diameter at 10% finer by weight) it is possible to conclude that particle size distribution has no major effect on ϕ_{cv}. The values of v_{max}, v_{min} and $v_{max} - v_{min}$ are increased and, compactability falls moving from a less uniform to a more uniform sand.

3.6 Summary of the review

The soil angle of internal friction (a.i.f.) is for one soil dependent on density, confining pressure and on the apparatus used.

The angle of internal friction ϕ may be separated into two different components: ϕ_{cv} when soil is deforming at constant volume (critical state), and ϕ_{dil} expressing the energy lost in the dilation process against the confining pressure applied by the apparatus.

At the crical state, (soil deforming at constant volume) the angle of internal friction is only dependent on the soil particle size distribution, particle shape, size and mineralogy.

The effect of confining pressure and soil density of the a.i.f. is present on the dilation component $\emptyset_{dil}$. The maximum expected value for $\emptyset_{dil}$ is associated with a fully dilating sand, i.e. at the maximum possible initial density and low confining pressure, and it seems to increase with soil compactability.

Based on the literature searched, the effect of grain shape, size and size distribution may be summarized as follows:

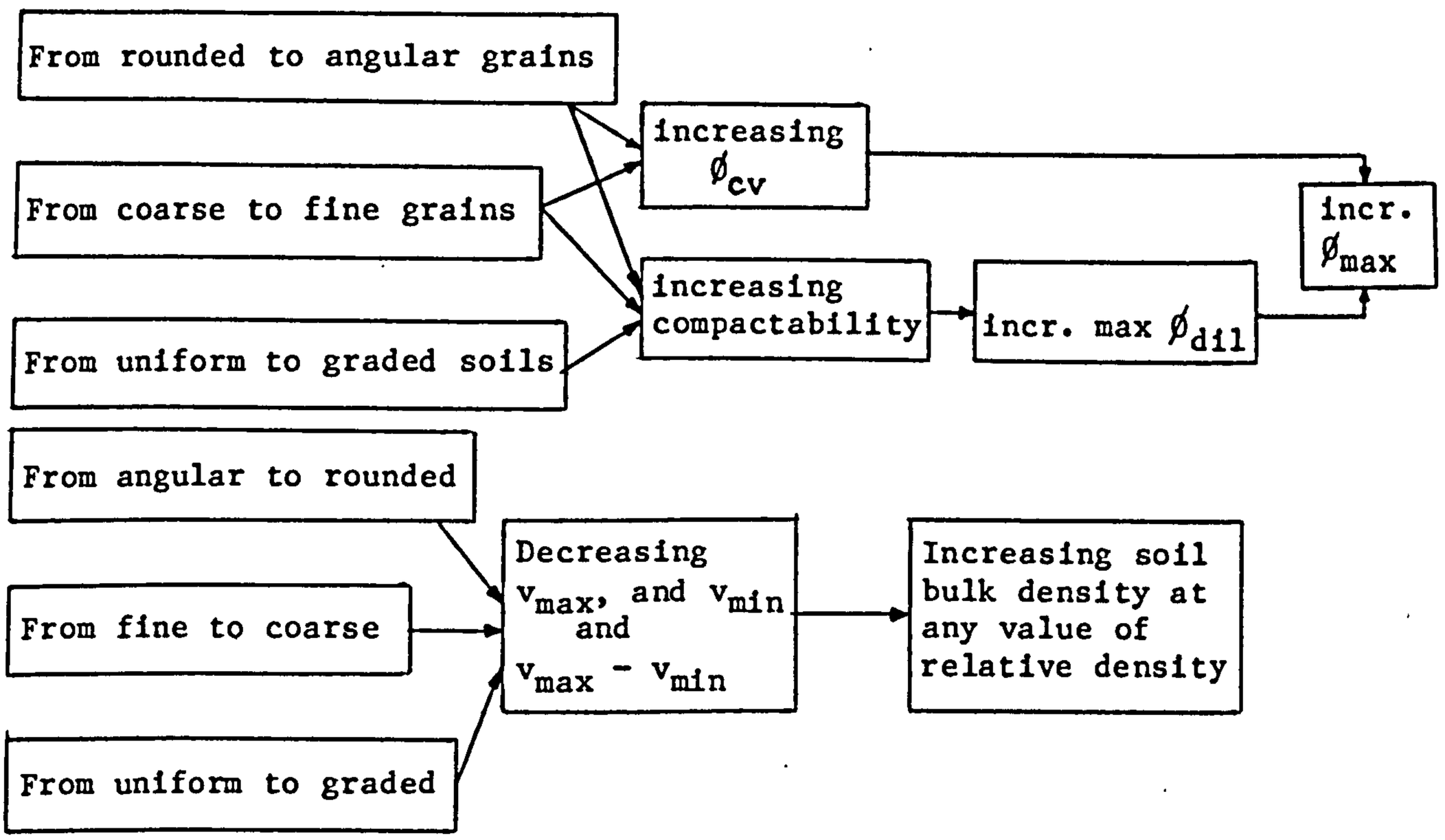

The relative importance of grain size, shape, and size distribution in contributing to variations on $\emptyset_{cv}$ and soil compactability may be summarized by stating that shape seems to be the important factor on the variation of $\emptyset_{cv}$, particle size distribution being mainly responsible for changes in compactability. Particle size alone, at least theoretically, should not affect any one of the above properties, however, it often does and it may be associated with unnoticed changes in particle shape.

Low compactability and low $\emptyset_{cv}$ may be associated with a coarse uniform soil made of well rounded particles in opposition to a soil with high compactability and $\emptyset_{cv}$ which is fine, non-uniform and made of angular grains.

3.7 The tested soils

The soils used in this work were Leighton Buzzard, Cresswell and Solway sands which were already available, plus Mix B sand, a specially blended sand, being a mixture of sieved samples from Leighton Buzzard, Cresswell, Lindisfarne and Solway sands. Reference is also made to Yuma, Mortar and Bayou Pierre sand (Melzer 1971) since these are three soils used in relevant work concerning traction on sand by W.E.S.

The same tests were performed on each of the four sands; these comprised a particle size analysis, a maximum density test using the standard compaction mould method, a minimum density test by the funnel method and a test for the measurement of the specific gravity of soil particles, using the Pycnometer method.

The procedure used in the four above tests may be found in Akroyd (1969).

The results are shown in Fig. 3.13 and in Table 3.1 which includes a microscopic observation of the soil grains. The shape of the grains was classified according to reference shapes published in Pettijohn (1972).

Shear resistance was measured in the shear box. There are objections to the use of this apparatus for measuring the shear resistance of soil, but it was decided that the advantage of being able to do a large number of tests in a reasonable short time outweighed the disadvantages.

A standard 60 x 60mm shear box apparatus was used into which the soil sample to be sheared was processed using the various techniques presented in Fig. 3.14 which aim to give various densities. It was found that different results could be obtained from tests at the same density prepared in different ways. The key thing seemed to be to avoid horizontal planes across the shear box. Vertical prodding was to be preferred to tapping. Fig. 3.15 shows results of shear tests using the tapping technique versus the results using the prodding method of Fig. 3.14c, where it seems that the tapping technique leaves weak layers of soil through which the shearing process is able to progress. In the prodding processing technique any irregularity in the packing is at least induced in a direction perpendicular to the plane of shear.

The succession of figures 3.16 to 3.19 show results of angle of internal friction against confining pressure and relative density, with singular values on Table 3.2.

In this work pressures were kept low, σ= 16kPa (2.3psi) to 98kPa (14.2psi) since it was thought to be more relevant to the problem of wheel soil interaction and cone penetration at shallow depth.

3.8 Discussion and conclusions

3.8.1 - Limit densities

The following table shows clearly a good agreement with the trend summarized in 3.6, insofaras there is a decrease in V_{max}, V_{min}, $V_{max} - V_{min}$ and an increase in bulk density at any value of relative density, when going from a fine, uniform sand with angular grains,like Solway,to coarser and much less uniform Bayou Pierre sand.

Sand	v_{max}	v_{min}	$v_{max}-v_{min}$	γ_{10}(kN/m^3) (D_d = 10%)	γ_{50}	γ_{90}
Solway	2.302	1.670	.632	11.62	13.10	15.01
Yuma	1.919	1.608	.311	13.86	14.84	15.96
Mortar	1.908	1.572	.336	13.96	15.04	16.30
Cresswell	1.775	1.525	.250	14.82	15.71	16.73
Leighton Buzzard	1.732	1.490	.242	15.17	16.08	17.11
Mix B	1.747	1.315	.432	15.27	16.99	19.16
Bayou Pierre	1.659	1.403	.256	15.90	16.96	18.18

3.8.2 - Compactability

In the same way the trend summarized in 3.6 shows a good agreement with the experimental results shown below where, a very uniform sand made of coarse rounded grains like Leighton Buzzard, showed the lowest value of compactability. In contrast, the highest compactability is, as expected, found in Mix B and Solway sands, in the former case because it is a non-uniform sand and in the latter case because it is a sand made of angular grains.

Leighton Buzzard	D' = 49.3%
Cresswell	47.6%
Mortar	58.7%
Yuma	51.2%
Bayou Pierre	63.3%
Solway	94.5%
Mix B	137.3%

3.8.3 - Angle of internal friction

If each soil is considered separately these are expected results insofaras the a.i.f. is rising with relative density and for a constant relative density is rising with decreasing confining pressure.

Loose soils are not very much influenced by confining pressure apart for very low pressures and therefore for the most common engineering problems strength of loose soils may be expressed by one number, dependent on the actual soil density regardless the confining pressure.

For dense soils it seems that the effect of confing pressure is more noticeable and,in fact,only at high confining pressures is it reasonable to use one number to express soil strength.

If a comparison among soils is attempted it should be made on a relative density basis and, for the reasons pointed out above, for a given confining pressure. The following points should be stressed from Fig. 3.20

1) The previous conclusion (Section 3.6) that uniform sands with rounded coarse grains would have relatively low values of ϕ_{cv} does not seem to stand from these tests judging from the results on Leighton Buzzard sand showing always the highest strength at a loose state regardless the test confining pressure. It should be stated, however, that the direct shear box is not adequated for tests up to the critical state since those tests require large values of strain and after about 4mm displacement the compression plate is no longer horizontal affecting the distribution of the normal load on the soil.

2) At any given pressure traces of soils with high compactability like Solway and Mix B sands run close to soil of much lower compactability, respectively Cresswell and Leighton Buzzard sands, concealing any possible influence of compactability on soil strength.

3) In part, the reason behind the much higher a.i.f. for Leighton Buzzard sand relative to Solway sand when all the grain features seem to indicate the opposite was found to be related with the component of friction expressing soil dilation.

Figure 3.21 shows the results of tests with three soils at D_d = 80% and it is shown that the higher the values of dilation the higher horizontal force has to be provided to make the soil fail. In the same way Fig. 3.22 shows tests results for Leighton Buzzard and Cresswell sand at similar values of relative density. It is clear that these two loose samples have a remarkably different behaviour under compression and shear insofaras the former dilates and the latter gets more compact with the obvious consequence concerning the angle of friction.

4 MEASUREMENT OF IN-SITU SOIL STRENGTH

In Soil-Vehicle Mechanics, and indeed in most Civil Engineering and Geotechnical studies, the measurement of in-situ soil strength is probably the most crucial practical problem. At the present time the cone penetrometer is the main tool used to perform this task in the field of Soil-Vehicle Mechanics. In purely cohesive soils and in cohesive-frictional soils the information required is the average of cone resistance with depth in terms of force on the cone divided by the cone base area (cone index - CI); in purely frictional soils is the average rate of increase of cone index with depth (cone resistance gradient - G).

The cone penetrometer is no new tool in the field of soil exploration, it is widely used in Civil Engineering and Geotechnical studies with a large number of designs either in its dynamic or in its static version. In Soil-Vehicle Mechanics the cone penetrometer most widely used has the simplest design of a 20.3mm cone base diameter, 30 degree apex angle attached to a 15.9mm cylindrical shaft (A.S.A.E. recommendation R313.1), and is pushed through a relatively shallow depth of soil at a steady rate of penetration, typically 150mm and 30mm/sec respectively. The modest size of the cone and above all the very shallow depth of penetration may place it on the threshold of application of the present theories meant for large cones and deep penetrations used for instance in foundation studies.

Howson (1977) and Smith and Dumas (1978) are examples of recent designs of cone penetrometers with recording capabilities for measuring soil resistance.

In the following sections will be described the experience gained with the cone penetrometer in sand at measured density and strength. Comparison will be made with relevant published work and a recent theory for cone indentation is checked against the experimental results.

4.1 Cone tests in air-dry sand

The four sands, Leighton Buzzard, Cresswell, Solway and Mix B, described in Section 3.7 were used in an extensive series of cone penetrometer tests with the primary target of establishing a relationship between cone resistance gradient (G) and soil density which could later be used for evaluation of in-situ density.

A cone penetrometer with the dimensions described in the previous section was driven by an hydraulic ram at a 30mm/sec penetration speed into the top 150 to 200mm thick layer of processed sand. A force transducer measured the force which was registered continuously against depth on a xy plotter.

The experiments were conducted in a cylindrical steel container 450mm in diameter and 250mm deep with a 200mm deep removable collar. Trials were done to make sure that the bottom of the mold would not affect the cone penetration force at least in the top 150mm of sand.

Initial experiments with a deeper 400mm mold, otherwise the same dimensions, proved to be less trustworthy for the simple reason that the cone resistance gradient (G) was obtained in a much smaller volume of sand than the one used to determine bulk density, let alone the fact that much more soil was involved in each test.

Sand bulk density (γ) was determined by weighing the mold on a lever type mechanical weighing machine with a discrimination of ½lb. Soil + mold weights vary from 142 to 204lb.

Various processing techniques were tried in order to get a volume of soil as uniform as possible with depth. Table 4.1 sums up the methods used in each test. Some of the techniques were only found after numerous other experiments had been discarded due to incorrect soil processing.

The results of the cone tests in the four tested sands are plotted in Fig. 4.1 to 4.4, with the actual values stated in Table 4.2. From these traces, values of cone index, CI, and cone resistance gradient, G, were computed using the following relations widely used in Soil-Vehicle Mechanics:

$$\text{CI at depth } z_1 = \frac{\text{Cone force at depth } z_1}{\text{Cone base area}}$$

$$\text{CI}_{av} \text{ over depth } z_1 = \frac{\int_0^{z_1} \text{CI}(z)\, dz}{z_1}$$

$$\text{G, averaged over depth } z_1 = \frac{\text{CI}_{av} \text{ over } z_1 - \text{CI}_{surf.}}{z_{1/2}}$$

The results are plotted against soil relative density in Figures 4.5 to 4.8 making the required set of charts for in-situ density measurements.

4.2 Cone resistance gradient and relative density

the straight lines in Fig. 4.8 may be represented by the following equation:

$$D_d = a_1 \log G + a_2 \quad ,$$

where D_d is measured in percentage and G in MP_a/m. This equation was put forward by Melzer (1971) who also suggested a correlation between the constants a_1 and a_2 respectively with soil compactability, D', and mean grain size, d_{50}. The actual values for the results in Fig. 4.8 are shown in the table below and plotted against D' and d_{50} in Fig. 4.9

Sand	a_1	D'(%)	a_2	d_{50}
Leighton Buzzard	74.7	49.3	13.5	0.95
Mix B	44.8	137.3	33.5	0.091
Cresswell	73.0	47.6	40.0	0.312
Solway	45.6	94.5	56.5	0.081
Bayou Pierre	77.0	63.3	29.5	0.46
Mortar	75.0	58.7	39.3	0.25
Yuma	71.1	51.2	51.6	0.12

The trends do not agree entirely with the conclusions in the original work by Melzer (1971); the same trend was found relative to constant a_2 but the opposite concerning constant a_1. This may be a result of the narrow range of compactability in the soils he used, making the results much more influenced by errors.

4.3 Cone resistance gradient and the angle of internal friction

At such shallow depths of penetration it is assumed that friction within the sand mass displaced by the cone is the main source of soil resistance. This assumption seems, at least qualitatively, to gain some credit by comparing the relative position of the curves shown in Figures 4.5 to 4.7 and the relative position of the curves in Fig. 3.20.

Various theories have been put forward describing the major factors involved in the process of probe indentation. Among others the theory by Durgunoglu and Mitchell (1975) was chosen because it seemed the most complete and recent developed. It is based on assumption of soil failing in a brittle way and therefore only applicable to dense soil. According to this theory cone index is given for a pure frictional soil by the following bearing capacity equation:

$$CI = \gamma d \; N_{\gamma q} \; \zeta_{\gamma q} \qquad (7)$$

where:

- CI - Cone index (kN/m^2),
- γ - Soil dry bulk density (kN/m^3),
- d - Cone diameter (m),
- $N_{\gamma q}$ - Bearing capacity factor for surcharge and friction,
- $\zeta_{\gamma q}$ - Probe shape factor for surcharge and friction.

The bearing capacity factor is a complex equation of several dimensionless parameters as follows:

$$N_q = f(\phi, \Psi, \delta, m, \beta, \lambda, \theta_o) \qquad (8)$$

where:

- ϕ - Mobilized angle of internal friction,
- δ - Soil-metal angle of friction
- m - Normalized depth (depth of penetration over cone base diameter),

and the remaining parameters as in Fig. 4.10.

The variables in equation 8 are not independent, in fact:

$$\lambda = f_1 (\delta, \phi)$$
$$\beta = f_2 (m, \phi, \Psi, \delta)$$
$$\theta_o = f_3 (\quad " \quad) \quad ,$$

so in the end,

$$N_{\gamma q} = f' (m, \phi, \Psi, \delta) \qquad (9)$$

The above equation was solved for the following values and the results are presented in Fig. 4.11.a

Ψ = 75 degrees
δ = ϕ/2 (dry sand smooth metal surface)
ϕ = 30, 40, 44, 48 degrees
m = 2.47, 4.93, 7.40, respectively
50, 100, 150mm of depth using a 20.3 diameter cone.

Figure 4.11a is valid within the range of values of ϕ and m shown above, for a circular base cone with a 30 degrees apex angle in pure frictional soil, assuming a soil-metal friction angle equal to half the soil angle of internal friction.

Figure 4.11b shows the computed values of cone shape factor which are valid for a circular base cone within the values of angle of friction and normalized depth presented.

Finally Fig. 4.12 shows the combination of the above two dimensionless parameters giving the dimensionless factor of equation 7. They are valid for the conditions stated for Fig. 4.11b.

Using equation 7, the values for the dimensionless factor $N_{\gamma q}\,\zeta_{\gamma q}$ were obtained from the experimental values (Table 4.2) of cone index at 150mm (π = 7.4), 100mm (π = 4.93) and at 50mm (π = 2.47). Subsequently, using Fig. 4.12b the dimensionless factor was translated into the correspondent angle of internal friction which in turn was plotted in Fig. 4.13 over the experimental values obtained in direct shear (Figs. 3.16 to 3.19). The results are closer to the values of the a.i.f. obtained in direct shear at low confining pressure. That may be regarded as a consequence of the relatively low earth pressure involved in shallow penetration.

Equation 7 also shows the relative importance of soil density and angle of friction in the resistance to penetration. As an example, Table 4.2 shows, for Leighton Buzzard sand, from Test No. 1 (very loose) to Test No. 10 (very dense), a variation in density by a factor of 1.15, whereas the factor for the variation in cone index, at 150mm depth, is above 20. This large variation may therefore be regarded as primarily the result of the ϕ dependent dimensionless factor $N_{\gamma q}\,\zeta_{\gamma q}$.

As pointed out in section 3.6 the range of densities from minimum to maximum is not the same for every sand. In the four sands tested the lowest and the highest densities were respectively 11.3 and 19.79 kN/m^3. This variation is still small compared with the very wide range of values taken by the dimensionless factor shown in Fig. 4.12. It follows, that it should be possible to relate the angle of internal friction with cone resistance quite independently on the soil type. An example is shown in Fig. 4.14, where values of the angle of internal friction obtained in direct shear (Table 3.2) were related to the correspondent values of soil resistance gradient using Fig. 4.8. At each confining pressure the correlation seems to be good; the separation according to values of confining pressure is due to the fact that in the shear box ϕ is dependent on the applied confining pressure, whereas in cone penetration at shallow depth the value of G is dependent on a constant value of ϕ, similar to the one found at low confining pressure in the shear box.

The relative distance of the curves in Fig. 4.14 suggests, that at high confining pressures, the relation ϕ; G should not be much affected by σ itself.

4.4 Conclusions

1) The cone penetrometer may be used to measure soil in-situ density. However that requires a soil sample to be collected and the time consuming process of cone calibration. In dry sand this means a sample of about 760N (170lb) that has to be processed uniformly into a cylindrical mold to produce at least three different densities. By doing at least three cone tests at each density charts can be drawn relating cone resistance to density.

2) It is possible that the relation $D_d = a_1 \log G + a_2$ may be proved of practical interest, since the tests required for the evaluation of the constants a_1 and a_2 are straight forward routine tests which can be done quickly and with much less soil involved.

   At the moment still more experimentation is required to assess the usefulness of the above relation.

3) Modern theories for cone indentation correctly relate cone resistance to shallow penetration of sand to the angle of internal friction mobilized, under low confining pressure, at the particular soil density. They also show the stronger role of friction angle, relative to soil density, on the effect on cone resistance.

4) There is some indication that cone resistance and the angle of friction at a particular confining pressure (e.g. measured in direct shear) can be correlated within a narrow band, even for widely different sands. Furthermore the correlation may even become independent on the pressure itself for angles of friction at high confining pressures.

5 WHEEL TESTING PROGRAMME

W.E.S. have performed a very large number of experiments on a very wide range of tyres. What, therefore, can be the aim of carrying out yet more tests with much more limited apparatus? There are several reasons.

First, to repair the great weakness of the W.E.S. programme, and to test on a variety of sands. In the light of the previous chapters it is clear that an ideal programme would use the following sands:

a) Yuma, to link up the two sets of results and expose any errors of technique either in W.E.S. or Newcastle.

b) Leighton Buzzard sand, because with its large rounded particles, and narrow range of particle sizes it is an extreme sand type.

c) Solway sand, because of its opposite characteristics of very small sharp particles and wider range of particles.

d) Cresswell sand, because of its variety of particle shapes due to a large shell content, probably responsible for its low angle of friction.

e) Mix B, because of its very wide range of particle sizes. (Probably not found naturally)

In practice in the time available work had to be limited to Cresswell and Leighton Buzzard. It is hoped to continue the experiments in Newcastle using Solway sand.

The tests used a single tyre size because of the limits of time, but different loads and inflation pressures because it had been found (Chapter 3) that the shearing strength of sand varied significantly with normal pressure.

The strength of the sand in the rut and the performance of the tyre on the second and third pass were investigated to see if the processes involved were of the brittle and dilating or soft and compressing types. It was desired to do tests at the widest posssible range of soil density; tests were conducted at the extreme values of density possible to process in the tank and at a density somewhere inbetween.

5.1 Apparatus and experimental techniques

The general experimental scheme is shown in Fig. 5.1 in the form of a block diagram. The final results are the combination of four separate sets of experiments:

1) The cone penetrometer resistance gradient is obtained as a function of soil density in carefully prepared molds containing soil in a uniform state.

2) Soil density is converted to specific volume.

3) The cone resistance gradient is obtained at several points along the soil tank for each experiment, giving the average specific volume in the tank.

4) Drawbar pull, torque and sinkage at 20% slip are measured at various wheel loads in tanks of soil prepared in such a way as to give a wide range of densities.

Steps 1 and 2 were discussed in previous chapters, respectively sections 4.1 and 3.7 and led to the results shown in Figures 4.5 to 4.8.

The information given herein deals with steps 3 and 4 i.e., the apparatus and experimental techniques for in-tank cone and wheel tests.

The tests were conducted using the single wheel tester and the general purpose soil-machine research facilities in the Soil Mechanics Laboratory of the Department of Agricultural Engineering, University of Newcastle upon Tyne. Fig. 5.2 presents a line diagram of the Newcastle wheel tester and Fig. 5.3 a general view of the set up. The wheel is driven by a variable speed D.C. motor and suspended from a carriage which can itself be hauled at any chosen speed by another D.C. motor driven winch. Detailed information concerning the wheel tester and the basic layout of the carriage-winch arrangements may be found respectively in Riley (1968) and Hettiaratchi (1968). A minor alteration to the circuit controlling the winch motor was introduced (Peca 1979), so that after fixing a wheel turning speed the carriage speed slows down as it moves along the tank making it possible to carry out a test over a range from say 100% skid to 100% slip in one pass down the tank. Alternatively steady runs can be made at a fixed slip. The winch and transmission driving the carriage were recently modernized and upgraded.

Drawbar pull, input torque, forward speed, rotational speed and sinkage are all measured by electric transducers and recorded on U.V. recorder. The wheel is loaded with a fixed deadweight and is free to move up and down on a sealed recirculating ball low friction slide.

As referred before, Cresswell sand, from Druridge Bay on the Northeast coast of England and Leighton Buzzard sand, a clean, sieved, course sand were used in this study. Detailed information on the physical and mechanical analysis of these two sand may be found in Table 3.1 and Figures 3.13, 3.16 and 3.17. Cresswell sand was used in air-dry and water saturated conditions; Leighton Buzzard was only used in air-dry conditions.

In the present work only tests in air-dry sand are presented and discussed. The special techniques required when testing in submerged sand may be found in Peca and Reece (1981).

The soil tanks used measured 6m long by .76m wide with about .3m depth of sand in them. Each experiment therefore involved the processing of about 2.2 tonnes (22kN) of sand, hopefully to produce a uniform bed of sand along the tank. A variety of soil processing methods were tried in the first sand to be tested (Cresswell sand in June 1980) always with the objective of obtaining similar cone traces to those obtained in the mold (Fig. 4.2). Fig. 5.4 shows schematicaly the soil processing methods used. Basic operations are digging the soil, raking and levelling. Following the above routine, various methods of soil compaction were tried like pushing of a spade vertically right to the bottom of the tank at very close centres. Also two types of vibratory soil compactors were used. Included in Fig. 5.4 are the range of relative density measured by the cone penetrometer. The techniques of in-tank soil processing were improved for the second programme of wheel tests (January 1982) providing a better uniformity of the results and easier processing. Fig. 5.5 summarizes the techniques and gives parameters used in the carriage and vibrator control set up.

A minimum of five equally spaced cone penetrometer tests were done along the central line of the tank prior to each wheel test. The experimental set up used was the same as for the tests in the mold, with the frame supporting the hydraulic ram clamped over the wheel tester. In the multipass experiments in Leighton Buzzard sand, cone tests were performed prior to each pass. A sample of in-tank cone traces are shown in Figs. 5.6 to 5.8 showing the results of tests after each wheel pass.

The main series of tests were conducted using a 6 x 16.00 - 2PR tractor tyre from which the tread had been removed, outside diameter 644mm, section with 145mm and section height 96mm. The tests were performed at various combination of loads and inflation pressures chosen to give a deflection of 30% of the carcass height on an unyielding surface. All dimensions and deflection were measured according to I.S.T.V.S. standards, Meyer (1977).

A tyre with the tread still on it was used to compare results of varying slip tests with results from fixed slip tests in air-dry Cresswell sand. Fig. 5.9 shows part of a test in which the slip was increased from -32% to 41%. The shape of the curves presented are in agreement with results obtained by W.E.S., showing a maximum value of pull and tractive efficiency around 20% slip. Also shown are the results of tests at fixed slip under the same conditions, producing lower values of drawbar pull, tractive efficiency and consistently higher values of sinkage than the corresponding values interpolated from the curves. This is because of the rate of slip increase that has to be imposed to range from skid to high slip along 4mm of tank, is too high.Insufficient travel at any slip is available to permit the wheel to attain its equilibrium sinkage at that slip. For this reason it was decided to perform all the tests at fixed 20% slip using the following routine:

1) After the sand has been processed and cone measurements taken, the wheel tester is lowered onto the soil until the tyre is entirely supported by it. Initial static sinkage and on-soil static carcass deflection are measured according to the procedure shown in Fig. 5.10a.

2) The U.V. recorder is switched on to produce a zero trace of pull, torque, initial sinkage, wheel and carriage speeds.

3) The pre-set controls of the carriage and wheel motor are switched on simultaneously.

4) The test is performed along the entire length of the tank, allowing the wheel to attain its steady value of sinkage. Pictures and slides are taken of relevant features.

In the case of multipass tests the above four steps were repeated in the rut of the previous pass after the cone measurements were taken.

Figure 5.10b shows a typical output trace from the wheel tester as recorded by the U.V. recorder. It enables the calculation of an average value of drawbar pull, torque and on-the-run sinkage which added to the initial sinkage gives the total sinkage. From the basic three quantities, drawbar pull, torque and total sinkage as well as soil and wheel parameters (Fig. 5.11), the following data concerning the energy involved in the wheel movement may also be computed:

1) Tractive efficiency - η

$$\eta = \frac{\text{Power output}}{\text{Power input}} = \frac{DP \times V_a}{T \times \omega} \quad ,$$

and taking into account the definition of slip

$$i = \frac{\omega r_r - V_a}{\omega r_r} \quad , \text{ it follows}$$

$$\eta = \frac{DP \times r_r (1 - i)}{T} \quad ,$$

where the rolling radius, r_r, is defined according to the I.S.T.V.S. standards (Meyer 1977) as the distance travelled on a rigid surface by the wheel in one complete revolution divided by 2π. Although not explicit in the standards it is assumed that the wheel is towed free rolling.

2) Power number, PN

Power input = Power output + power losses

$$T\omega = DP \times V_a + \frac{E_s}{t} \quad ,$$

being E_s the energy lost in soil and tyre deformation in time t. PN is defined by Melzer (1976) as the energy supplied at the wheel axle per unit of vertical load, per unit of distance travelled by the wheel:

$$PN = \frac{T\omega}{WV_a} = \frac{DP}{W} + \frac{E_s}{WV_a t} = \frac{T}{Wr_r (1-i)}$$

or

$$PN = \frac{DP}{W} + \frac{\varepsilon_s}{W} \quad ,$$

where ε_s is the energy consumed in soil and tyre deformation per unit of distance travelled by the wheel. In soft soil, ε_s is basically the energy wasted in soil deformation per unit length of rut.

5.2 Results from single wheel tests

Tables 5.1 and 5.2 present the bulk of information obtained from the single wheel tests. Figures 5.12 to 5.16 show the results compared with those obtained by WES in Yuma and Mortar sands, both against the original WES sand number N_s, and Turnage's sand number N_{se}. Each point is shown as a bar due to the range in values of G found for several tests along the tank. There was negligible variation in DP in each test.

Figures 5.17 to 5.20 show in the same plot the performance of the 6 x 16 tyre in Leighton Buzzard and Cresswell sand against the sand relative density.

The results in Figs. 5.12 to 5.14 add further proof of the inadequacy of the sand number N_s in correlating traction performance in different sands. The process of normalization to Yuma sand proposed by Patin (1971) to make the results collapse in a single curve is also proved to be unacceptable, since it is based on the hypothesis that the same traction performance is obtained in dry-sands at the same relative density no matter how different the sands may be. The results in Cresswell and Leighton Buzzard sand, Figs. 5.17 to 5.20, do not confirm such an assumption. Under the same combination of tyre load and inflation pressure, Cresswell sand, relative to Leighton Buzzard sand at the same relative density, consistently sustains a lower coefficient of traction, allows deeper sinkage and consequently lower tractive efficiency. Cresswell sand is a worse media for traction. These results cannot come entirely as a surprise, after all, as revealed by Fig. 3.20, Cresswell sand is a worse media for transmitting power by friction, at a given relative density.

The process of normalization to Yuma sand (or to any sand for that matter) being incorrect, there is not much hope of success for Turnage's method, as shown in Fig. 5.15 and 5.16.

6 CHANGES IN SAND STRENGTH DUE TO WHEEL TRAFFIC - MULTIPASS WHEEL PERFORMANCE

The set of figures 6.1 to 6.9 show the results of probing soil strength after each of the three passes in the same rut, compared with the initial soil strength.

Figures 6.10 to 6.12 show the actual performance parameters obtained for each pass. Sinkage data was measured both relative to the free soil surface and relative to the rut surface of the previous pass.

Tables 6.1 to 6.3 show relevant data concerning the multipass tests carried out, respectively on very dense, medium dense and very loose Leighton Buzzard sand.

On very dense Leighton Buzzard sand it was found that wheel traffic causes soil dilation. The soil strength measured in the rut was revealed to be quite unaffected by the combination of load carried by the wheel and inflation pressure; neither did it change appreciably after the second and third subsequent wheel passes. As a result the substantial changes in performance were observed between the first and second pass. The third pass showed performance similar to the second pass.

On medium dense sand soil dilation was always present during the first pass. Neither the soil strength nor the depth of the dilated zone seemed to be influenced by the combinations of vertical load and inflation pressure used. A second pass in the same rut made the soil denser, mainly under the larger vertical load, resulting in a better traction performance on the third pass.

On very loose sand the results of traffic are deep ruts with a slight soil compaction. This was observed for all the loads and inflation pressures used. The compaction is only noticeable by comparison of the cone penetrometer traces; it is so small that it cannot be felt by probing manually using a welding rod.

In loose sand the comparison between cone traces pre and post-traffic, respectively relative to the free soil surface and to the rut surface require some judgement; there is now a large surcharge on the rut level leading itself to an increase in penetration resistance which could be interpreted as soil compaction. In a situation of a rut with depth z_r, it is assumed that there is soil compaction whenever the value of cone force at depth z below the rut surface is greater than the pre-traffic cone force at a depth $z + z_r$ below the soil free surface, and quantified by expressing the difference, in percentage, between those two values.

Subsequent passes in the same rut do not alter substantially the depth of the rut neither do they appear to increase compaction at the rut surface, though towards the deeper layers there is some compaction as shown in the following table:

Test	LB6 (W=2002N)	LB3 (W=1413N)	LB9 (W=864N)
Depth below rut level (cm)	Difference, in percentage, between cone force after 3rd pass and after 1st pass		
5	-4.4	2.9	15.7
10	21.0	28.0	27.6
15	37.3	44.1	40.9

There is an improvement in performance after the first pass both in terms of coefficient of traction and tractive efficiency, although the value of power number (PN) remained quite unaffected.

Figure 6.13 replots the information obtained in multipass tests in an attempt to make clear that in dry sand, despite adjusting inflation pressure to maintain a maximum practicable deflection, the effect of increasing weight on the tyre is to decrease the absolute value of tractive effort obtained, with the exception of the tests performed in conditions of very dense sand; the efficiency goes down accordingly. This, of course, applies to a given tyre size; if absolute traction is to be increased then both tyre size and load have to be increased. In Fig. 6.13a the result for W = 1413N, at the first pass, was obtained from interpolation in Figs. 5.17 and 5.18, instead of using the result from the actual test, which was performed on a slightly looser sand than the one used in the tests with the other two loads.

It is apparent from multipass tests in Leighton Buzzard sand that soil resistance to cone penetration after the first pass is primarily influenced by the soil initial density. For each initial density the combinations of vertical load and inflation pressure used seem to have a minor effect. This gives support to what is apparent from Turnage's method (Fig. 1.7): for a given tyre the change in soil density due to traffic is only dependent on the pre-traffic density. However, the present results contest the generality of Fig. 1.7b; according to this figure, for a tyre shape factor b/d = 0.225 (6.00 - 16 tyre), soil dilation due to wheel traffic is present for values of initial relative density greater than 75% and soil compaction for values below 75%. The results in Leighton Buzzard sand show that for values of D_d as low as 10% the compaction is very small and show definite soil dilation above 60% relative density.

7 DISCUSSION

7.1 Relevant soil properties

From the point of view of soil mechanics, the passage of wheels on sand is usually a dilating process and the relevant properties are the sand's internal friction and its density. The measurement of the in-situ density of a 150mm thick layer at the surface can at present be best achieved by an in-situ cone test followed by a calibration of cone gradient against density in a fairly large sample. The relation obtained $\gamma = f(G)$ is particular to any given sand.

The measurement of the angle of internal friction can be done by a series of standard tests, e.g. the direct shear test, at various pressures over a wide range of specific volumes. The relation obtained $\phi = f(\gamma,\sigma)$ is again particular to any given sand as is shown for example in Fig. 7.1

The combination of the previous two relations yields $\phi = f(G,\sigma)$. This relation is the same for Leighton Buzzard, Cresswell, Solway and Mix B and is shown in Fig. 4.14. This common relationship is surprising, and it is likely that different relations are obtained for most sands, i.e. the state of packing of two different sands may be such that they produce the same value of G, although they do not have the same value of ϕ when sheared under equal confining pressure. An example of different behaviour is given by Plantema (1957).

The influence of confining pressure, σ, on ϕ means that it is necessary to determine the appropriate pressure at which the sand is sheared beneath the wheel. At shallow depths below the wheel this depends on the vertical load applied to the wheel axle, tyre pressure, carcass stiffness and tyre size. The problem is even more complex due to the change in the relative importance of the above factors with the strength of the sand. There are two ways of taking this effect of pressure into account. One is to correct the value of G to correspond to the value of ϕ expected under the particular contact pressure, instead of the in-situ measured G which is based on ϕ at very low confining pressure. This approach could be easy to apply to a stiff track where the contact pressure is the load divided by the contact area, but rather difficult for tyres and wheels.

The other way to take the effect of pressure into account is to appreciate that a numeric in which the soil strength is represented by a single value of G appropriate to low pressure cannot possibly produce a single curve, i.e. to accept that the results will be represented by a family of curves separated by a suitable parameter which represents contact pressure in an empirical way. It will be shown later how this can be achieved.

The two relations $\gamma = f(G)$ and $\phi = f(G)$, after taking account of σ in the way just described, suggest that, for a quick prediction, the two relevant soil parameters γ and ϕ may be replaced by the cone resistance gradient, G, for which it is only required to register the force-depth diagram of a cone being pushed into the soil. It carries, however, the disadvantage of restricting the relation to each particular sand. This is what WES experienced in Yuma and Mortar sand, and example of which is shown in Fig. 7.2.

In some cases the performance may be similar in different sands at the same G. This is what Newcastle experienced in Leighton Buzzard and Cresswell sands, Fig. 7.3; this is because in these two particular sands G happens to correspond to similar values of ϕ in both sands (Fig. 4.14) and although it does not define the same values of γ, the differences here are too small to influence the overall result.

At the present it seems that to keep the cone based traction predicting system in dry sand as a practical proposition, the soil strength should be defined by G, accepting that this leads generally to a separation of results according to the sand type; at the same time effort should be placed on the identification of which property or combination of properties are affecting the separation. At least in the beginning this may be accomplished by studying the relations $\gamma = f(G)$ and $\phi = f(G)$. Relations like $\cot\phi = c_1 - c_2 \times D_d$, presented in section 3.2, and $D_d = a_1 \times \log G + a_2$, presented in section 4.2, suggest that this objective can be achieved and above all the key properties, may be relatively easy to measure, e.g. sand mean grain size and compactability.

The idea that two different sands may sustain the same traction performance at the same value of relative density, everything else the same, is the basis of the process of "normalization to Yuma sands", introduced by Patin (1971). Although supported by some evidence by WES, as in Fig. 7.4, it cannot be generally accepted since at the same value of relative density neither γ nor ϕ are generally the same for different sands, as it was shown in Fig. 3.20. In particular, at the same value of D_d, the values of and ϕ are higher for Leighton Buzzard than for Cresswell sand leading to the conclusion that, at the same D_d, traction is the better in Leighton Buzzard sand, as indeed it was proved by Fig. 5.17.

7.2 The effect of vertical load and inflation pressure

Using G to define the sand strength, WES published a large number of tests performed in Yuma sand with a wide variety of tyres. Some results with a 9.00 - 14, 2PR tyre are shown in Fig. 7.5 plotted as a relation $\frac{DP}{W} = f(G)$.

It can be seen that there is a pronounced separation according to values of pressure and vertical load. When plotting these tests as a relation $\frac{DP}{W} = f(\frac{G}{W})$, Fig. 7.6, the separation becomes more clear insofaras the combinations of W and i.p. which give a particular value of deflection, δ, on an unyielding surface are clustered along a well defined curve. To emphasize the separation accourding to δ, or δ/h as WES choose to represent, the results for two rigid wheels were also included.

WES attempted to overcome the separation by plotting the results as a relation $\frac{DP}{W} = f(\frac{G}{W} \times \frac{\delta}{h})$, shown in Fig. 7.7. It worked well for the values of δ/h from 15 to 35, indeed very representative values of deflection, however one should expect that as the tyre is made stiffer by over-inflating (lower values of δ/h, in the limit a rigid wheel $\delta/h = 0$) the relation $\frac{DP}{W} = f(\frac{G}{W} \times \frac{\delta}{h})$ is no longer able to collapse the δ/h curves into a single one. This also brings up the suspicion that if the tyre is made stiffer by increasing the number of ply-rating, then the relation may also become unable to collapse into a single curve all the curves for various values of δ/h, even within the range 15% to 35%. This is what seems to be suggested by Figs. 7.8 and 1.6, plotted using WES data.

Unfortunately it is not only highly inflated tyres or stiff tyres that condemn a sand number of the form $\frac{G}{W} \times \frac{\delta}{h}$; using data published by Turnage (1972b) it is possible to trace the pressure-load curves for some of the tyres tested, and then to superpose on the diagram curves for equal-values

of $\frac{\delta/h}{W}$. These are shown in Figs. 7.9 and 7.10, where it can be seen, that for any given tyre, the ratio is a function of i.p. and W, as expected; however in some instances the effect of load, W, becomes quite negligible, leaving $\frac{\delta/h}{W}$ mainly influenced by i.p. This means that in certain instances the effect of load on the sand number, N_s, is represented by the inflation pressure alone. As a consequence, during a wheel test, if the axle load is increased by ΔW this should not contribute to any substantial change in the sand number. Should the same be expected concerning the traction performance? In the situation of a low pressure, very flexible pneumatic tyre operating on dense sand, it is reasonable to expect that ΔW will change the tyre deflection, with minor increase in the contact pressure on the soil surface. As a consequence no substantial change in the coefficient of traction, or on sinkage-diameter ratio are to be expected, with the tractive efficiency around its maximum value. The following examples illustrating this, and subsequent points, were obtained from Turnage (1972b).

9.00 - 14 - 2PR tyre on Yuma sand (low pressure/dense sand)

i.p. (psi)	W (N)	D_d (%)	DP/W	PN	z/d	η	N_S
7.5	1010	92.5	0.449	0.586	0.029	76.6	32.3
7.2	1922	89.2	0.465	0.629	0.027	73.9	25.5

i.e. a 90% increment in the vertical load results in a 97% increment in drawbar pull and virtually the same sinkage and efficiency.

For stiffer tyres and/or on looser soil conditions it is reasonable to think that the adjustment required to accommodate an increasing load is made by increasing deformation in the soil. In the limit a highly inflated tyre in loose sand behaves as a rigid wheel whose shape does not change as the load changes. Increasing soil deformation leads to a significant increase in losses. The following sequence of examples show clearly these facts:

31 x 15.50 - 13 - 4PR tyre on Yuma sand (low pressure/loose sand)

i.p. (psi)	W (N)	D_d (%)	DP/W	PN	z/d	η	N_S
6	3840	47	0.206	0.509	0.073	40.5	8.7
7	5923	47	0.188	0.52	0.079	36.2	8.0

i.e. a 54% increment in the vertical load results in a 41% increment in DP for slightly higher sinkage and slightly lower efficiency.

16 x 6.50 - 8 - 2PR in Yuma sand (high pressure/dense sand)

i.p. (psi)	W (N)	D_d (%)	DP/W	PN	z/d	η	N_S
30.8	1496	82	0.075	0.4613	0.126	16.3	4.8
30.8	2910	83	-0.032	0.476	0.15	<0	4.2

i.e. a 96% increment in vertical load leads to a complete deterioration in performance.

4.00 - 20 - 2PR tyre on Yuma sand (high pressure/medium dense sand)

i.p. (psi)	W (N)	D_d (%)	DP/W	PN	z/d	η	N_s
21.5	877	59	0.137	0.536	0.092	25.6	4.43
20	2680	61	-0.038	0.538	0.203	<0	3.59

i.e. a 200% increase in vertical load leads to a complete deterioration in the performance.

The last two examples show clearly that large differences in performance are not related with the sand number N_s, simply because the factor $\frac{\delta/h}{W}$ is primarily influenced by tyre pressure.

7.3 The effect of tyre size

By including the factor $(bd)^{3/2}$ in the sand number, WES attempted to reduce the results obtained with a wide variety of tyre dimensions to a single curve. That is shown in Fig. 7.11 for Yuma sand.

In view of the above comments concerning the factor δ/h in the sand number, it seems a better idea to restrict the number to $\frac{G(bd)^{3/2}}{W}$ and accept the separation of the results according to tyre deflection. This is shown in Fig. 7.12 for all the results published by WES in Yuma sand with different tyres at three values of δ/h, 35%, 25% and 15%, as well as for three rigid steel wheels. For the sake of clarity a series of figures, 7.13 to 7.16, show separately the results for each value of deflection. In particular the last figure reveals that the number $\frac{G(bd)^{3/2}}{W}$ is unable to collapse results for rigid wheels. This is of crucial importance since in many situations pneumatic wheels operating on loose sands are effectively behaving like rigid wheels.

7.4 An alternative way

The correlation can be improved just by modifying the sand number to $\frac{Gbd^2}{W}$ as shown in Fig. 7.17. This new number was applied to all the results as shown in Figs. 7.18 to 7.20, and finally presented in a single plot in Fig. 7.21. To emphasize the importance of the number $\frac{Gbd^2}{W}$, Fig. 7.21 was replotted as Fig. 7.22, in which the tests carried out at tyre pressures greater than 30 psi are represented by the same symbol used for rigid wheels. The result is a set of curved bands of points, a band for each value of δ/h. These bands of points have two common features: towards lower values of the sand number they become tangent to the same curve; towards higher values of the sand number they tend to a similar maximum value of $\frac{DP}{W}$.

The first of these features is a consequence of the fact that towards looser packings, there is a density at which the soil is so loose that it does not provide enough support to deflect the tyre. Therefore, from this stage onwards the tyre is effectively a rigid wheel, whatever was the value of deflection on hard ground, δ/h. The common tangent band is the curve for $\delta/h = 0$ which can be easily obtained by a set of tests with rigid wheels of different sizes.

The second of these features arises from the fact that the maximum coefficient of traction is developed at conditions of very dense sand and low tyre-soil contact pressure, when sinkage is small. In this situation the sand is sheared on a horizontal plane, and the strength developed is mainly a function of the shear-displacement characteristics of the sand and also dependent on the dimensions of the contact surface, mainly on its length. Either for a large diameter tyre, even at low deflection, δ/h, or for a smaller, but deflected tyre, the length of the contact surface may be sufficiently large to bring the value of $\frac{DP}{W}$ close to its maximum, possibly $\frac{DP}{W} = \tan \phi_{cv}$.

Figures 7.23 and 7.24 show respectively all the tests published by WES in Mortar sand, and all the tests performed at Newcastle University, against the number $\frac{Gbd^2}{W}$.

A further improvement to the WES system would be to get rid of the h on the δ/h ratio. It is very difficult to see that h can have anything to do with what the soil experiences as the wheel rolls over it. It arose because in the beginning tyres were toroidal with h = b and it was the way in which tyre manufacturers expressed the maximum deflection that the tyre could tolerate before experiencing fatigue failure of the carcass. This becomes less and less acceptable as tyres tend towards even lower aspect ratios. Time has not permitted an investigaton of this point, but an obvious alternative to be examined is δ/d (Appendix 2).

7.5 Summary

It has been proposed that considerable advantages are to be gained by using the numeric $N_s = \frac{Gbd^2}{W}$ and plotting separate curves for δ/h = 0; .15; .25; .35. These advantages are:

1) Rigid wheel results can be included.

2) Better predictions can be obtained because each band is much narrower.

3) The separate effects of load and inflation pressure are both taken into account in a proper way.

4) The soil mechanics of sand, which shows that strength is a function of both density and normal pressure is taken account of in an empirical way.

5) The WES results mainly consist of tests on dense sands; if more tests had been carried out on loose sands the above advantages would have become even clearer.

The new numeric does not eliminate the large differences between performance in Yuma and Leighton Buzzard and Cresswell sands. This is due either to some consistent errors in either Newcastle or WES or, perhaps, to a considerable difference in the relationships $\phi = f(G)$ between Yuma and the sands used in Newcastle. This should be the main topic of future research.

8 CONCLUSIONS

1) From the point of view of soil mechanics the passage of wheels on dry or submerged sand is usually a dilating process. So, however disappointing, the mathematical model for the plastically deforming, compacting behaviour of soil described by Critical State Soil Mechanics does not seem of much use to the present work.

2) For traction on sands the scope of the relevant soil mechanics is reduced to the question of the way the angle of internal friction varies with specific volume and the range of specific volume available to any particular sand.

3) The angle of internal friction for any sand is dependent on the specific volume, confining pressure and on the apparatus used. It increases with decreasing specific volume and for a constant specific volume it increases with decreasing confining pressure.

4) The angle of internal friction may be separated into two different components: $\emptyset_{cv}$, when soil is deforming at constant volume (critical state), and $\emptyset_{dil}$ expressing the energy lost in the dilation process against the confining pressure applied by the apparatus.

5) $\emptyset_{cv}$, for dry sand, is only dependent on the particle size distribution, particle shape, size and mineralogy of the sand.

6) The state of the art based on observations of triaxial compression tests, show that, for each mineralogy, the main factor influencing $\emptyset_{cv}$ is the shape of the particles, possibly associated with size in natural sands (fine with angular and coarse with rounded). The limits seem to be: at one end, form glass beads to subrounded Ottawa sand, $\emptyset_{cv}$ varies from 24 to 30 degrees; on the other end, from crushed quartz stones to crushed glass $\emptyset_{cv}$ varies from 38 to 43 degrees.

7) The value of $\emptyset_{dil}$ depends on the specific volume and confining pressure, increasing with decreasing specific volume and decreasing confining pressing. The maximum value of $\emptyset_{dil}$, max $\emptyset_{dil}$, according to the Rowe-Horne stress dilatancy theory, is about 9 to 10 degrees, and this was experimentally confirmed by triaxial tests in sands as well as glass beads and crushed glass. In contrast, and from a different source, it was possible to deduce that there is a correlation between max $\emptyset_{dil}$ and soil compactability with the experimental values of max $\emptyset_{dil}$ increasing linearly from 8 to 18 degrees when compactability increases from 35 to 90%.

8) Direct shear tests in four sands, by the author, produced, in some instances, results contradicting the trends from triaxial tests described in conclusions 6 and 7; for instance higher values of the angle of friction were consistently found in a coarse sand with smooth rounded grains and low compactability, than in a fine sand with sharp angular grains and high compactability. Nevertheless the results are consistent with the effect of dilation, since the coarse sand dilated more than the fine sand against the same normal pressure.

9) Soil compactability depends on the combination of size and shape, increasing from coarse rounded grains to fine angular grains. However the main factor influencing compactability is the particle size distribution, increasing for less uniform sands.

10) For a given mineralogy the range of densities a sand can take depends on its grain features. Two extreme examples are Solway sand with densities varying from 11.3 to 15.6 kN/m^3 and Mix B sand with densities varying from 14.9 to 19.8 kN/m^3. The extremes seem to be: for lower densities, fine, angular and uniform sand; for higher densities, coarse rounded and less uniform sand.

11) At the same value of relative density neither γ nor ϕ are generally the same for different sands.

12) Cone resistance gradient in sand is a function of the bulk density and mainly of the angle of internal friction. As a consequence of conclusion 11, cone resistance gradient, G, is not generally the same for different sands at the same value of relative density.

13) As a consequence of the previous conclusion, if G is correlated with γ or ϕ separately, then the results are not the same for different sands. For instance at a given value of G there is not just one value of γ for any sand, but several values of γ, according to the sand; this is due to the fact that for a particular value of γ, different sands have different values of ϕ.

    The same can be said if a correlation between G and ϕ is attempted separately of γ. However in this case the separation according to sand type may not be as pronounced as in the previous case due to the relatively modest contribution of γ in the relation $G = f(\gamma,\phi)$, and also to the fact that γ does not change very much from sand to sand (see concl. 10).

    The practical implication of this, is that if the cone penetrometer is to be used to measure the in-situ density or the in-situ angle of friction, then calibration of the cone to each individual sand is required first.

14) To use the cone penetrometer as a tool for measuring in-situ density, it requires a soil sample to be collected for the process of cone calibration. In dry sand this is a sample weighing about 760N (170lb) that has to be processed uniformly into a cylindrical mould to produce at least three different densities. By doing at least three cone tests at each density a chart can be drawn relating cone resistance gradient, G, to density, γ.

15) It is possible that the relation $D_d = a_1 \log G + a_2$ may be proved of practical interest, since the tests required for the evaluation of the constants a_1 and a_2 are straightforward routine tests which can be done quickly and with much less soil involved.

16) The process of cone calibration required if the cone is to be used as a tool for measureing the in-situ angle of friction, was already partially described in conclusion 14. This has to be complemented with a series of tests, e.g. direct shear tests, at various pressures over a wide range of specific volumes. The final result is a chart showing curves, one for each confining pressure, of $\phi = f(G)$.

17) If G is used to describe soil strength instead of γ and ϕ in the problem of wheel-sand interaction, then the relations describing traction performance are not generally the same for different sands.

The actual soil strength sensed by the tyre is also dependent on the tyre sand contact pressure, a factor not included in the cone-sand interaction. However, since tyre-sand contact pressure is unknown and itself dependent on the sand strength, it is not at present possible to correct G to take pressure into account. A possible exception is the situation of a stiff track on sand where the contact pressure can be reasonably predicted.

18) At the same relative density traction performance in two different sands is not generally the same; this is because in these conditions γ and ϕ are also not generally the same for different sands (conclusion 11).

19) The additional wheel test results in Cresswell an Leighton Buzzard sand confirm the fact that the WES system, in its original or recently developed form, does not adequately describe the performance of tyres in a range of sand types.

20) The original WES system, and indeed any other system in which sand strength is described by cone gradient, G, is not likely to give the same correlation for different sands.

21) Recent developments of the WES system made it more complex, probably acknowledging the fact that there is no easy solution to the problem due to the large number of independent variables involved. With the objective of improving the correlation for each sand and also of reducing the separation according to sand type, two main assumptions were put forward: first, the relevant soil strength is not the initial strength measured by the cone, but a soil strength somewhere in between the initial and the post-traffic value; a method was presented by which the value of the relevant soil strength can be predicted based on the initial value and tyre geometry. The second assumption is the normalization to Yuma sand, which itself is based on the proposition that two sands, however different, sustain the same traction at the same value of relative density.

The first asumption, however correct, is not promising insofaras it requires the knowledge of parameters resultant from the actual traffic situation to predict the traffic ability. The second assumption, as seen in conclusion 18, is generally incorrect.

Finally the use of $\tan\phi_{70}$ associated with the performance factor, e.g. $\eta\tan\phi_{70}$, is incorrect since in the limit the maximum value of tractive efficiency of a tyre at 20% slip is 0.8 and is independent of the media supporting taction.

22) Multipass tests at 20% slip on Leighton Buzzard sand showed that after the first pass the soil strength is primarily influenced by its original strength and only mildly affected by the combination of tyre load and inflation pressure. For instance after one pass on very dense sand the cone force at 10cm below the rut surface is 50% to 63% of the pre-traffic value, depending on the load (2002N and 864N respectively); similar conclusions for medium dense sand are 62% to

76%, and for very loose sand 148 to 120%. As a direct consequence of these soil changes, the second pass performance relative to the first pass performance will be reduced in the case of very dense and medium dense sand, and increased in the case of very loose sand. As an example, for a load W = 2002N, the 14 psi inflated 6.00 - 16 - 2PR tyre on Leighton Buzzard had its coefficient of traction reduced from 0.187 to 0.089 on very dense sand; 0.11 to 0.037 on medium dense sand, and increased from 0.01 to 0.037 on very loose sand.

For a single sand, a G based system could work and the very extensive original WES data has been reviewed in the light of the much more limited results obtained at Newcastle on Cresswell and Leighton Buzzard sand with the following results.

23) Inflation pressure and load have separate independent effects on wheel performance. Soft tyres on hard sand are most affected by inflation pressure; stiff tyres on soft sand are most influenced by load.

24) The ratio $\frac{\delta}{Wh}$ in the WES sand number, for some tyres represents inflation pressure almost entirely; it leaves out the effect of W. In order to consider both parameters, a more complex representation of the data is required. This can be done by replacing $\frac{\delta}{Wh}$ by $\frac{1}{W}$ and plotting separate curves for $\frac{\delta}{h}$.

25) The numeric $\frac{G(bd)^{3/2}}{W}$ does not reduce the WES data on rigid wheels to a narrow band of data. This is accomplished much better by $\frac{G\ bd}{W}$, without affecting very much the scatter for the tyre data.

26) If the coefficient of traction obtained from wheel tests on sand at 20%, are plotted against the sand number $\frac{Gbd^2}{W}$, the result is a set of curved bands of points, a band for each value of δ/h. These bands of points have two common features: towards high values of the sand number they tend to a similar maximum value of $\frac{DP}{W} = \tan\phi_{cv}$; towards low values of the sand number they become tangent to the curve for $\delta/h = 0$ (Rigid wheels).

27) The study of the effect of G in different sands may be done simply by testing rigid wheels.

28) The maximum possible coefficient of traction should be possible to predict by measuring $\tan\phi_{cv}$.

R E F E R E N C E S

Akroyd, T.N.W. - "Laboratory testing in soil engineering", Soil Mechanics Limited, 1969.

Atkinson, J.H.; Bransby, P.L. - "The mechanics of soils - An introduction to Critical State Soil Mechanics", McGraw-Hill Company, 1978.

Durgunoglu, H.T.; Mitchell, J.K. - "Static penetration resistance of soils: I - Analysis
II - Evaluation of theory and implications for practice". Proc. of the Conf. on In-situ Measurements of soil Properties, Vol. 1, A.S.C.E., 1975.

Dwyer, M.J.; Comely, D.R.; Evernden, D.W. - "Development of the N.I.A.E. handbook of agricultural tyre performance". Proc. of the 5th Conf. of I.S.T.V.S., 1975.

Freitag, D.R. - "A dimensional analysis of the performance of pneumatic tyres on clay". Journal of Terramechanics, Vol. 3, No. 3, 1966.

Freitag, D.R. - "Dimensional analysis of performance of pneumatic tyres on sand". Transactions of A.S.A.E., 1968.

Frossard, E. - "Effect of sand grain shape on interparticle friction; indirect measurements by Rowe's stress dilitancy theory". Géotechnique 29, No. 3, 1979.

Hettiaratchi, D.R.P. - "A general purpose soil-machine research facility". Journal of Terramechanics, Vol. 5, No. 4, 1968.

Hettiaratchi, D.R.P.; O'Callaghan, J.R. - "Mechanical behaviour of agricultural soils". J. Agric. Engng. Res., 25, 1980.

Holubec, I.; D'Appolonia, E. - "Effect of particle shape on the engineering properties of granular soils". Evaluation of Relative Density and its role in geotechnical projects involving cohensionless soils, A.S.T.M., STP 523, 1973.

Horne, M.R. - "The behaviour of an assembly of rotund, rigid, cohesionless particles". Part I and Part II. Proc. Roy. Soc. A 286, 1965.

Horne, M.R. - "The behavior of an assembly of rotund, rigid, cohesionless particles". Part III, Proc. Roy. Soc. A 310, 1969.

Howson, D.F. - "A recording Cone Penetrometer for measuring soil resistance". J. Agric. Engng. Res. 22, 1977.

Josselin De Jong, G. De - "Rowe's stress-dilatancy relation based on friction". Géotechnique 26, No. 3, 1976.

Kirkpatrick, W.M. - "Effects of grain size and grading on the shearing behaviour of granular materials". Proc. 6th Int. Conf. on Soil Mech. and Found. Engng., Vol. I, 1965.

Koerner, R.M. - "Behaviour of single mineral soils in triaxial shear". Proc. AM. Soc. Civil Eng., Soil Mech. Found. Div., SM 4, 1970 a.

Koerner, R.M. - "Effect of particle characteristics on soil strength". Proc. Am. Soc. Civil Eng., Soil Mech. Found. Div., SM 4, 1970 b.

R E F E R E N C E S (cont.)

Kolbuszewski, J.; Frederick, M.R. - The significance of particle shape and size on the mechanical behaviour of granular materials". Proc. Europ. Conf. on Soil Mech. and Found. Engng., Vol. I, 1963.

Kurtay, T.; Reece, A.R. - "Plasticity Theory and Critical State Soil Mechanics". J. Terramechanics, Vol. 7 Nos. 3 and 4, 1970.

Lee, K.L. et al - "Effect of moisture on the strength of clean sand". Proc. Am. Soc. Civil Eng., Soil Mech. Found. Div., SM 6, 1967.

Melzer, K-J. - "Measuring soil properties in vehicle mobility research". Report 4: Relative density and cone penetration resistance. Technical Report No. 3-652, Waterways Experiment Station, C.E. Vicksburg, Miss., 1971.

Melzer, K-J. - "Relative density - Three examples of its use in research and practice". Evaluation of Relative Density and its role in geotechnical projects involving cohesionless soils. A.S.T.M., STP 523, 1973.

Melzer, K-J. - "Power requirments for wheels operating in sand". J. of Terramechanics, Vol. 13, No. 2, 1976.

Meyer, M.P., et al - "International Society for Terrain-Vehicle Systems Standards". J. of Terramechanics, Vol. 14, No. 3, 1977.

Parikh, P.V. - "The shear behaviour of sand under axisymmetric loading". Ph.D. thesis, Manchester University, 1967.

Patin, T.R. - "Prediction of performance of rectangular cross-section tyres in sand." Paper No. 71-603, Winter Meeting of the A.S.A.E., Chigago, Ill., 1971.

Peca, J.O. - "The comparative performance of tyres and rigid wheels in clay". Unpublished M.Sc. thesis, University of Newcastle upon Tyne, U.K., 1979.

Peca, J.O.; Reece, A.R. - "Tyre performance on submerged sand". Proc. 7th I.S.T.V.S. Conf., Vol. II, 1981.

Pettijohn, F.J. et al - "Sand and Sandstones". Springer-Verlag, Berlin, 1972.

Plantema, G. - "Influence of density on sounding results in dry, moist and saturated sands". Proc. 4th Int. Conf. Soil Mech. and Found. Engng., Vol. I, 1957.

Procter, D.C.; Barton, R.R. - "Measurements of the angle of interparticle friction". Géotechnique 24, No. 4, 1974.

Reece, A.R. - "Machines and soil". J. Terramechanics, Vol. 6, No. 3, 1969.

Reece, A.R. - "Soil Mechanics and Agricultural Soils", Soil Science, Vol. 123, No. 5, 1977.

Reece, A.R.; Peca, J.O. - "An assessment of the value of the cone penetrometer in mobility prediction. Proc. 7th I.S.T.V.S. Int. Conf., Vol. III (appendix), 1981.

R E F E R E N C E S (cont.)

Riley, J.G. - "The design of single-wheel tester". Unpublished M.Sc thesis, Univeristy of Newcastle upon Tyne, 1968.

Rowe, P.W. - "The Stress-dilatancy relation for static equilibrium of an assembly of particles in contact". Proc. Roy. Soc. A 269, 1962.

Rowe, P.W. - "The relations between the shear strength of sands in triaxial compression, plane shear and direct shear". Géotechnique 19, No. 1, 1969.

Smith, L.A. and Dumas, W.T. - "A recording soil penetrometer", Transactions of the A.S.A.E., Vol. 21, No. 1, 1978.

Swanson, G.D. - "Scale-model tyre tests in clay". J. Terramechanics, Vol. 10, No. 3, 1973.

Turnage, G.W.; Green, A.J. - "Performance of soils under tyre loads; analysis of tests in sand from September 1962 through November 1963". Technical Report No. 3-666, report 4. Waterways Experiment Station, Vicksburg, Miss., USA, 1966.

Turnage, G.W. - "Tyre selection and performance prediction for off-road wheeled vehicle operations". Proc. 4th Int. Conf. I.S.T.V.S., 1972 a.

Turnage, G.W. - "Performance of soils under tyre loads; application of test results to tyre selection for off-road vehicles". Technical Report No. 3-666, report 8, Waterways Experiment Station, Vicksburg, Miss., USA, 1972 b.

Turnage, G.W. - "In-soil tractive performance of selected radial and bias-ply tyres". American Society of Agric. Engs., Paper No. 76-1520, 1976.

Turnage, G.W. - "A synopsis of tyre design and operational considerations aimed at increasing in-soil tyre drawbar performance". Proc. 6th Int. Conf. I.S.T.V.S., 1978.

Vésic, A.S.; Clough, G.W. - "Behaviour of granular materials under high stresses". Proc. Am. Soc. Civil Eng., 94, SM 3, 1968.

Wismer, R.D.; Luth, H.J. - "Off-road traction prediction for wheeled vehicles". Transactions of A.S.A.E., Vol. 17, 1974.

Youd, T.L. - "Factor controlling maximum and minimum densities of sands". Evaluation of Relative Density and its role in geotechnical projects involving cohesionless soils, A.S.T.M. STP 523, 1973.

TABLE 3.1

Soil Type	Specific gravity G_s	Effective size d_{10} (mm)	d_{50} (mm)	Coefficient of uniformity C_u	v_{max}	v_{min}	$v_{max} - v_{min}$	γ_{max} (kN/m³)	γ_{min} (kN/m³)	Compactability D' (%)
Solway	2.655	0.049	0.081	1.735	2.302	1.670	0.632	15.58	11.30	94.5
Cresswell	2.646	0.312	0.459	1.647	1.775	1.525	0.250	17.00	14.61	47.6
Leighton Buzzard	2.644	0.950	1.120	1.220	1.732	1.490	0.242	17.39	14.97	49.3
Mix B	2.654	0.091	0.288	3.867	1.747	1.315	0.432	19.79	14.89	137.3

T A B L E 3.1 (cont.)

MICROSCOPIC EXAMINATION OF THE SANDS STUDIED

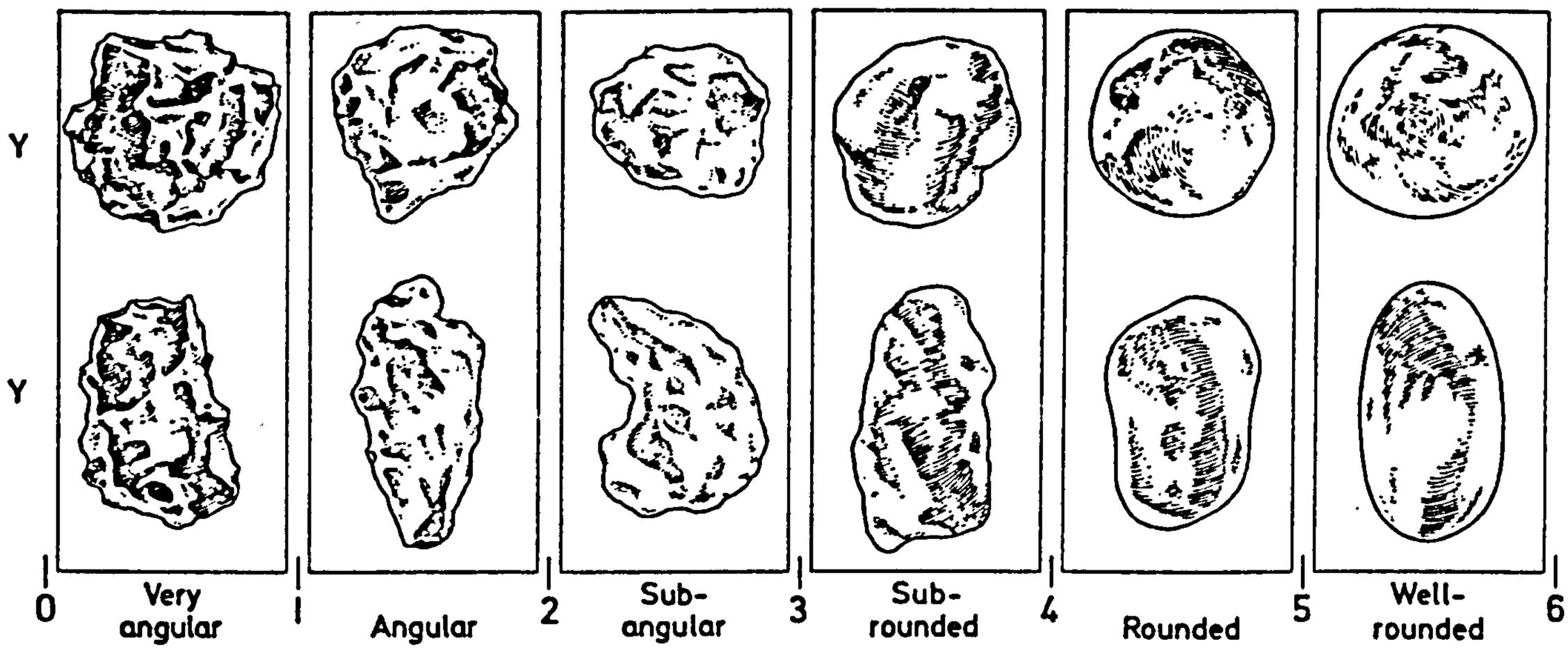

Roundness images and classes. Columns show grains of similar roundness but different sphericity (Redrawn from Powers, 1953, Fig. 1)

Solway sand - Angular grains of silica.

Cresswell sand - Large quantity of flat and concave shell fragments; otherwise sub-angular and sub-rounded silica grains.

Lindisfarne sand - Sub-angular and sub-rounded silica grains.

Leighton Buzzard sand - Rounded massive silica grins and predominantly non-spherical.

Mix B sand - Sub-rounded and sub-angular particles from the Cresswell + Lindisfarne contents.

T A B L E 3.2

Air-dry MIX B sand

γ = 15.58 kN/m^3 v= 1.67 D_d = 17.9%

Test Nº	σ (kPa)	Displacement (mm)	ϕ (Degrees)
1/2/2A	15.99	3.8	35.9
3/4/5	56.82	5.2	34.2
6/7/8	97.65	6.4	33.9 to 34.4

γ = 17.55 kN/m^3 v= 1.483 D_d = 61.2%

Test Nº	σ (kPa)	Displacement (mm)	ϕ (Degrees)
9/10/11	15.99	1.2	49.5 to 50.5
12/13/14	56.82	2.2	44.8 to 45.0
15/16/17/18	97.65	2.8 to 3.0	42.7 to 43.5

γ = 19.70 kN/m^3 v= 1.321 D_d = 98.7%

Test Nº	σ (kPa)	Displacement (mm)	ϕ (Degrees)
20	56.82	1.9	49.5

Air-dry CRESSWELL sand

γ = 15.12 kN/m^3 v= 1.716 D_d = 23.8%

Test Nº	σ (kPa)	Displacement (mm)	ϕ (Degrees)
34	15.99	2.2	33.3
14	56.82	3.0	32.9
35	97.65	5.2	31.8

γ = 16.48 kN/m^3 v= 1.574 D_d = 80.4%

Test Nº	σ (kPa)	Displacement (mm)	ϕ (Degrees)
24/33/32	15.99	1.2	47.0 to 48.2
28	56.82	2.0	43.4
29	97.65	2.8	41.7

T A B L E 3.2

Air-dry LEIGHTON BUZZARD sand

γ = 14.90 kN/m^3 v = 1.739 D_d = -2.89%

Test Nº	σ (kPa)	Displacement (mm)	ϕ (Degrees)
38	15.99	3.8	38.4
37	56.82	5.0	34.7
35/36	97.65	5.4	33.3

γ = 15.55 kN/m^3 v = 1.667 D_d ≒ 26.9%

Test Nº	σ (kPa)	Displacement (mm)	ϕ (Degrees)
56/68	15.99	2.0/2.2	41,8/41.0
58	56.82	3.6	36.6
59/60/67	97.65	3.8	35.2

γ = 15.81 kN/m^3 v = 1.639 D_d = 38.4%

Test Nº	σ (kPa)	Displacement (mm)	ϕ (Degrees)
2	15.99	2.0	41.0
7/8	56.82	2.9	37.5
14	97.65	3.2	36.5

γ = 16.55 kN/m^3 v = 1.565 D_d = 69.0%

Test Nº	σ (kPa)	Displacement (mm)	ϕ (Degrees)
40/41/42 51/52/53	15.99	1.4/1.8	51.5 to 52.9
43/44/45 54/55	56.82	2.0 to 2.6	46.8 to 47.9
46/47/48 49/50	97.65	2.6/2.8	43.2 to 45.2

γ = 16.84 kN/m^3 v = 1.538 D_d = 80.0%

Test Nº	σ (kPa)	Displacement (mm)	ϕ (Degrees)
64	15.99	1.2	54.5
65	56.82	2.2	50.7
66	97.65	3.0	49.2

T A B L E 3.2

Air-dry Solway sand

γ = 12.61 kN/m^3 v = 2.063 D_d = 37.8%

Test Nº	σ (kPa)	Displacement (mm)	ϕ (Degrees)
2/11/12/15	15.99	8$^+$	37.7
1/13/14	56.82	"	34.7
3	97.65	"	34.4

γ = 14.54 kN/m^3 v = 1.789 D_d = 81.2%

Test Nº	σ (kPa)	Displacement (mm)	ϕ (Degrees)
16/17/18	15.99	1.6/1.8	46.2 to 48.1
19/20	56.82	2.1/2.6	41.2/41.8
21/22	97.65	3.0/3.2	39:0/40.2

NOTE: The values of horizontal displacement and of angle of internal friction were obtained at the maximum of shear stress.

T A B L E 4.1

SOIL PROCESSING TECHNIQUES FOR IN-MOLD CONE PENETRATION TESTS

A - Pouring through a funnel.

B - Pushing a 4mm diameter welding rod right to the bottom of the full loaded mold at very close centers, systematically over the whole area.

C - A circular board with an electric vibrator bolted on the top, compacting 50mm thick layers of soil for about 3 min.

D - Placing 700N dead weight on the surfuce of the sand of the full loaded mold and tapping all around the outside of the mold with a soft hammer.

E - Placing 20mm thick layers with a scoop.

F - Stirring the full loaded mold over the whole depth with a circular rod.

G - Electric vibrator running for 10 min on the surface of the sand of a full loaded mold.

H - Stirring about 80mm thick layers of sand at a time.

SAND/Test No./Processing technique:

LB	S	C	MB
1A	2A	1E	1A
3A	3A	2E	2A
4EB	6D	3E	3A
5EB	8E	4EB	4EB
6EB	11EFD	5EB	5EH
8C	12C	6EB	6EH
9C	13C	7EG	7EH
10C	14C	8EG	8C
	15EH	9EG	9C
	16EH	10C	10C
	17EH	11C	

LB - Leighton Buzzard
S - Solway
C - Cresswell
MB - Mix B

T A B L E 4.2

Air-dry MIX B sand

Test N°	γ (kN/m^3)	D_d (%)	v	CI_{av} (kPa)	G (MPa/m)	CI_{50}	CI_{100}	CI_{125} (kPa)	CI_{150}
1	15.29	10.5	1.702	32.99	0.356	28.49	41.59	45.42	47.43
2	15.38	12.4	1.694	33.23	0.369	27.47	42.21	46.84	51.26
3	15.62	18.8	1.666	33.58	0.358	28.15	42.39	47.18	51.17
4	16.98	49.8	1.532	203.70	2.244	164.59	242.05	293.99	370.15
5	16.73	44.3	1.556	156.07	1.772	109.44	198.48	241.40	281.10
6	16.76	45.0	1.553	165.23	1.903	119.29	216.71	257.74	306.41
7	16.76	45.0	1.553	138.62	1.591	95.50	178.52	224.04	271.43
8	18.74	83.1	1.388	981.46	12.130	498.87	1254.43	1808.51	2476.00
9	18.74	83.1	1.388	1089.48	13.039	607.25	1381.91	1914.05	2682.28
10	18.73	82.9	1.389	1085.62	13.044	590.11	1489.18	2059.98	2639.36

Air-dry CHESSWELL sand

Test N°	γ (kN/m^3)	D_d (%)	v	CI_{av} (kPa)	G (MPa/m)	CI_{50}	CI_{100}	CI_{125} (kPa)	CI_{150}
1	14.78	8.4	1.754	36.25	0.401	27.62	46.04		59.22
2	14.77	8.4	1.754	33.04	0.358	27.13	42.75		52.63
3	14.85	11.6	1.746	35.76	0.394	27.92	43.11		57.51
4	15.64	46.8	1.658	104.69	1.187	79.69	141.63	168.80	198.28
5	15.73	50.8	1.648	116.79	1.351	80.52	149.48	181.15	227.19
6	15.80	53.6	1.641	127.83	1.498	86.72	165.17	207.91	226.43
7	16.35	75.6	1.596	209.03	2.499	140.18	277.07	339.87	404.21
8	16.30	73.6	1.591	228.23	2.652	156.68	296.86	363.40	437.20
9	16.33	74.8	1.588	281.08	3.295	188.01	370.25	452.19	543.62
10	16.90	96.4	1.534	443.33	5.398	230.93	576.42	786.40	1077.60
11	16.92	97.2	1.532	551.88	6.788	305.76	718.39	980.31	1294.81

T A B L E 4.2 (cont.)

Air-dry LEIGHTON BUZZARD sand

Test N°	γ (kN/m^3)	D_d (%)	v	CI_{av} (kPa)	G (MPa/m)	CI_{50}	CI_{100} (kPa)	CI_{125} (kPa)	CI_{150} (kPa)
1	14.82	-7.0	1.749	54.69	0.662	40.14	70.75	83.98	100.32
3	14.87	-4.5	1.743	56.11	0.672	36.24	76.19	92.07	107.68
4	15.79	37.7	1.641	173.77	1.918	121.46	218.07	271.53	333.54
5	15.84	40.0	1.635	198.45	2.304	132.55	252.71	320.71	406.24
6	15.78	37.2	1.642	176.96	2.211	101.78	225.77	291.86	378.03
8	16.95	84.0	1.529	649.30	8.230	342.09	846.68	1175.95	1667.71
9	16.92	83.1	1.531	729.82	8.961	374.17	940.76	1351.26	1870.83
10	16.98	85.1	1.526	820.36	9.655	449.00	1069.04	1496.66	2063.25

Air-dry SOLWAY sand

Test N°	γ (kN/m^3)	D_d (%)	v	CI_{av} (kPa)	G (MPa/m)	CI_{50}	CI_{100} (kPa)	CI_{125} (kPa)	CI_{150} (kPa)
2	11.91	18.8	2.183	29.38	0.239	24.28	34.85	38.78	41.12
3	11.89	18.1	2.187	23.33	0.260	19.19	28.77	33.15	36.86
6	13.96	69.5	1.863	117.39	1.388	79.10	150.75	193.69	249.09
8	12.51	35.1	2.080	41.13	0.409	37.51	48.08	56.26	61.21
11	14.07	71.8	1.848	172.53	2.009	110.12	214.89	286.51	381.64
12	14.95	89.0	1.740	475.44	5.700	280.52	617.91	828.57	1021.15
13	14.98	89.5	1.737	425.04	4.903	264.26	545.21	709.25	910.82
14	15.02	90.3	1.732	474.15	5.581	295.07	614.05	797.06	1015.59
15	13.45	58.2	1.934	92.15	1.000	70.57	118.68	134.28	159.92
16	13.47	58.7	1.931	106.85	1.162	80.39	134.71	158.22	189.43
17	13.44	58.1	1.935	90.49	1.000	62.01	111.82	144.97	175.31

T A B L E 5.1

TYRE TESTS ON AIR-DRY CRESSWELL SAND

Tyre: 6.00-16-2PR, b=145mm, d=644mm, h=96mm.

TEST No.	CS10	CS11	CS12	CS13	CS14	CS15	CS16	CS17	CS18	CS19	CS20	CS21
W (N)	1413	962	864	864	1413	962	864	864	864	1413	962	714
i.p.(psi)	11	7.5	6	6	11	7.5	6	6	6	11	7.5	12.5
δ/h (%)	30	30	30	30	30	30	30	30	30	30	30	20
i (%)	20	20	20	20	20	20	20	20	20	20	20	20
G (MPa/m)	3.491 ↕ 4.081	6.146 ↕ 6.911	0.574 ↕ 0.765	0.708 ↕ 1.030	0.708 ↕ 1.030	0.708 ↕ 1.030	3.654 ↕ 3.888	2.583 ↕ 3.606	2.418 ↕ 2.803	2.418 ↕ 2.803	2.418 ↕ 2.803	4.854 ↕ 6.597
D_d (%)	80 ↕ 84.5	97.3 ↕ 100	22.3 ↕ 31.5	29 ↕ 41	29 ↕ 41	29 ↕ 41	81 ↕ 83	70 ↕ 80.5	68.5 ↕ 73	68.5 ↕ 73	68.5 ↕ 73	90 ↕ 99.5
γ (kN/m^3)	16.46 ↕ 16.58	16.93 ↕ 17.00	15.08 ↕ 15.29	15.23 ↕ 15.50	15.23 ↕ 15.50	15.23 ↕ 15.50	16.49 ↕ 16.54	16.21 ↕ 16.48	16.17 ↕ 16.28	16.17 ↕ 16.28	16.17 ↕ 16.28	16.73 ↕ 16.99
DP (N)	212	221	86.4	86.4	42.4	96.2	233.3	198.7	155.5	141.3	163.5	85.8
T (Nm)	130.5	98.4	84.8	93	151	103	93.5	90	84.7	119.3	97	53.3
z_1 (mm)	14	7	42	39	48	31	12.5	14	20.5	23	14.5	11
z (mm)	26	11	64	64	77	58	19	26	32	39	26	23
DP/W	.15	.23	.10	.10	.03	.10	.27	.23	.18	.10	.17	.12
η (%)	40	55	25	22	7.4	22.5	58.8	52	45	28.2	41.3	40.2
PN	.375	.418	.4	.455	.39	.444	.459	.442	.4	.355	.412	.299
ξ_s/W	.225	.188	.3	.355	.36	.344	.189	.212	.22	.255	.242	.179
z/d	.04	.02	.1	.1	.12	.09	.03	.04	.05	.06	.04	.036
N_s	21.13 ↕ 24.7	54.62 ↕ 61.42	5.68 ↕ 7.57	7.00 ↕ 10.20	4.28 ↕ 6.23	6.29 ↕ 9.16	36.16 ↕ 38.47	25.56 ↕ 35.69	23.93 ↕ 27.73	14.63 ↕ 16.96	21.49 ↕ 24.91	38.75 ↕ 52.66
D_{de} (%)	77.9	85.5	57.2	60	60	60	77.9	74.8	73.8	73.8	73.8	84.1
G_e (MPa/m)	2.33	3.0	1.2	1.3	1.3	1.3	2.33	2.1	2.04	2.04	2.04	2.9
N_{se}	14.1	26.66	11.87	12.86	7.87	11.55	23.06	20.78	20.19	12.34	18.13	23.15
$\tan \phi_{TO}$	.8496	.8941	.9196	.9196	.8496	.8941	.9196	.9196	.9196	.8496	.8941	
on soil δ/h (%)	15.6	23	12				24.5	20.8	17.2	14.1	21.9	9.9
$\frac{Gbd^2}{W}$	148.6 ↕ 173.7	384.2 ↕ 432.0	39.9 ↕ 53.3	49.2 ↕ 71.7	30.1 ↕ 43.8	44.2 ↕ 64.4	254.4 ↕ 270.6	179.8 ↕ 251	168.3 ↕ 195.1	102.9 ↕ 119.3	151.2 ↕ 175.2	408.8 ↕ 555.6

T A B L E 5.2

TYRE TESTS ON AIR-DRY LEIGHTON BUZZARD SAND

Tyre : 6.00-16-2PR, b=145mm, d=644mm, h=96mm.

TEST No.	LB6	LB3	LB9	LB4	LB2	LB8	LB5	LB1	LB7
W (N)	2002	1413	864	2002	1413	864	2002	1413	864
i.p.(psi)	14.5	11	6.5	14.5	11	6.5	14.5	11	6.5
δ/h (%)	30	30	30	30	30	30	30	30	30
i (%)	20	20	20	20	20	20	20	20	20
G (MPa/m)	0.9 | 0.936	0.772 | 0.862	0.856 | 0.941	4.732 | 5.00	4.37 | 4.87	4.1 | 4.6	7.623 | 8.388	5.643 | 6.684	7.746 | 9.014
D_d (%)	10 | 11	5 | 9	9 | 12	64 | 66	62 | 65.5	61 | 63	79 | 82	70 | 75	79 | 83
γ(kN/m)	15.07 | 15.1	14.95 | 15.04	15.03 | 15.1	16.43 | 16.49	16.37 | 16.46	16.32 | 16.42	16.83 | 16.9	16.58 | 16.72	16.83 | 16.96
DP (N)	20	63	92	221	233	253	375	253	317
T (Nm)	232	173	94	175	134	104	198	128	113
z_1(mm)	54	38.5	31.5	12.5	13	9	6	10	7
z (mm)	102	79.5	58.5		28	14	15	20	10
DP/W	.01	.044	.106	.11	.165	.293	.187	.179	.367
η(%)	2.1	8.6	23.3	30.2	41.8	58.4	45.4	47.4	67.3
PN	.483	.510	.454	.364	.395	.502	.412	.378	.545
ε_s/W	.473	.466	.348	.254	.230	.209	.225	.199	.178
z/d	.158	.123	.091		.043	.022	.023	.031	.015
N_s	3.85 | 4.00	4.68 | 5.22	8.49 | 9.32	20.2 | 21.4	26.5 | 29.5	40.6 | 45.6	32.6 | 35.9	34.2 | 40.5	76.8 | 89.3
D_{dc}(%)	51.7	50.9	51.9	71.8	71.3	70.8	77	74	77.2
G_e(MPa/m)	1	.97	1	1.9	1.88	1.85	2.26	2.1	2.28
N_{se}	4.28	5.88	9.89	8.13	11.36	18.28	9.65	12.42	22.57
tan ϕ_{70}	1	1.035	1.15	1	1.035	1.15	1	1.035	1.15
on soil δ/h	5	11.5	10	18	16	23.4	25	25	24
$\frac{Gbd^2}{W}$	27.0 | 28.1	32.9 | 36.7	59.6 | 65.5	142.1 | 150.2	186 | 207.3	285.4 | 320.2	229 | 252	240.2 | 284.5	539.1 | 627.4

T A B L E 5.2 (cont.)

SECOND PASS TESTS ON AIR-DRY LEIGHTON BUZZARD SAND

Tyre : 6.00-16-2PR, b=145mm, d=644mm, h=96mm

TEST No.	LB6	LB3	LB9	LB4	LB2	LB8	LB5	LB1	LB7
DP (N)	75	35	174	74	105	222	163	271	222
T (Nm)	188	135	98	163	131	99	168	137	90
z_i (mm)	74	59.5	52	35.5	28.5	19	16	26	11
z (mm)	95	85.5	62		61.5	25	27	40	20
z^* (mm)	26	23.5	20		51.5	20	23	36	20
DP/W	.037	.025	.2	.037	.074	.257	.081	.192	.257
η (%)	9.5	6.3	42.3	10.9	19.2	53.8	23.1	47.5	59.2
PN	.391	.398	.473	.339	.386	.478	.350	.404	.434
ε_s/W	.354	.373	.273	.302	.312	.221	.269	.212	.177
z/d	.147	.133	.096		.095	.039	.042	.062	.031

T A B L E 5.2 (cont.)

THIRD PASS TESTS ON AIR-DRY LEIGHTON BUZZARD SAND

Tyre : 6.00-16-2PR, b=145mm, d=644mm, h=96mm.

TEST No.	LB6	LB3	LB9	LB4	LB2	LB8	LB5	LB1	LB7
DP (N)	34	82	194	149	138	228	143	234	255
T (Nm)	206	139	94	173	118	99	179	122	100
z_i (mm)	78.5	59.5	57	44.5	42	26	29	33	19
z (mm)	102.5	82.5	65	58.5	62	33	39	44	24
z^* (mm)	23.5	13.5	15	25.5	40	22	21	30	16
DP/W	.017	.058	.224	.074	.098	.264	.071	.166	.295
η (%)	4.0	14.1	46.9	20.6	28.2	55.2	19.0	46.1	61.1
PN	.429	.410	.478	.360	.348	.478	.373	.360	.483
ε_s/W	.412	.352	.254	.286	.250	.214	.302	.194	.188
z/d	.159	.128	.100	.091	.096	.051	.061	.068	.037

T A B L E 6.1

MULTIPASS TESTS IN VERY DENSE LEIGHTON BUZZARD SAND

TEST	LB5 (W=2002N)	LB1 (W=1413N)	LB7 (W=864N)
1st pass			
Depth below rut surf. (cm)		After 1st pass cone force as a percentage of the initial value	
5	32		39
10	50		63
15	68		78
Performance data (Nm/m)			
DP	375		317
ε_s	450		154
PN×W	825		471
2nd pass			
Depth below rut surf. (cm)		Difference, in percentage, between cone force after 2nd and 1st passes	
5	13.5	14.3	1.8
10	19.4	14.2	11.9
15	17.0	9.9	3.1
Performance data (Nm/m)			
DP	163		222
ε_s	539		153
PN×W	701		375
3rd pass			
Depth below rut surf. (cm)		Difference, in percentage, between cone force after 3rd and 2nd passes	
5	7.1	12.5	1.8
10	8.1	-3.3	-6.2
15	0.6	-2.0	-1.3
Performance data (Nm/m)			
DP	143		255
ε_s	605		162
PN×W	747		417

T A B L E 6.2

MULTIPASS TESTS IN MEDIUM DENSE LEIGHTON BUZZARD SAND

TEST	LB4 (W=2002N)	LB2 (W=1413N)	LB8 (W=864N)
1st pass			
Depth below rut surf. (cm)	After 1st pass cone force as a percentage of the initial value		
5	40.2	43.6	55.3
10	61.9	59.8	76.4
15	80.1	78.5	83.9
Performance data (Nm/m)			
DP	221	233	253
ε_s	508	325	181
PN×W	729	558	434
2nd pass			
Depth below rut surf. (cm)	Difference, in percentage, between cone force after 2nd and 1st passes		
5	20.0	6.0	1.4
10	17.4	22.4	9.1
15	18.0	16.7	4.3
Performance data (Nm/m)			
DP	74	105	222
ε_s	605	441	191
PN×W	679	546	413
3rd pass			
Depth below rut surf. (cm)	Difference, in percentage, between cone force after 3rd and 2nd passes		
5	9.5	11.1	13.5
10	3.9	8.3	16.7
15	-1.2	1.7	14.6
Performance data (Nm/m)			
DP	149	138	228
ε_s	572	354	185
PN×W	721	492	413

T A B L E 6.3

MULTIPASS TESTS IN VERY LOOSE LEIGHTON BUZZARD SAND

TEST	LB6 (W=2002N)	LB3 (W=1413N)	LB9 (W=864N)
1st pass			
Depth below rut surf. (cm)	Difference, in percentage, between cone force after 1st pass and pre-traffic cone force at depth = z + rut depth.		
5	20	16.6	2.1
10	47.6	40.8	19.5
Performance data (Nm/m)			
DP	20	63	92
ε_s	947	658	301
PN*W	967	721	393
2nd pass			
Depth below rut surf. (cm)	Difference, in percentage, between cone force after 2nd and 1st passes		
5	-2.2	0.5	11.9
10	12.9	14.5	13.3
15	21.7	26.1	19.4
Performance data (Nm/m)			
DP	75	35	174
ε_s	708	527	235
PN*W	783	562	409
3rd pass			
Depth below rut surf. (cm)	Difference, in percentage, between cone force after 3rd and 2nd passes		
5	-2.3	2.4	4.0
10	7.1	11.8	12.6
15	12.8	14.3	18.0
Performance data (Nm/m)			
DP	34	82	194
ε_s	825	497	219
PN*W	859	579	413

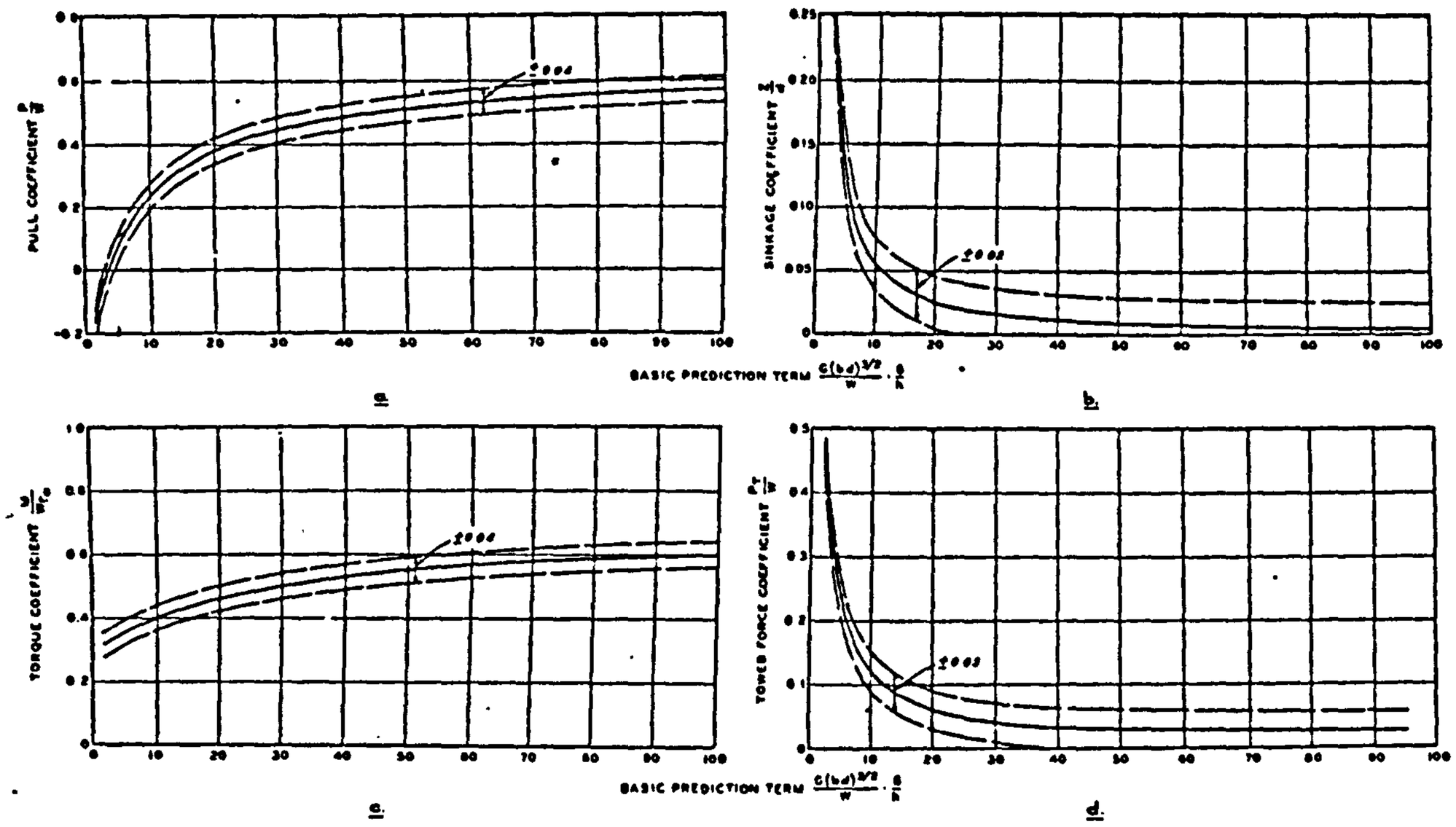

Fig. 1.1 - Relation of the performance coefficients to the W.E.S. sand number for Yuma sand (after Turnage 1972a)

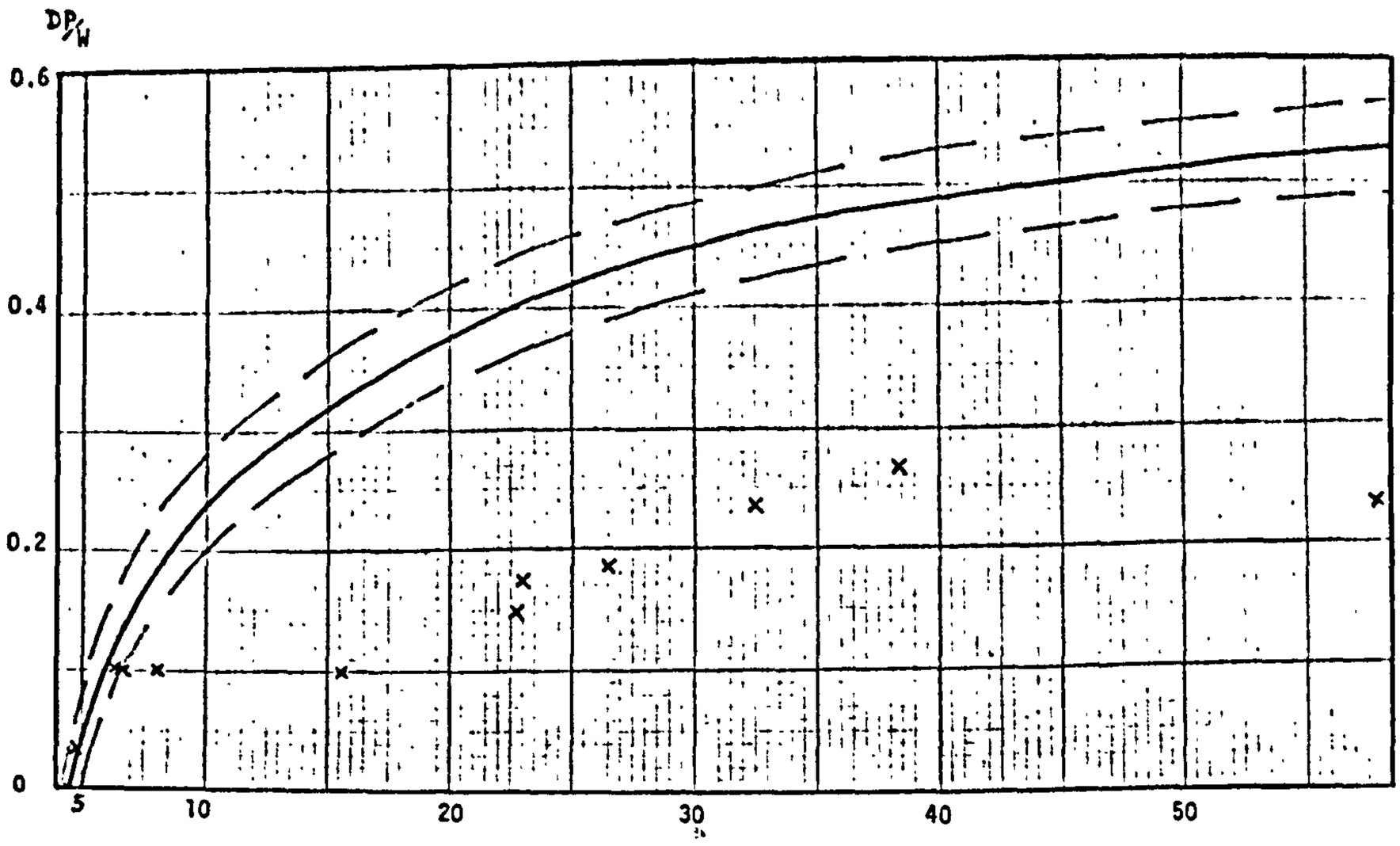

Fig. 1.2.a Drawbar pull/vertical load ratio against the sand number $N_S = \frac{G(bd)^{3/2}}{W} \frac{\delta}{h}$, showing the measured results for Cresswell sand compared with the W.E.S. curve.

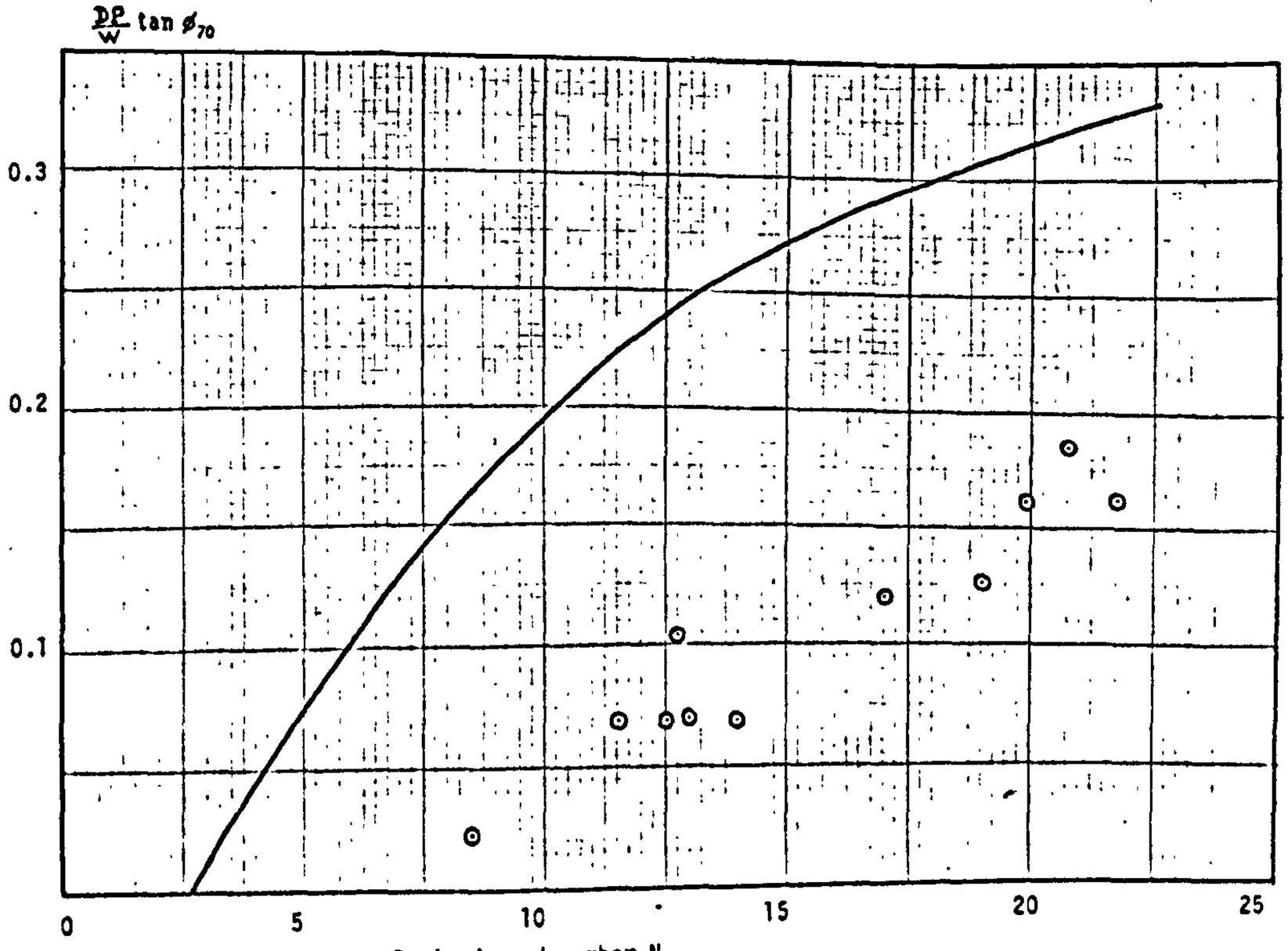

Fig. 1.2.b Drawbar pull/vertical load ratio against the revised sand number N_{se}.
Results for Cresswell sand compared with proposed curve.

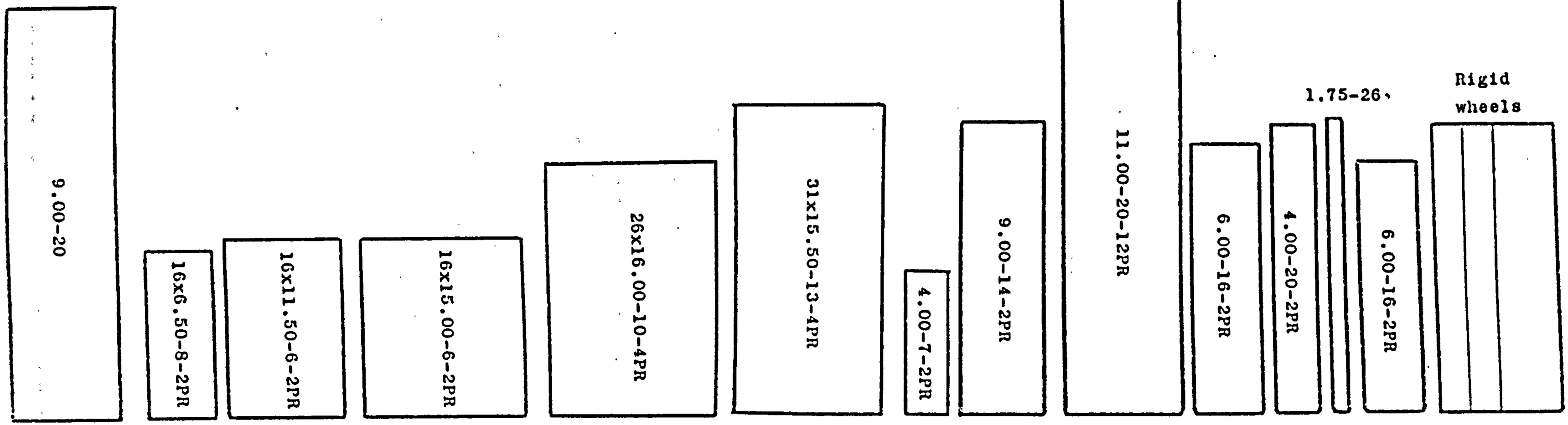

	b (cm)	d (cm)	h (cm)	b/d	h/b
16x6.50-8-2PR	16.3	40.6	8.6	.401	.528
16x11.50-6-2PR	28.2	43.9	13.4	.642	.475
16x15.00-6-2PR	38.6	44.5	13.4	.867	.347
26x16.00-10-4PR	41.0	62.1	15.6	.660	.380
31x15.50-13-4PR	38.1	75.9	19.7	.502	.517
4.00-7-2PR	10.6	35.8	7.8	.296	.736
4.00-20-2PR	10.4	70.9	7.9	.147	.760
11.00-20-12PR	28.4	104.9	22.9	.271	.806
6.00-16-2PR	16.8	71.8	13.4	.234	.798
9.00-14-2PR	21.0	71.9	16.2	.292	.771
(Newcastle)6.00-16-2PR	14.5	64.4	9.6	.225	.660
Rigid wheels	30.5	70.9	-	.430	-
"	15.2	70.6	-	.216	-
"	7.6	70.9	-	.108	-

Fig. 1.3 - Tyres and wheels used by W.E.S. in traction research on sand.

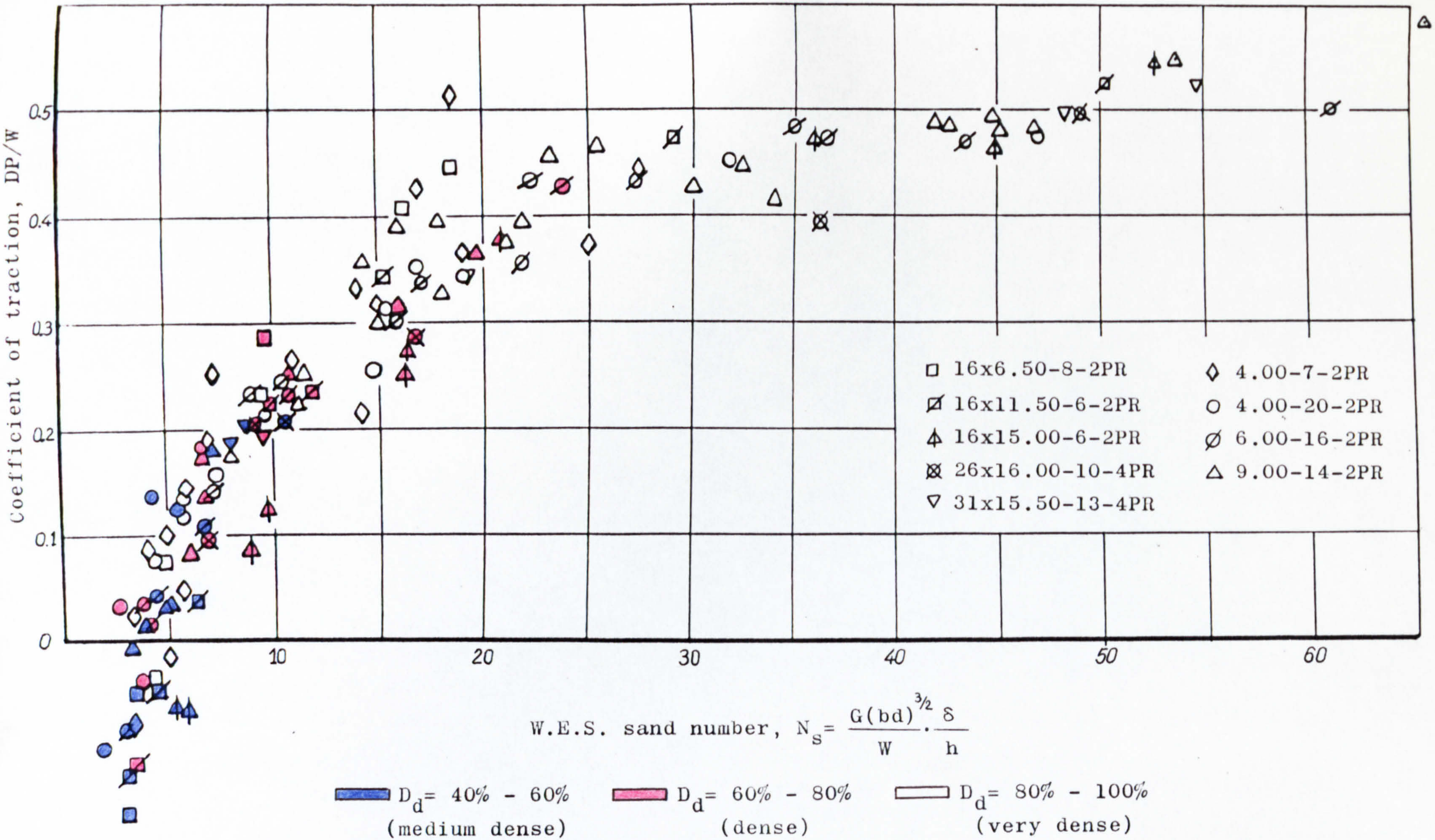

W.E.S. sand number, $N_s = \frac{G(bd)^{3/2}}{W} \cdot \frac{\delta}{h}$

D_d= 40% - 60% (medium dense) D_d= 60% - 80% (dense) D_d= 80% - 100% (very dense)

Fig. 1.4 - Tyre tests on Yuma sand at 20% slip, δ/h=15% to 35%.

Data from Turnage (1972b).

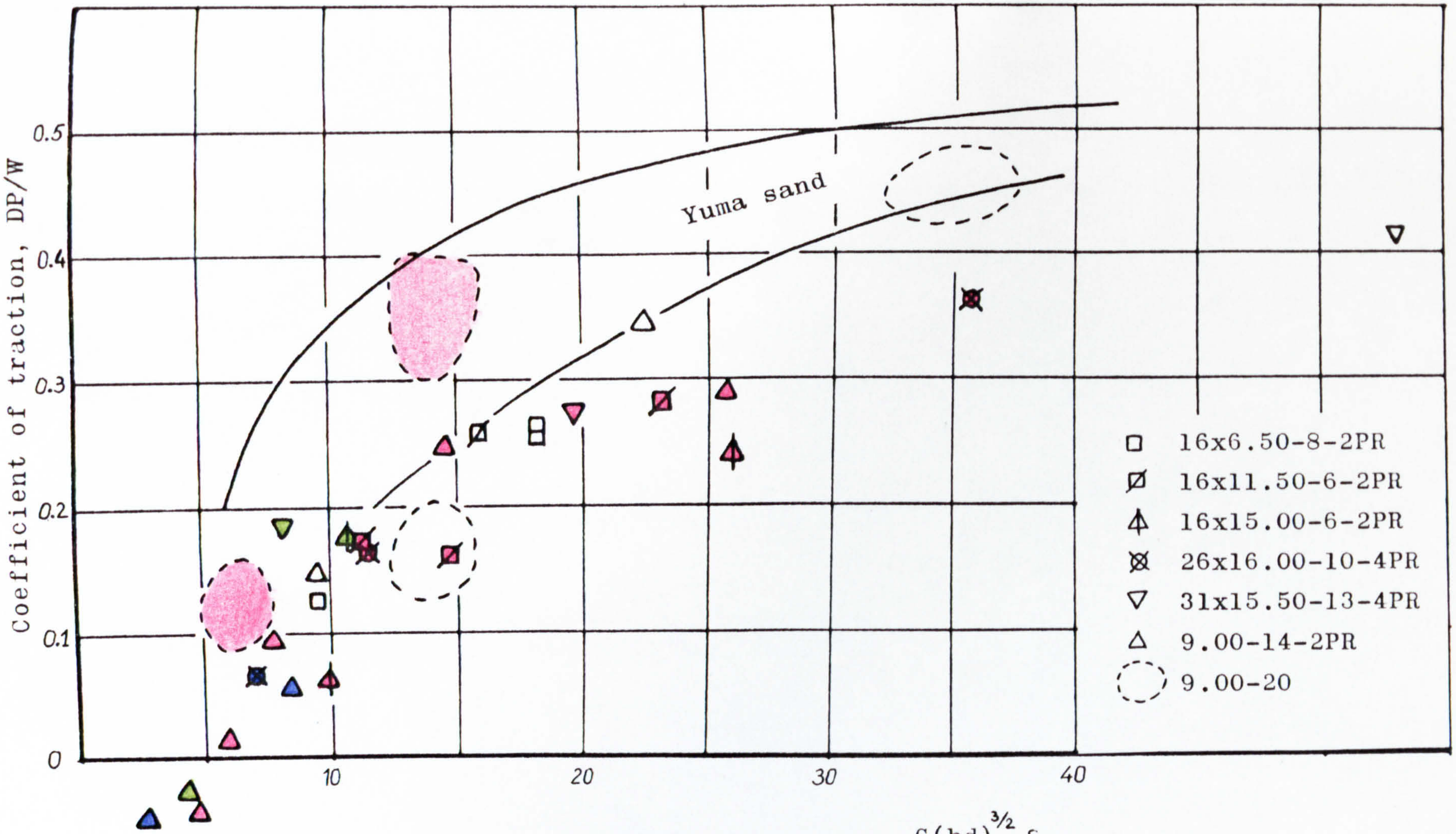

W.E.S. sand number, $N_s = \frac{G(bd)^{3/2}}{W} \cdot \frac{\delta}{h}$

D_d= 40% (loose) D_d= 40% - 60% (medium dense) D_d= 60% - 80% (dense) D_d= 80% - 100% (very dense)

Fig. 1.5 - Tyre tests on Mortar sand at 20% slip, δ/h=15% to 35%. Data from Turnage (1972b) and Turnage (1976).

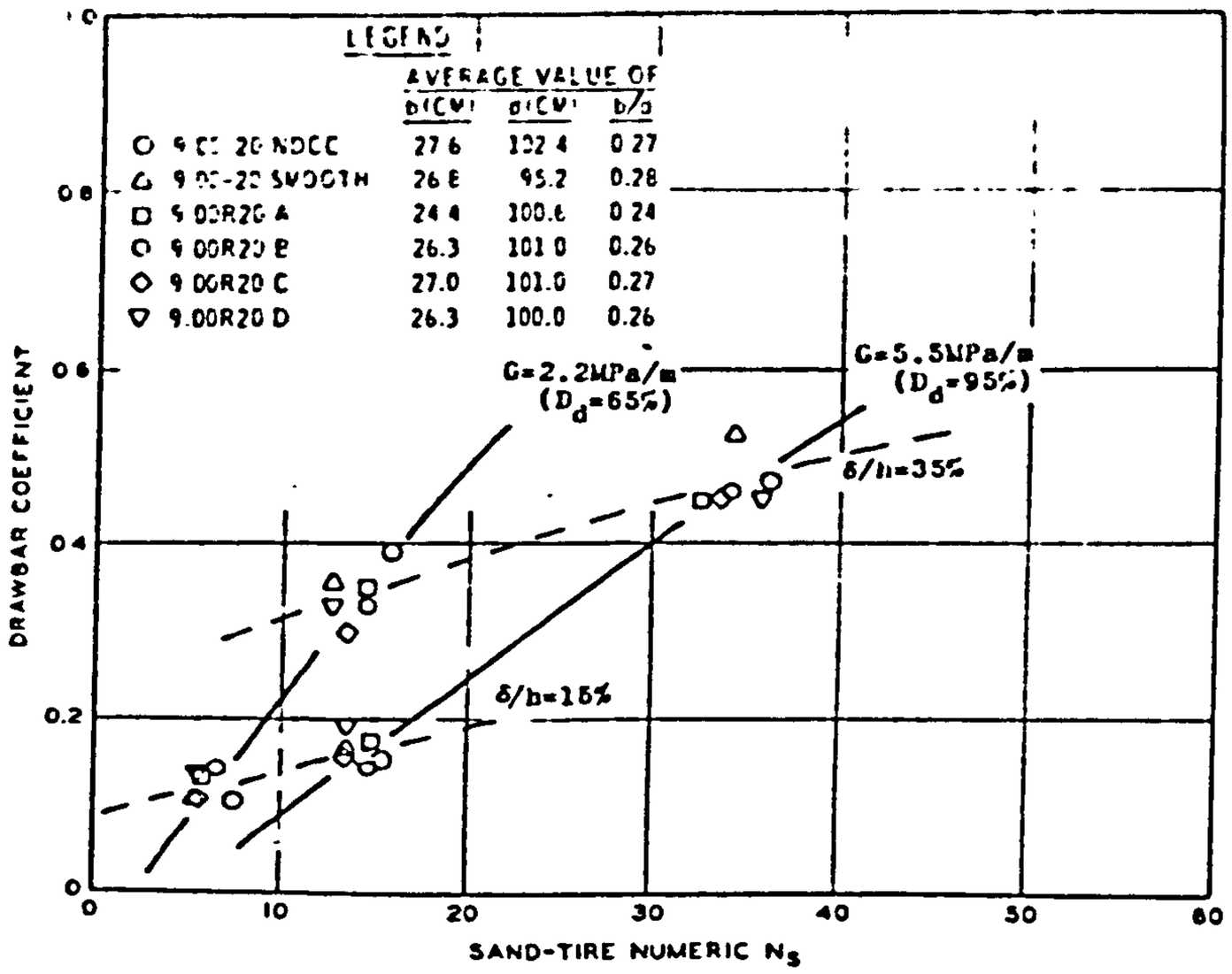

Fig. 1.6.a - Relation of coefficient of traction to sand number N_s for a set a 9.00 -20 tyres in Mortar sand.

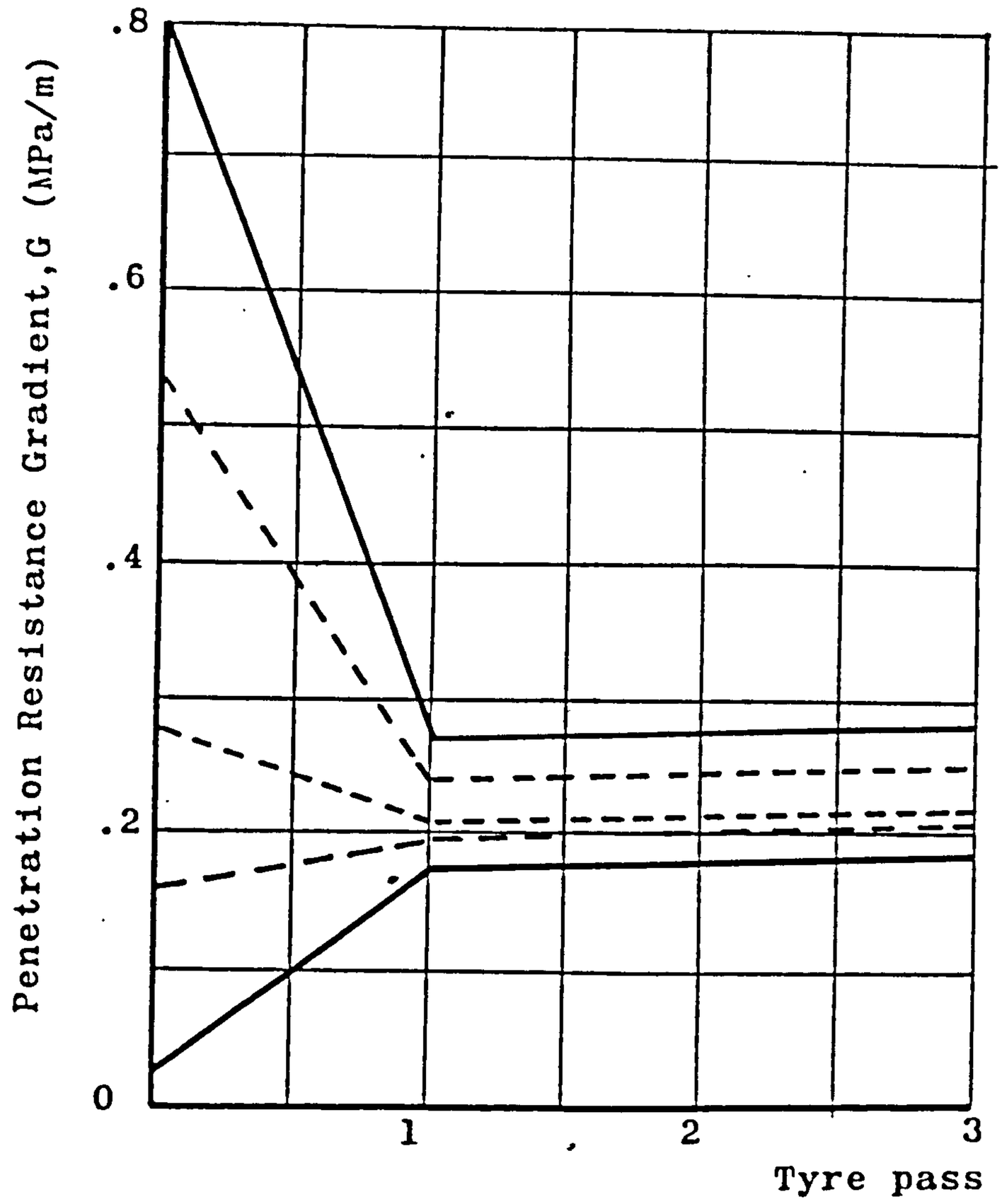

Fig. 1.6.b - Relations of penetration resistance gradient to tyre pass number for tests in Mortar sand (after Turnage, 1976).

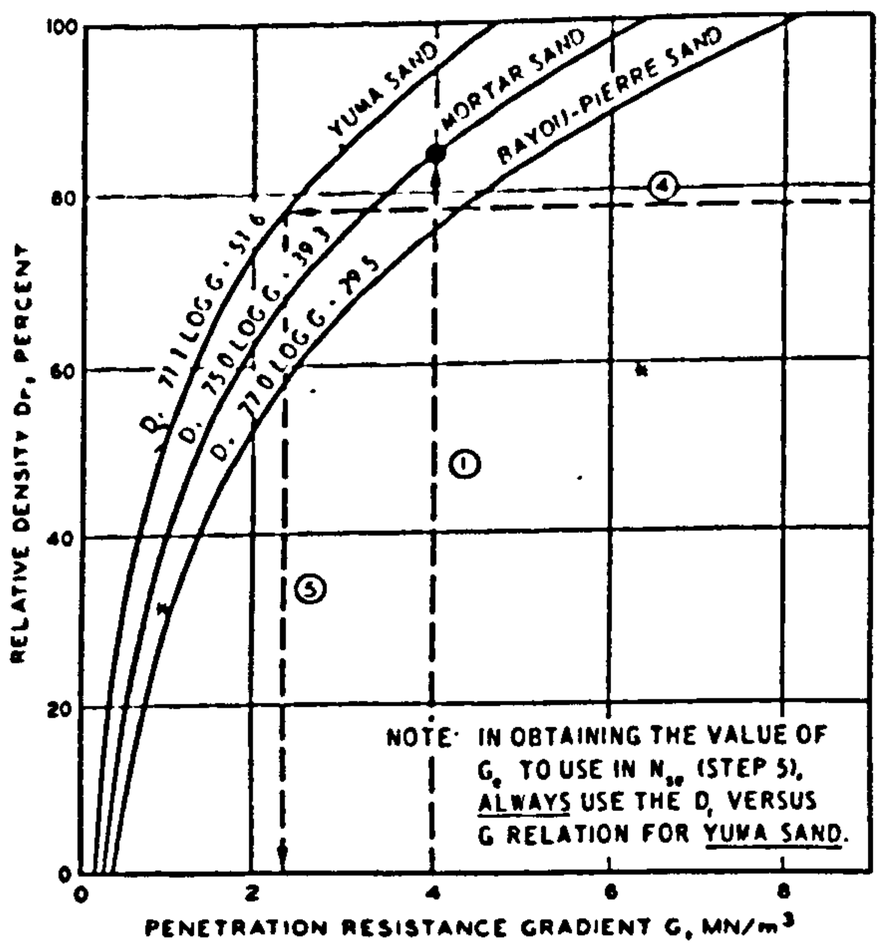

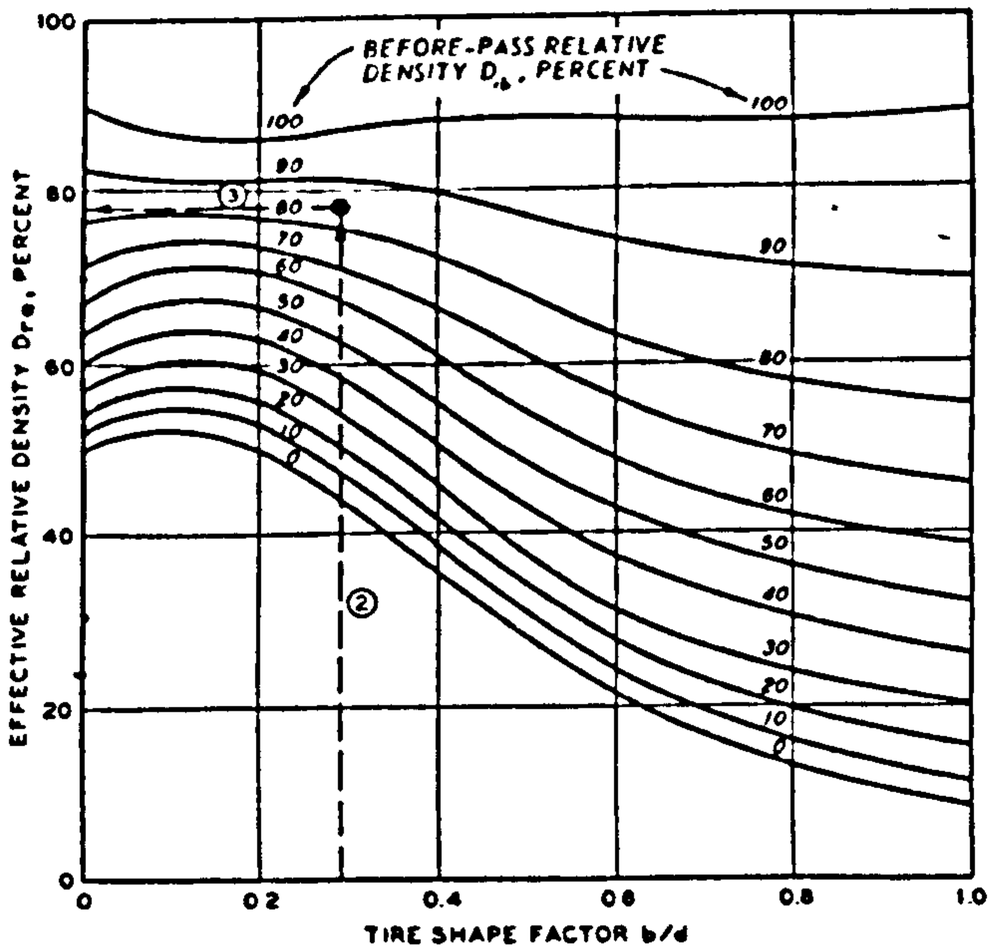

Step 1: Using a relation like those shown in Fig. 1.7.a, translate the known G value for the frictional soil of interest to the D_d value of the same soil. (In Fig. 1.7.a, example line 1 shows that a mortar sand G value of 4.0 MPa translates to a mortar sand D_d value of 84.5%.)

Steps 2 and 3: Use the D_d value from Step 1 and the tyre's b/d value in the relation in Fig. 1.7.b to estimate D_{de} for the frictional soil of interest. (In fig. 1.7.b, example lines 2 and 3 show that mortar sand D_d=84.5% translates to mortar sand D_{de}=78%)

Steps 4 and 5: Translate the D_{de} value from step 3 for the frictional soil of interest to the D_d versus G curve for Yuma sand in fig. 1.7.a and read off the corresponding G value on the abscissa scale. This is Yuma sand G_e. (In fig. 1.7.a, example lines 4 and 5 show that the D_{de} value of 78% for mortar sand from step 3 translate to a value G_e=2.35 MPa for Yuma sand.)

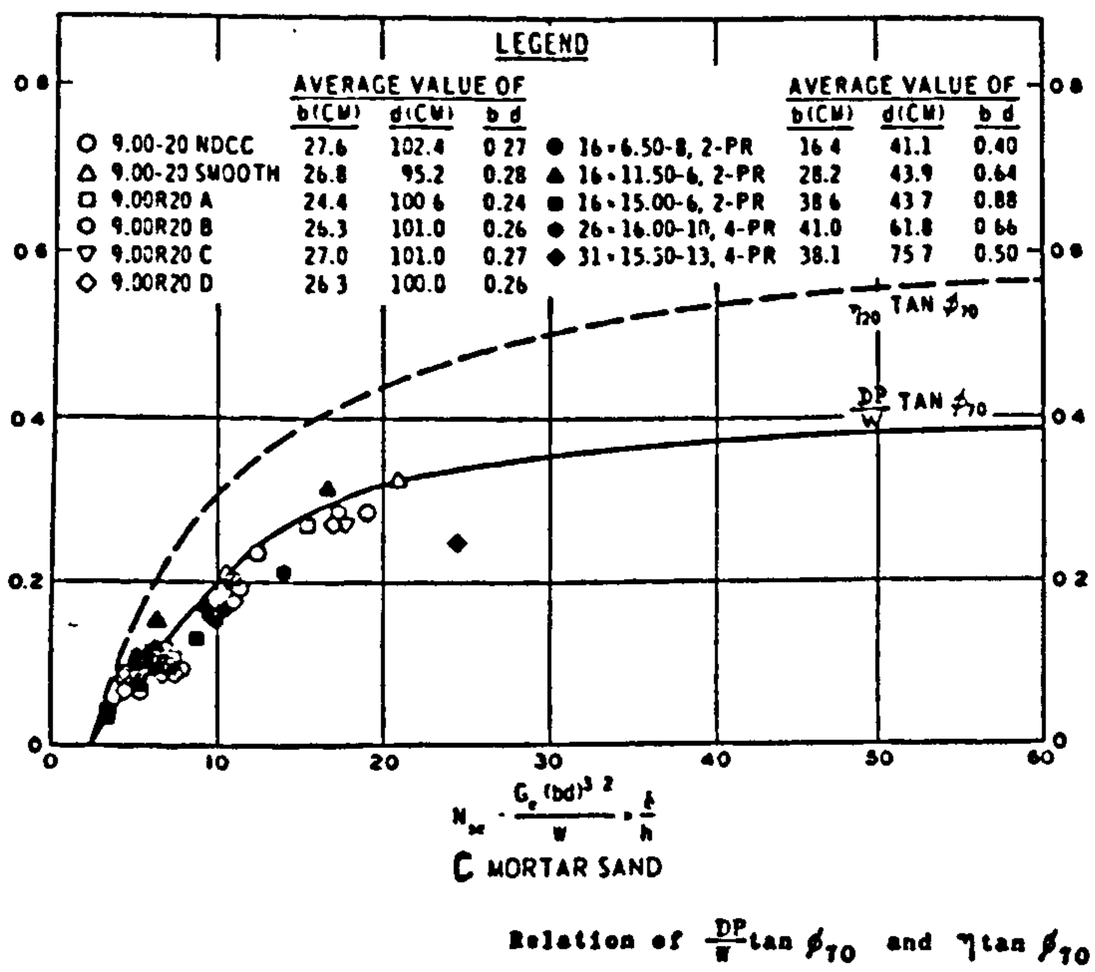

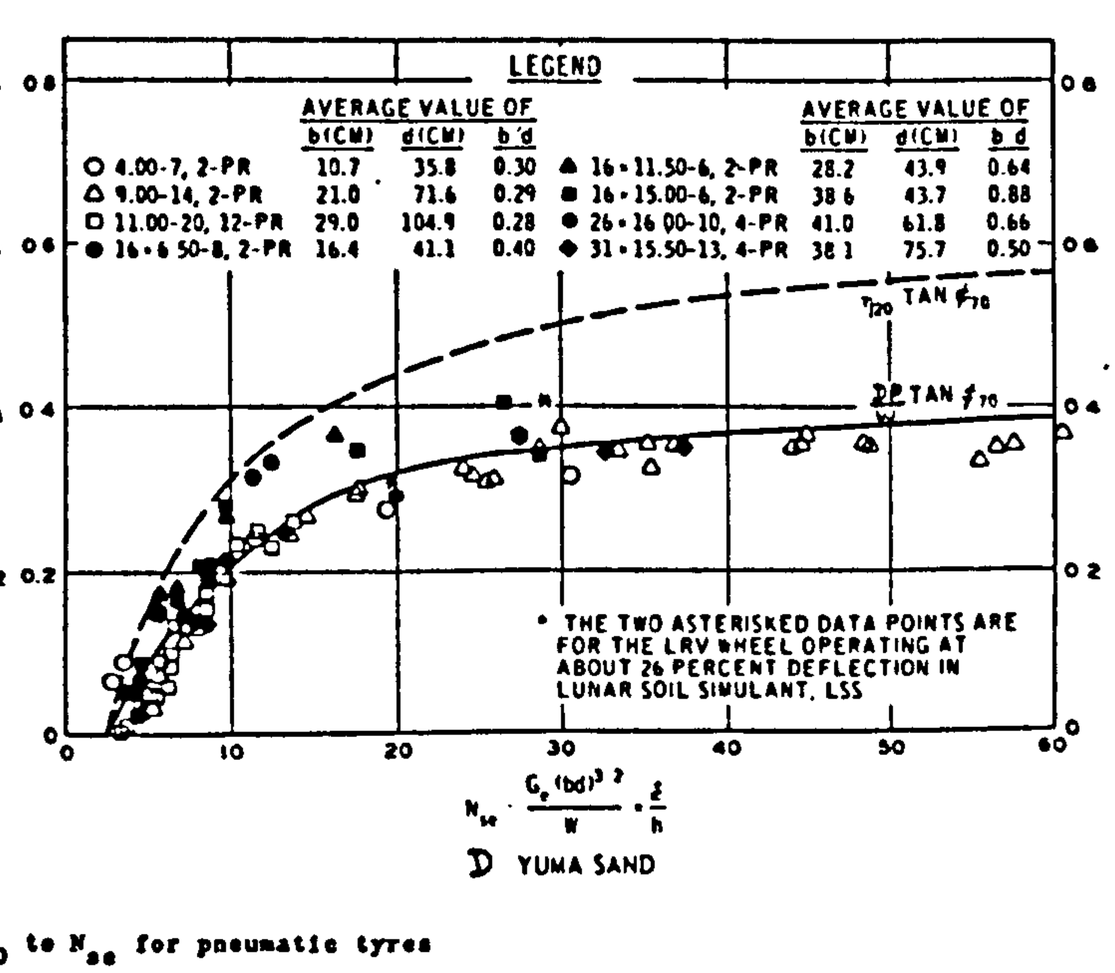

Relation of $\frac{DP}{W}\tan\phi_{70}$ and $\eta\tan\phi_{70}$ to N_{se} for pneumatic tyres operating at deflections up to 35% (d) in mortar sand and (d) in Yuma sand.

Fig. 1.7 - Turnage's Method for predicting traction on air-dry sand. Transcribed from Turnage 1978.

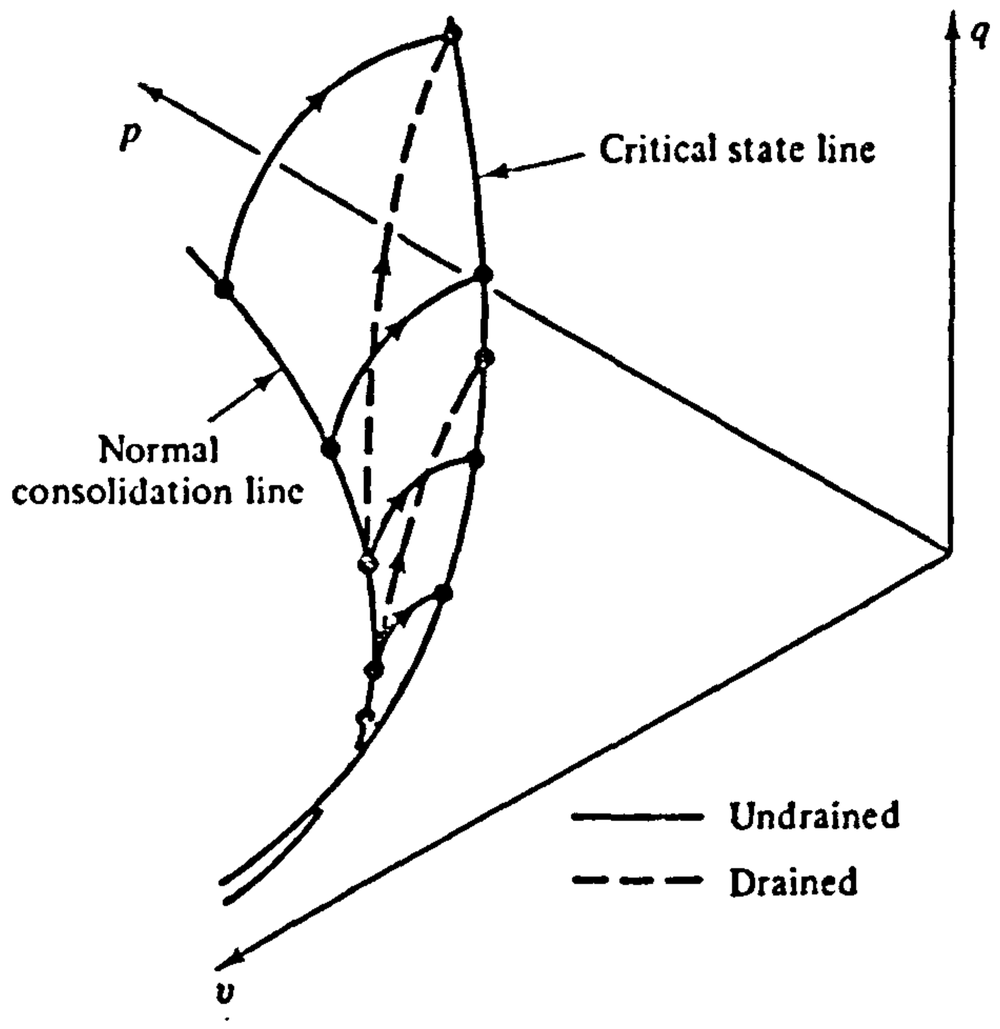

Fig. 2.1 - Roscoe surface obtained in triaxial compression of samples of normally consolidated clay (after Atkinson and Bransby, 1978).

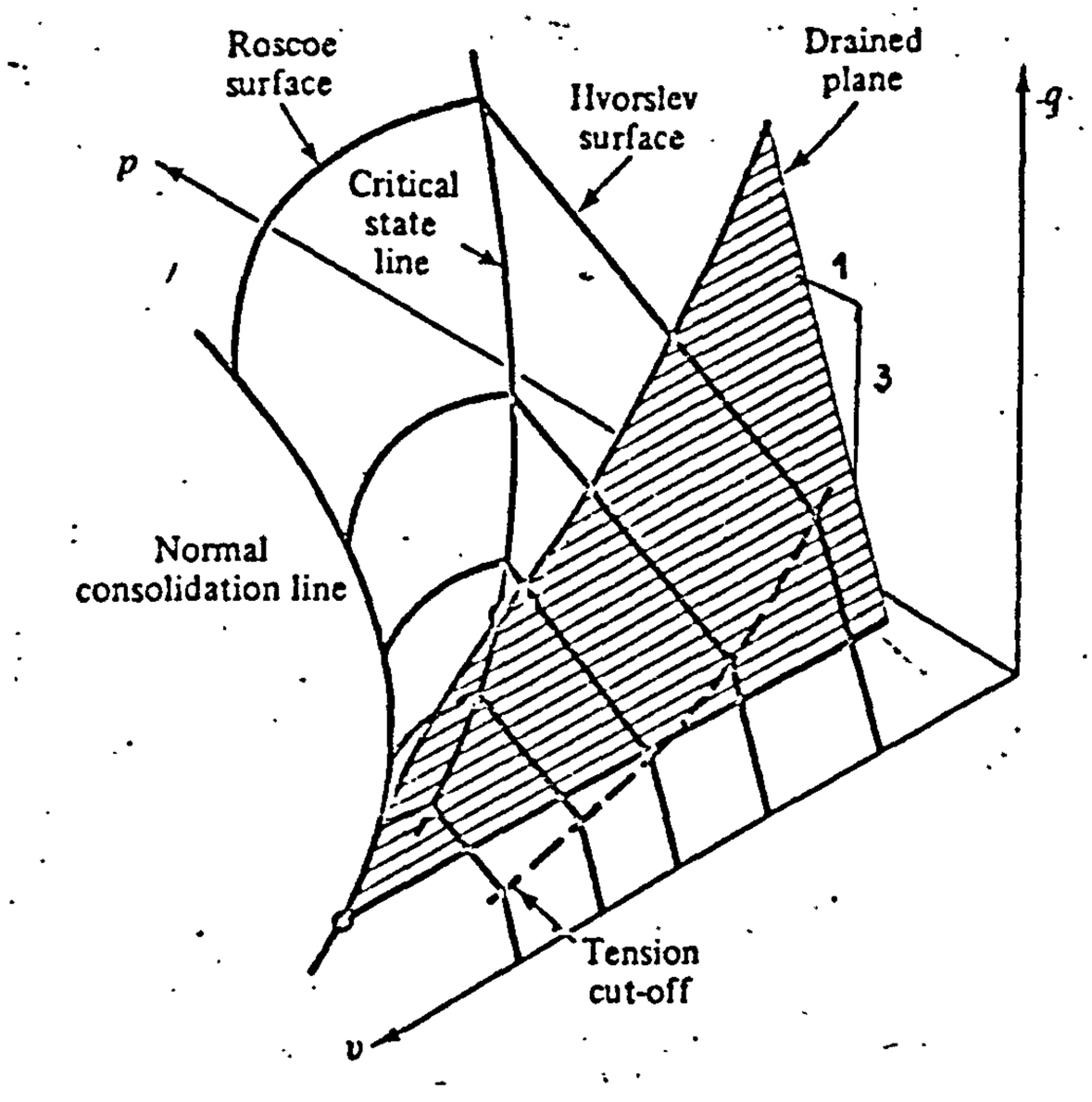

Fig. 2.2 - Complete state boundary surface representing the behaviour of samples of normally and overconsolidated clay in triaxial compression (after Atkinson and Bransby, 1978).

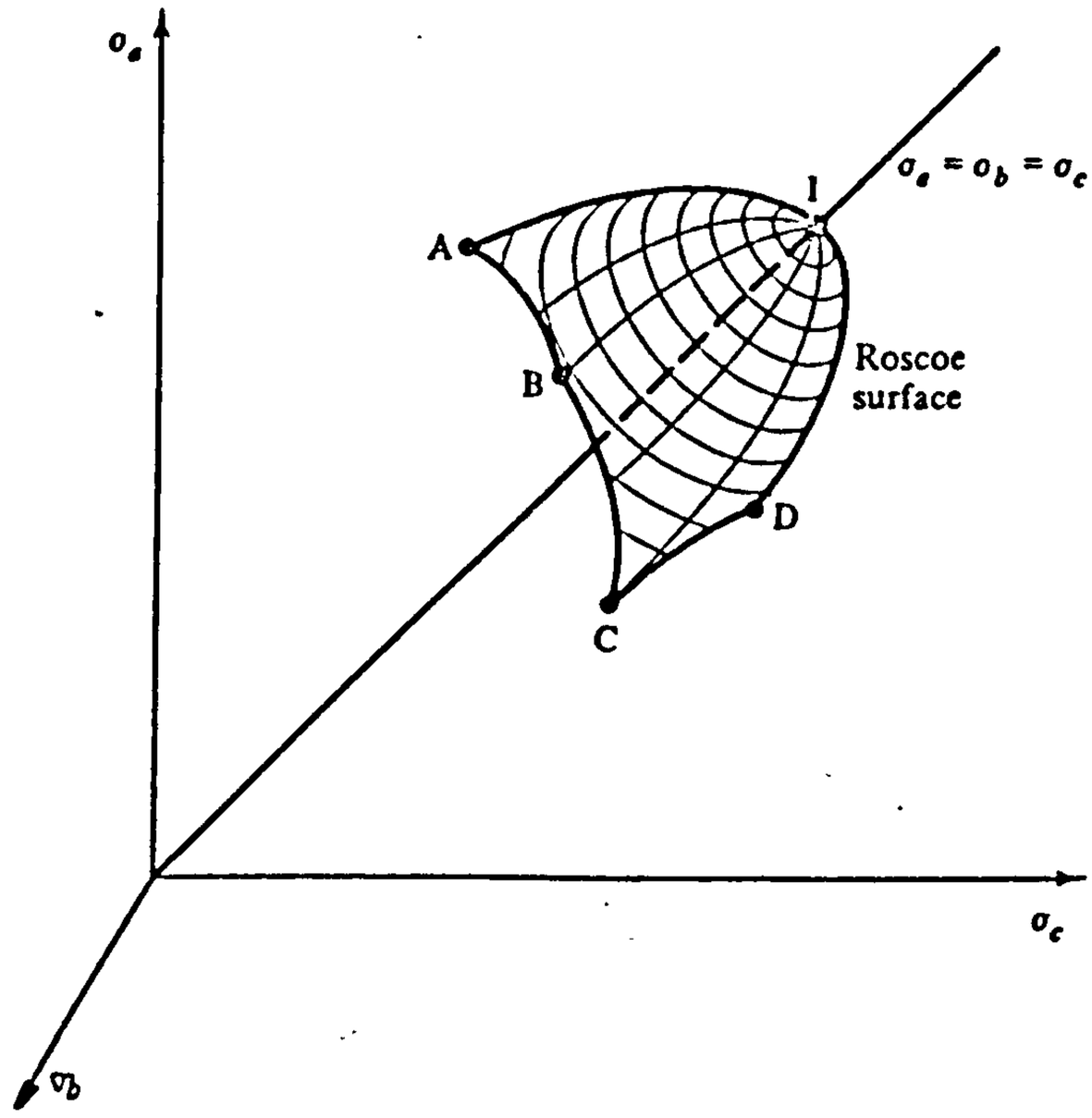

Fig. 2.3 - Generalized Roscoe surface in the principal stress diagram (after Atkinson and Bransby, 1978).

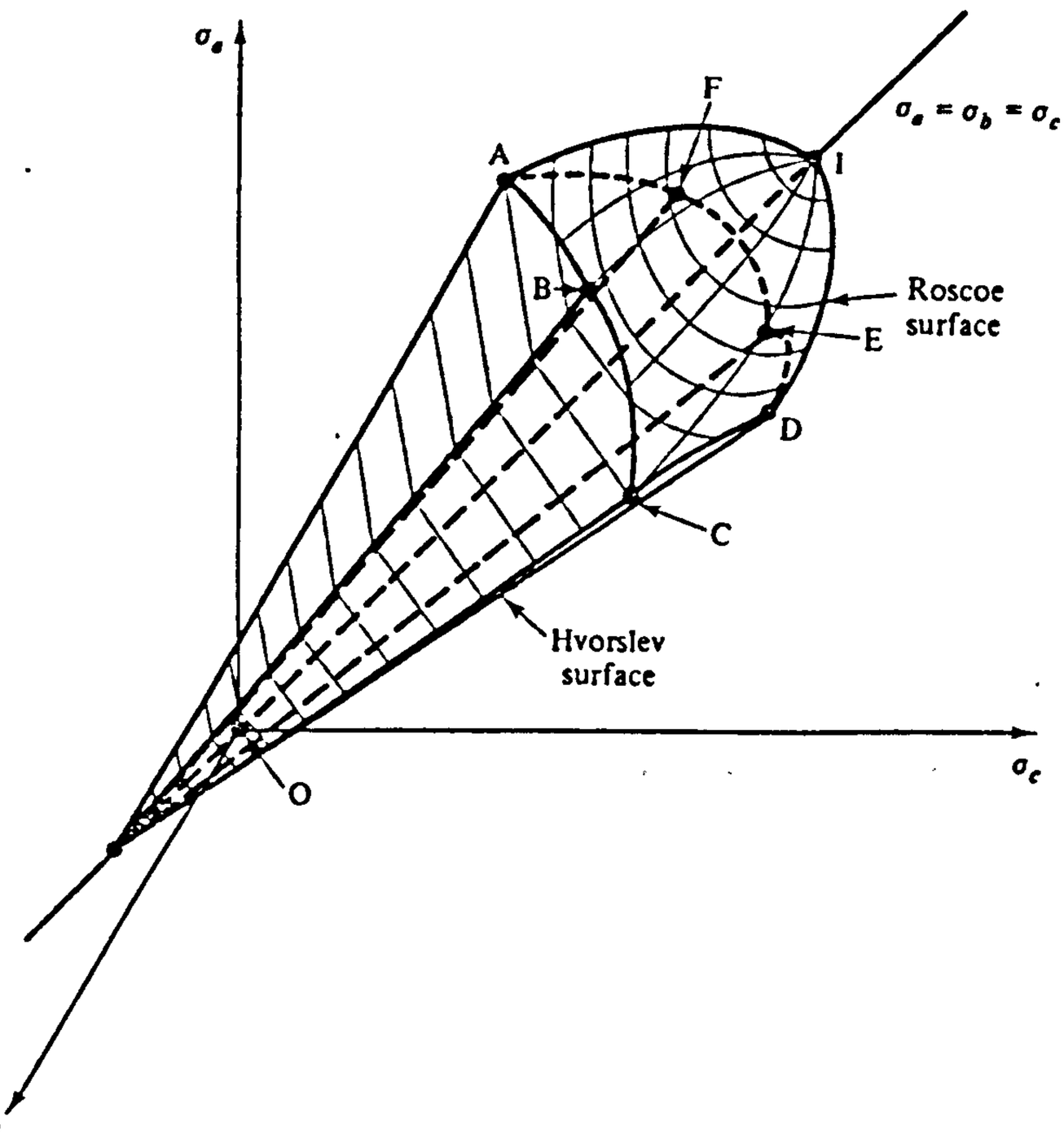

Fig. 2.4 - Generalized complete boundary surface in the principal stress diagram (after Atkinson and Bransby 1978).

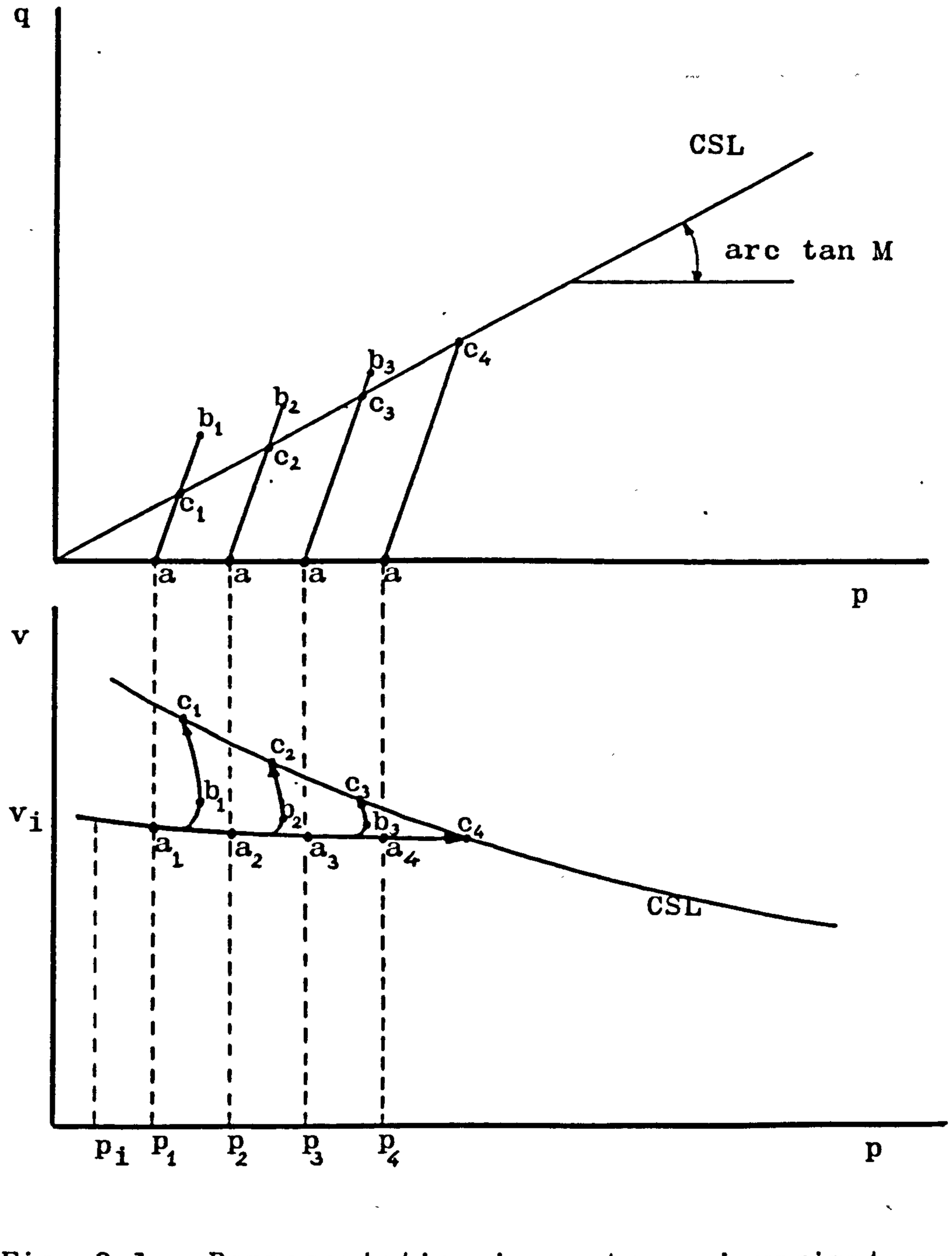

Fig. 3.1 - Representation in a stress invariant space of a set of drained triaxial tests in dense soil.

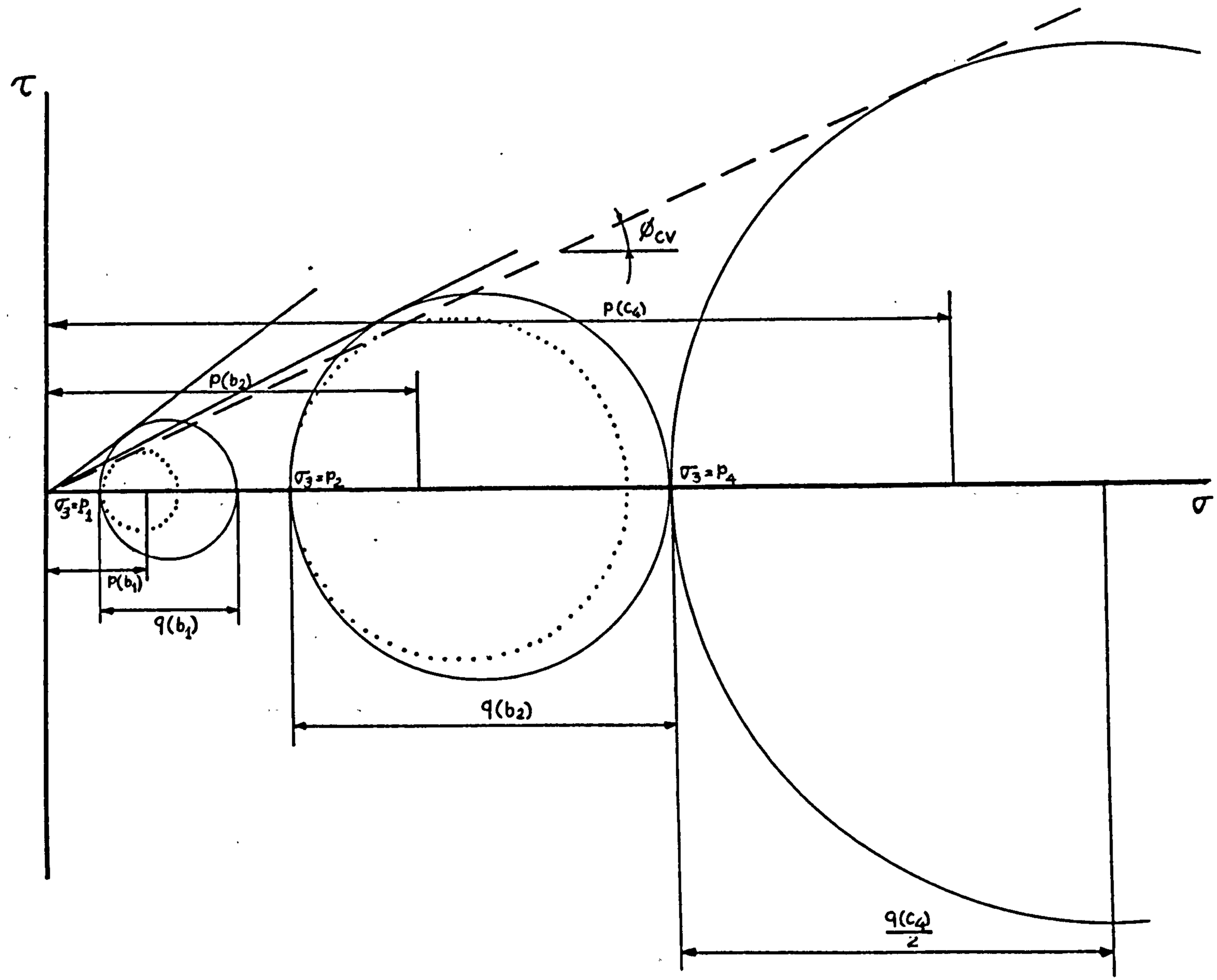

Fig. 3.2 - Mohr's space representation of the state of stress at points b_1 , b_2 and c_4 in fig. 3.1 .

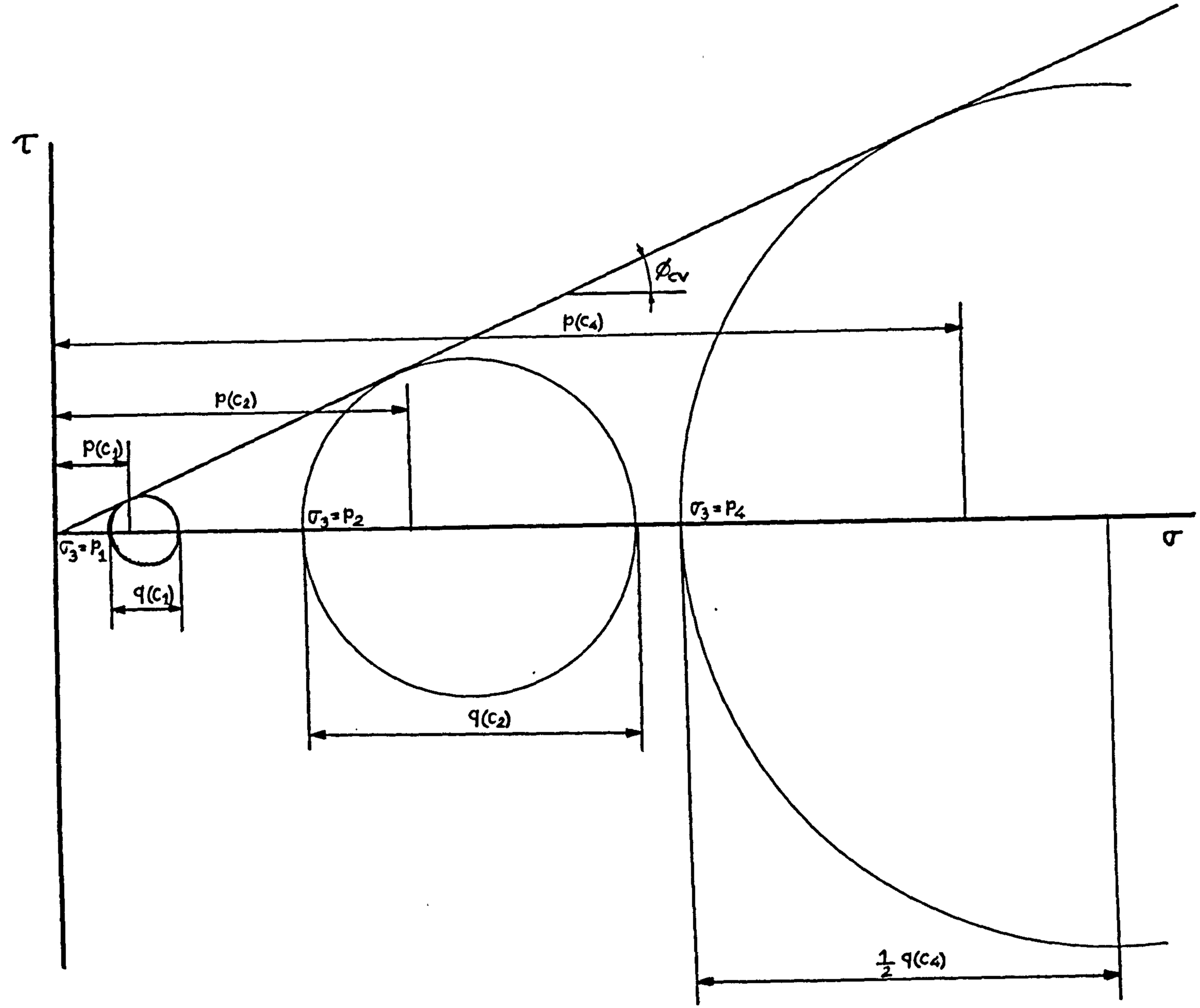

Fig. 3.3 - Mohr's space representation of the stace of stress at points c_1 , c_2 and c_4 in fig. 3.1 .

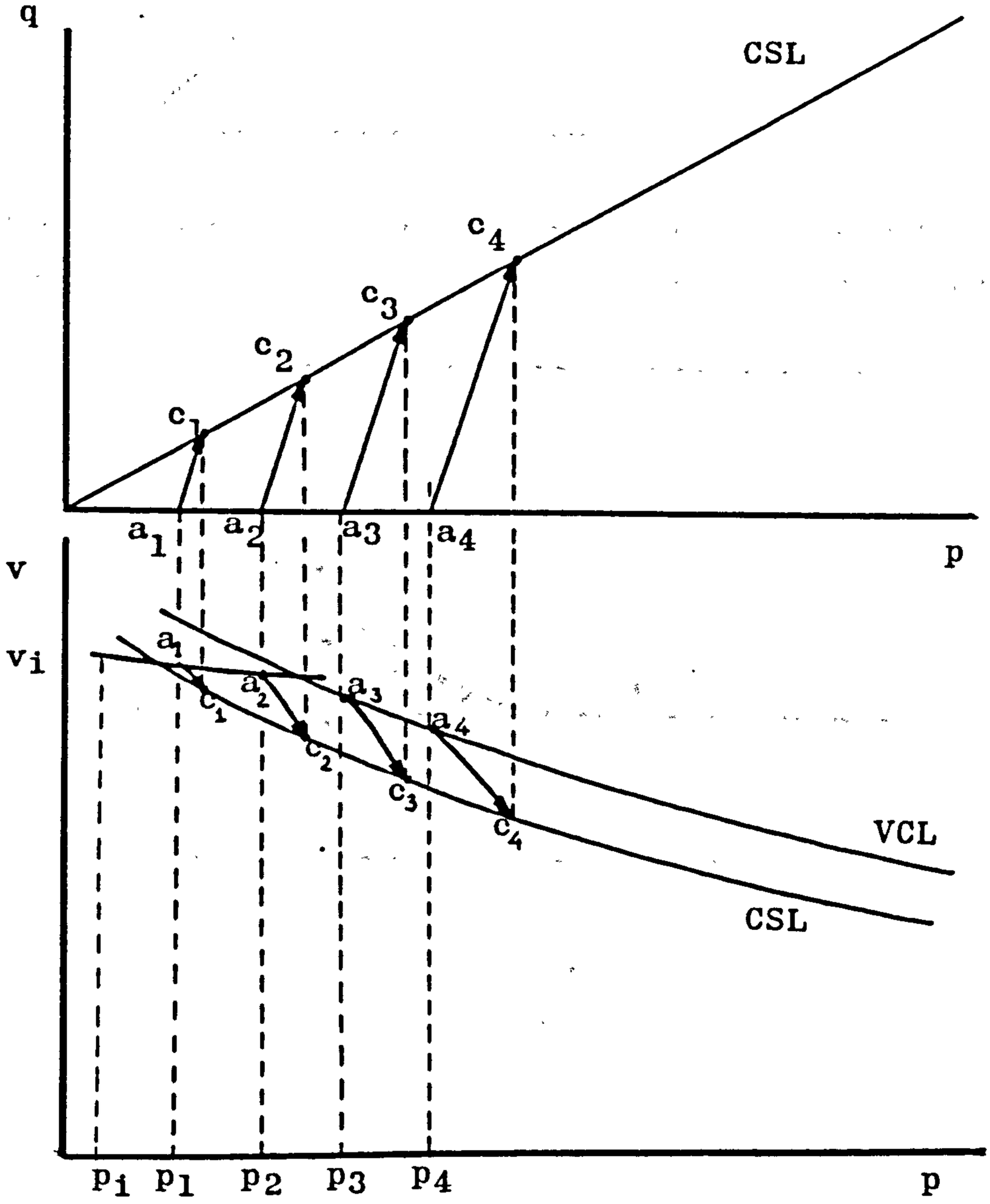

Fig. 3.4 - Representation in a stress invariant space of a set of drained triaxial tests in loose soil.

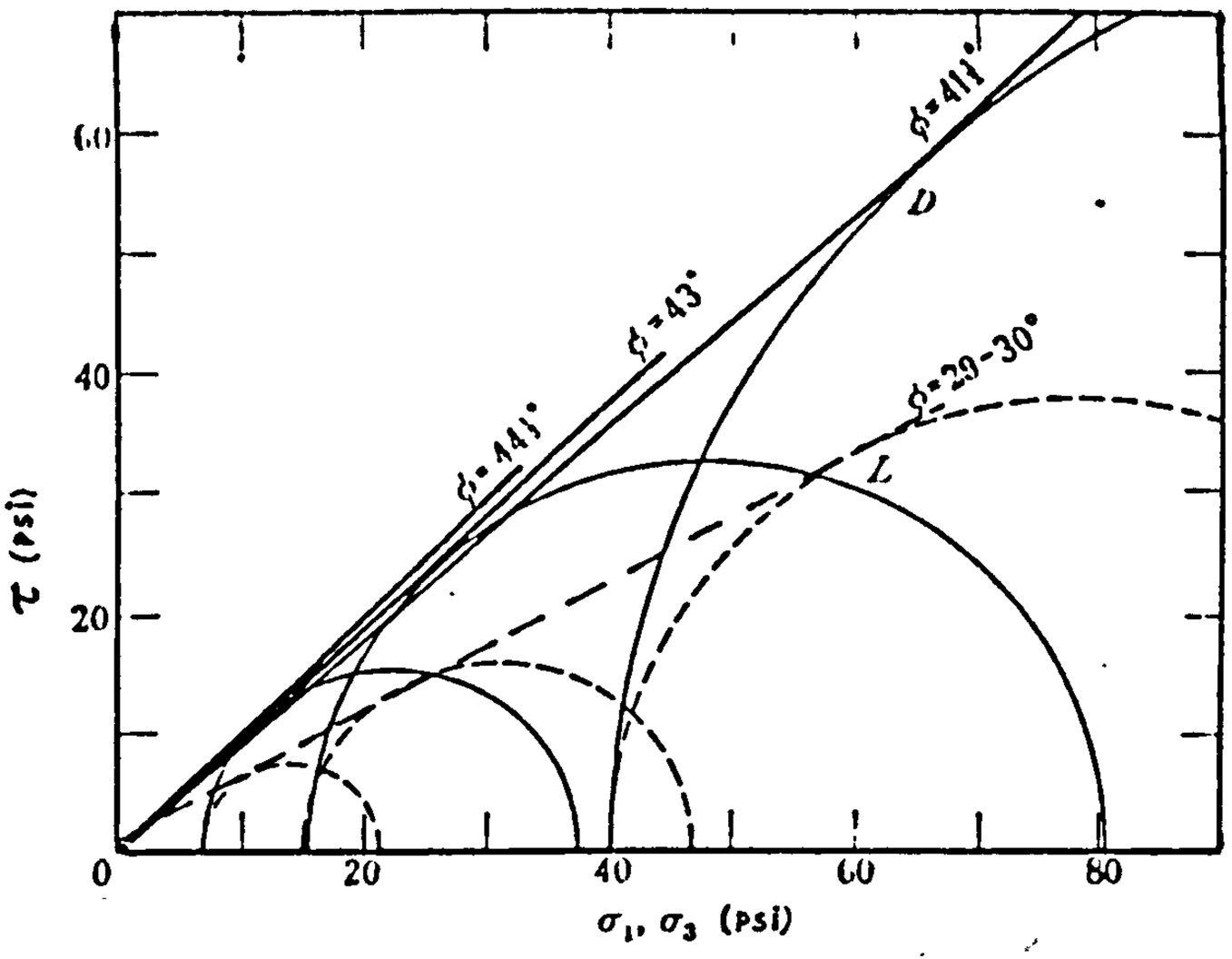

Fig. 3.5 - Fine sand, ϕ_μ= 28 degrees. D, dense state; relative porosity = 0.9. L, loose state; relative porosity = 0.2. Adapted from Rowe (1962).

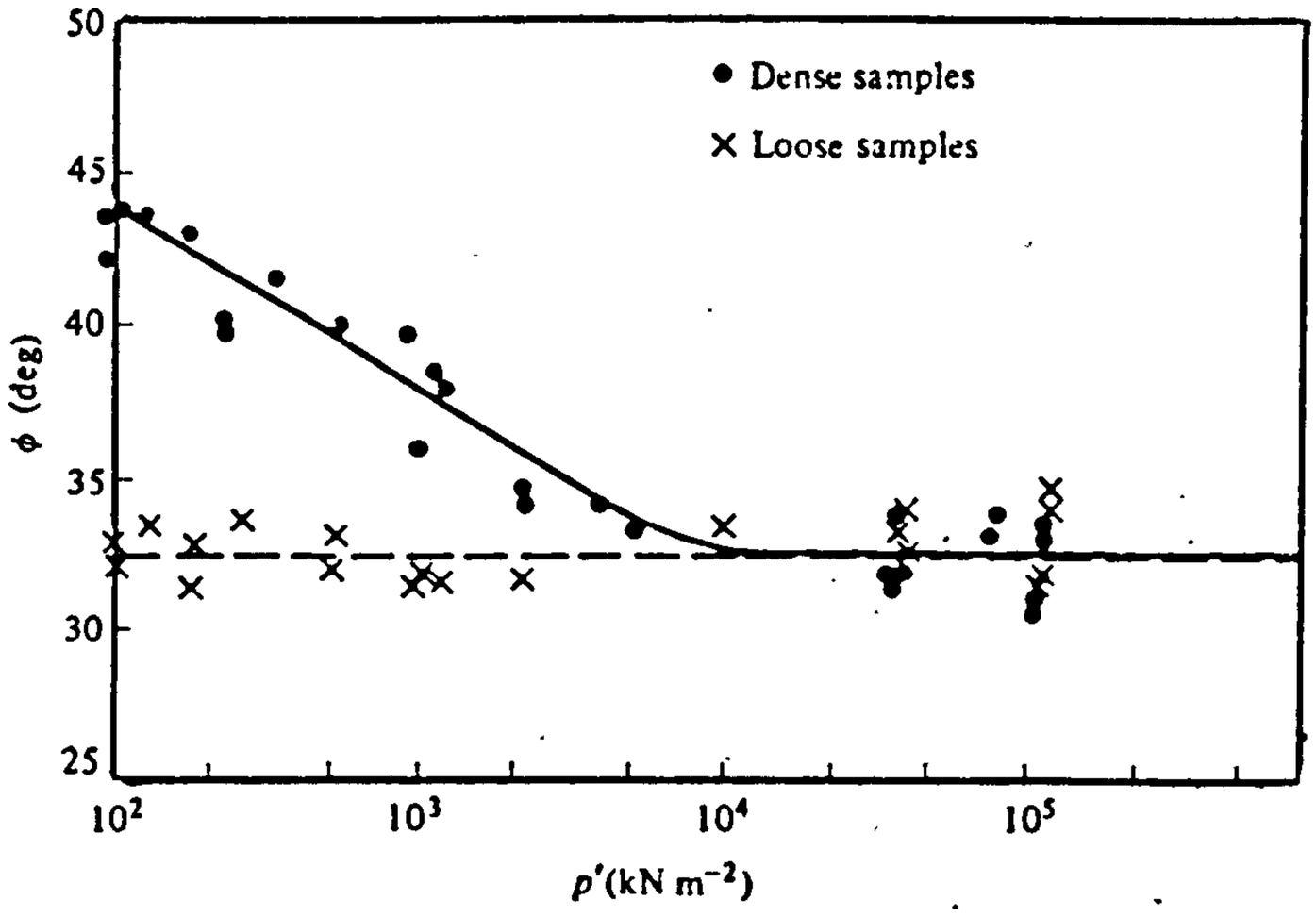

Fig. 3.6 - Angle of internal friction for Chattahoochee River sand tested at different stress levels in triaxal apparatus (after Vesic and Clough, 1968).

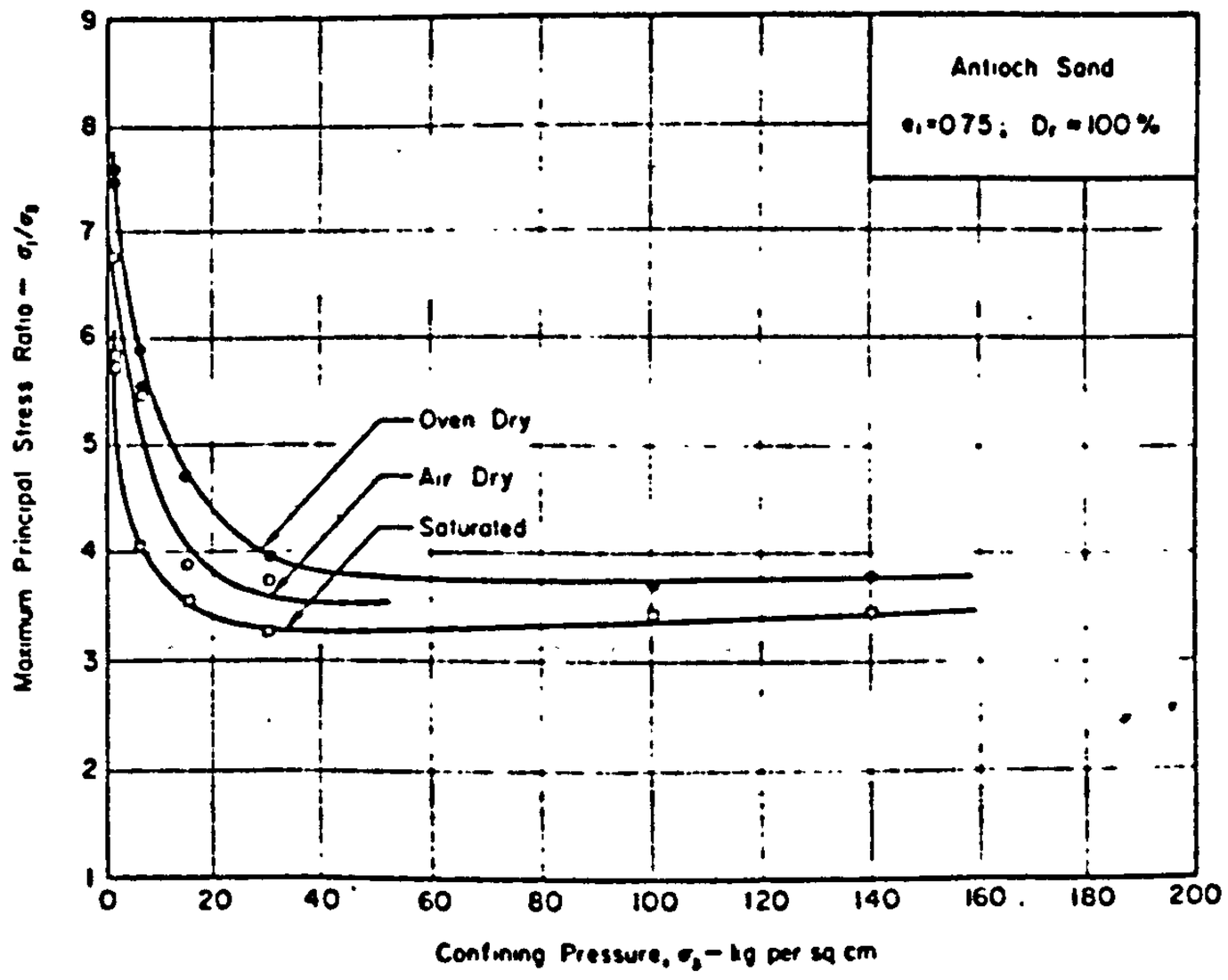

Fig. 3.7 - Drained strength of dense Antioch sand at various moisture conditions (after Lee et al, 1967).

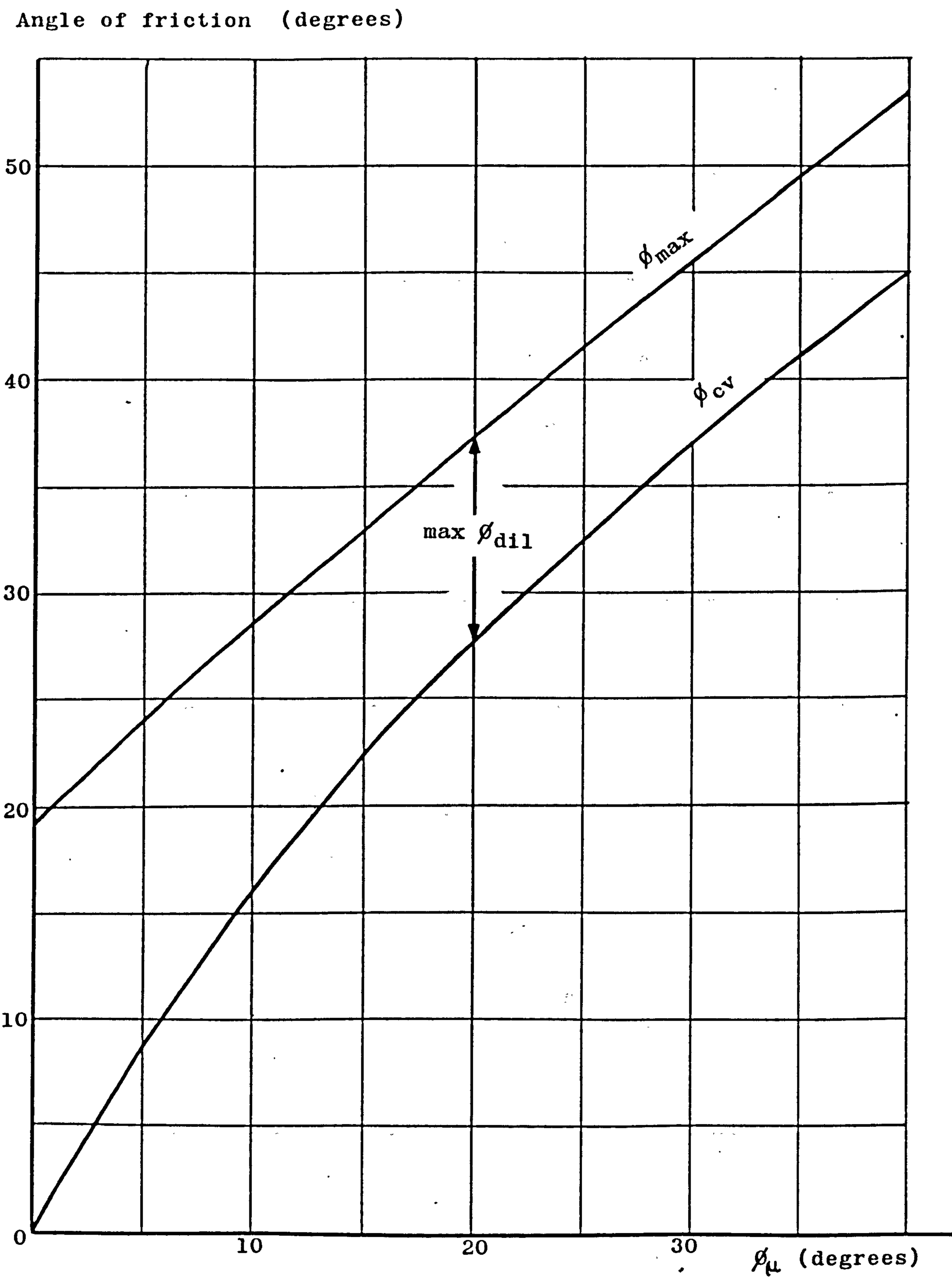

Fig. 3.8 - Angle of friction of a very dense specimen tested in triaxial compression at low confining pressure, ϕ_{max}, and angle of friction at the Critical State, ϕ_{cv}, as a function of the angle of interparticle friction, ϕ_μ .

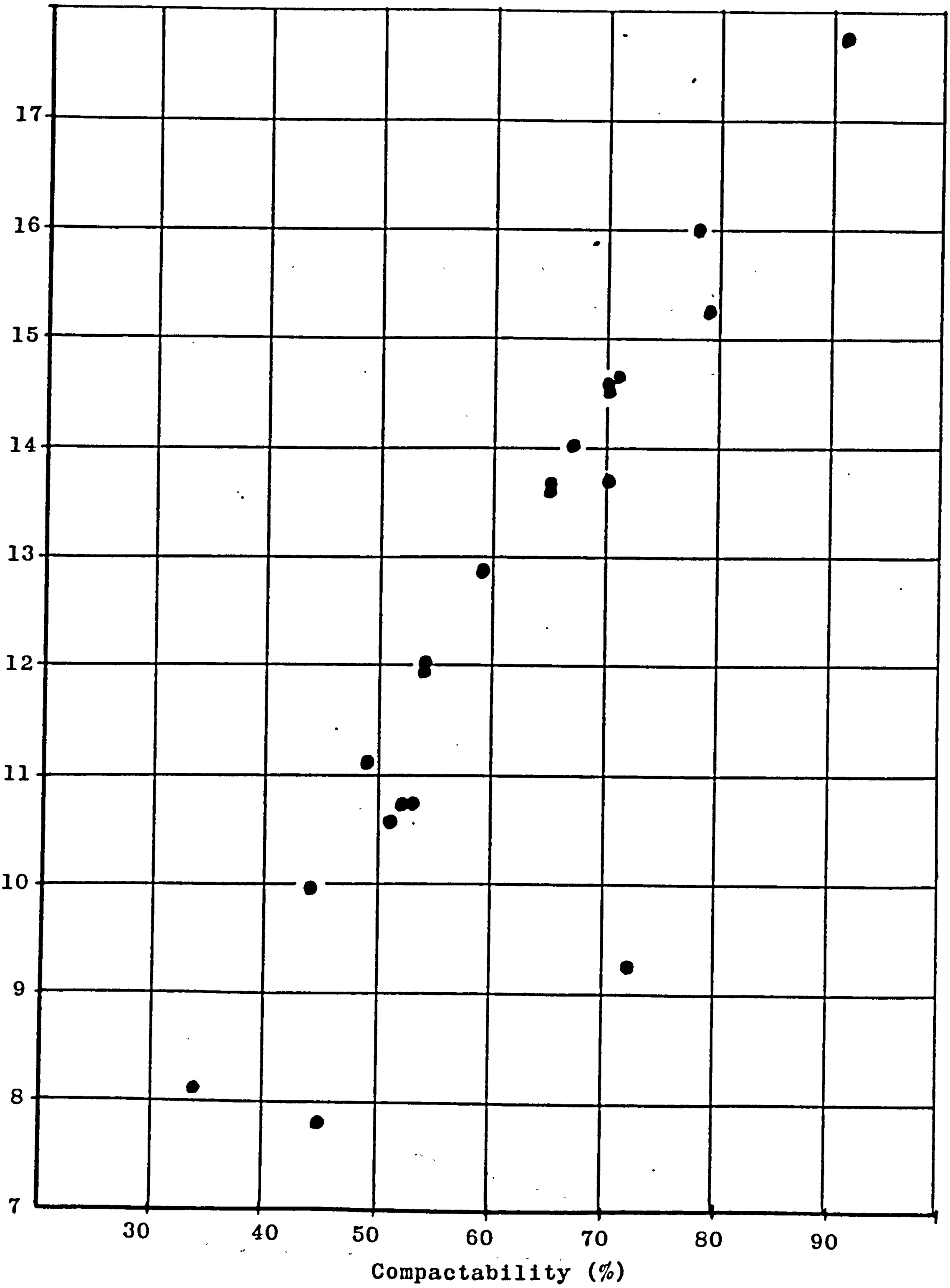

Fig. 3.9 - $\phi_{max} - \phi_{cv}$ versus compactability for dry sand from results published by Melzer (1973).

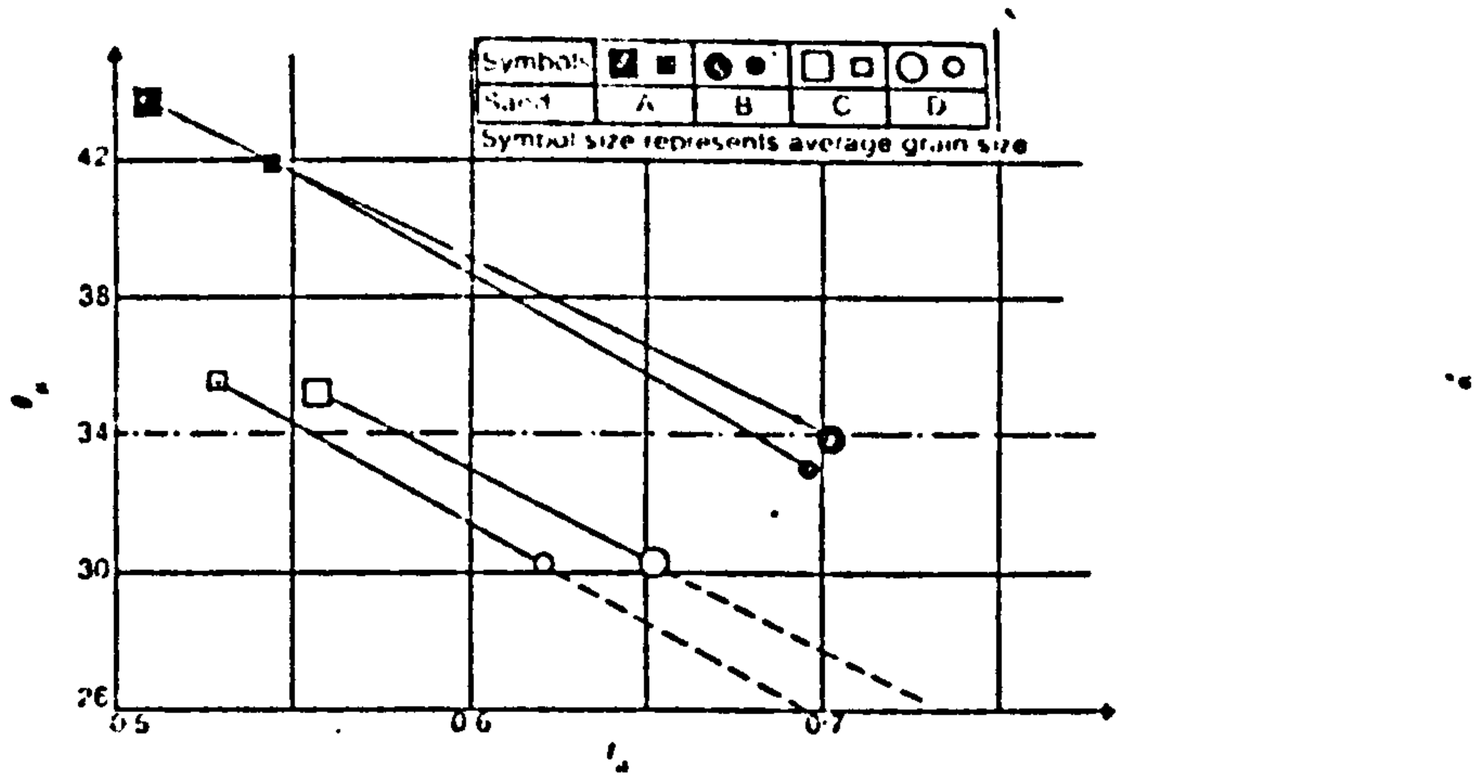

Fig. 3.10 - Relation between the angle of interparticle friction and the asperity index I_a according to Frossard (1979). Close symbols: calcareous sands ; open symbols: quartz sands.

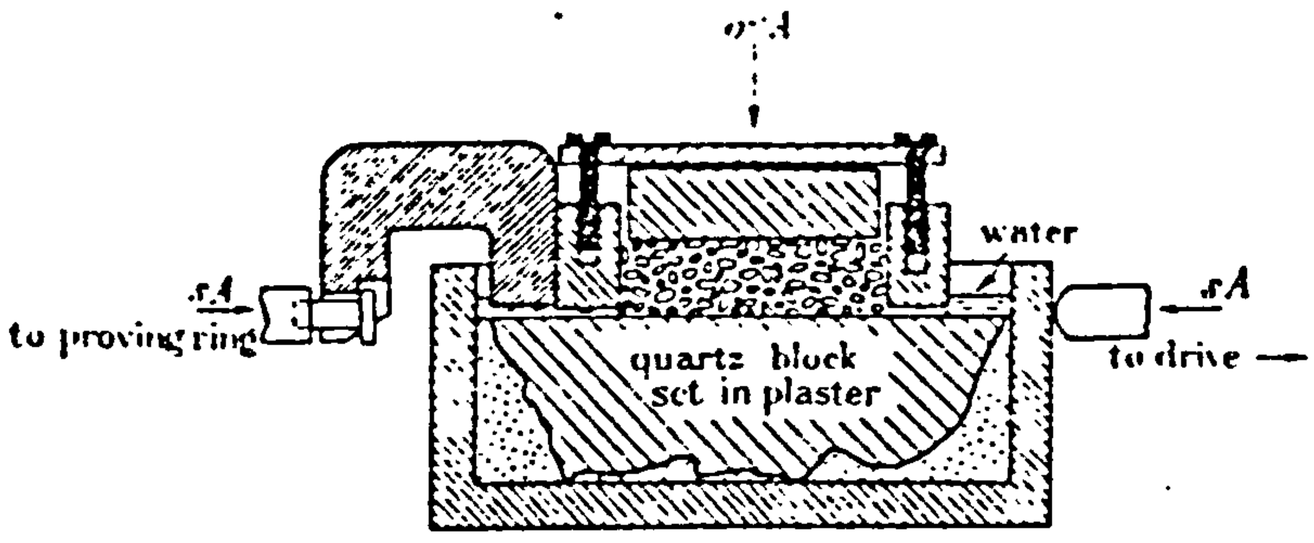

Standard shear box modified to record particle friction.

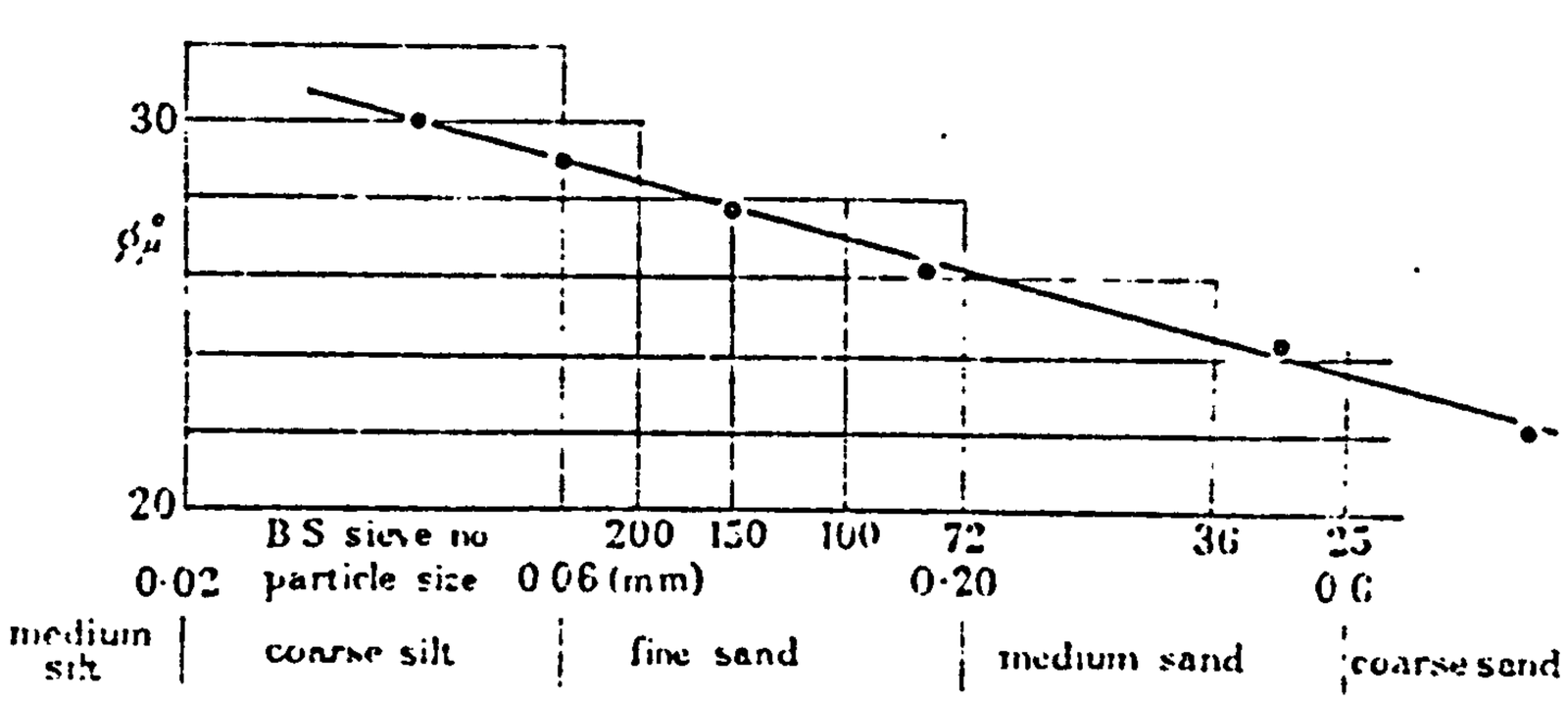

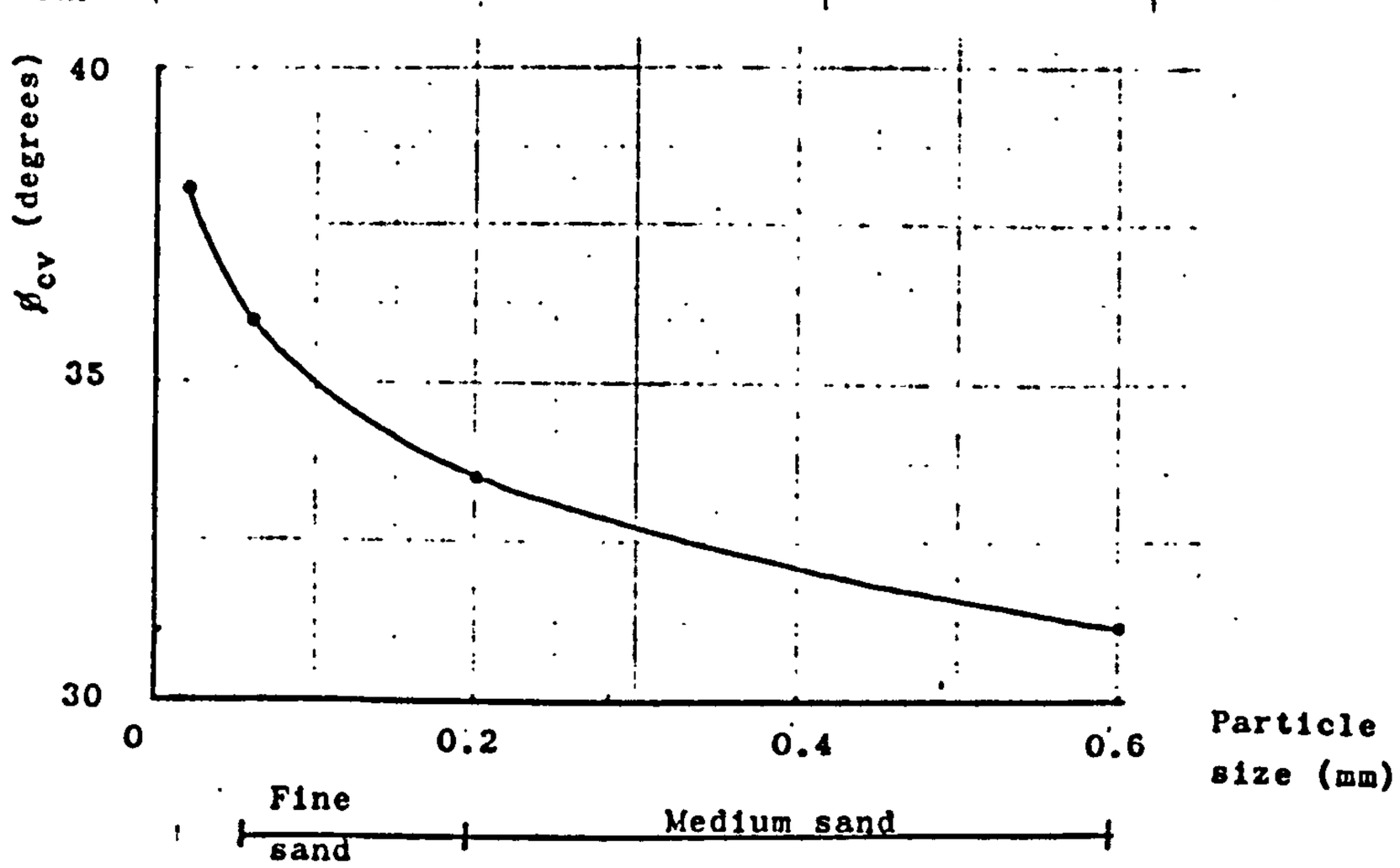

Fig. 3.11 - The influence of particle size on the angle of interparticle friction after Rowe (1962).

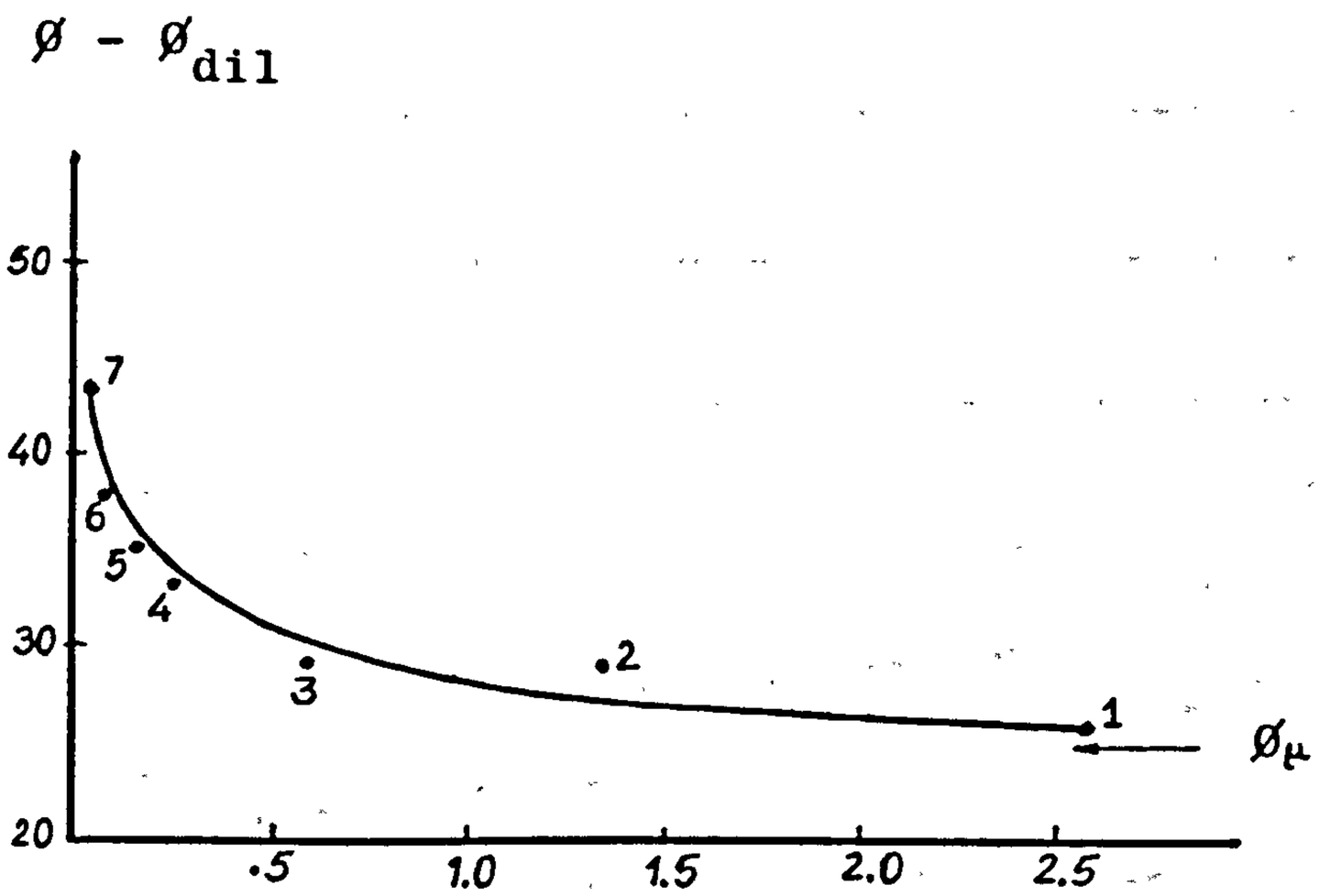

Sand No.	d_{10} (mm)	C_u	v_{min}	v_{max}	Angularity	Sphericity	Compactability	Soil type
1	2.6	1.31	1.633	2.118	Angular	0.48	76.6	Fine gravel
2	1.35	1.22	1.680	2.060	"	0.47	55.9	Coarse sand
3	0.59	1.27	1.773	2.218	"	0.52	57.6	Medium sand
4	0.25	1.25	1.594	1.919	Subangular	0.58	54.7	Medium sand
5	0.15	1.25	1.639	2.146	"	0.51	79.3	Fine sand
6	0.074	1.25	1.709	2.350	"	0.49	90.4	Fine sand
7	0.037	1.25	1.754	2.458	"	0.49	93.4	Coarse silt

Fig. 3.12 - The effect of particle size on the angle of friction corrected for the dilation component, after Koerner (1970b).

LB - Leighton Buzzard ; BP - Bayou Pierre ; C - Cresswell ; MB - Mix B

M - Mortar ; Y - Yuma ; S - Solway

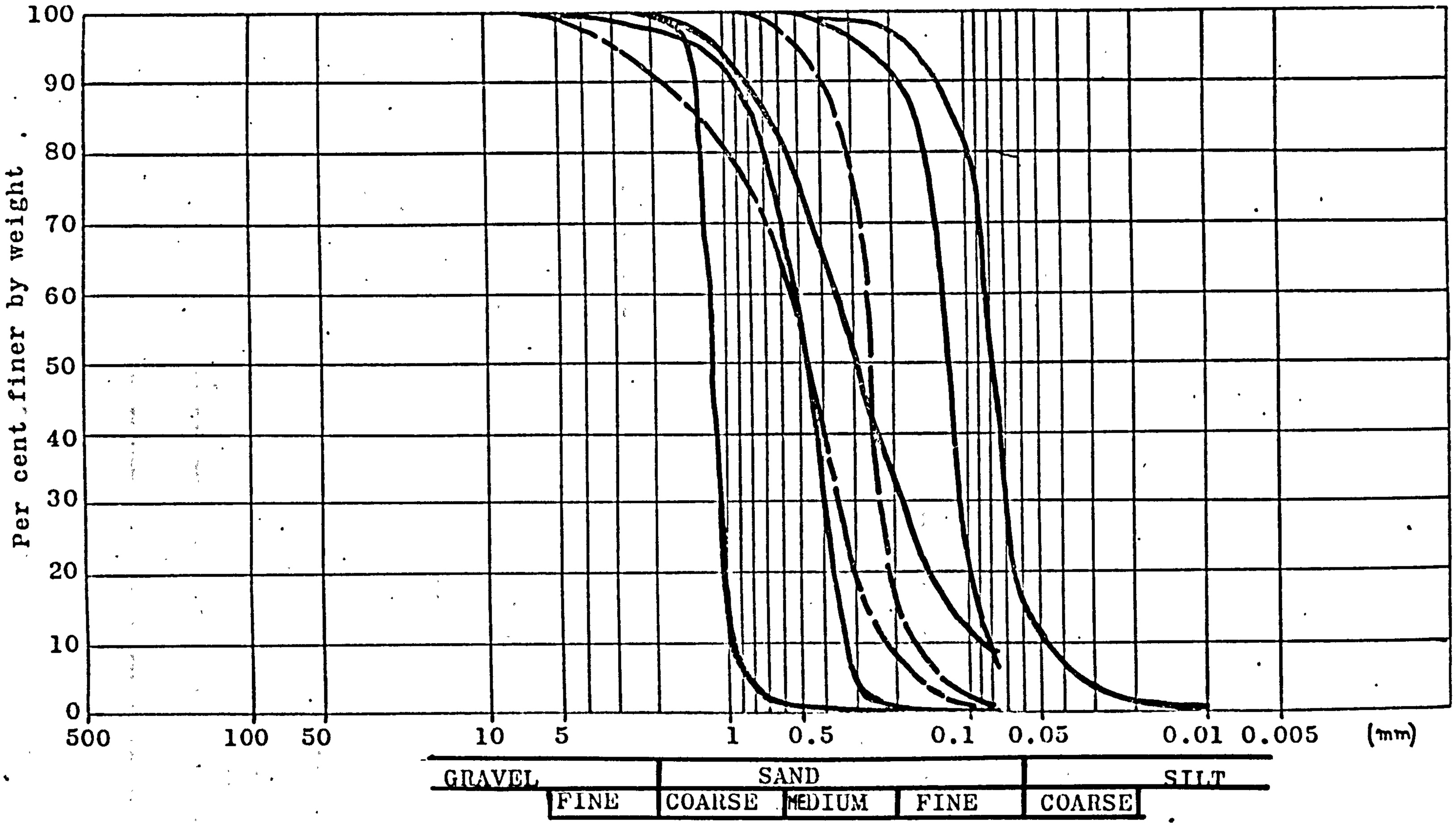

Fig. 3.13 - Particle size distribution chart

(a)

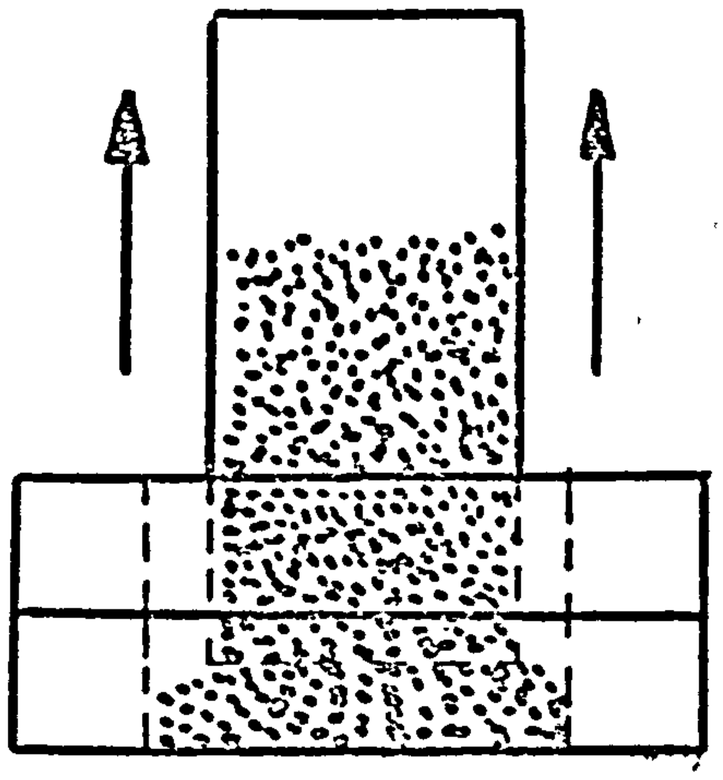

	D_d(%)
LB	27 - 38
C	23.4
MB	18
S	39

(b)

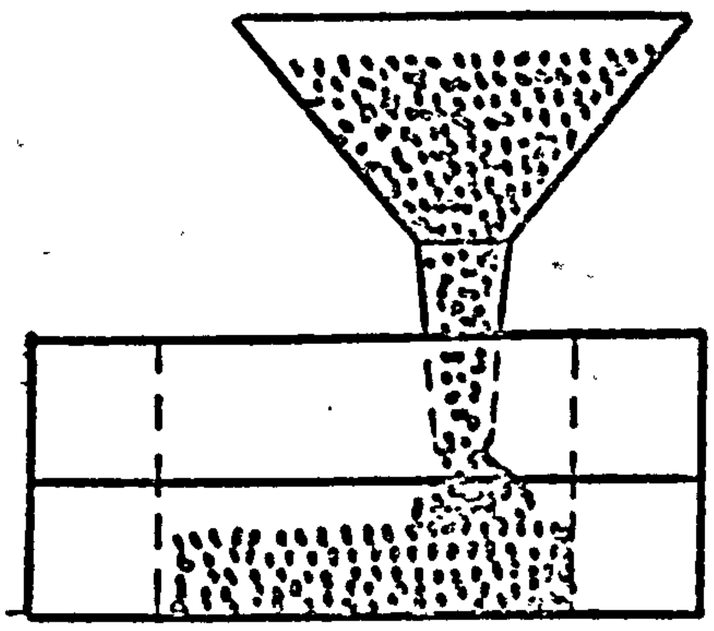

	D_d (%)
LB	69
C	80
MB	61.4
S	81.2

(c)

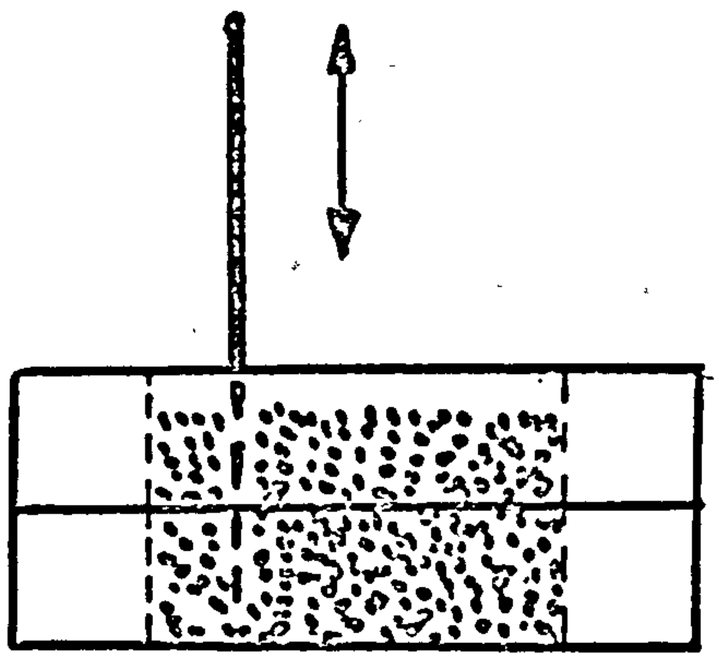

	D_d(%)
LB	80
MB	99

(d)

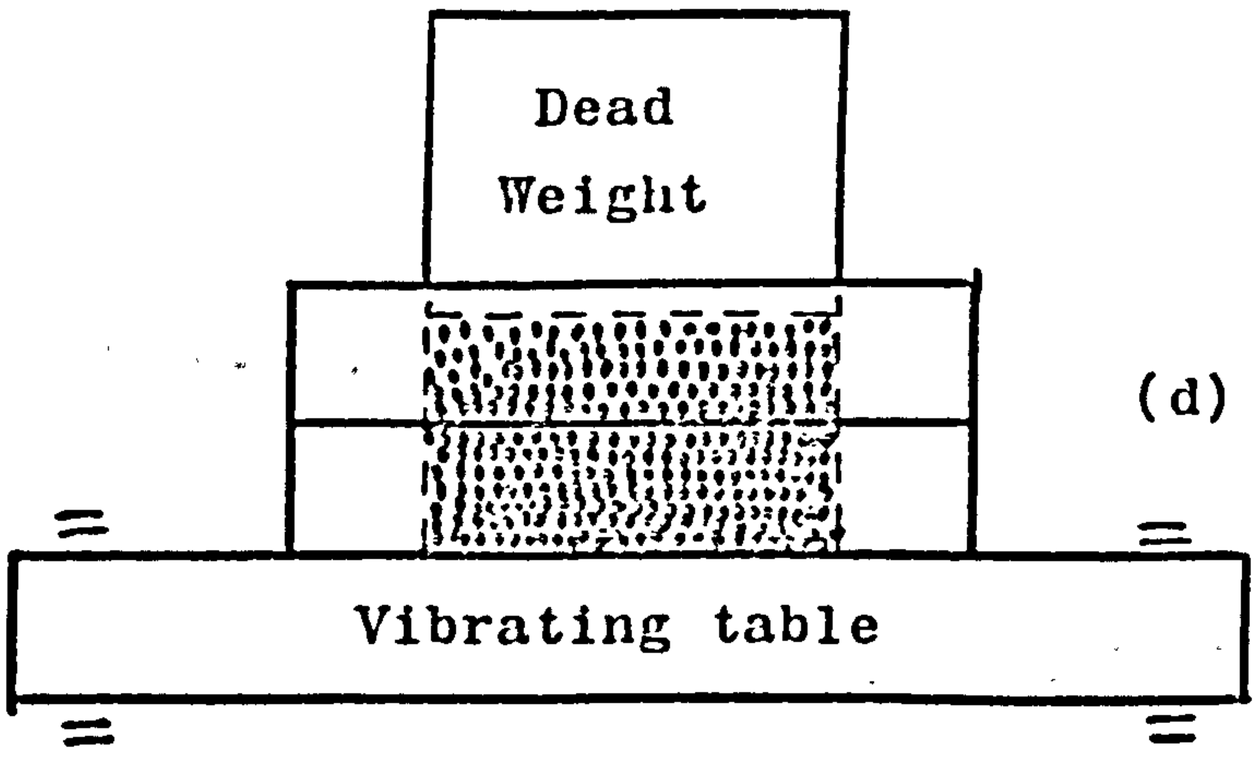

LB - D_d= -3%

Fig. 3.14 - Processing techniques used in Shear Box tests.

Symbols: LB - Leighton Buzzard ; MB - Mix B

C - Cresswell ; S - Solway.

D_d - Relative density.

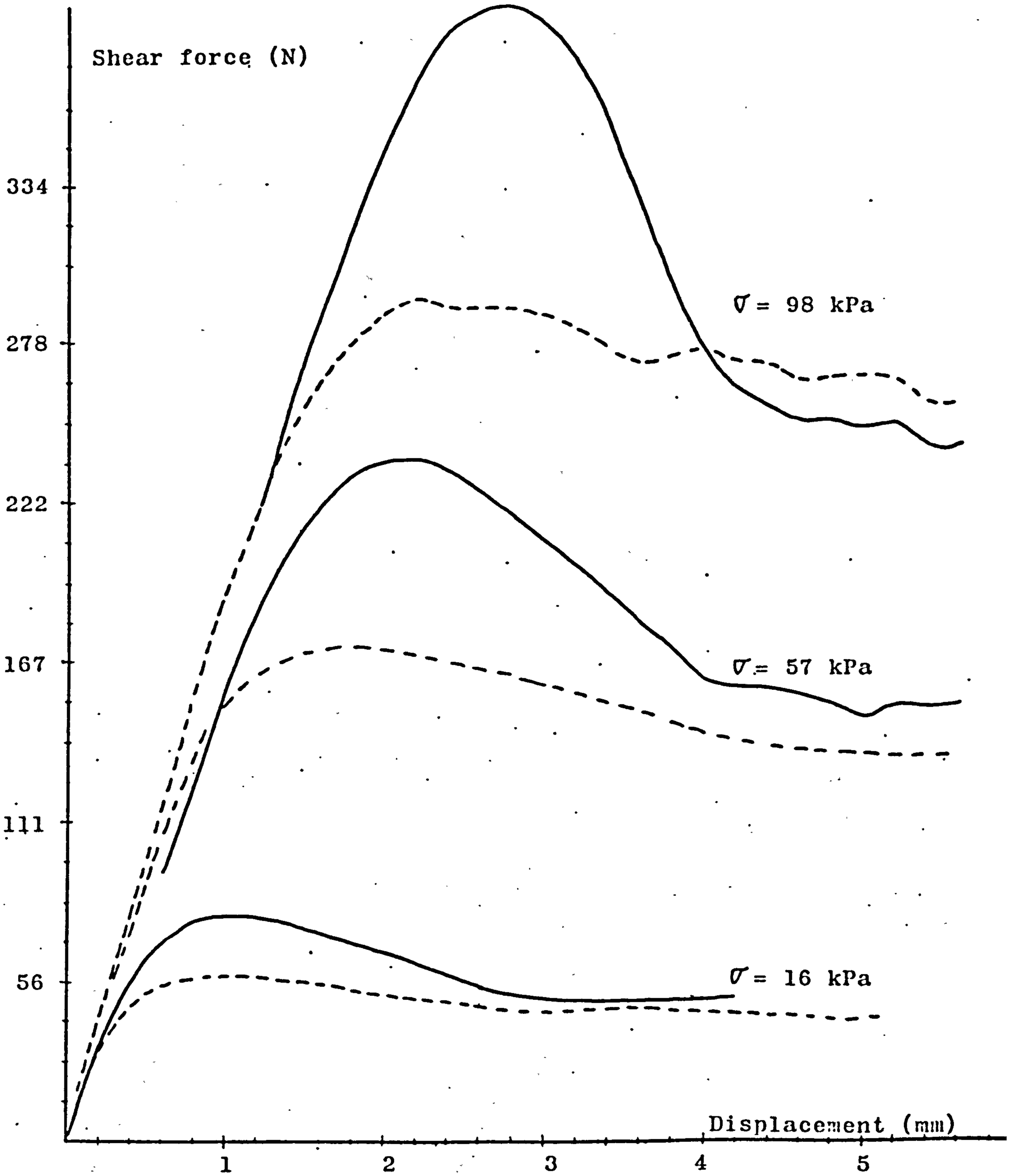

Fig. 3.15 - Direct Shear tests in air-dry Cresswell sand.
Comparison between processing techniques.
--- γ = 16.40 kN/m^3 (tapping) ; — γ = 16.48 kN/m^3 (prodding as in fig. 3.14.c).

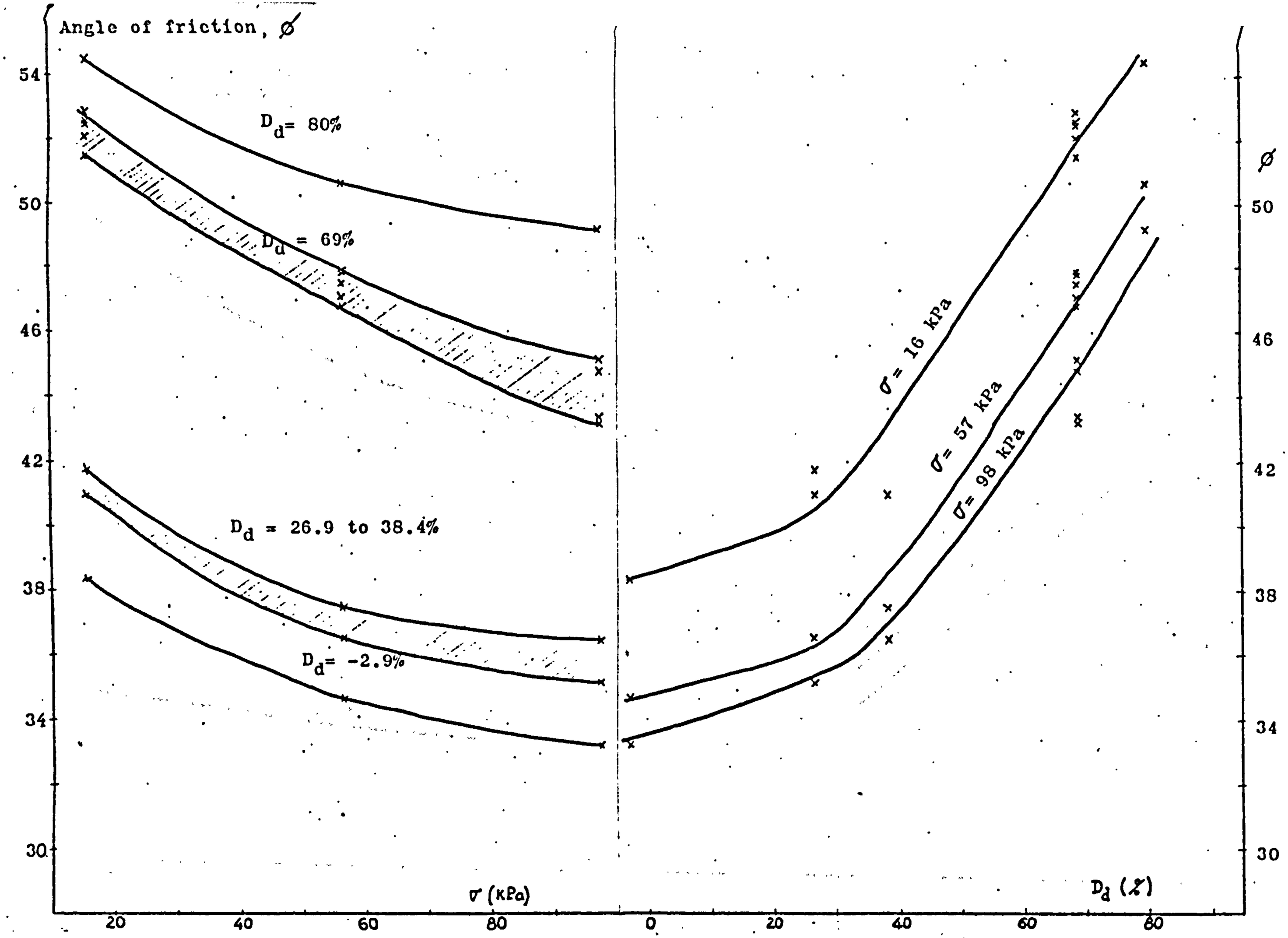

Fig. 3.16 - Angle of internal friction of air-dry LEIGHTON BUZZARD sand from direct shear tests.

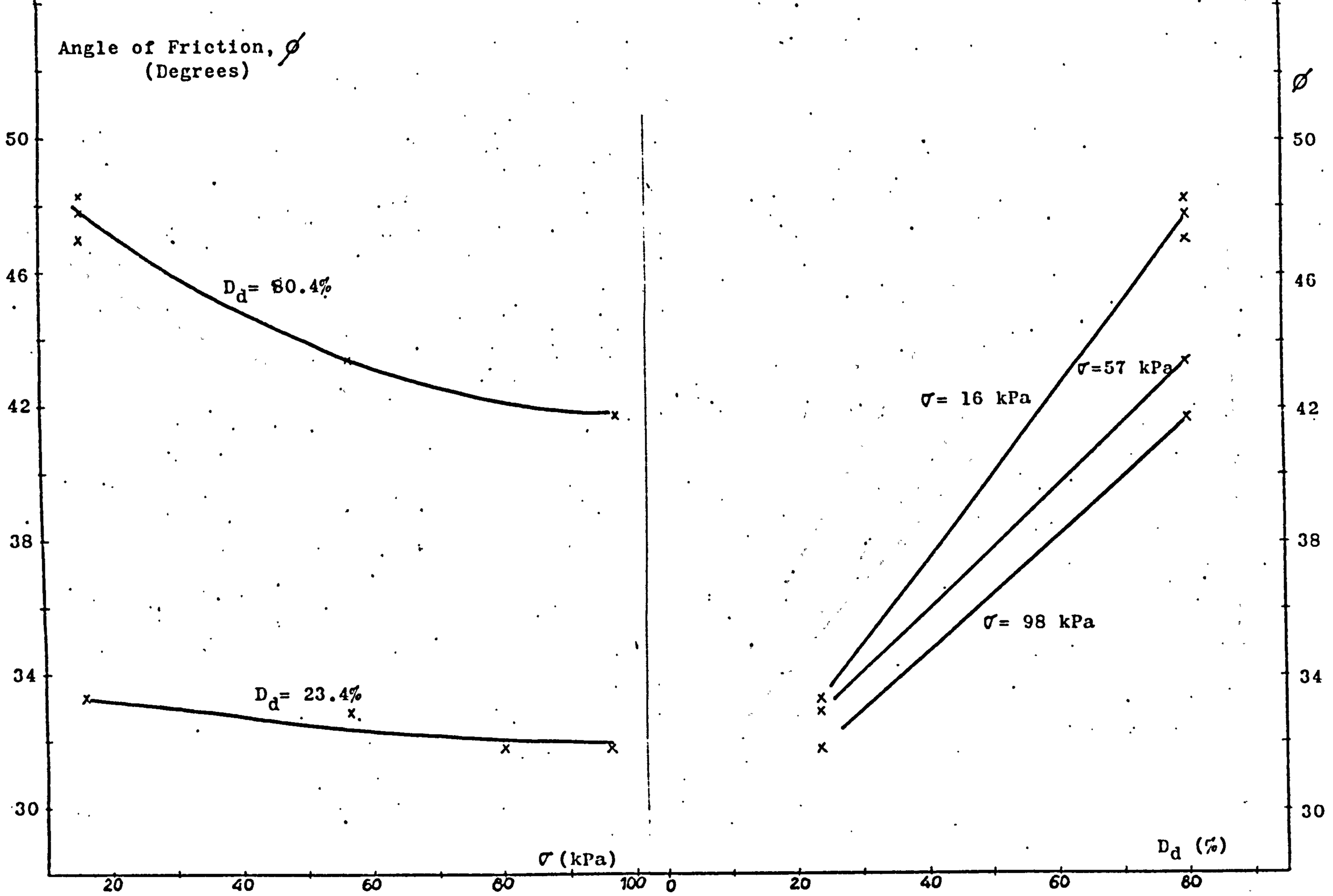

Fig.3.17 - Angle of internal friction of air-dry CRESSWELL sand from direct shear tests.

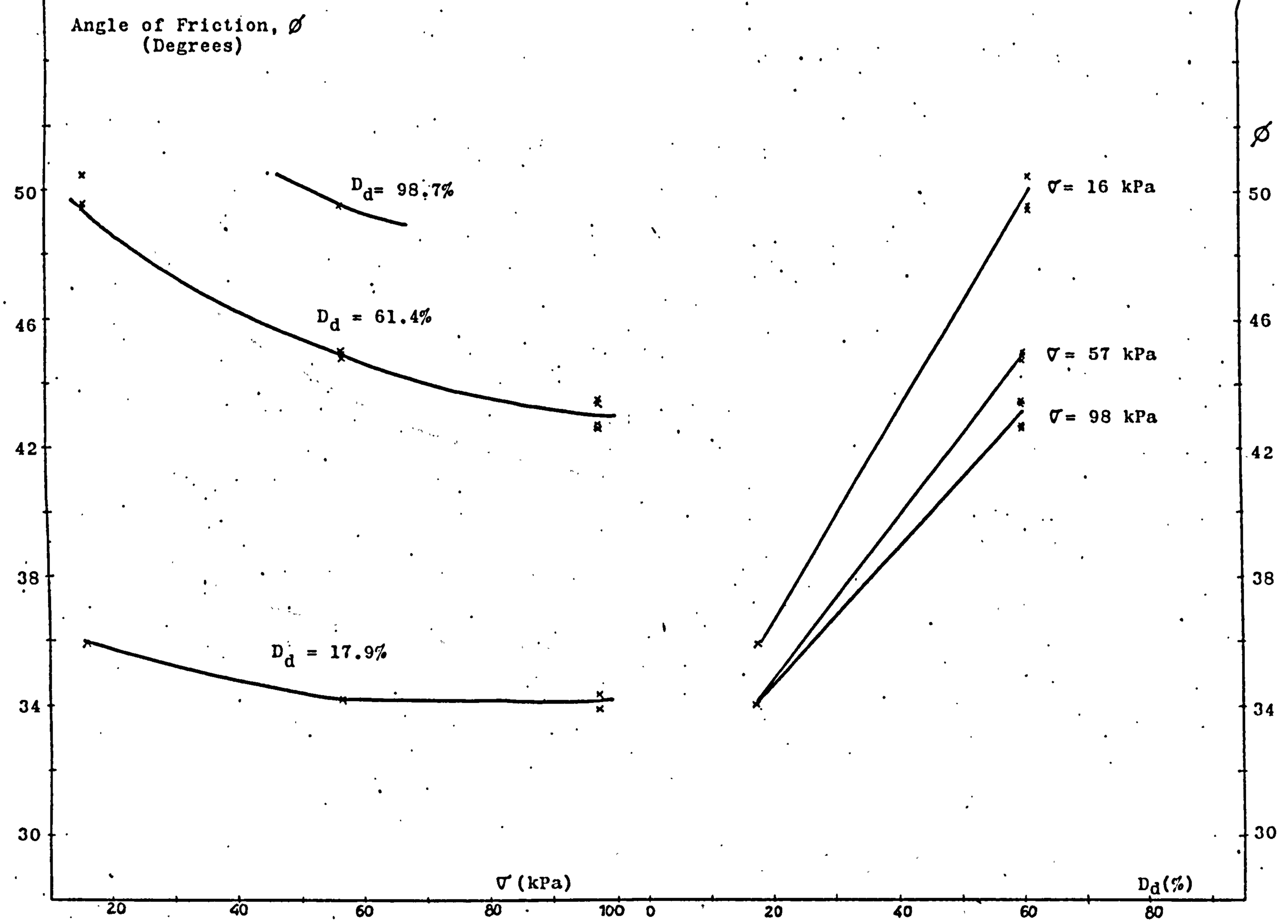

Fig. 3.18 - Angle of internal friction of air-dry MIX B sand from direct shear tests.

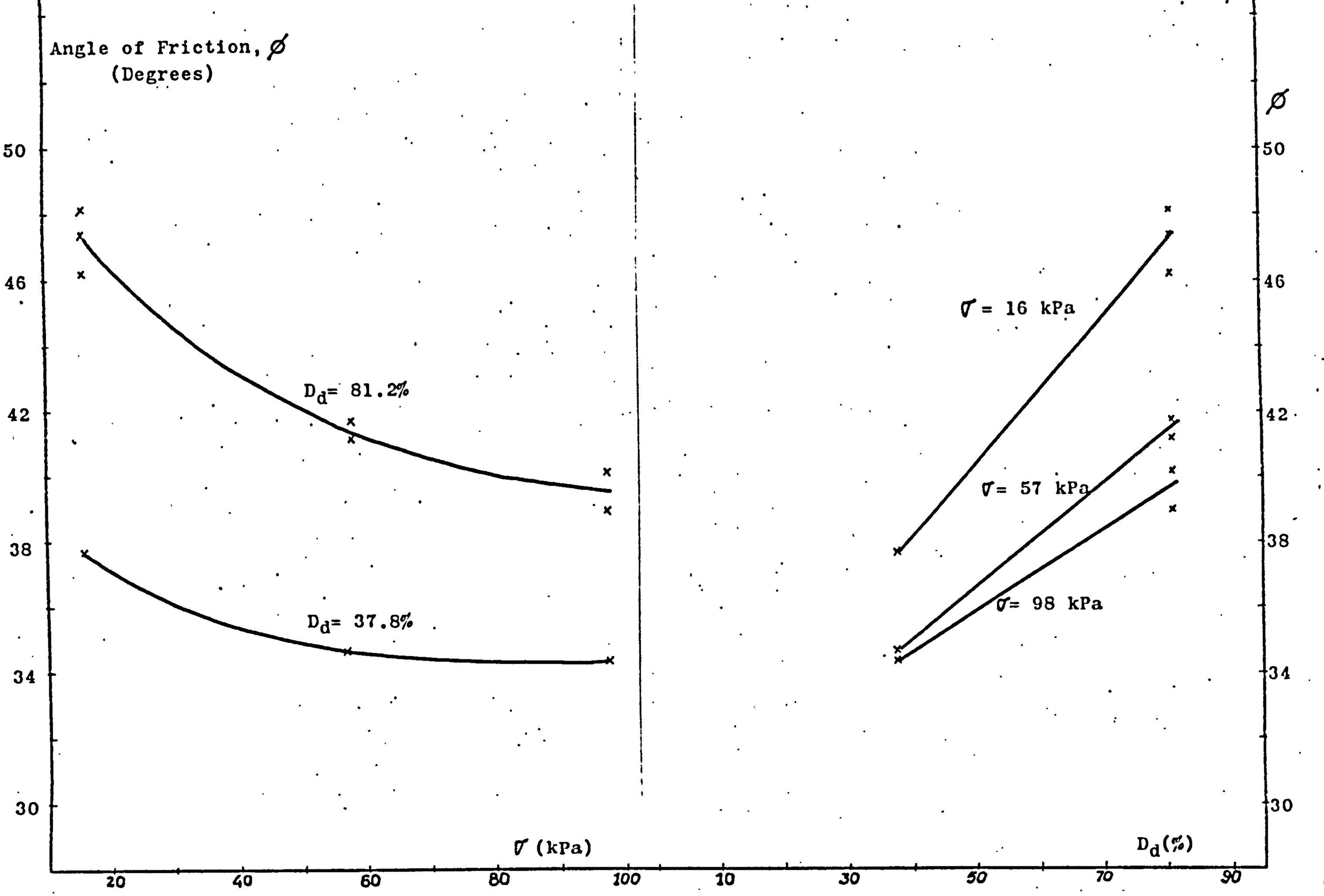

Fig.3.19 - Angle of internal friction of air-dry SOLWAY sand from direct shear tests.

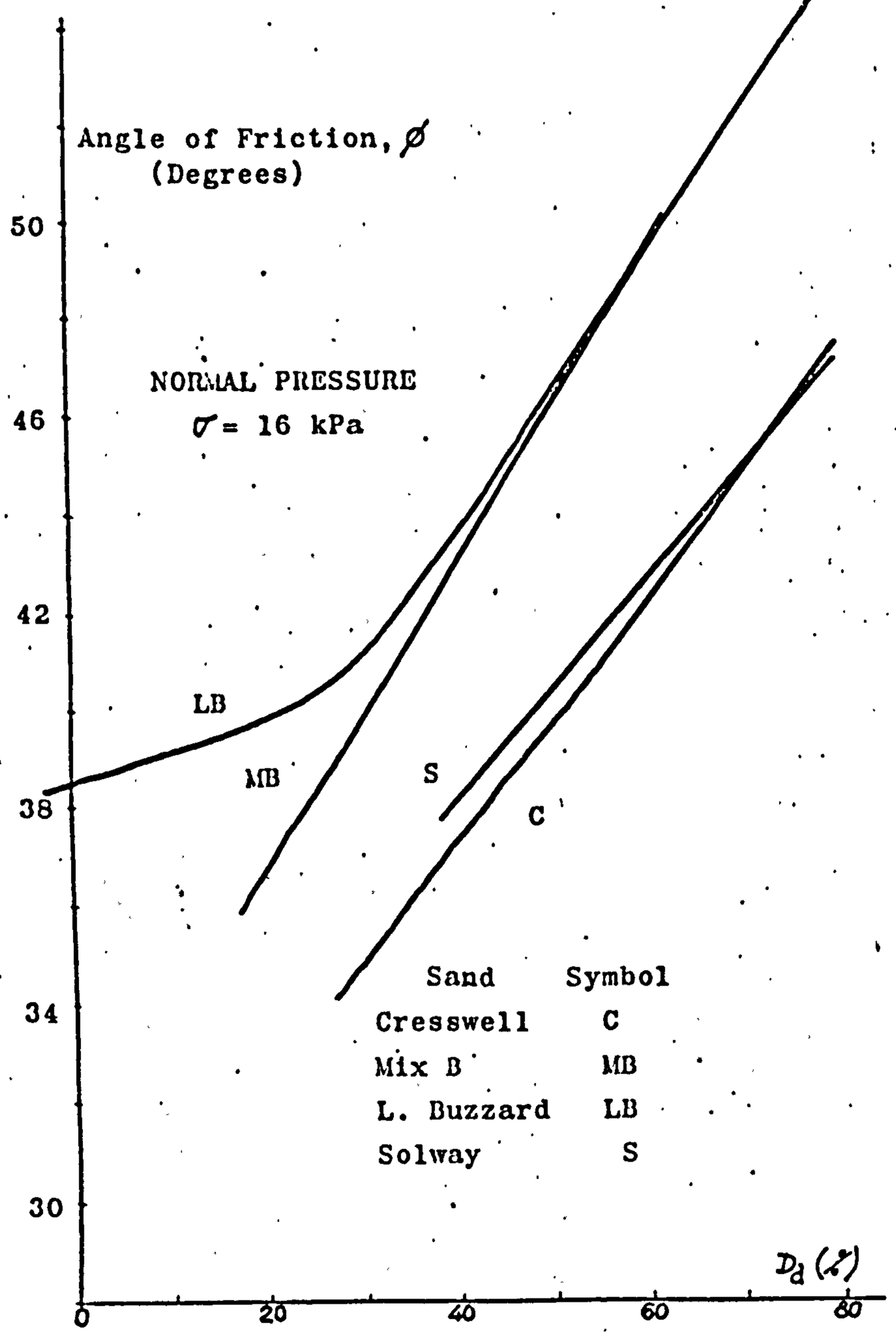

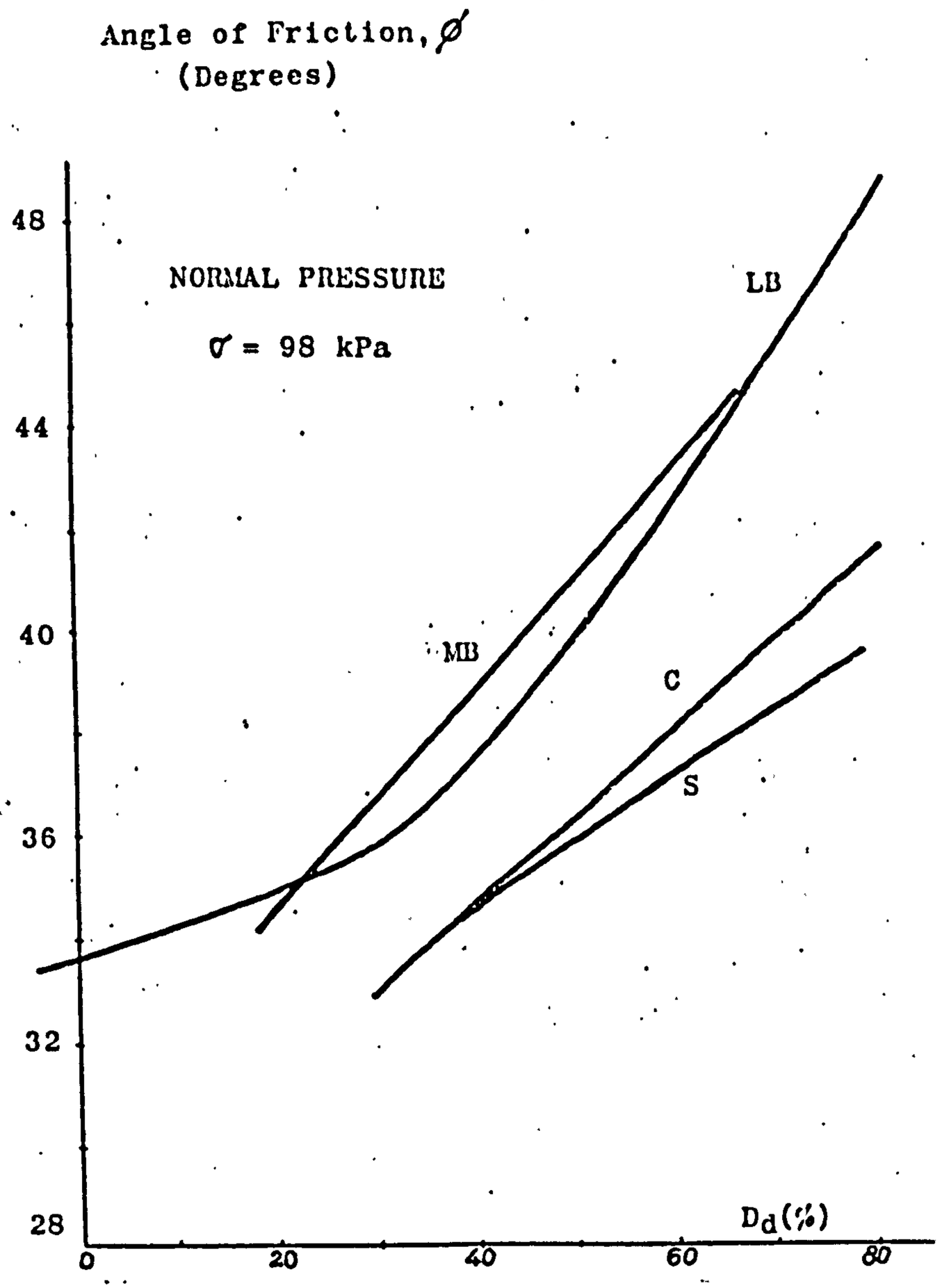

Fig. 3.20 - Angle of internal friction from direct shear tests for the four air-dry sands.

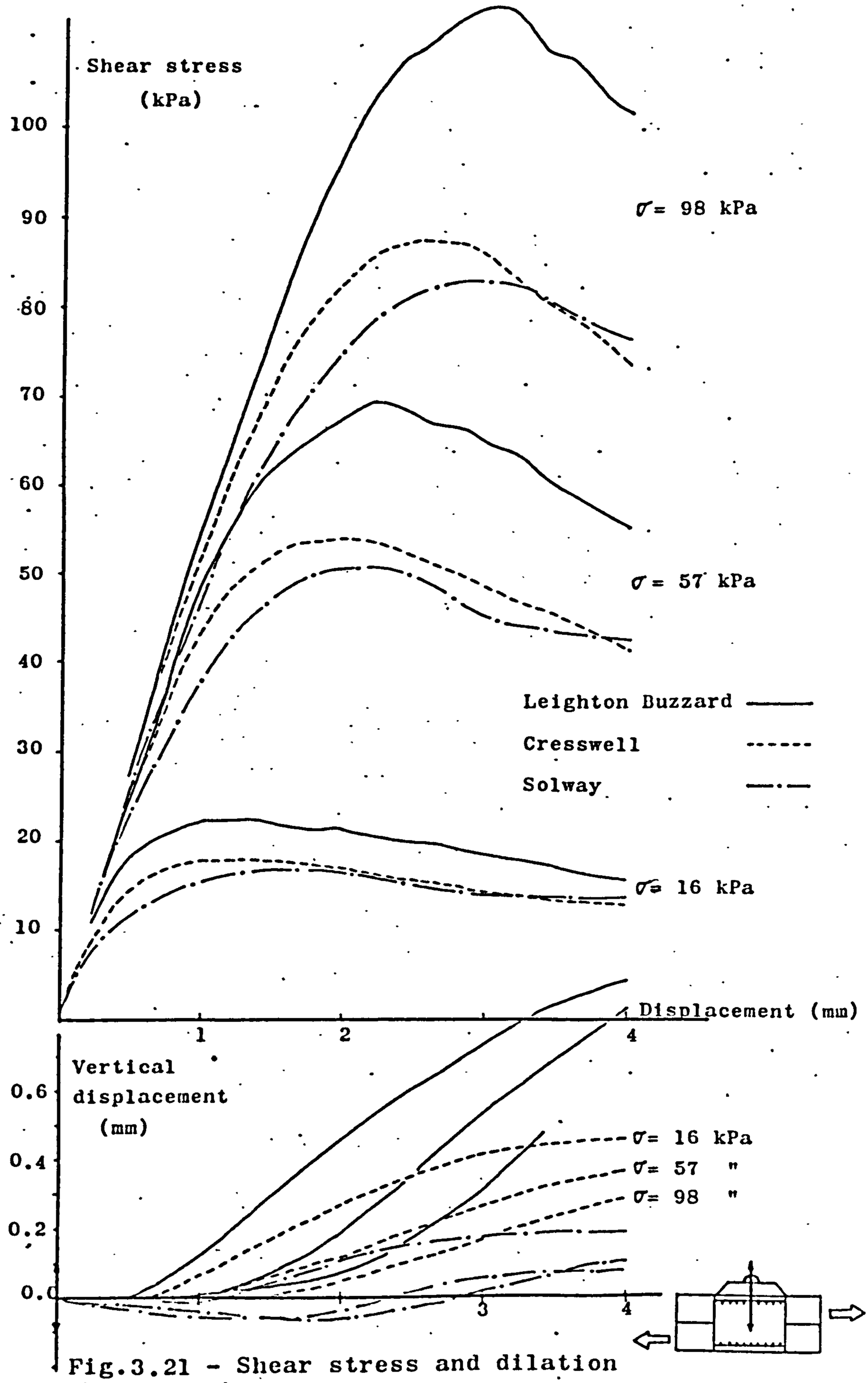

Fig.3.21 - Shear stress and dilation from direct shear tests in dense air-dry sand, D_d= 80%

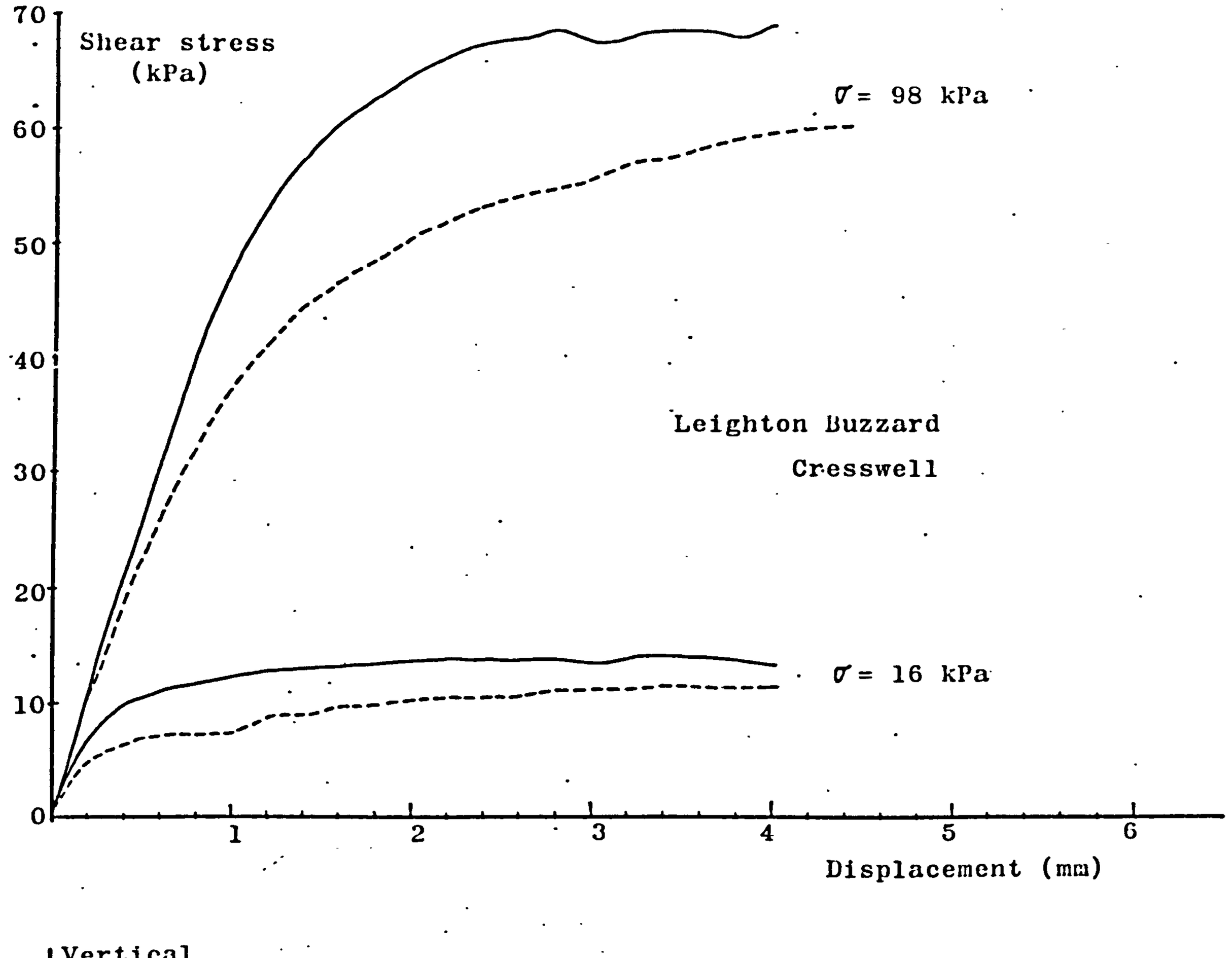

Fig.3.22 - Shear stress and dilation diagram from direct shear tests in air-dry loose sand, D_d = 25% .

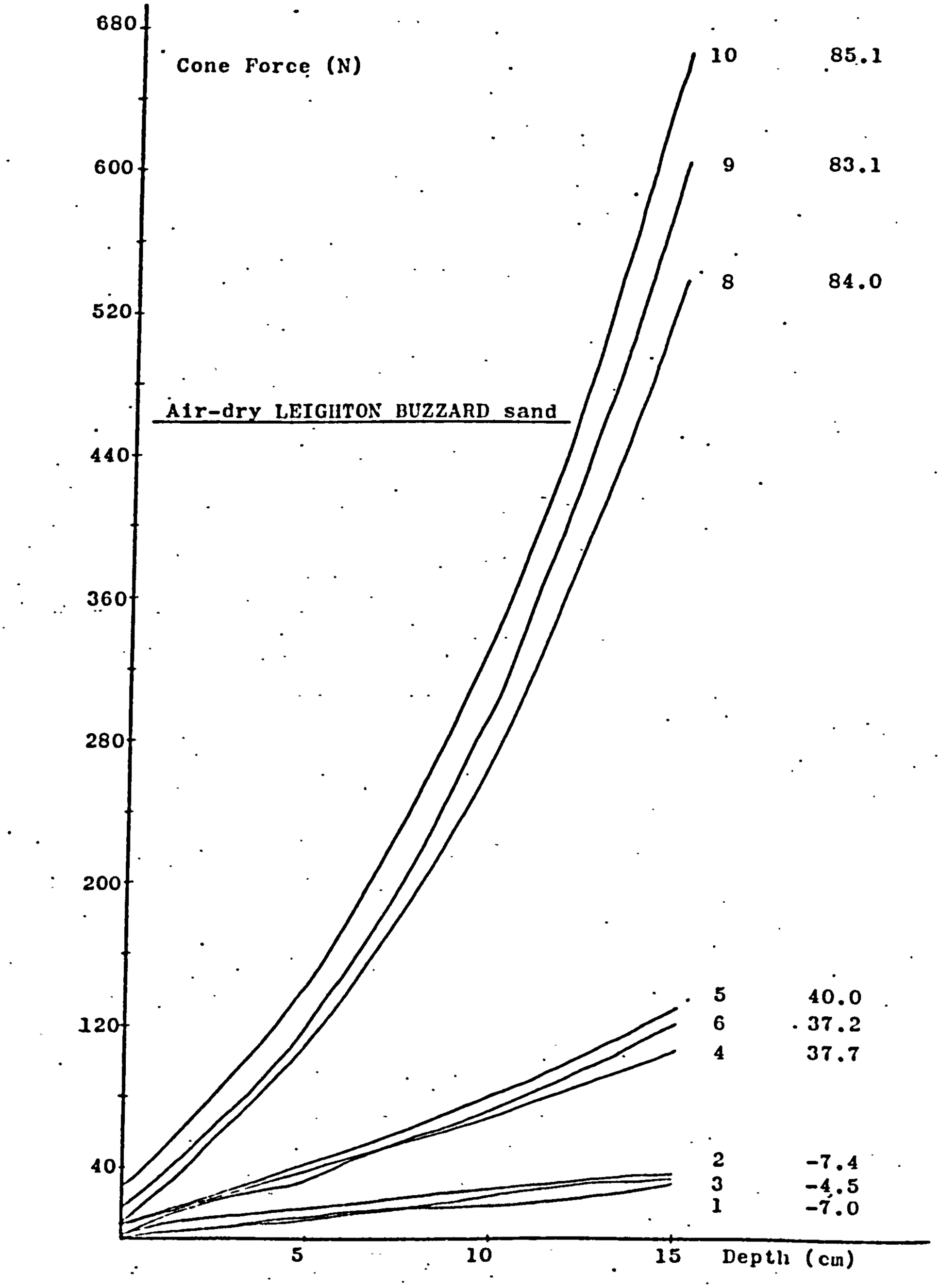

Fig. 4.1 - Cone force /depth diagram for air-dry LEIGHTON BUZZARD sand

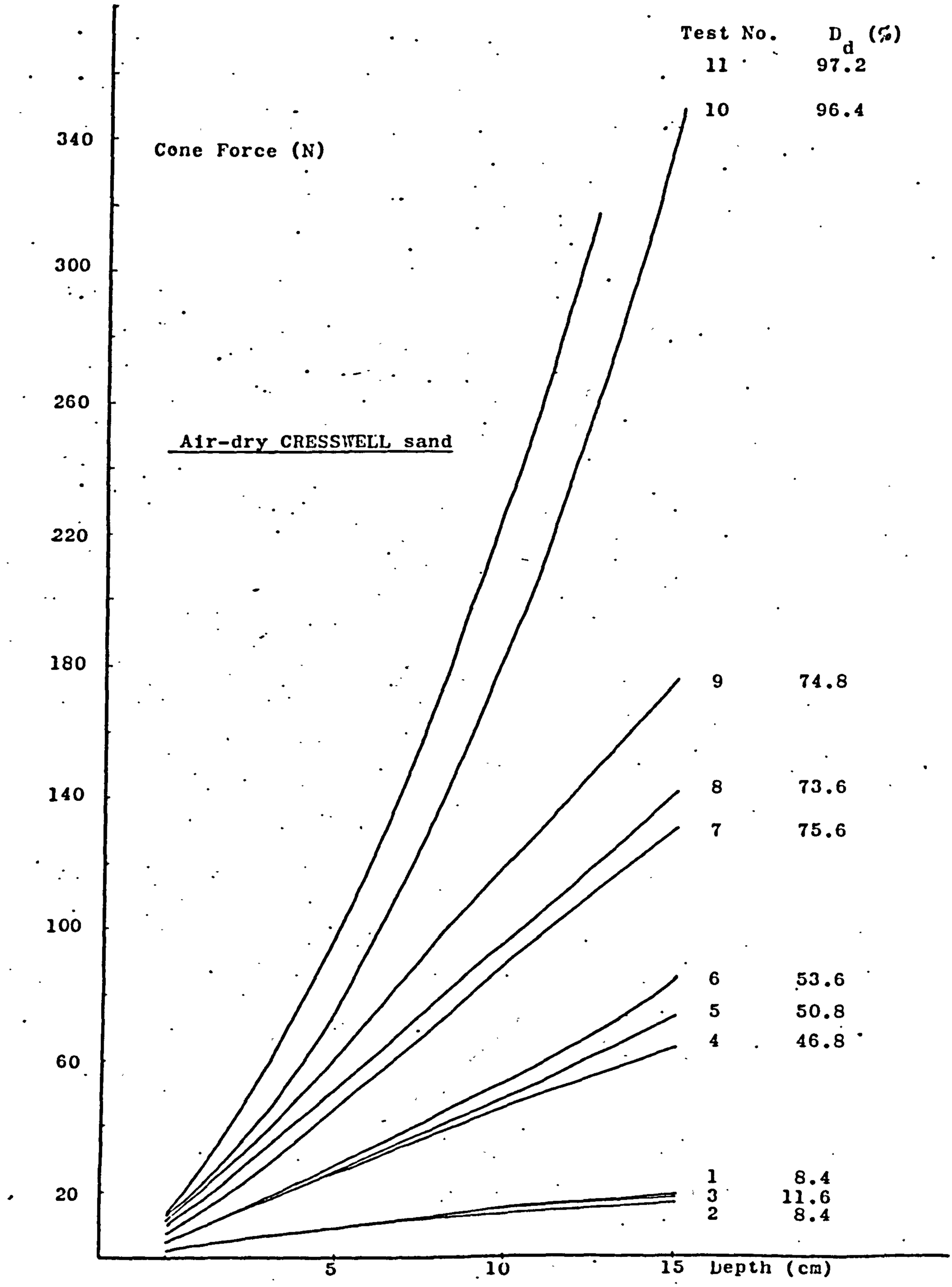

Fig. 4.2 - Cone force / depth diagram for air-dry CRESSWELL sand.

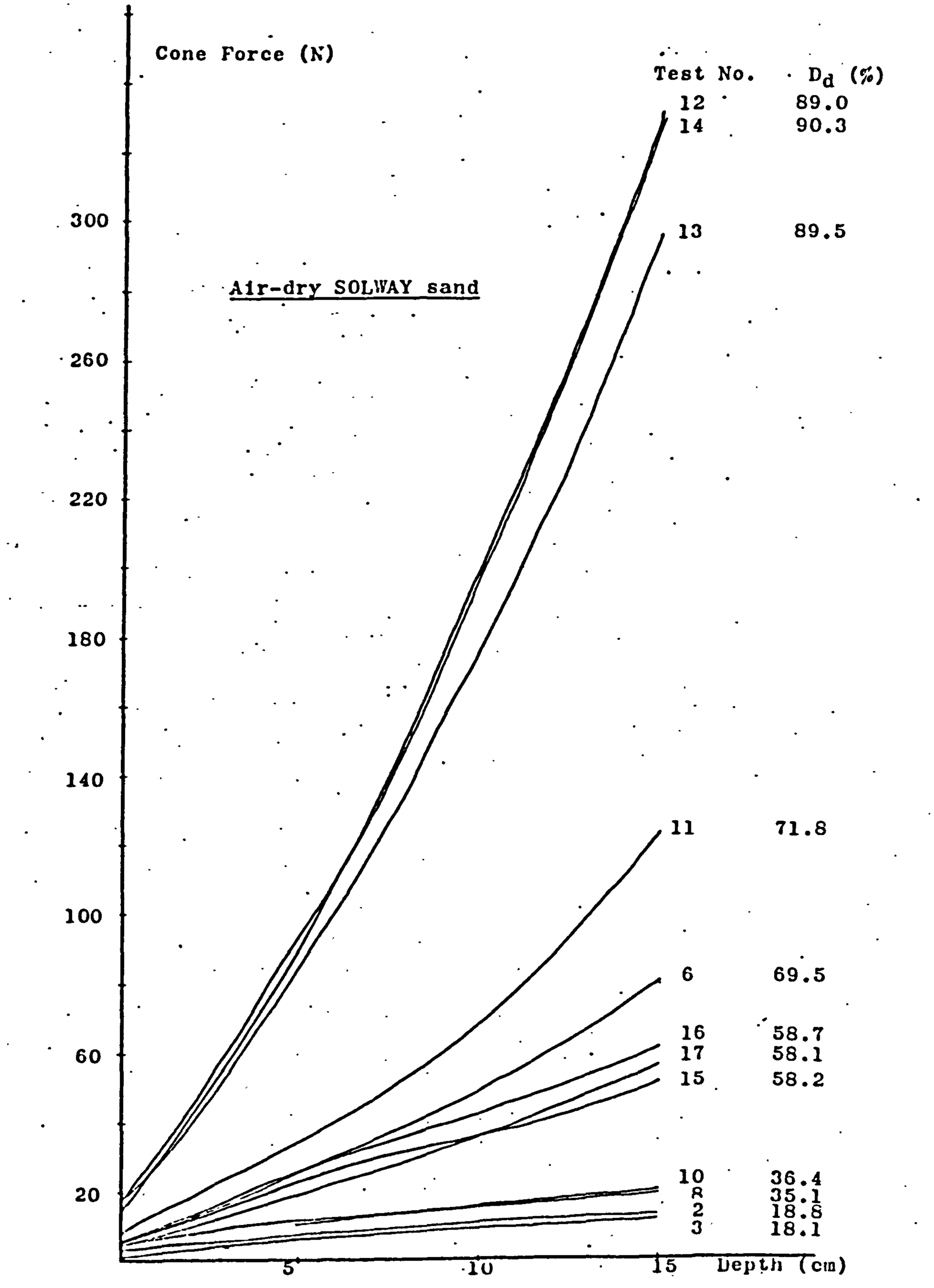

Fig. 4.3 - Cone force/depth diagram for air-dry SOLWAY sand.

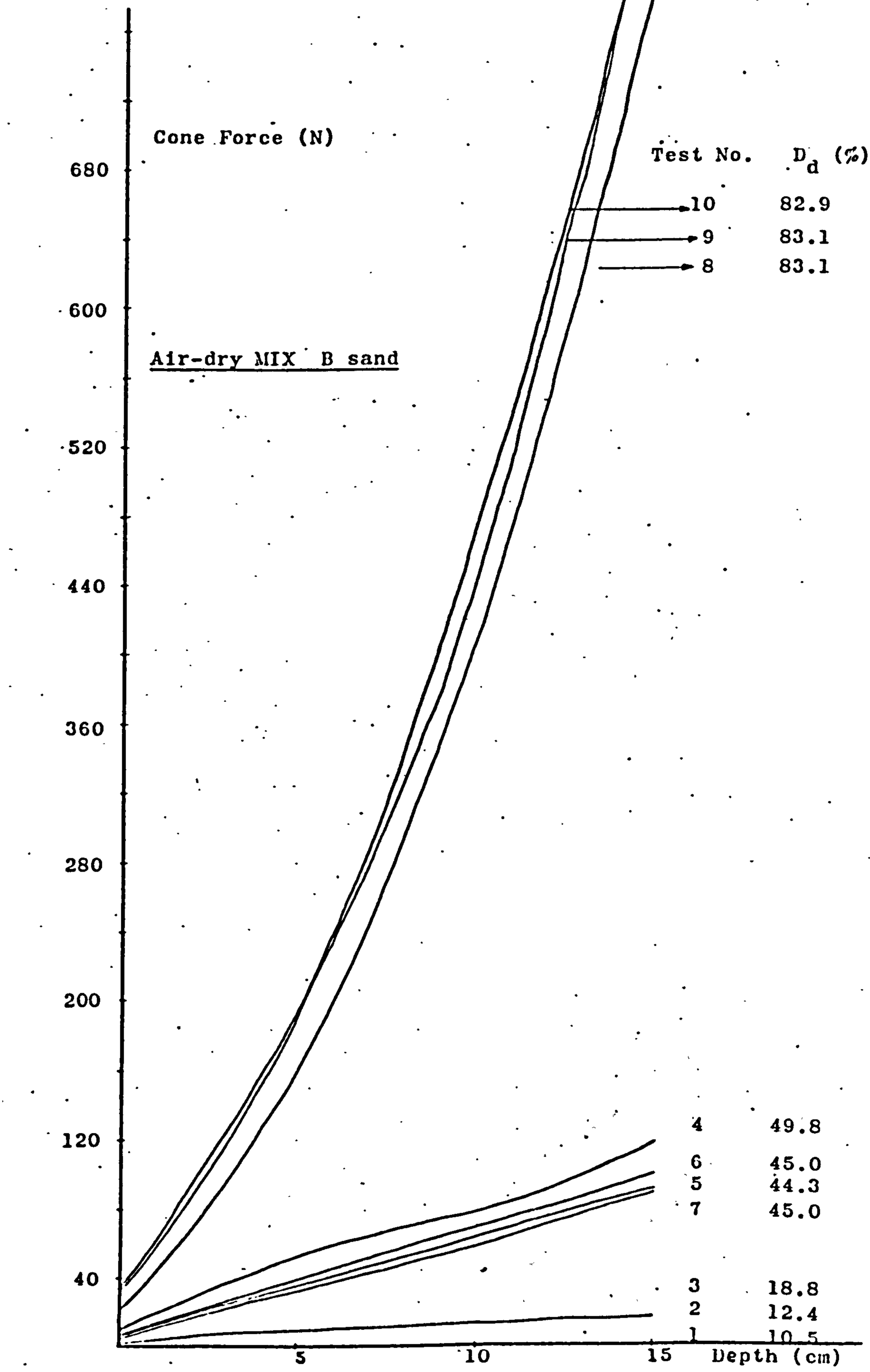

Fig. 4.4 - Cone force / depth diagram for air-dry MIX B sand.

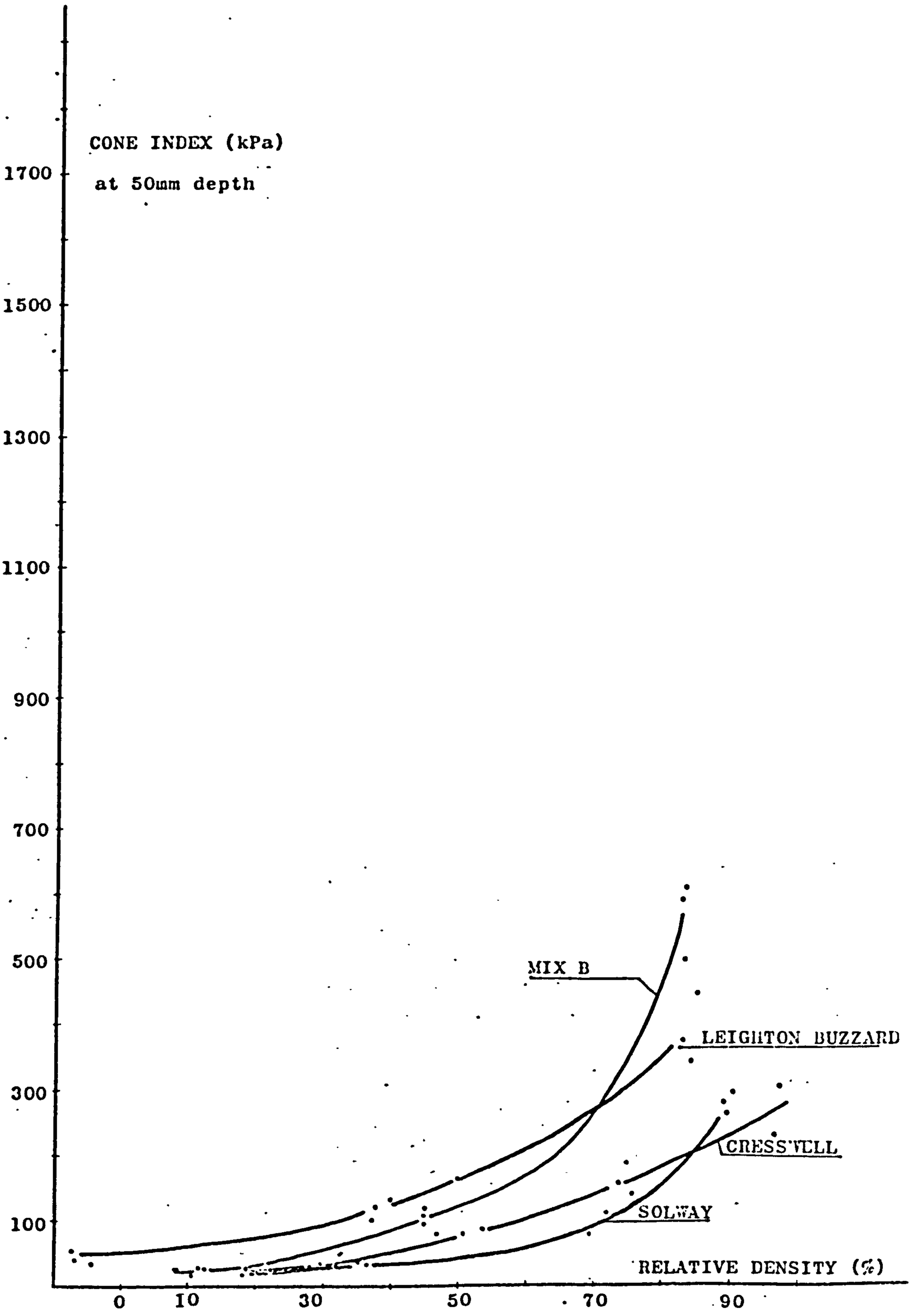

Fig. 4.5 - Cone index at 50mm deep for the four air-dry sands.

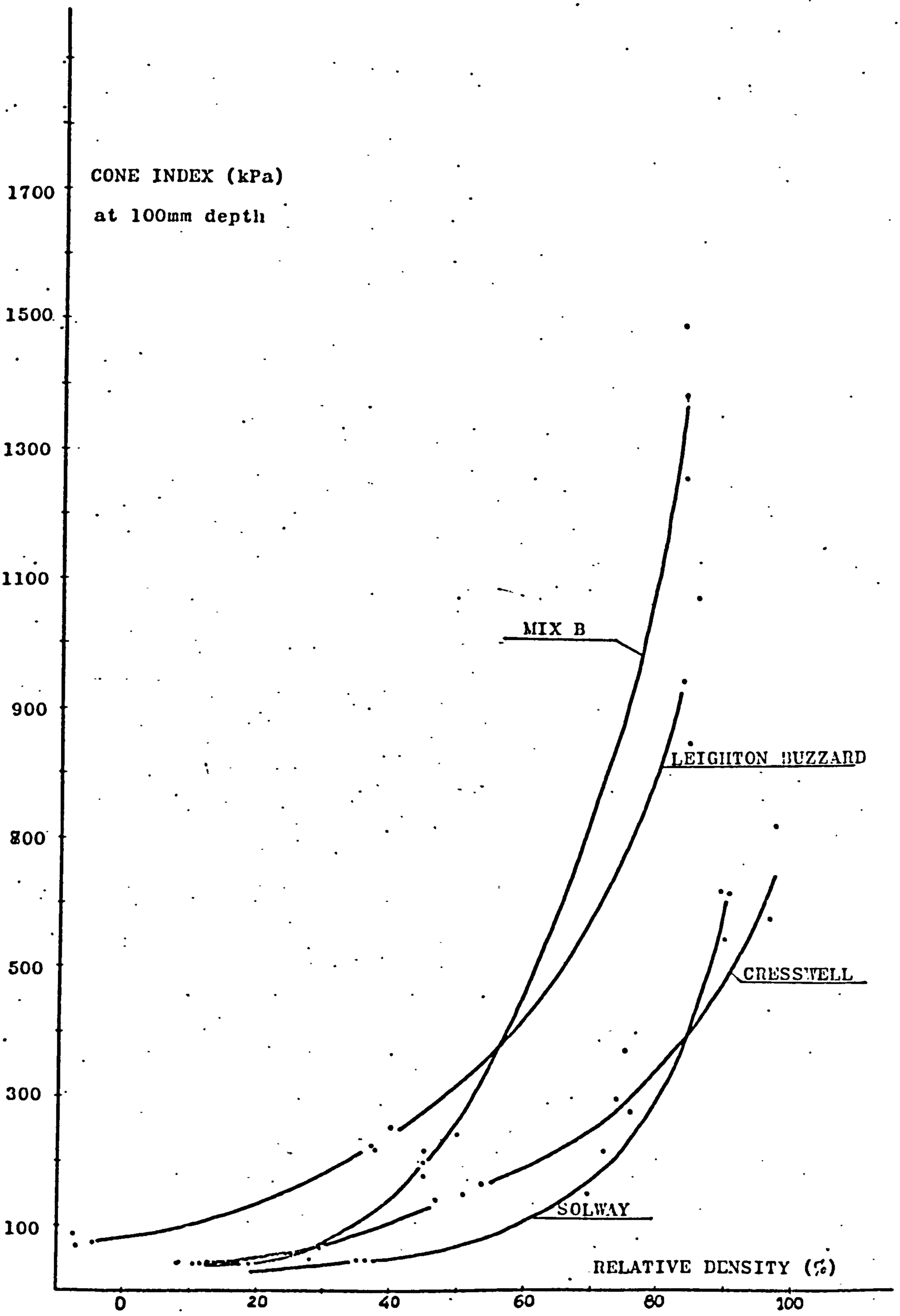

Fig. 4.6 - Cone index at 100mm deep for the four air-dry sands.

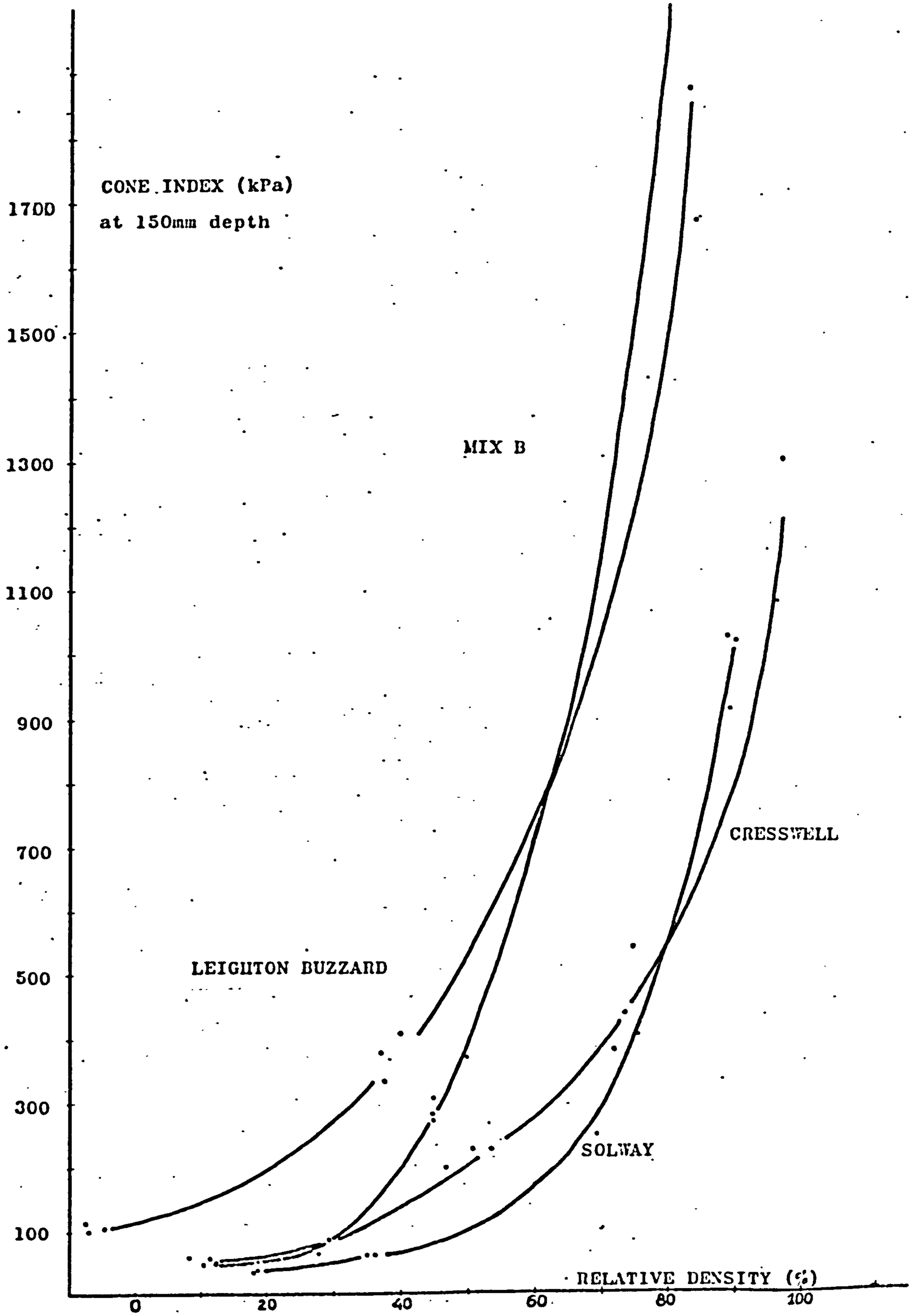

Fig. 4.7 - Cone index at 150mm deep for the four air-dry sands .

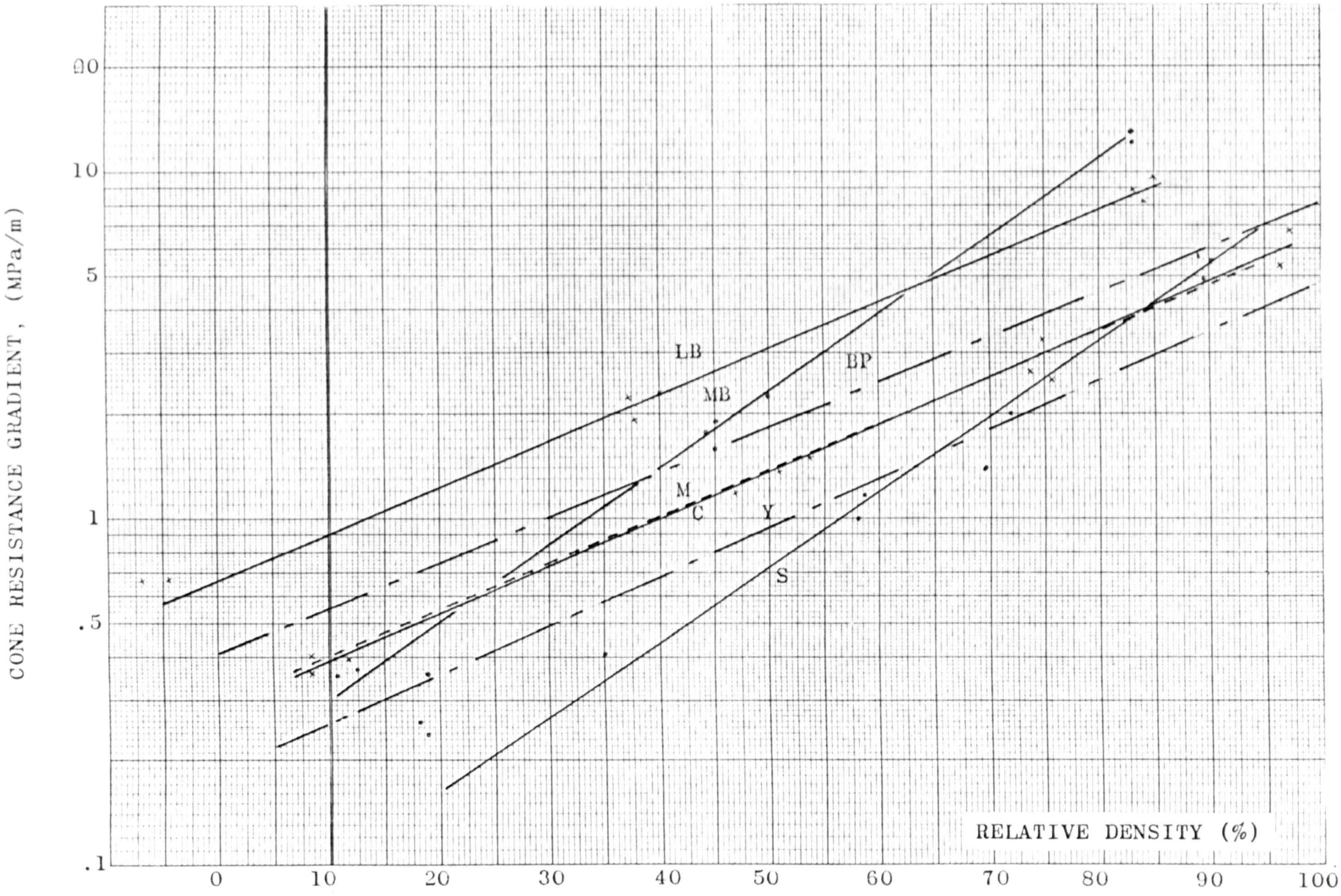

Fig. 4.8 - Results of cone resistance gradient averaged over the top 150mm of penetration.

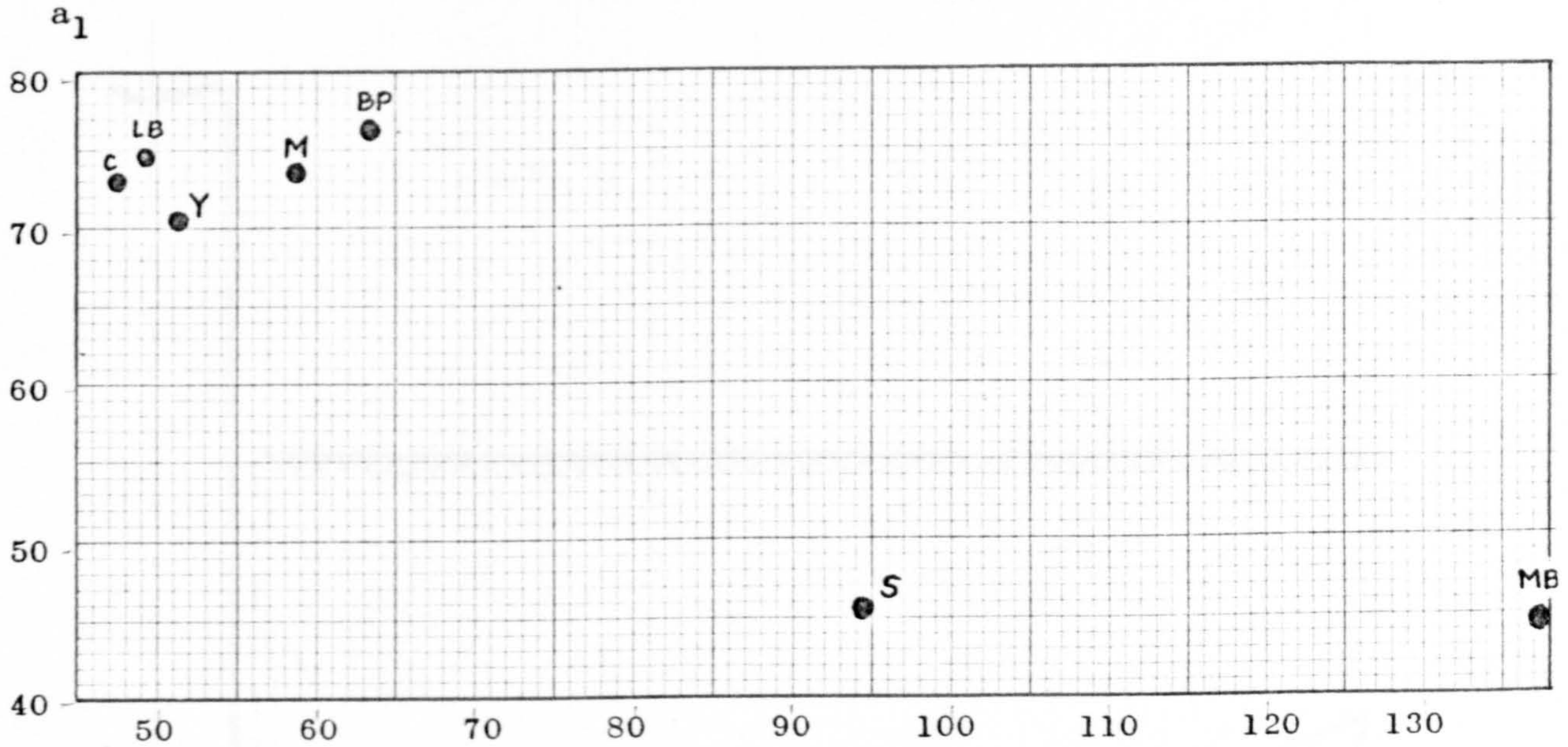

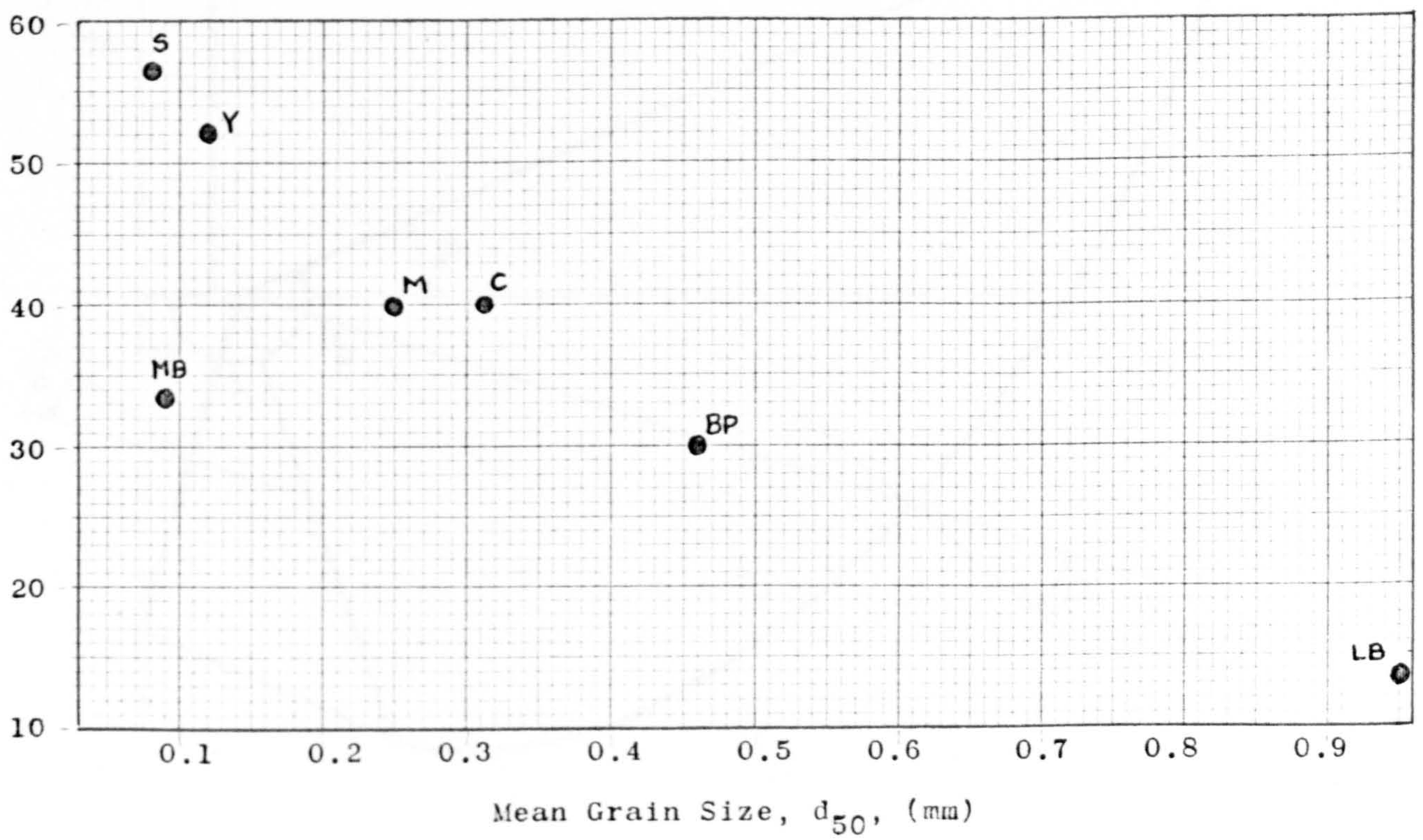

Fig. 4.9 - Factors affecting the relation $D_d = a_1 \log G + a_2$, with D_d in percentage and G in MPa/m. Y - Yuma, M - Mortar and BP - Bayou Pierre sands were tested by Melzer (1971).

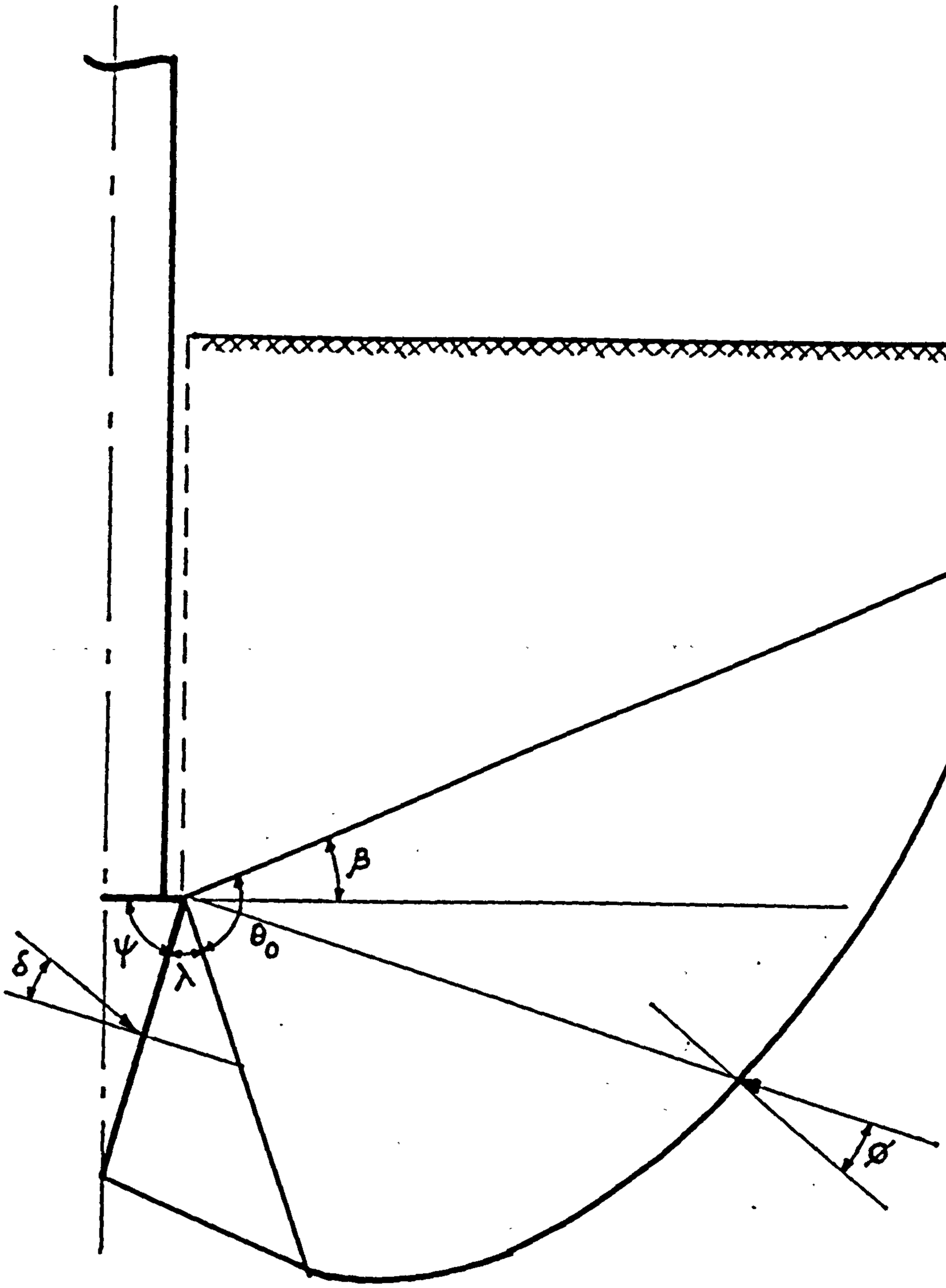

Fig. 4.10 Proposed failure mechanism according to Durgunoglu and Mitchell theory (1975).

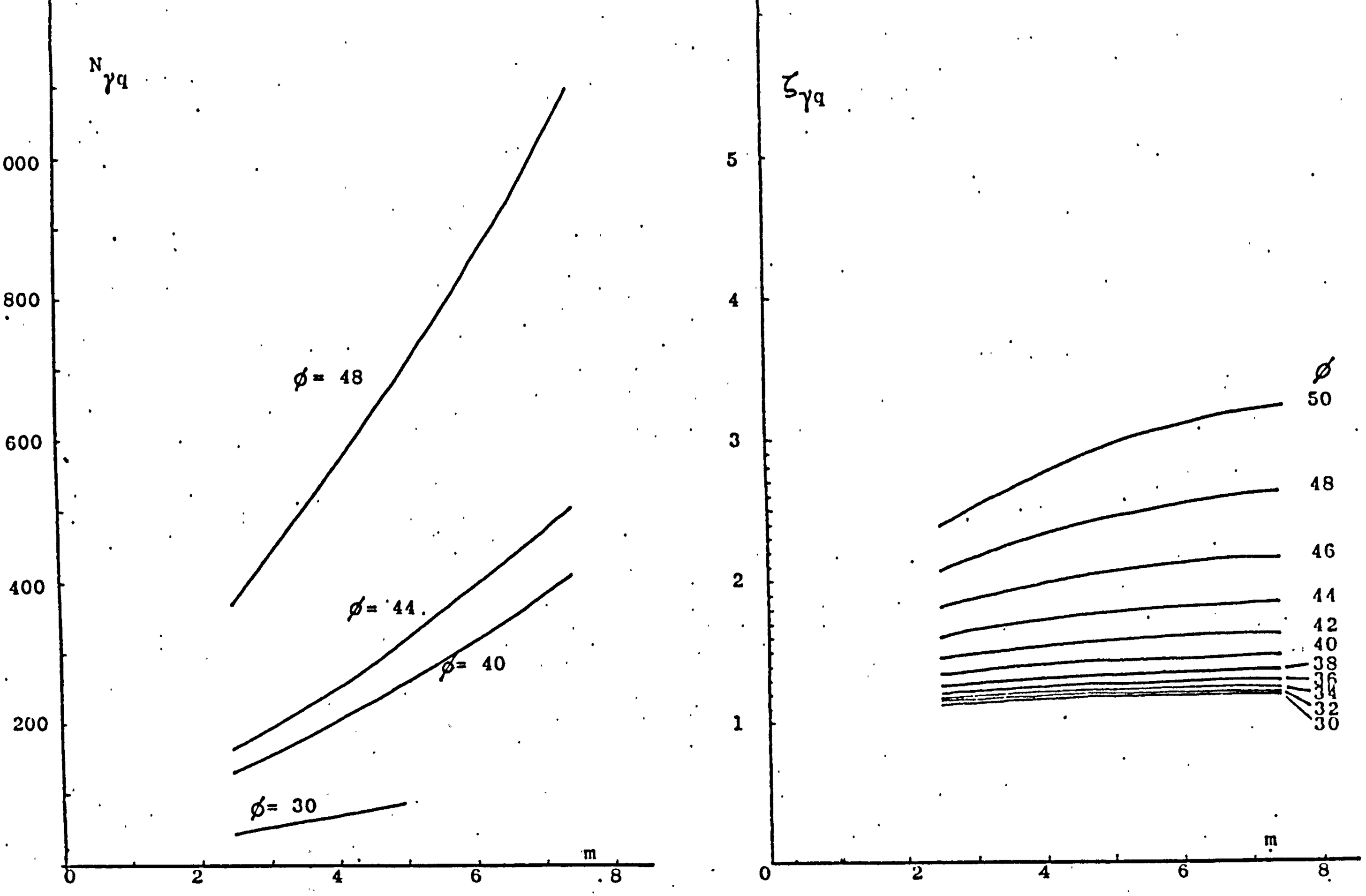

Fig. 4.11 - Bearing capacity factor and Shape factor in Durgunoglu and Mitchell (1975) theory.

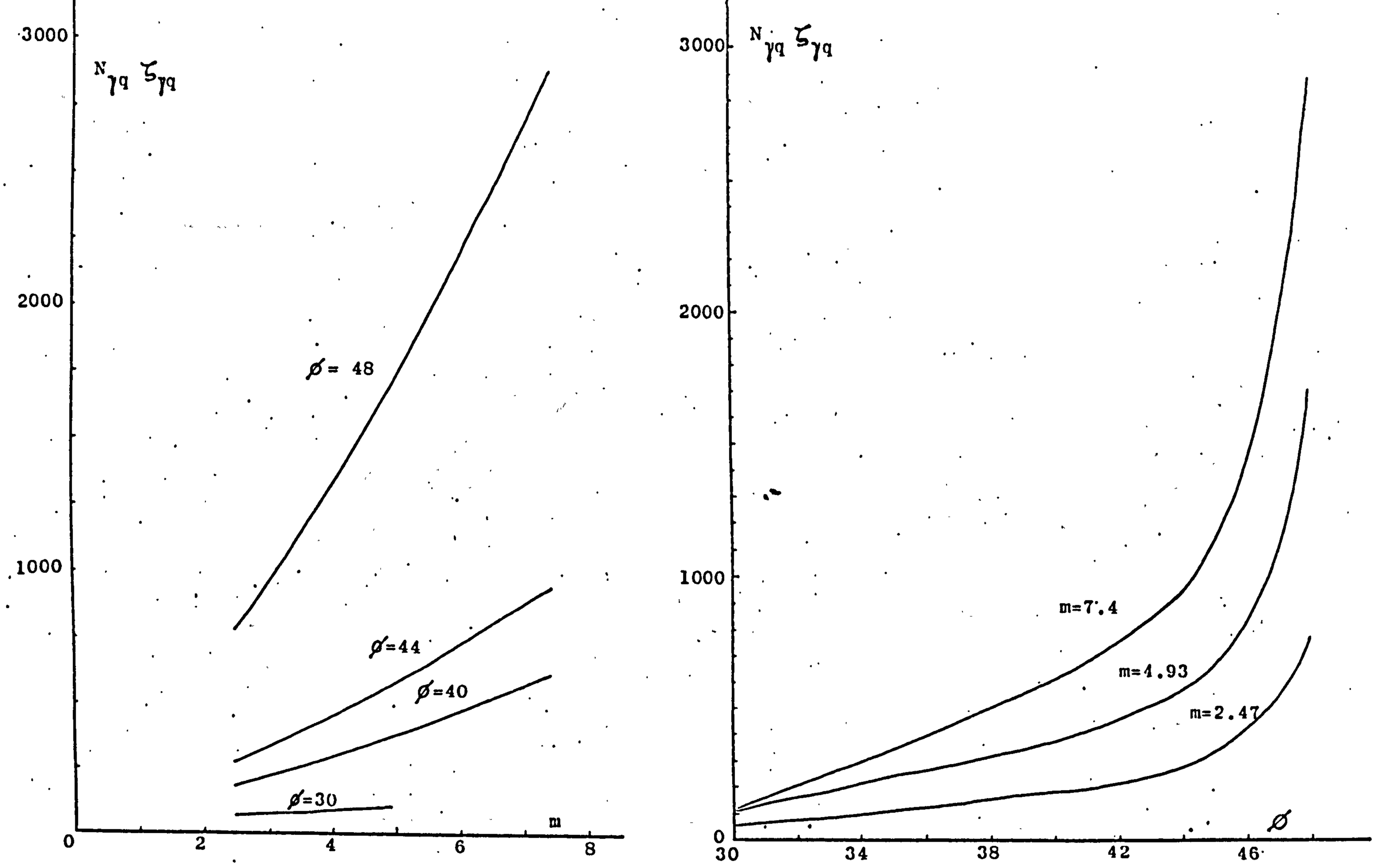

Fig. 4.12 - Dimensionless factor on Durgunoglu and Mitchell (1975) equation for Cone Index.

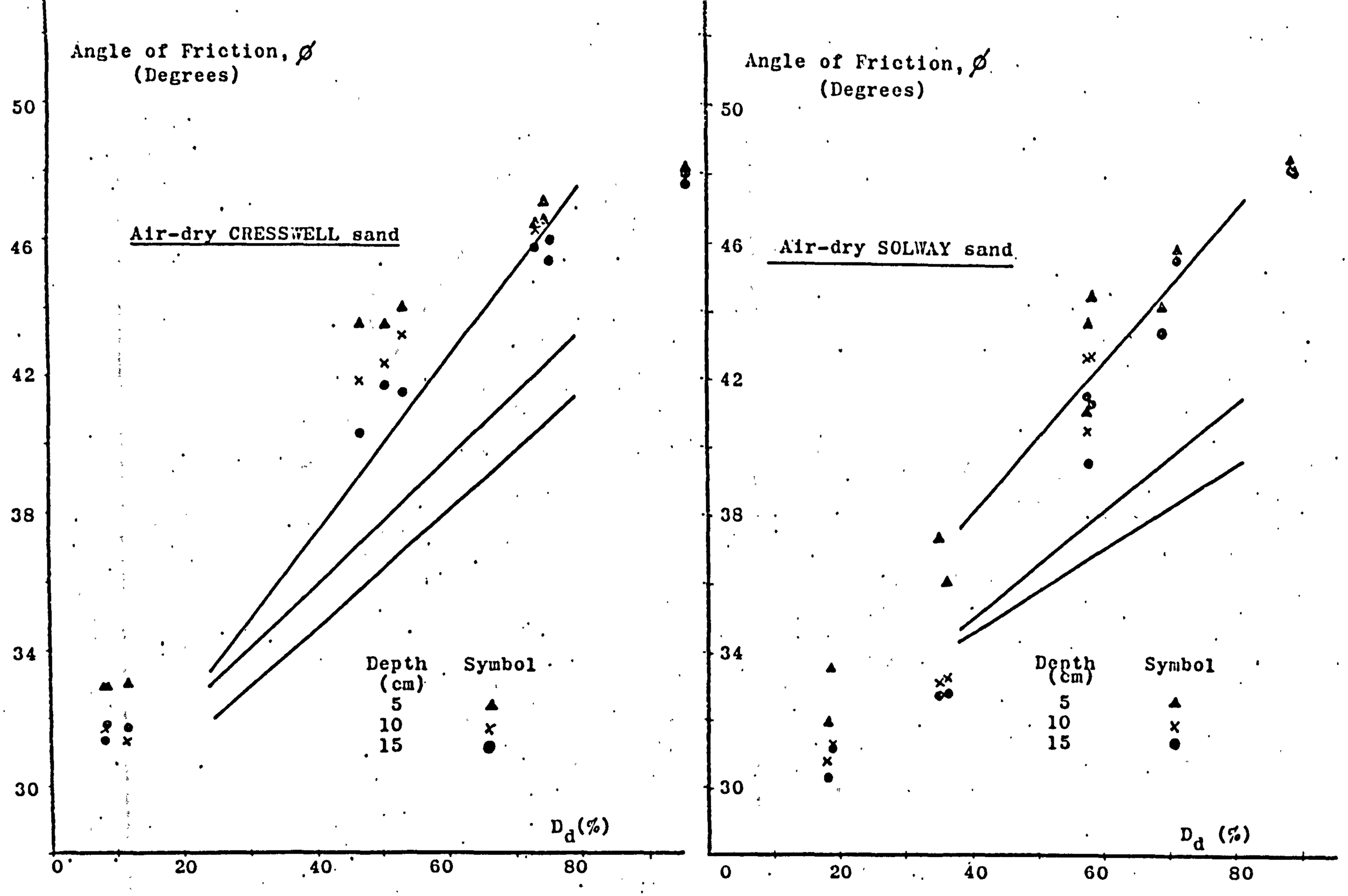

Fig. Fig. 4.13 - Angle of friction computed from cone penetrometer results using Durgunoglu & Mitchell theory compared with the a.i.f. from direct shear tests.

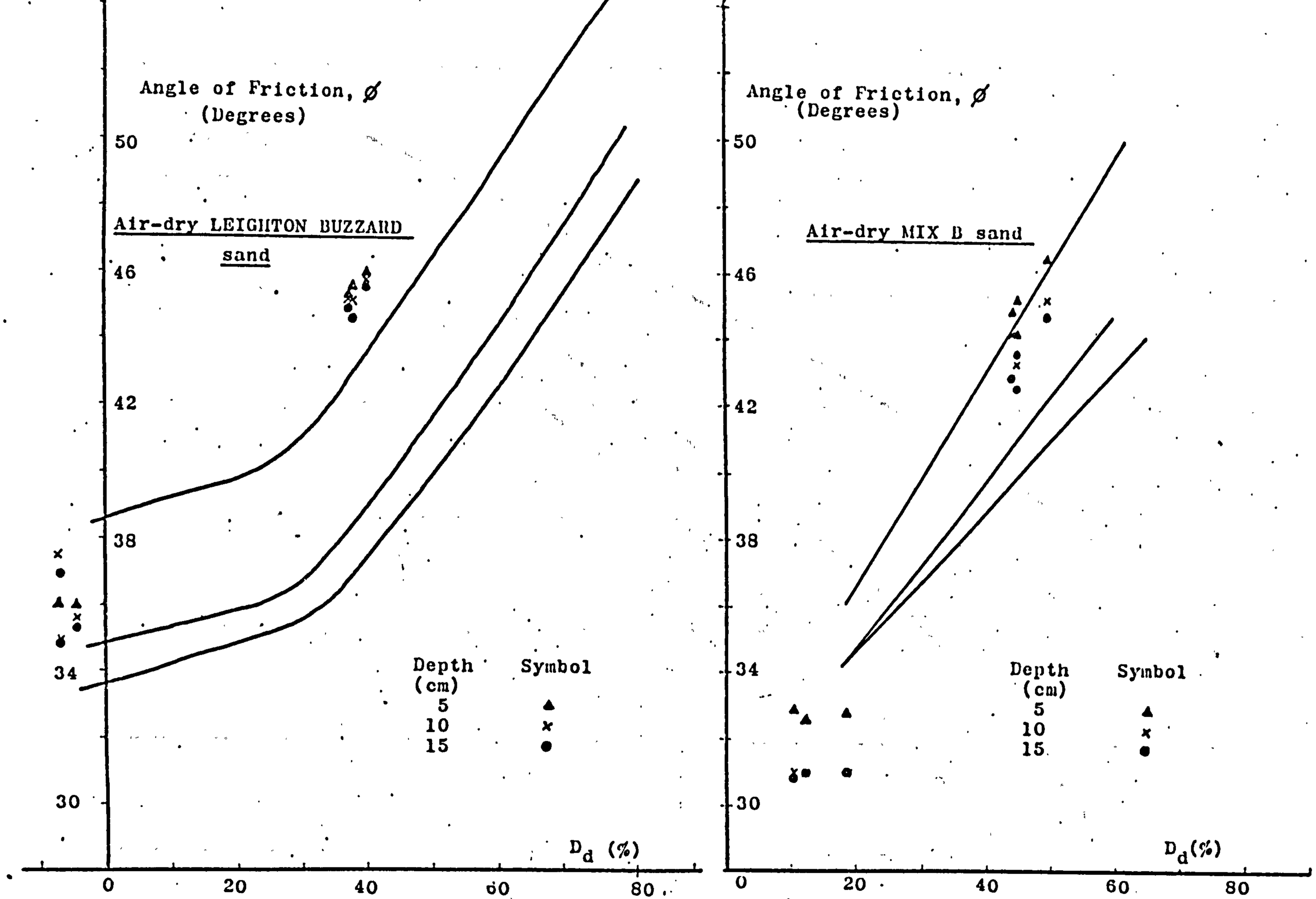

Fig. 4.13 (cont.) - Angle of internal friction from cone penetrometer tests using Durgunoglu & Mitchell theory compared with the a.i.f. from direct shear tests.

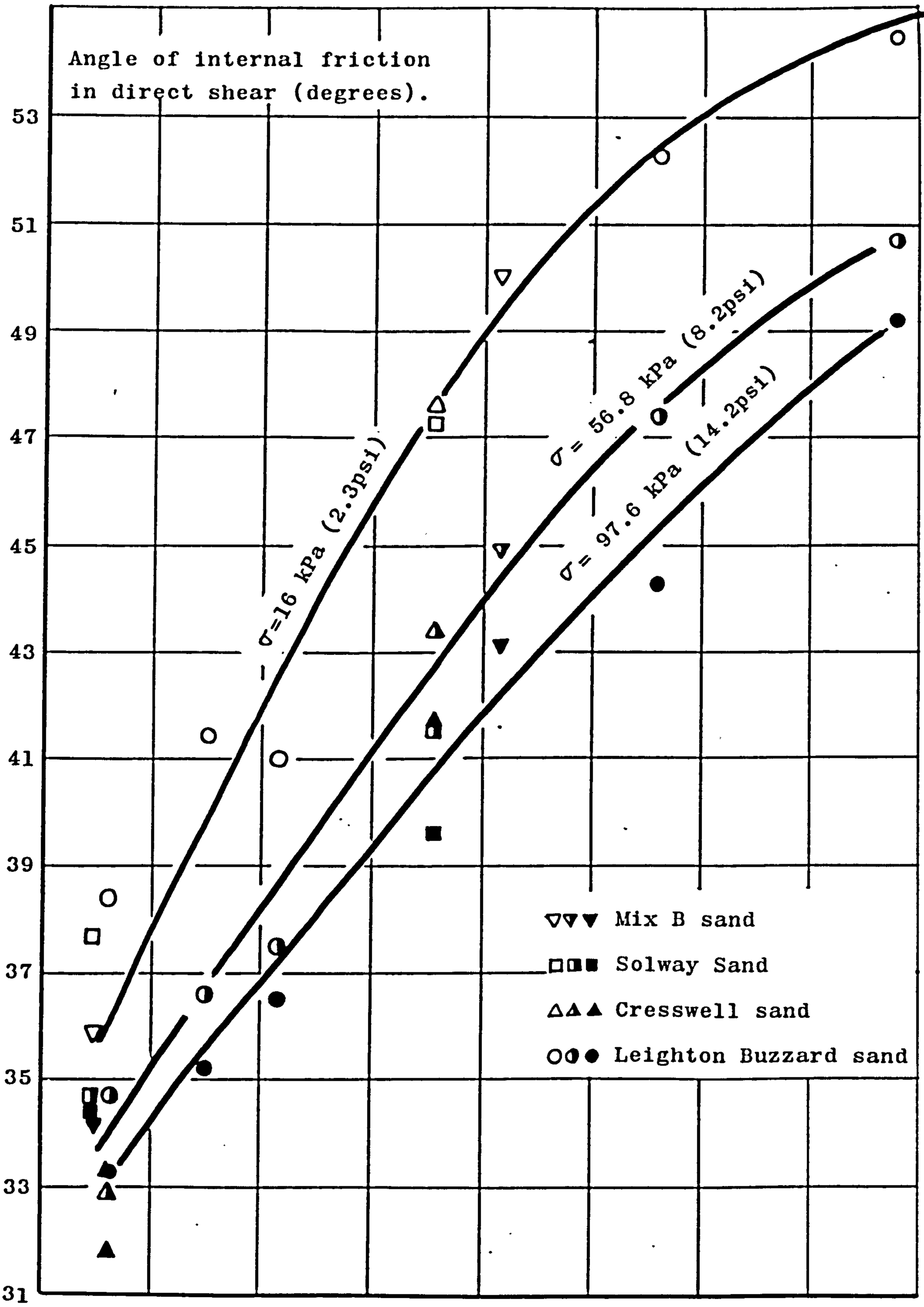

Fig. 4.14 - Relation between the angle of internal friction from direct shear tests and cone resistance gradient, G, for dry sands.

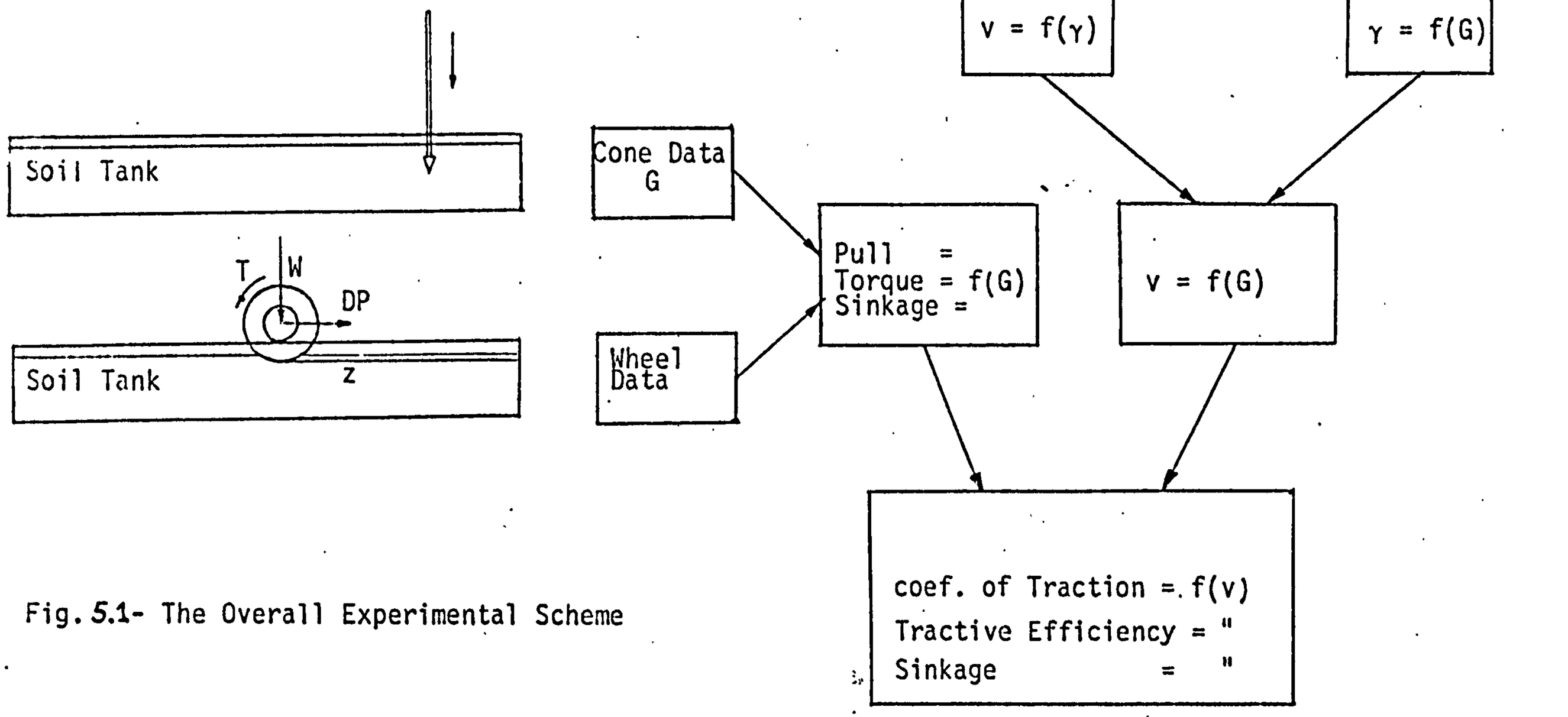

Fig. 5.1- The Overall Experimental Scheme

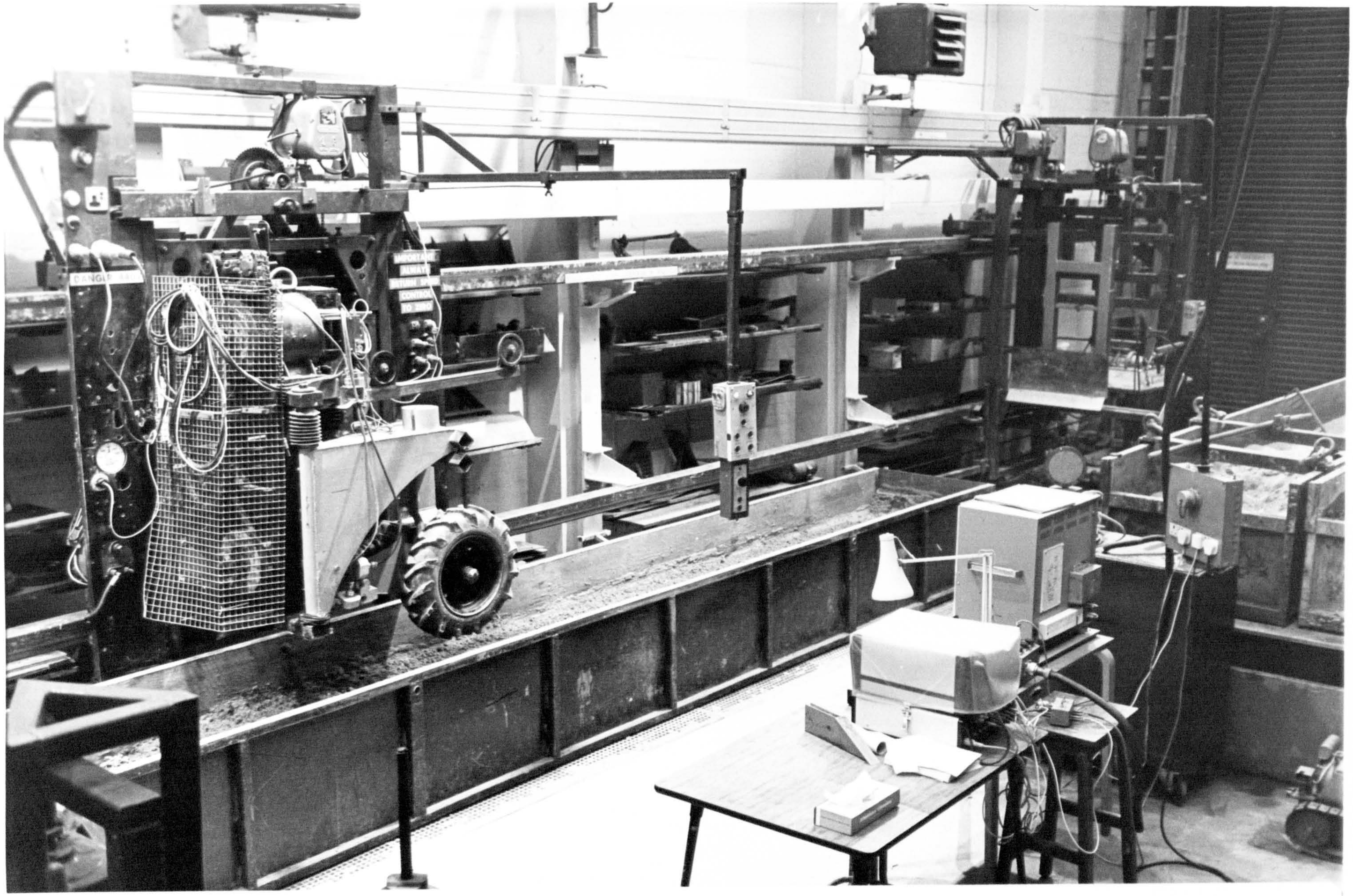

Fig. 5.3 - General view of the wheel tester and soil-tank facilities at Newcastle University.

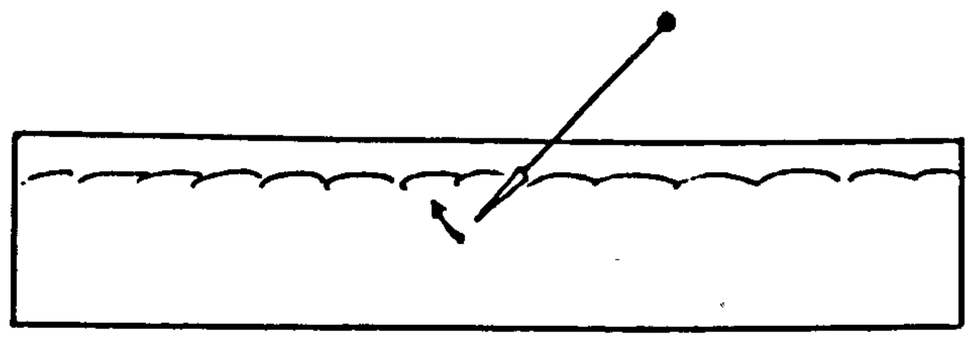

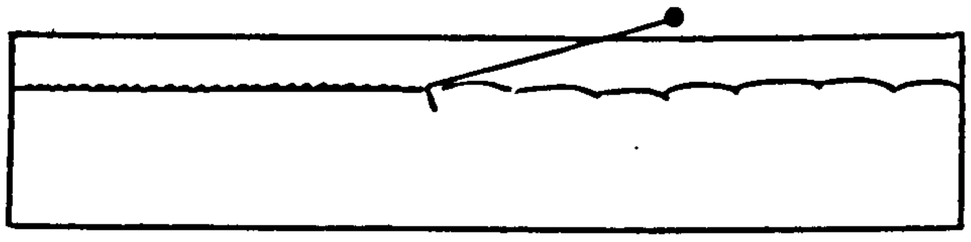

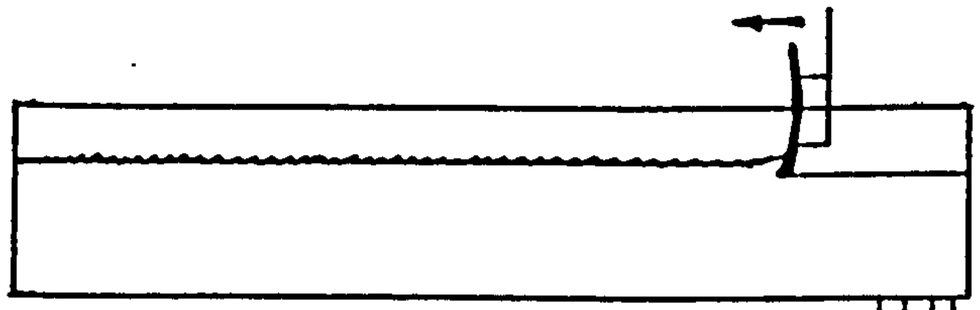

Tests CS13/14/15, D_d=29 to 41%

Tests CS18/19/20, D_d=68.5 to 73%

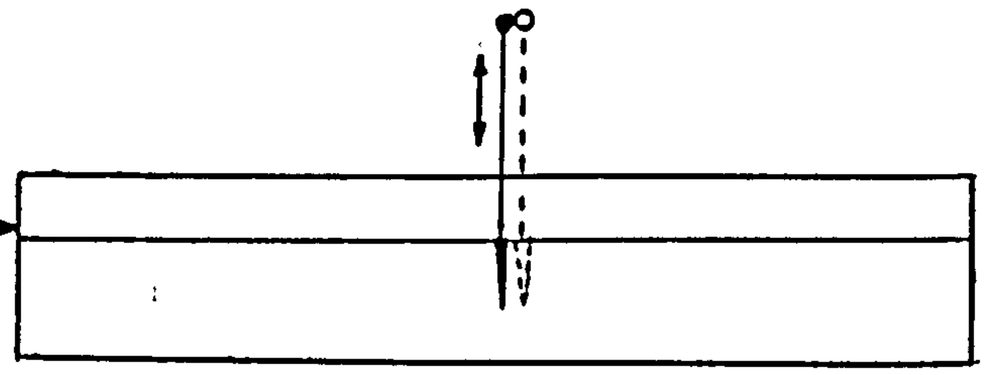

Test CS16 (two passes)
D_d=81 to 83%
Test CS17 (one pass)
D_d=70 to 80.5%

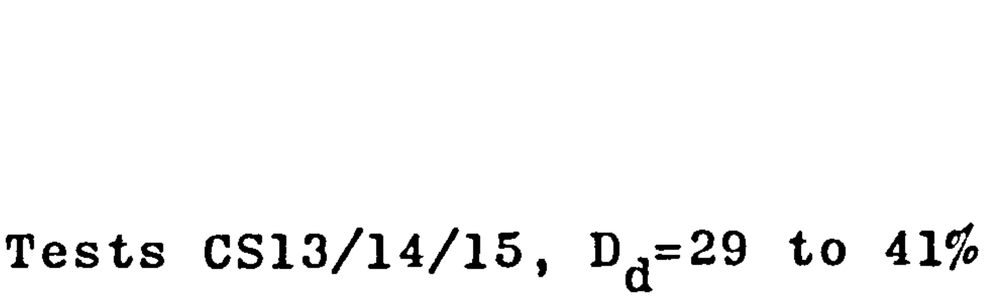

Test CS10, D_d=80 to 84.5%

Test CS11, D_d=97.3 to 100%

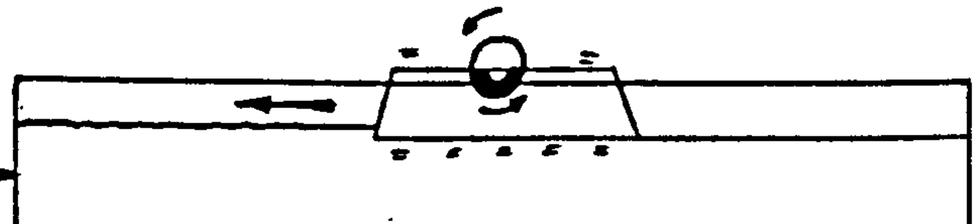

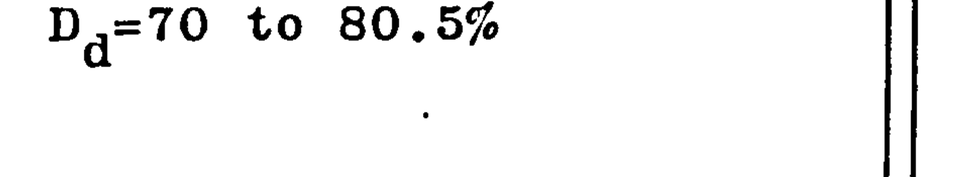

Test CS12, D_d=22.3 to 31.5%

Fig. 5.4 - In-tank soil processing methods used in air-dry Cresswell sand.

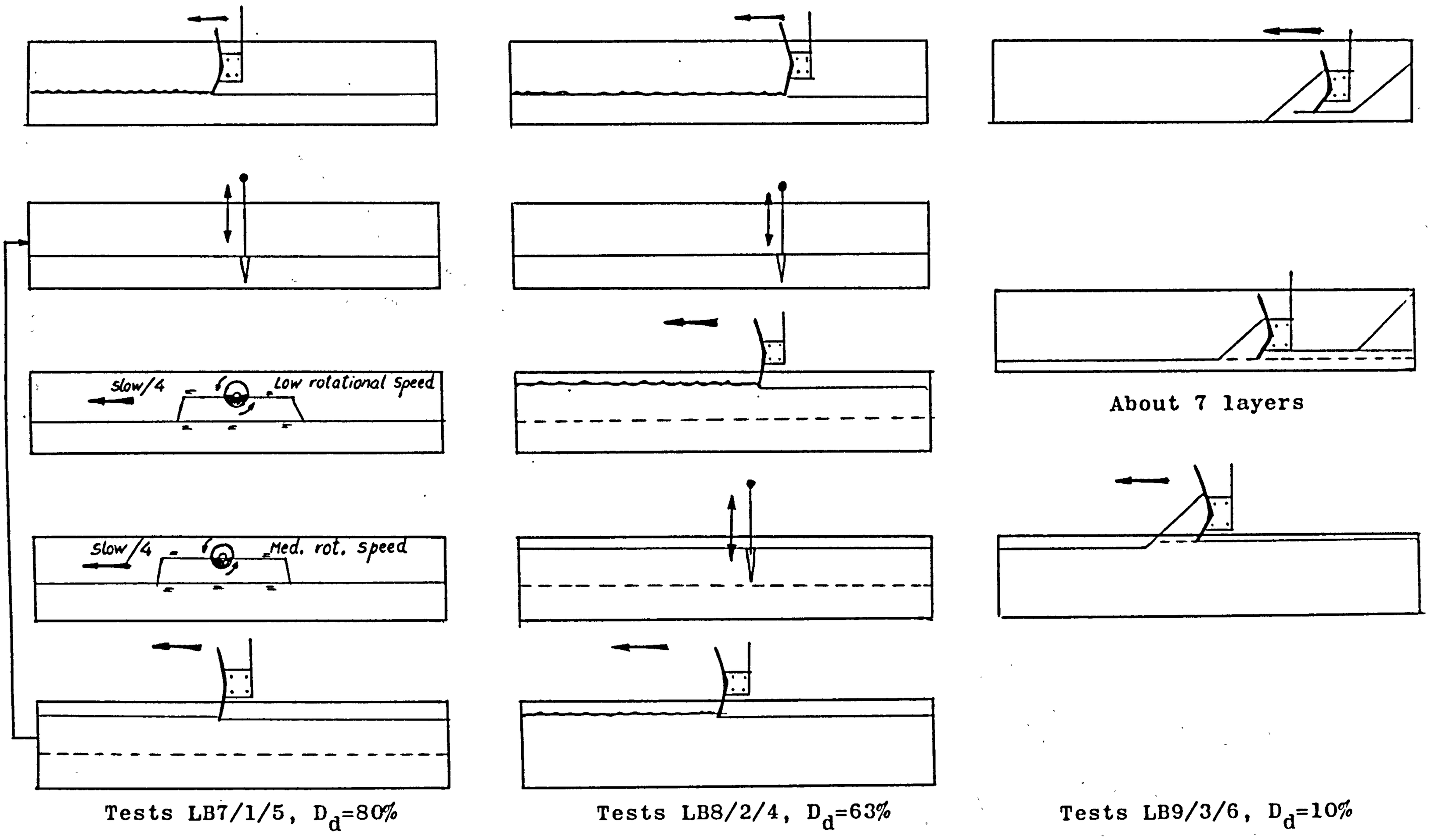

Tests LB7/1/5, D_d=80%

Tests LB8/2/4, D_d=63%

Tests LB9/3/6, D_d=10%

Fig. 5.5 - In-tank soil processing methods for air-dry Leighton Buzzard sand

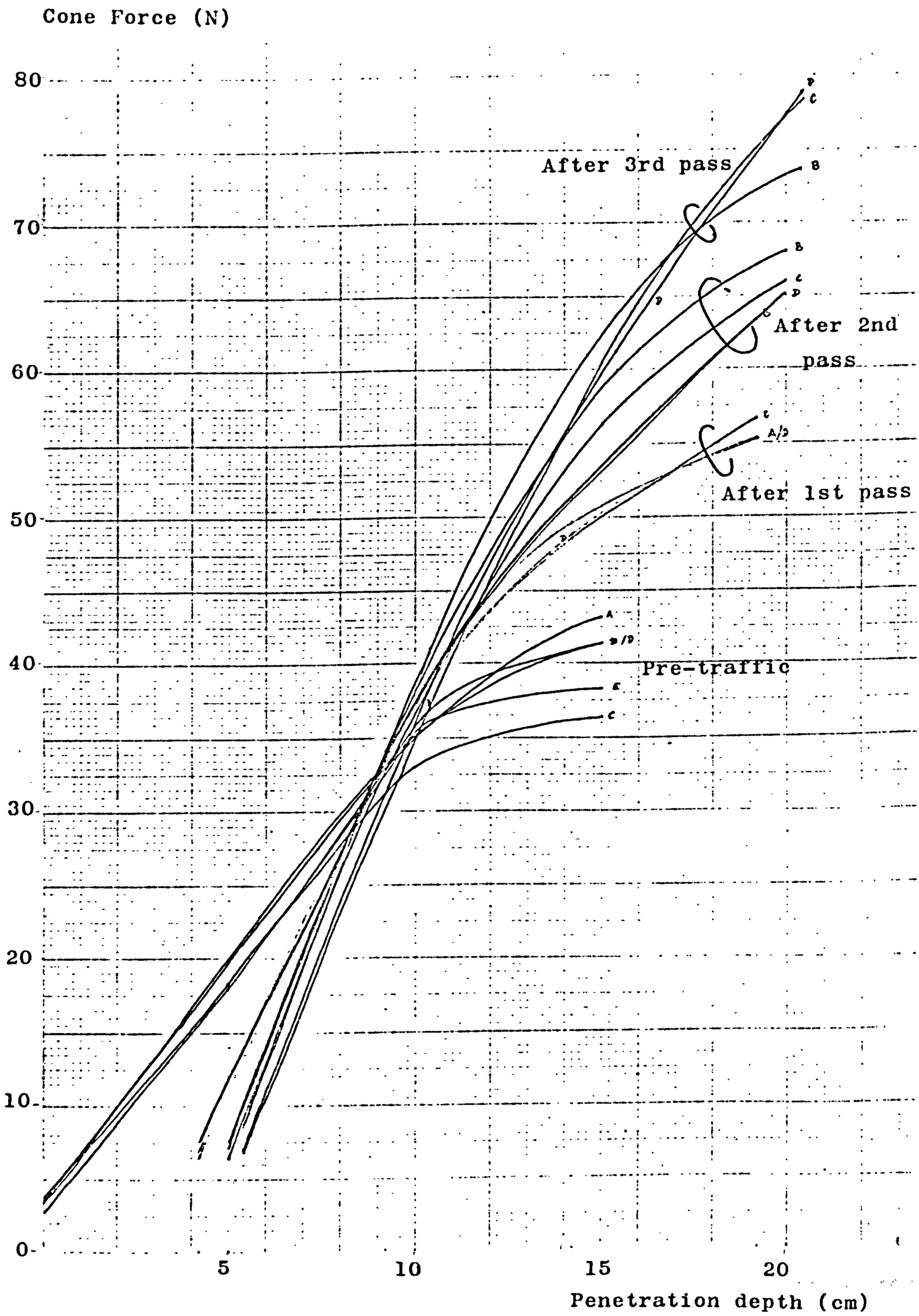

Fig. 5.6 - Cone trace of test LB9 (very loose sand)

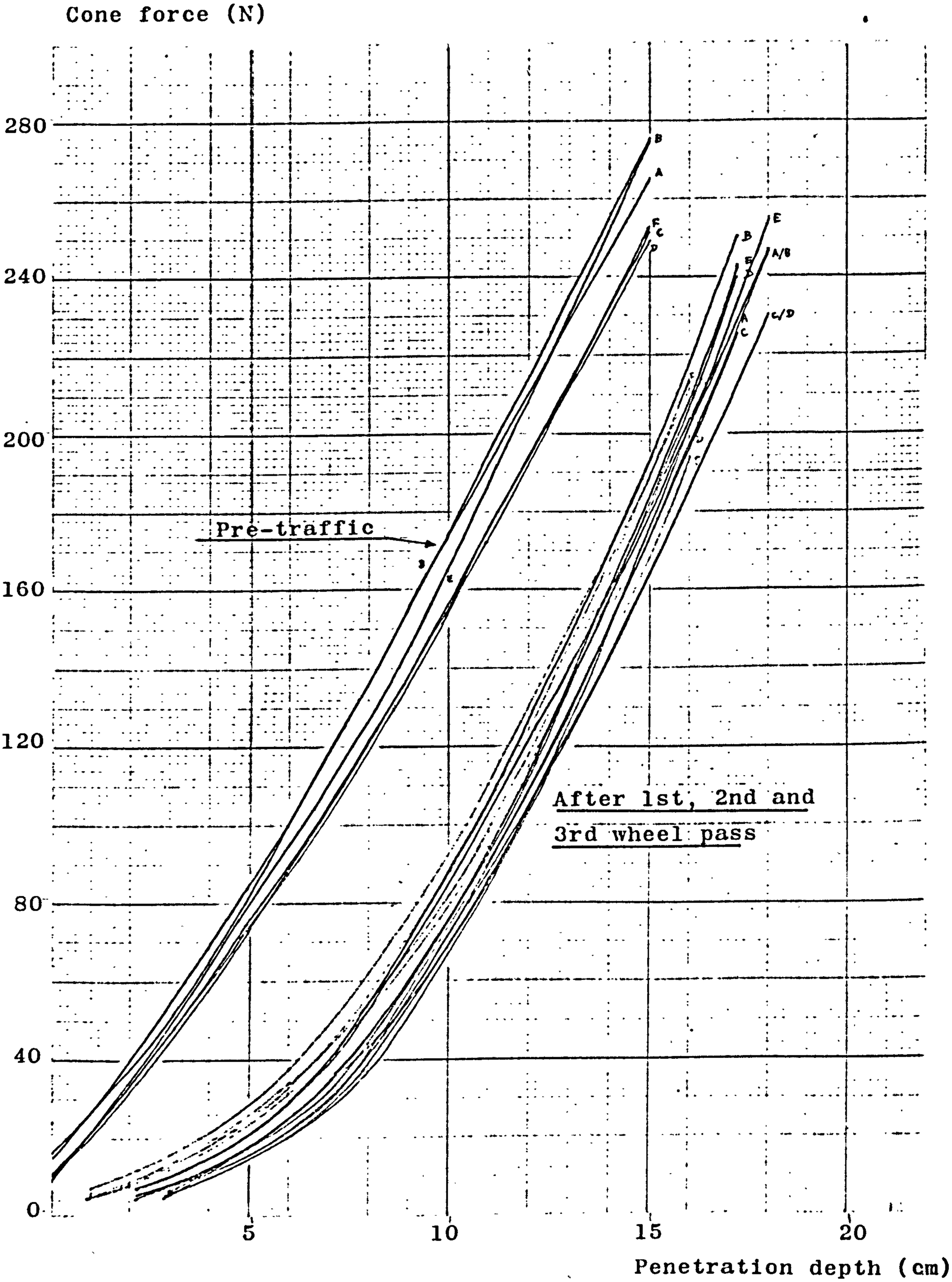

Fig. 5.7 - Cone trace of wheel test LB2 (medium dense sand)

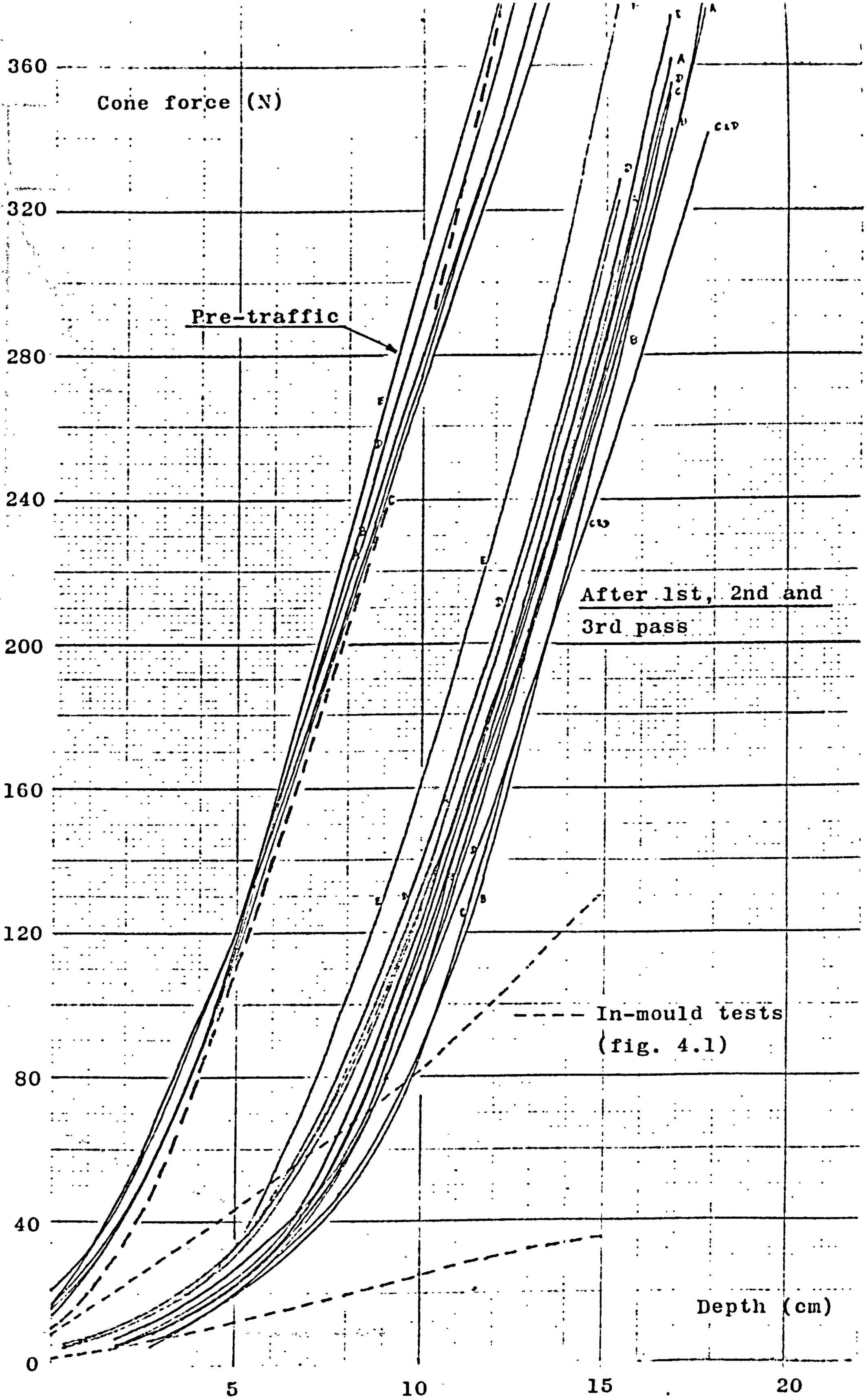

Fig. 5.8 - Cone trace of wheel test LB5 (very dense sand)

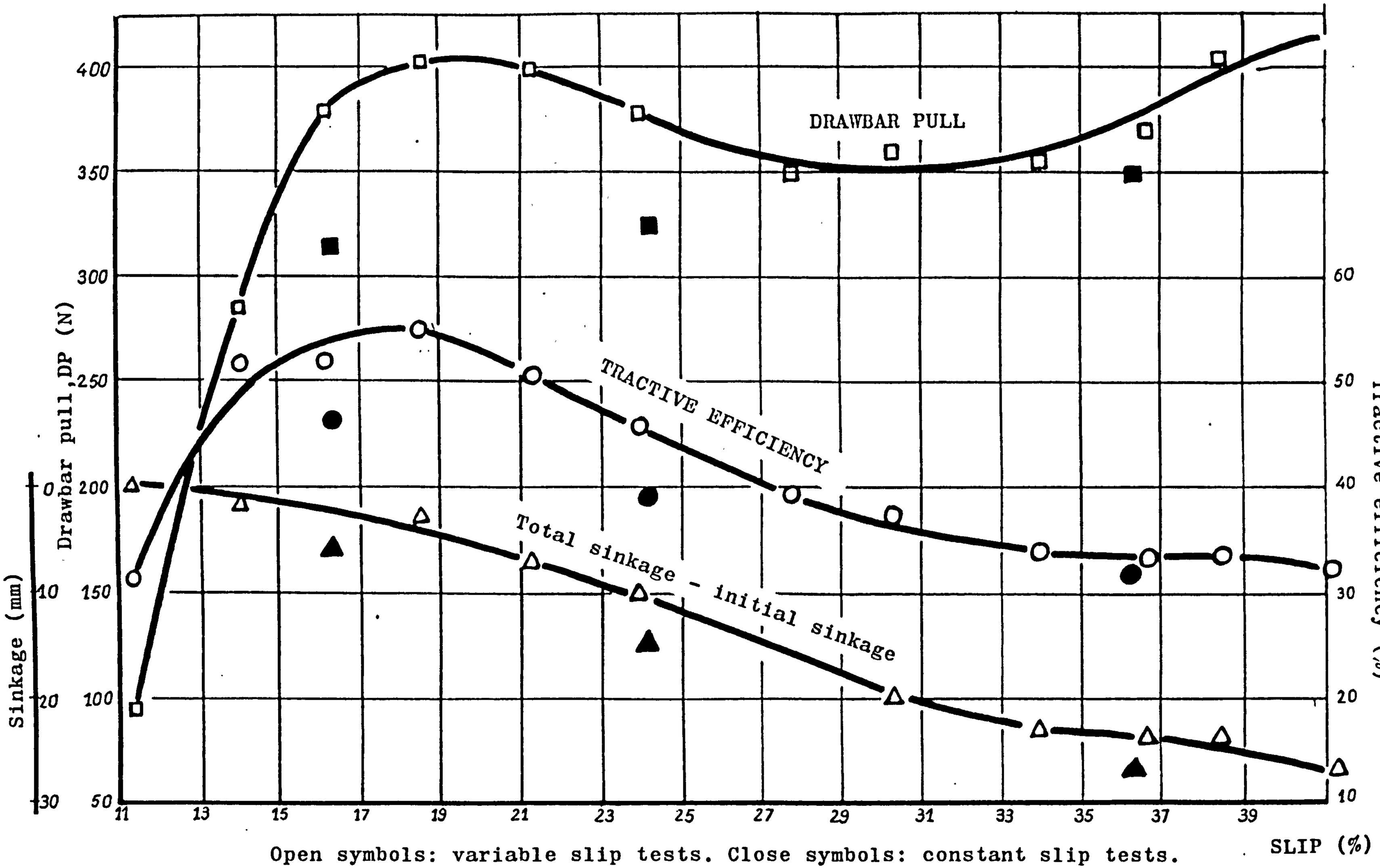

Open symbols: variable slip tests. Close symbols: constant slip tests.

Fig. 5.9 - Variable and constant slip tests on Cresswell sand with a 6.00-16-2PR Goodyear tyre, W=1.6kN, 39% deflection.

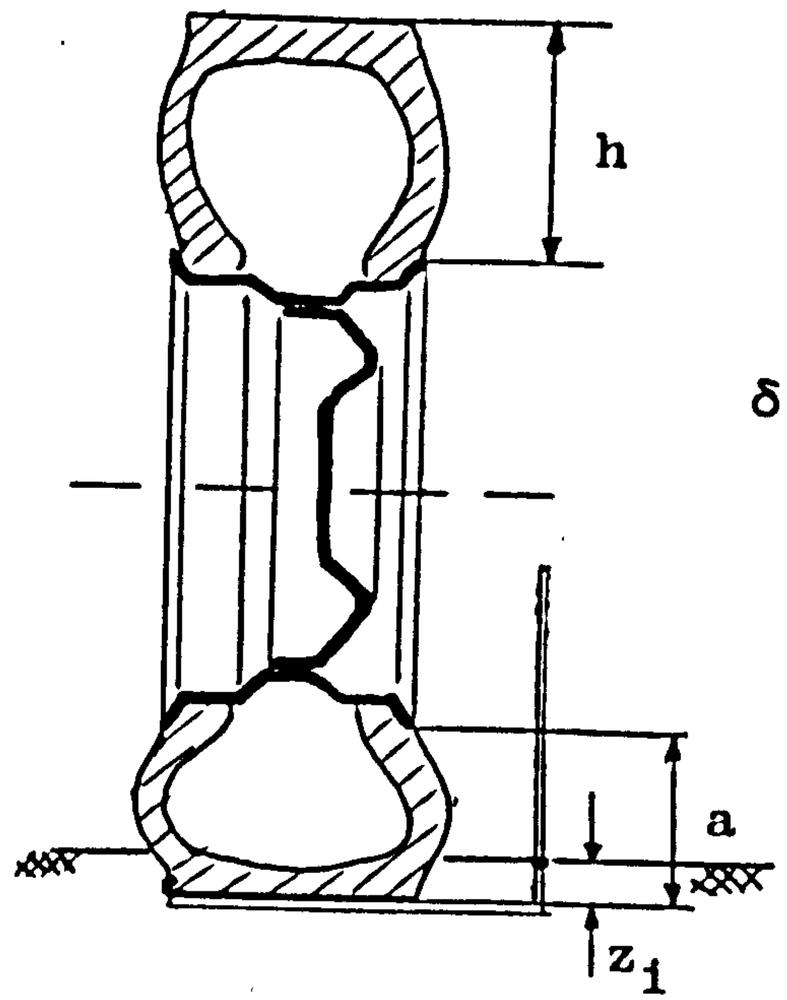

$$\delta = h - a$$

(a)

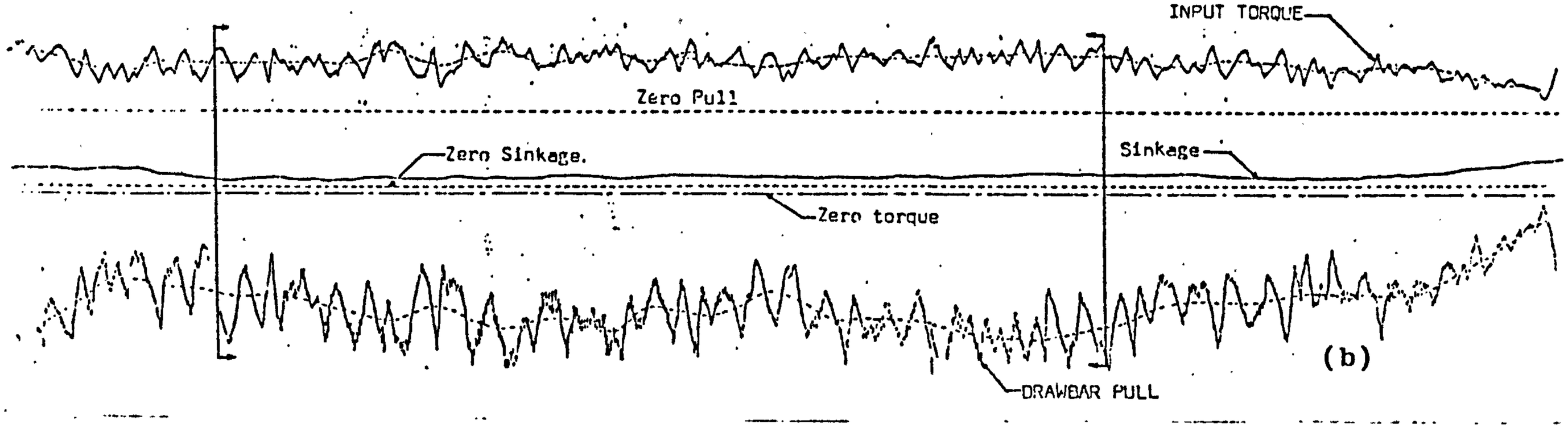

Fig. 5.10 - (a): technique for measuring on-soil tyre deflection and initial (static) sinkage. (b): U.V. recorder trace showing torque input, drawbar pull and sinkage.

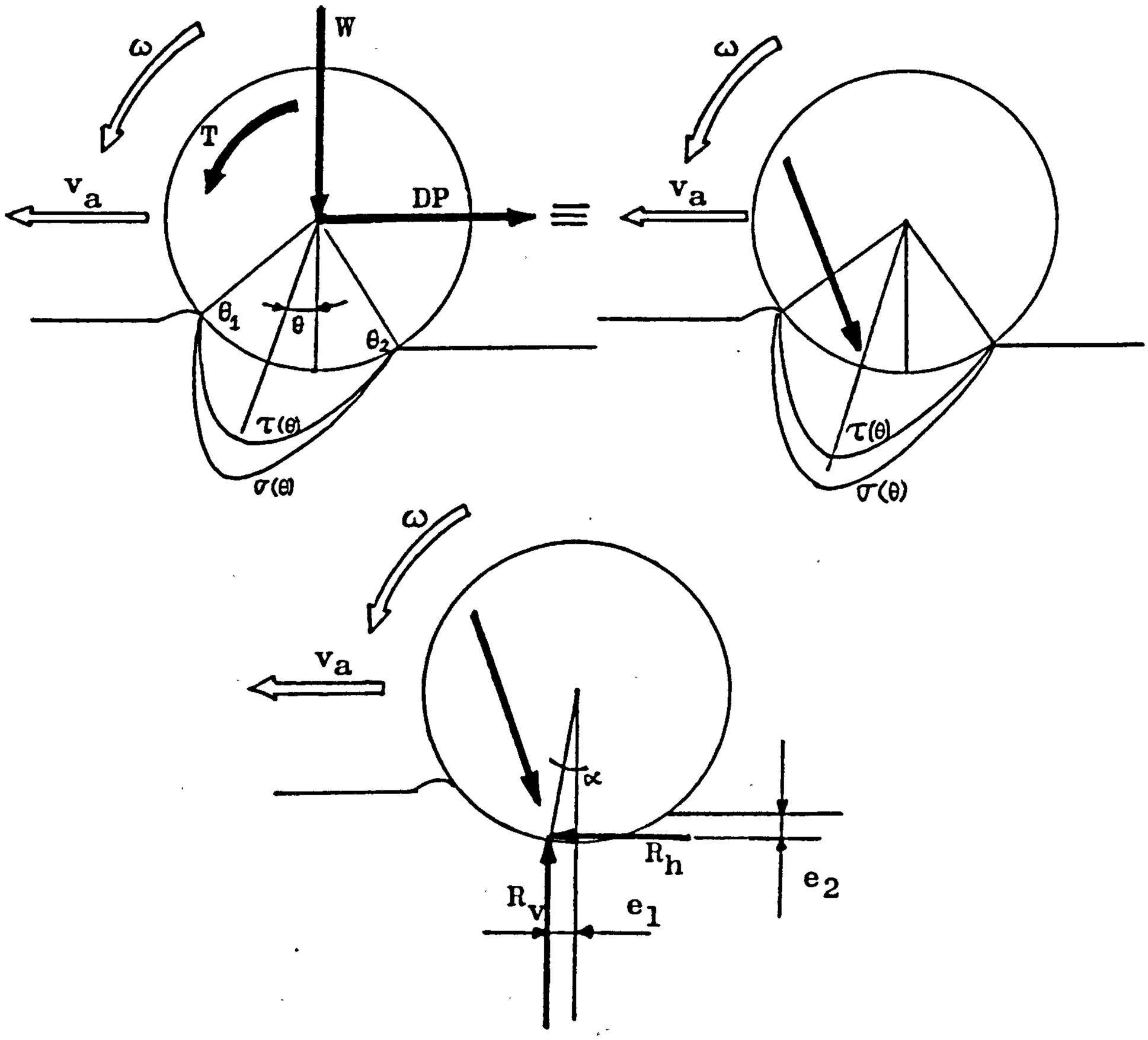

Fig. 5 11 - Basic statics of soil- wheel interaction.

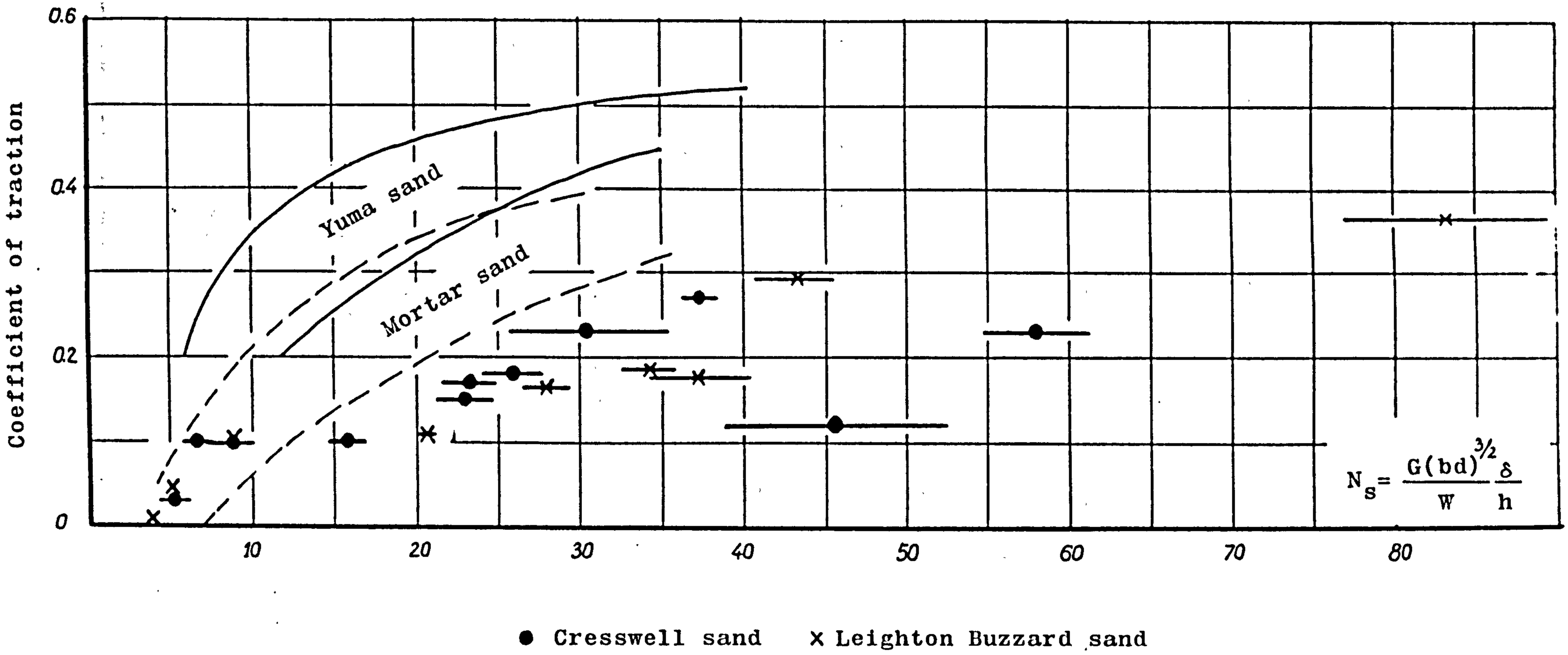

Fig. 5.12 - Coefficient of traction from tests in Cresswell and Leighton Buzzard sands against the original W.E.S. sand Number.

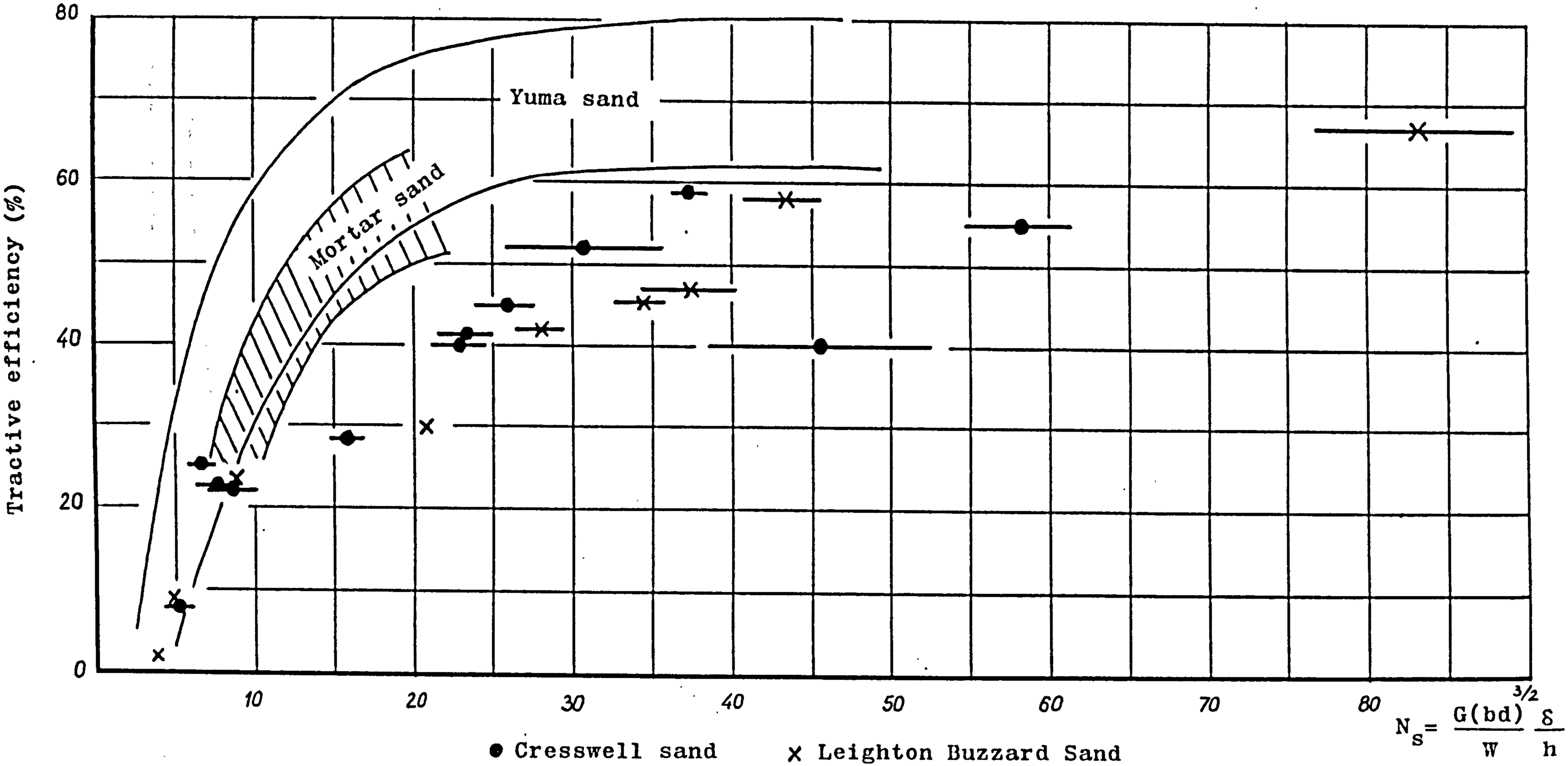

Fig. 5.13 - Tractive efficiency from tests in Cresswell and Leighton Buzzard sands against the original W.E.S. sand number.

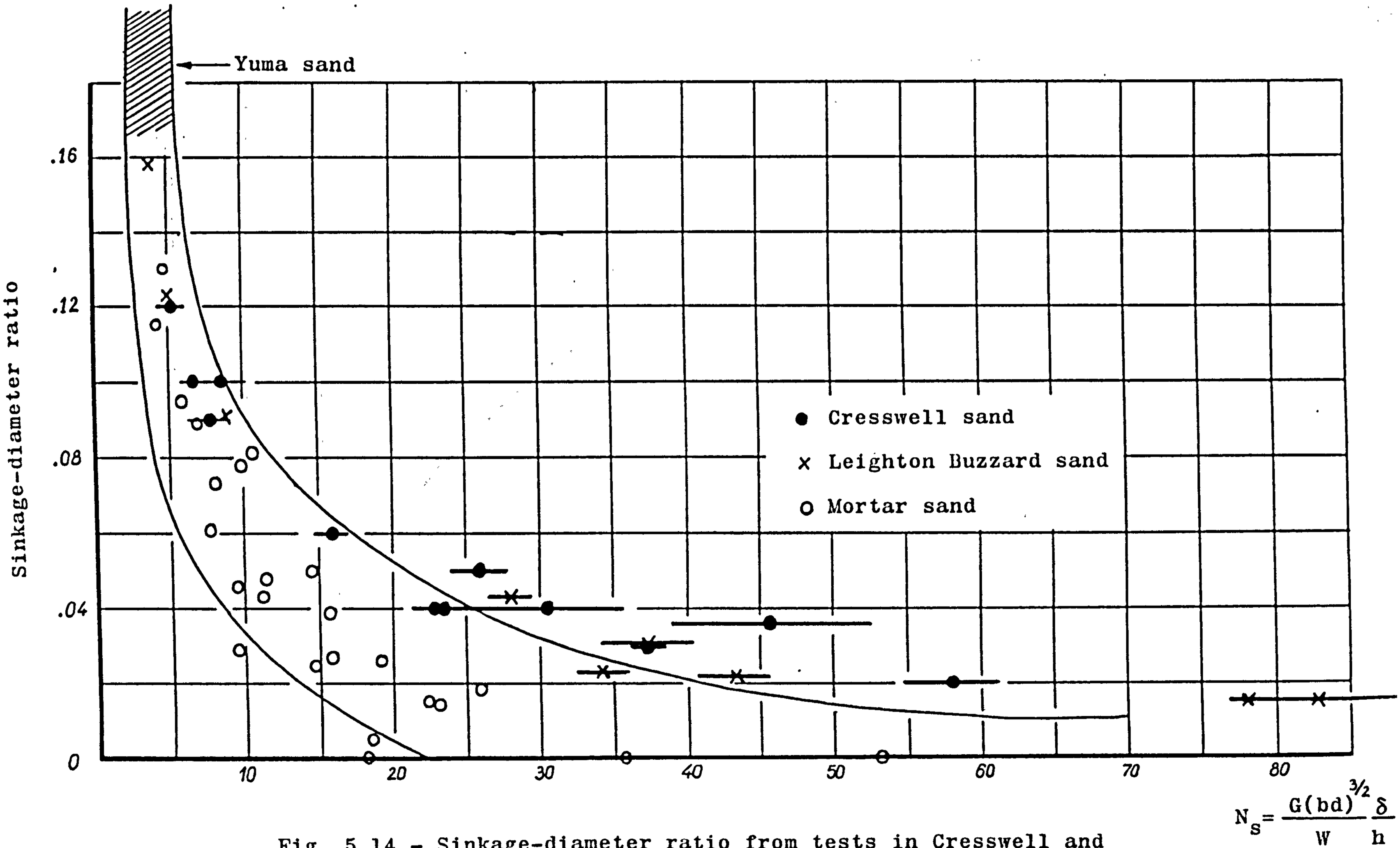

Fig. 5.14 - Sinkage-diameter ratio from tests in Cresswell and Leighton Buzzard sands against the original W.E.S. sand number.

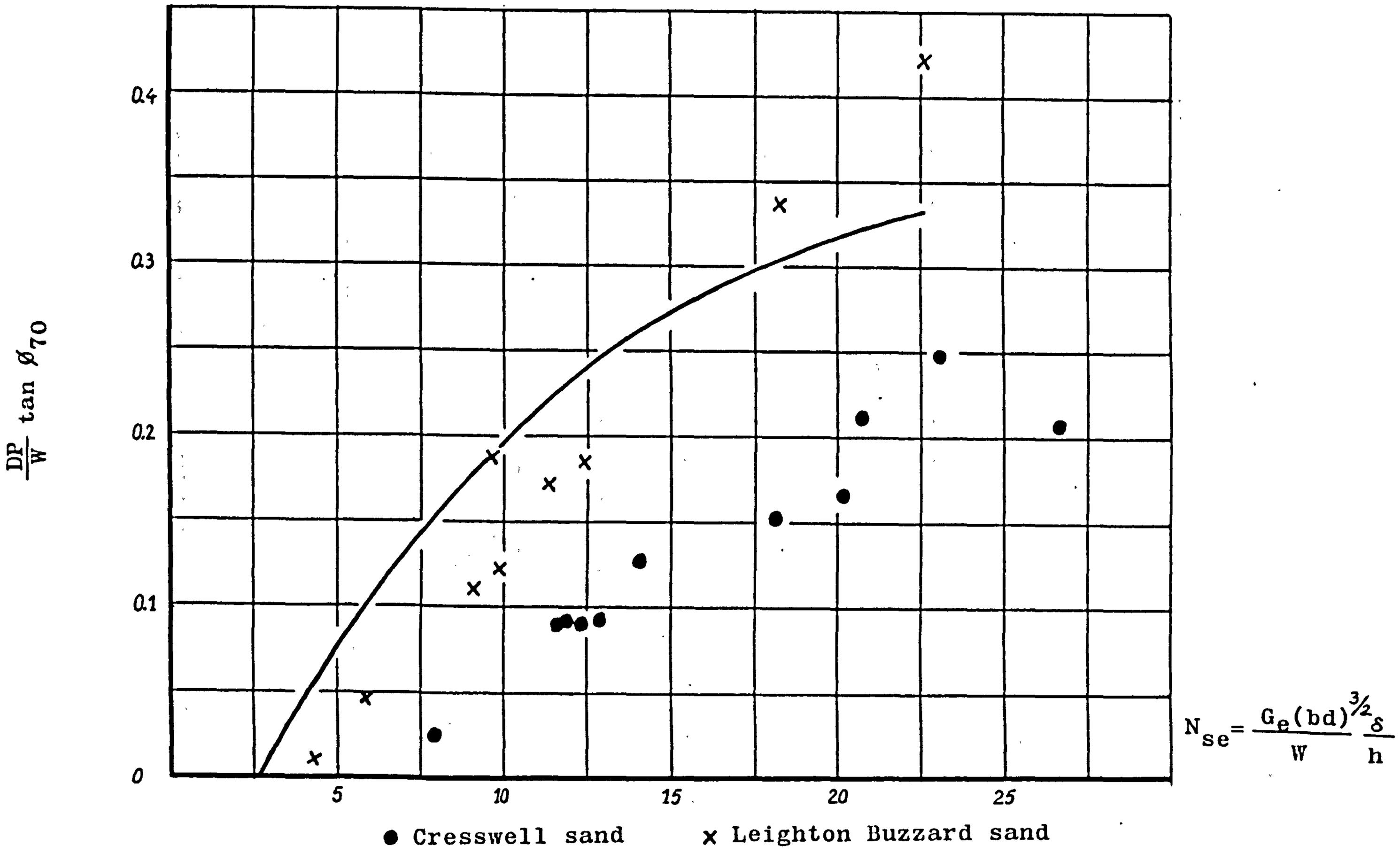

Fig. 5.15 - Results of tyre tests on Cresswell and Leighton Buzzard sands against Turnage's (1978) prediction curve for the coefficient of traction

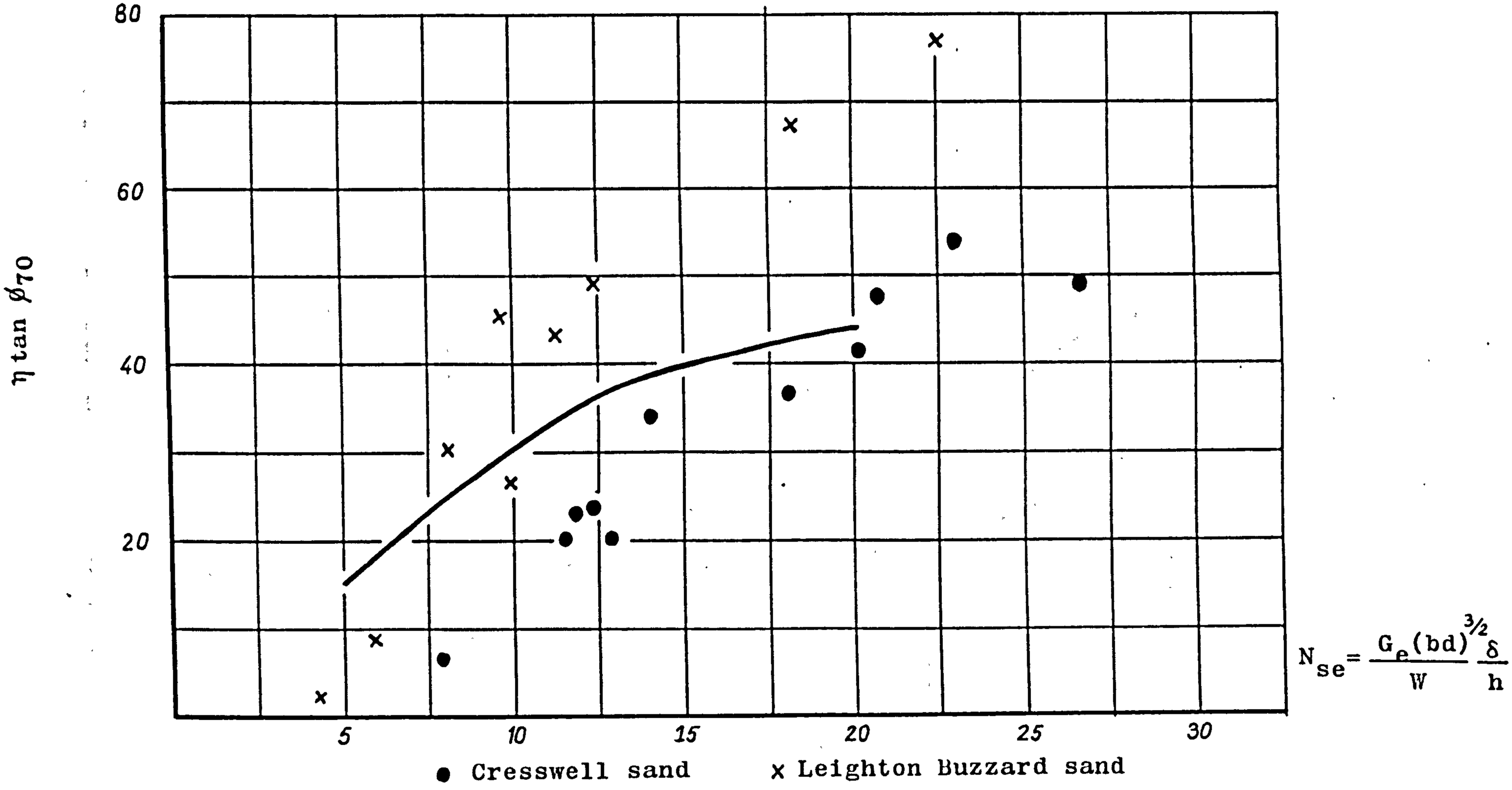

Fig.5.16 - Results of tyre tests on Cresswell and Leighton Buzzard sands against Turnage's (1978) prediction curve for the tractive efficiency

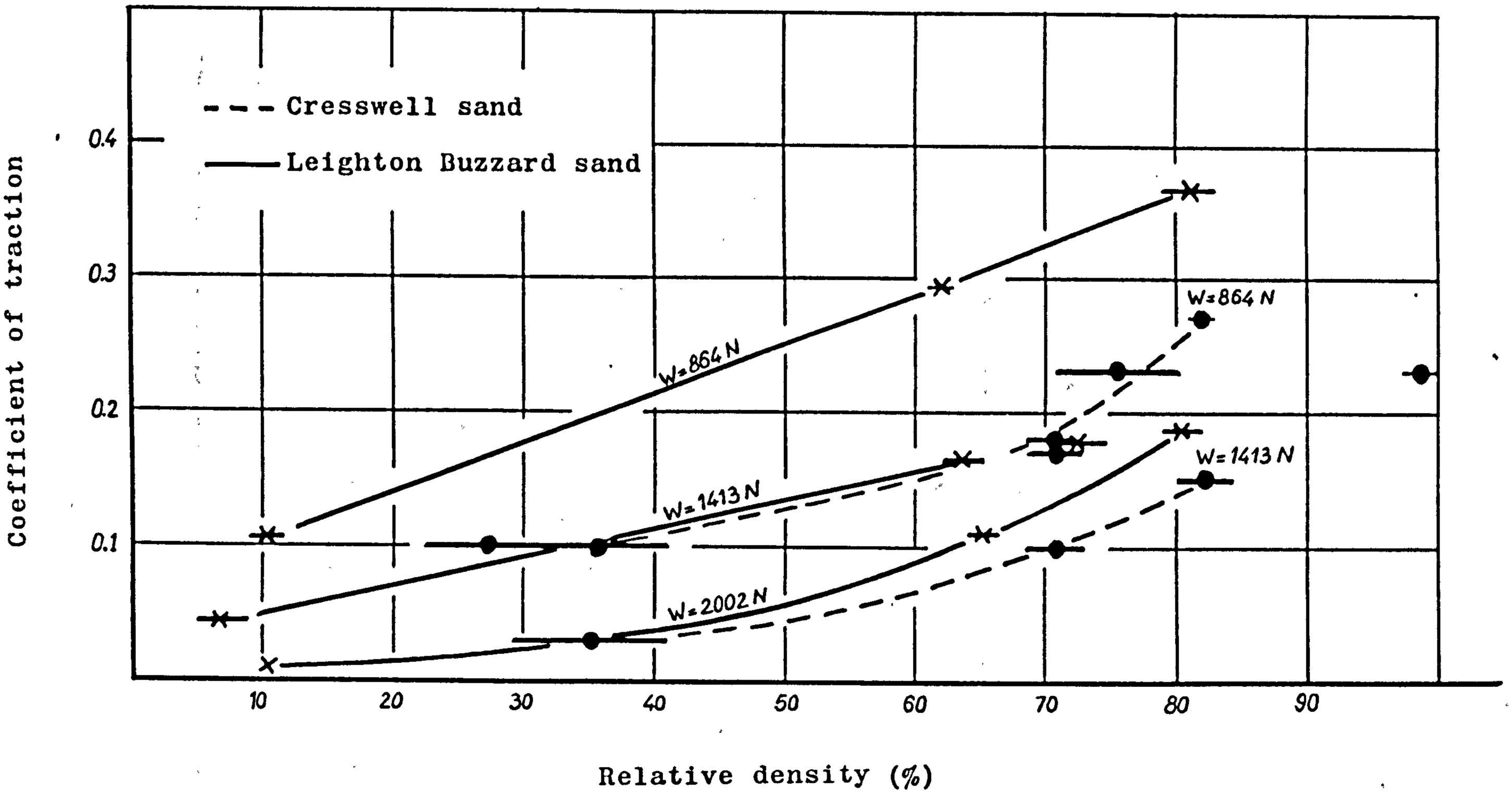

Fig. 5.17 - Coefficient of traction from tests on Cresswell and Leighton Buzzard sands with a 6.00-16-2PR tyre at 20% slip, 30% deflection plotted versus the soil relative density.

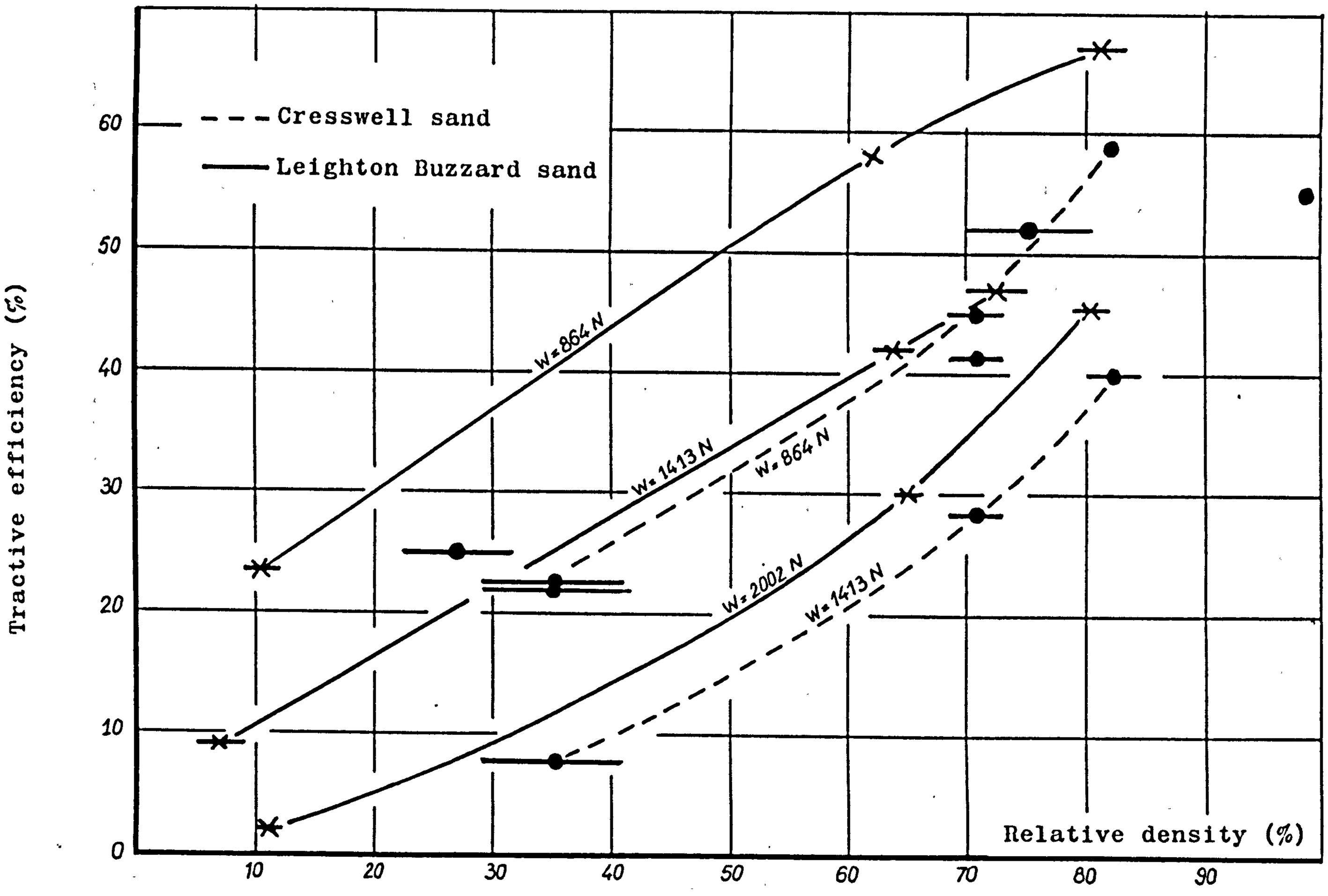

Fig. 5.18 - Tractive efficiency from tests on Cresswell and Leighton Buzzard sands with a 6.00-16-2PR tyre at 20% slip, 30% deflection plotted versus the soil relative density.

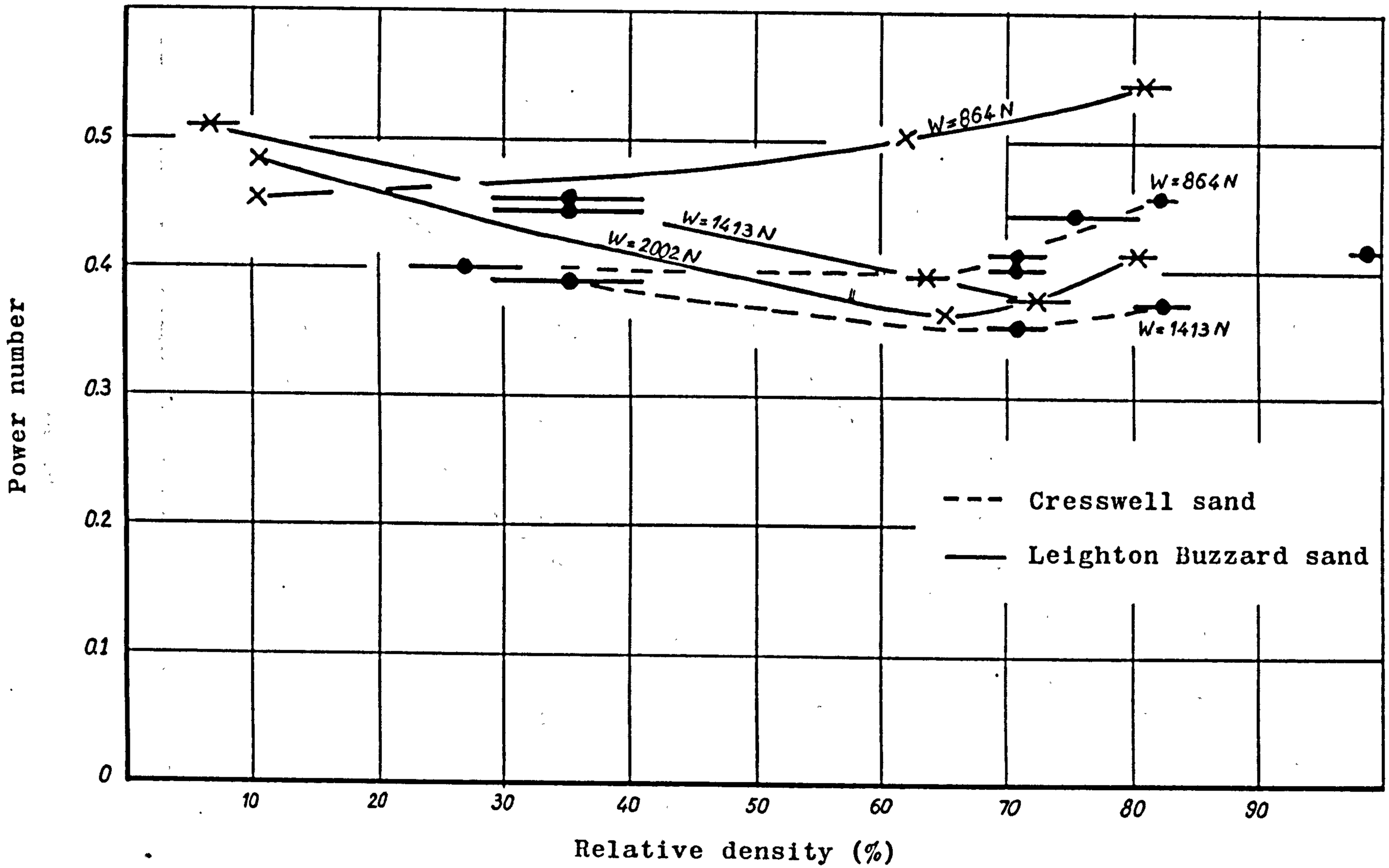

Fig. 5.19 - Power number from tests on Cresswell and Leighton Buzzard sands with a 6.00-16-2PR tyre at 20% slip, 30% deflection plotted against the soil relative density.

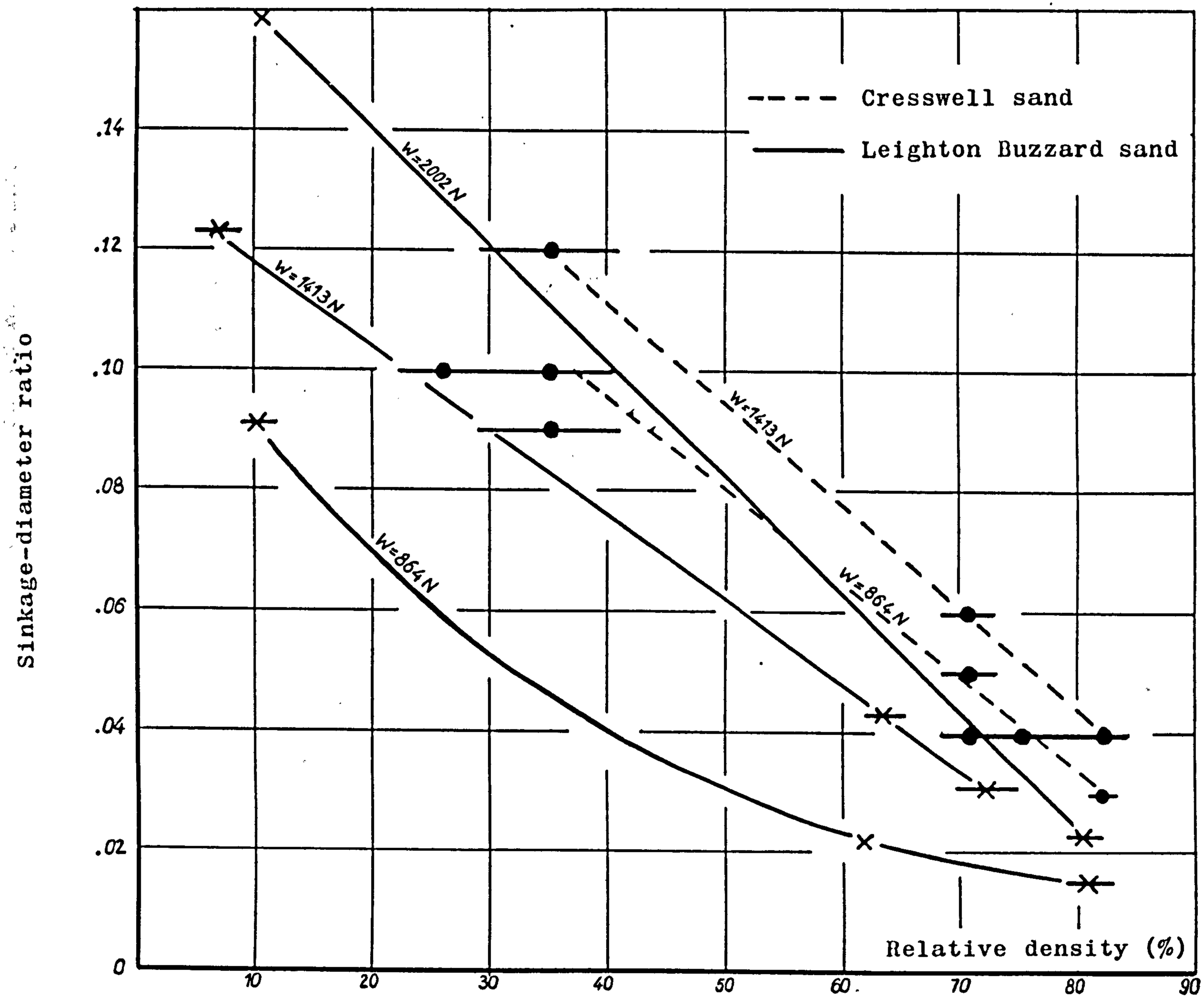

Fig. 5.20 - Sinkage-diameter ratio from tests on Cresswell and Leighton Buzzard sands with a 6.00-16-2PR tyre at 20% slip, 30% deflection plotted against the soil relative density.

Fig. 6.1 - Test LB5: 6.00-16-2PR smooth tyre on very dense Leighton Buzzard sand, D_d=79 to 82%. Vertical load = 2002N, 30% deflection on an unyielding surface , 20% slip.

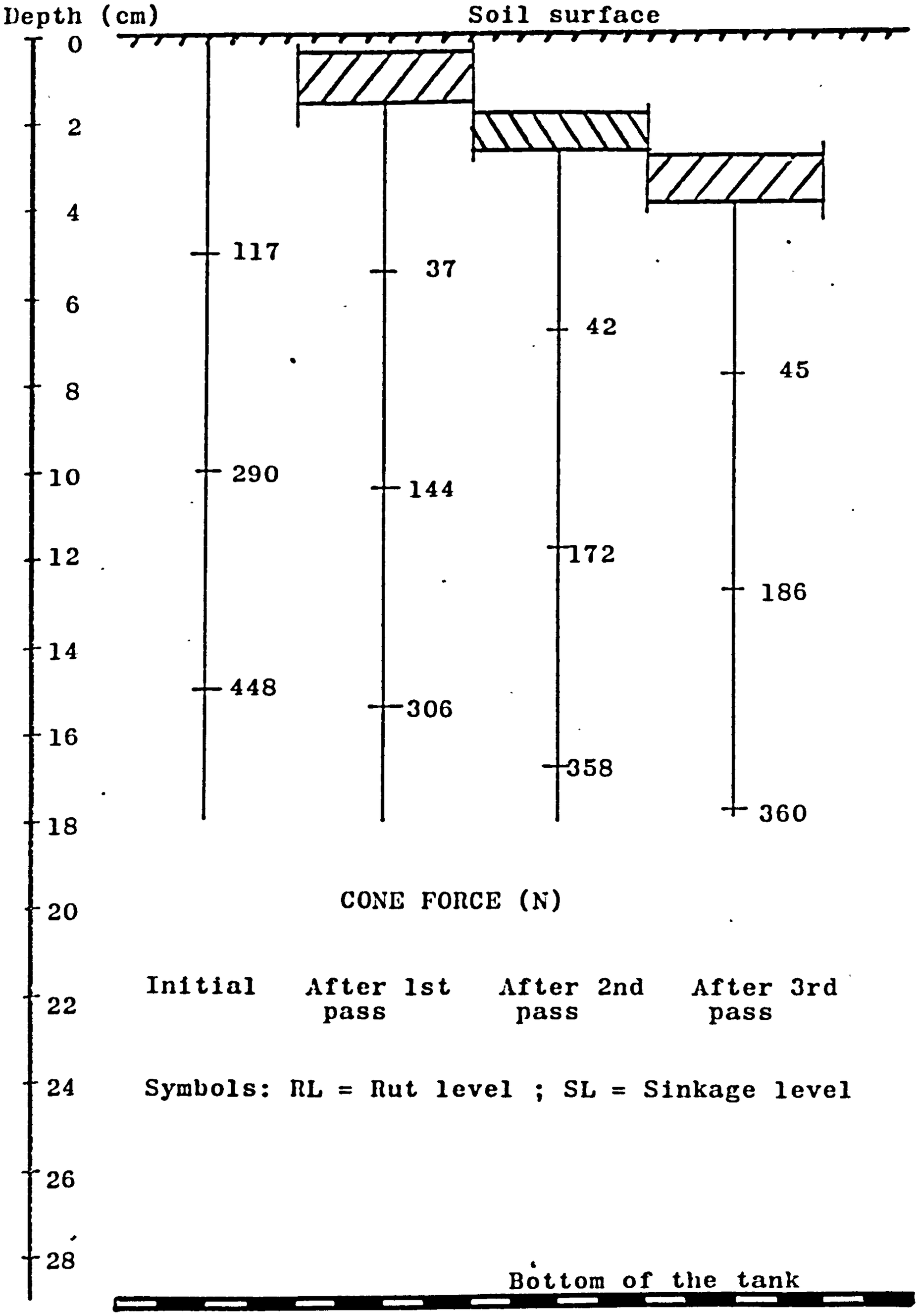

Fig. 6.2 - Test LB1, 6.00-16-2PR smooth tyre on very dense Leighton buzzard sand, D_d=70 to 75%. Vertical load = 1413N, 30% deflection on an unyielding surface, 20% slip.

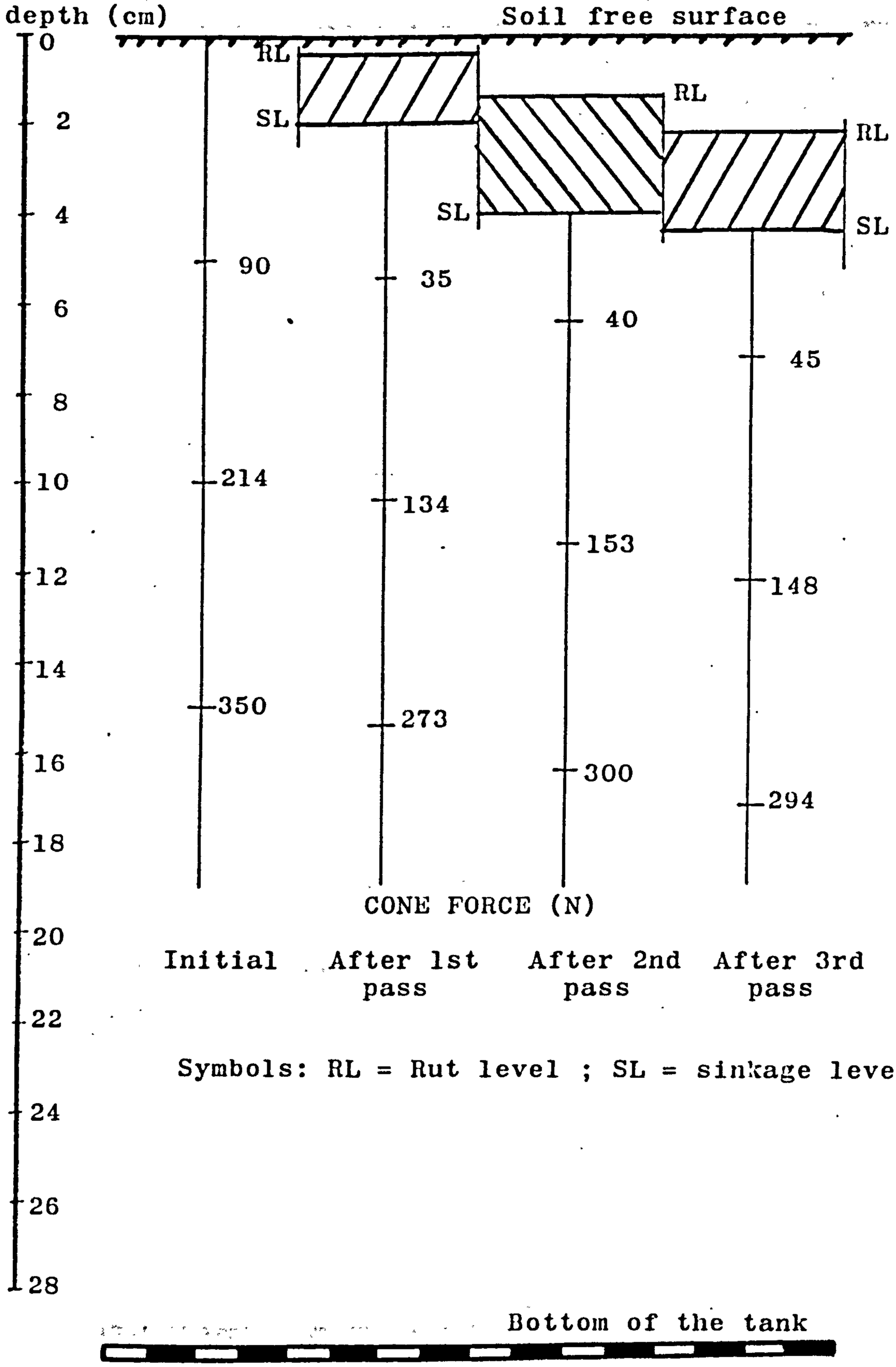

Fig. 6.3 - Test LB7, 6.00-16-2PR smooth tyre on very dense Leighton Buzzard sand, D_d=79 to 83%. Vertical load = 864N, 30% deflection on an unyielding surface, 20% slip.

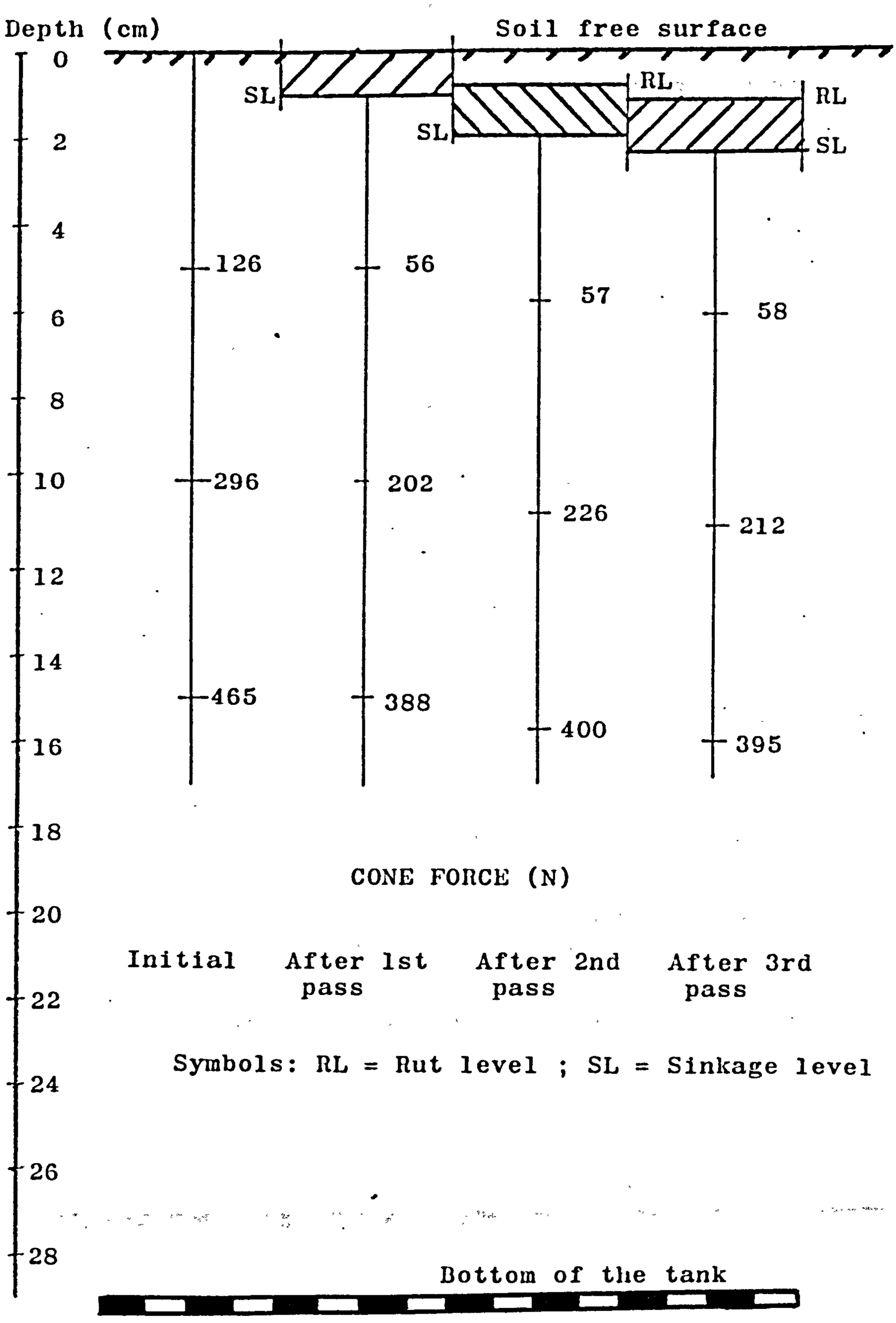

Fig. 6.4 - Test LB4, 6.00-16-2PR smooth tyre on medium dense Leighton Buzzard sand, D_d=64 to 66%. Vertical load = 2002N, 30% deflection, 20% slip.

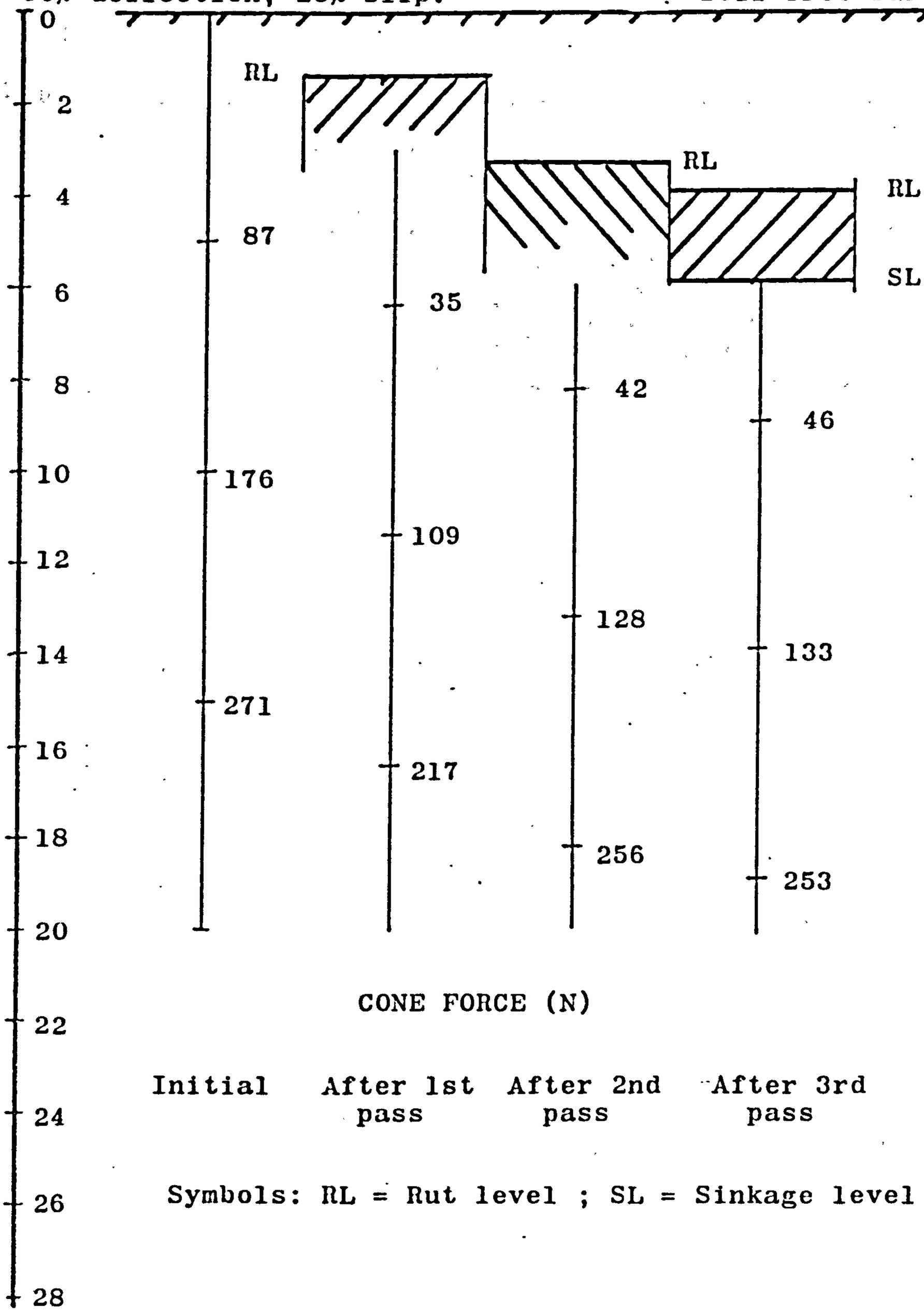

Fig. 6.5 - Test LB2, 6.00-16-2PR smooth tyre on medium dense Leighton Buzzard sand, D_d=62 to 65.5%. Vertical load = 1413N, 30% deflection on an unyielding surface, 20% slip.

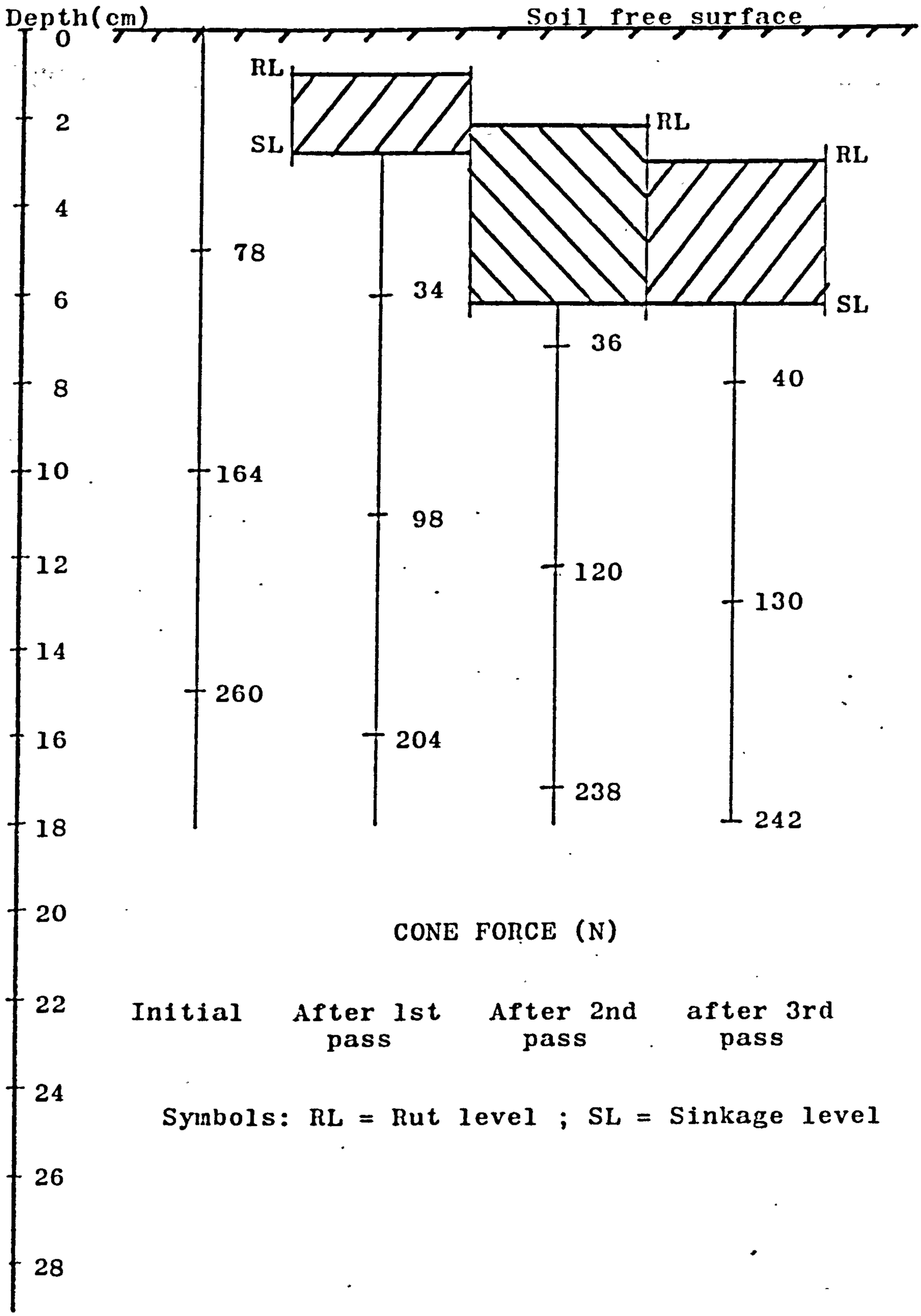

Fig. 6.6 - Test LB8, 6.00-16-2PR smooth tyre on medium dense Leighton buzzard sand, D_d=61 to 63%. Vertical load = = 864N, 30% deflection on an unyielding surface, 20% slip.

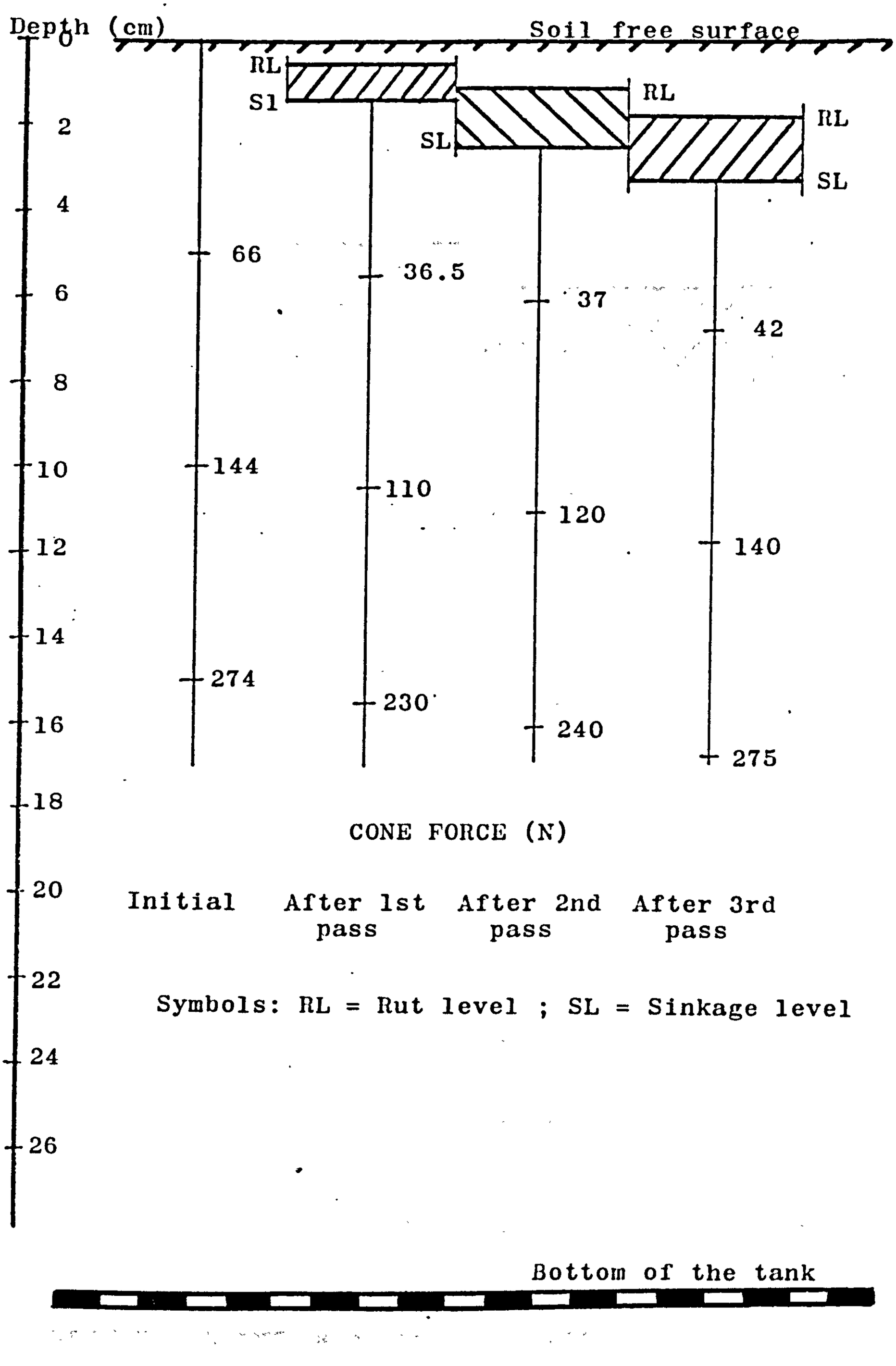

Fig. 6.7 - Test LB6, 6.00-16-2PR smooth tyre on very loose Leighton Buzzard sand, D_d= 10 to 11%. Vertical load = 2002N, 30% deflection on an unyielding surface, 20% slip.

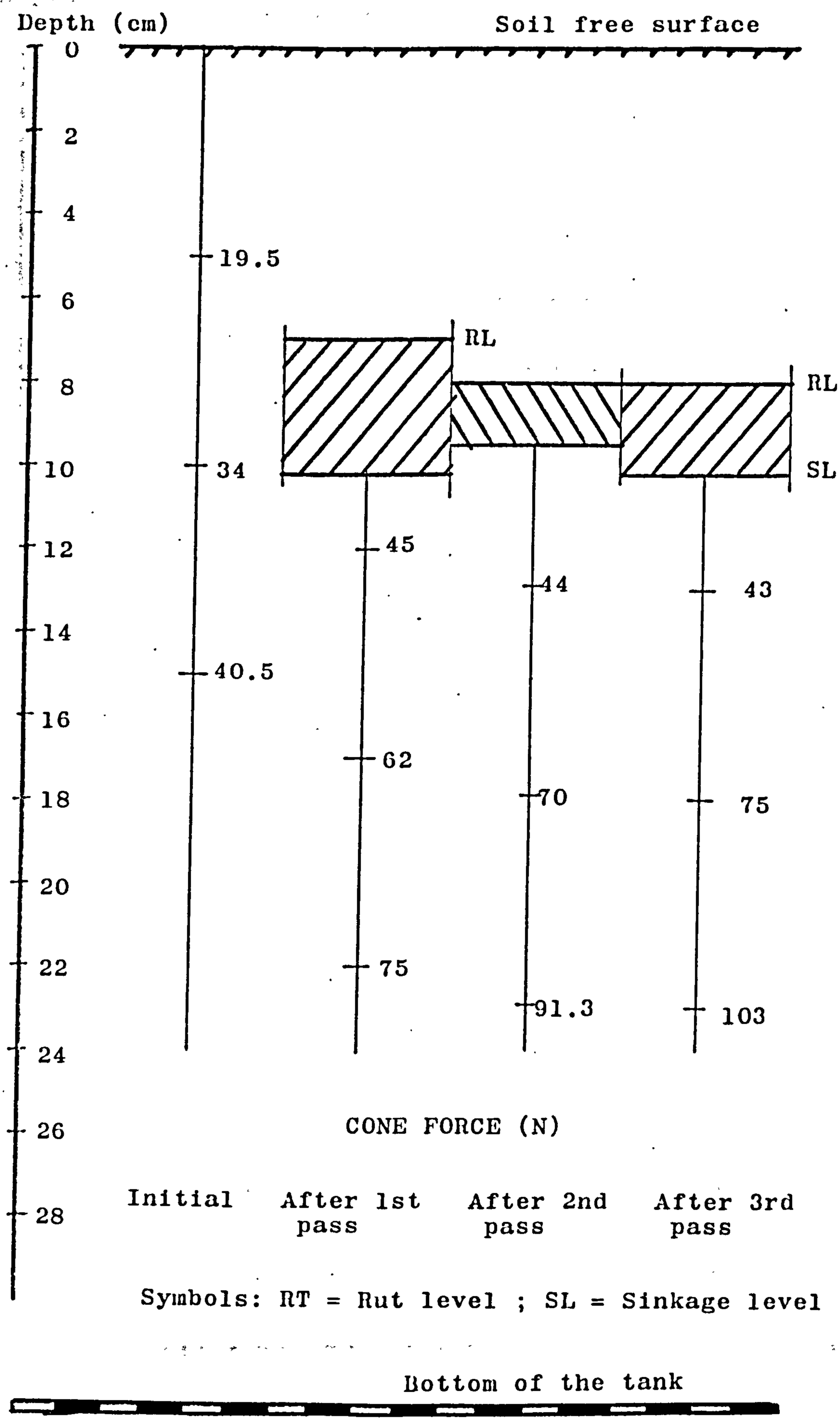

Fig. 6.8 - Test LB3/3A: 6.00-16-2PR smooth tyre on very loose Leighton Buzzard sand, D_d=5 to 9%. Vertical load = = 1413N, 30% deflection on hard surface, 20% slip.

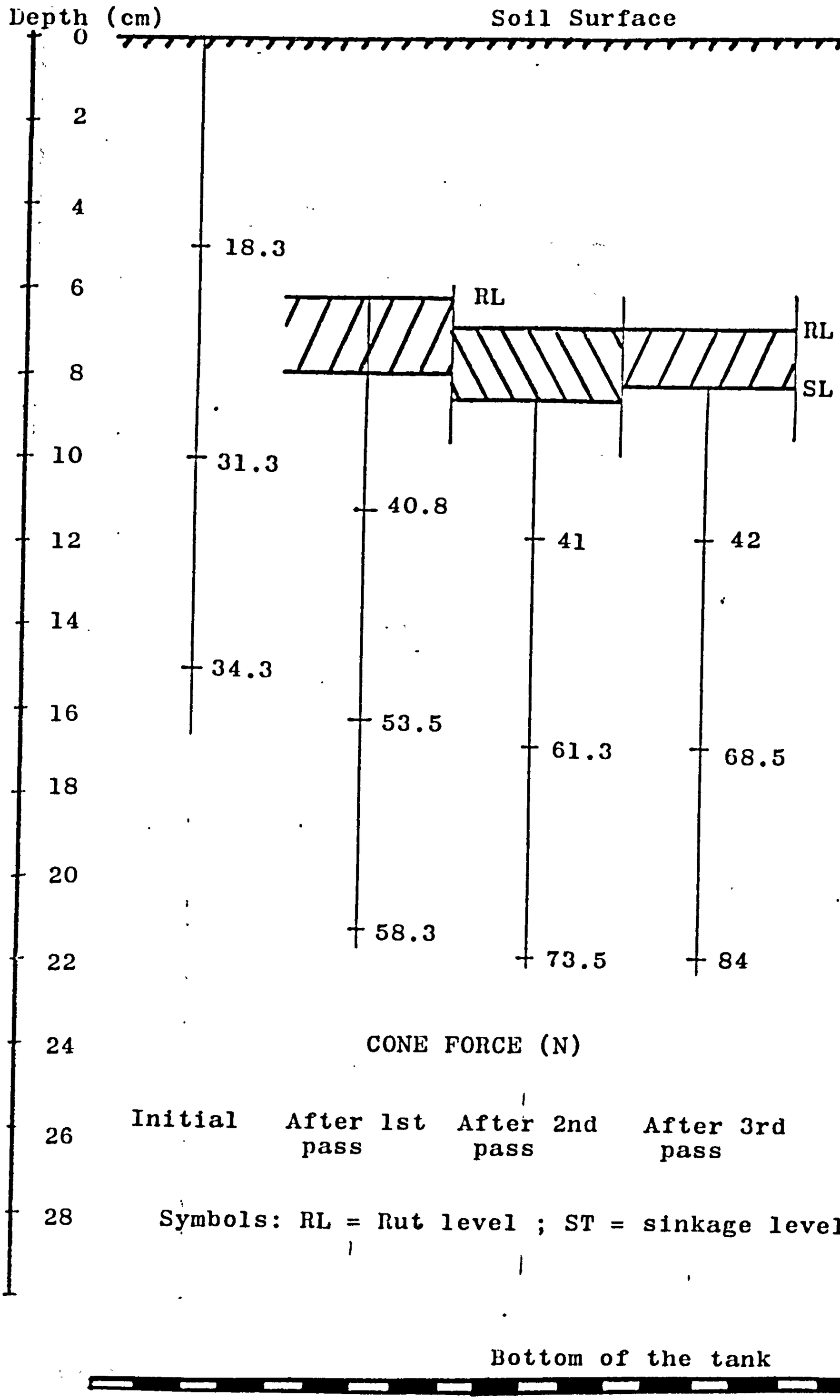

Fig. 6.9 - Test LB9, 6.00-16-2PR smooth tyre on very loose Leighton Buzzard sand, D_d=9-12%. Vertical load = 864N, 30% deflection on unyielding surface, 20% slip.

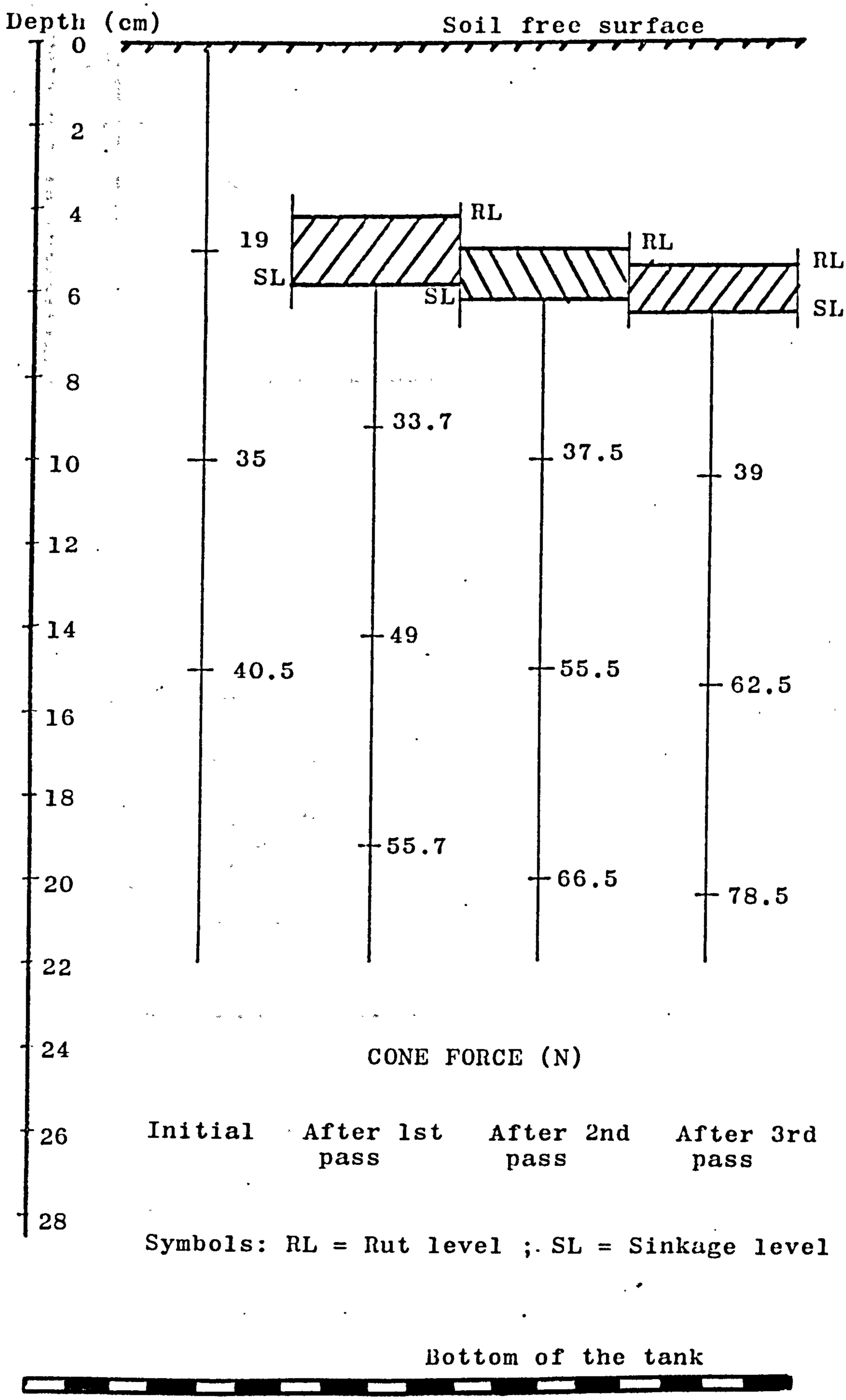

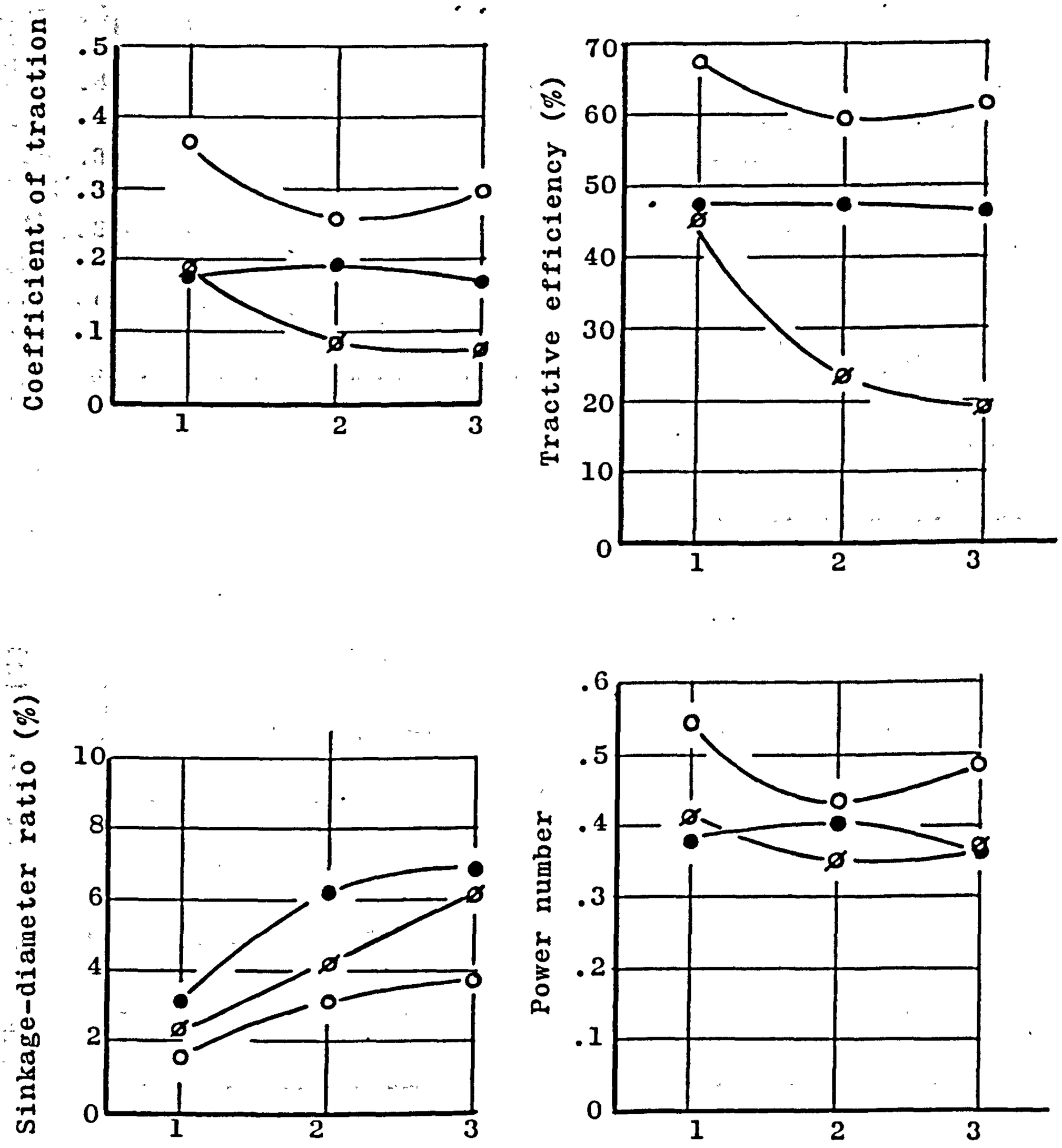

Fig. 6.10 - Traction performance of a 6.00-16-2PR smooth tyre at 20% slip on very dense air-dry Leighton Buzzard sand recorded on three consecutive passes.

Symbol	Test	W(N)	i.p.(psi)	D_d(%)
O	LB7	864	6.5	79-83
●	LB1	1413	11	70-75
⌀	LB5	2002	14.5	79-82

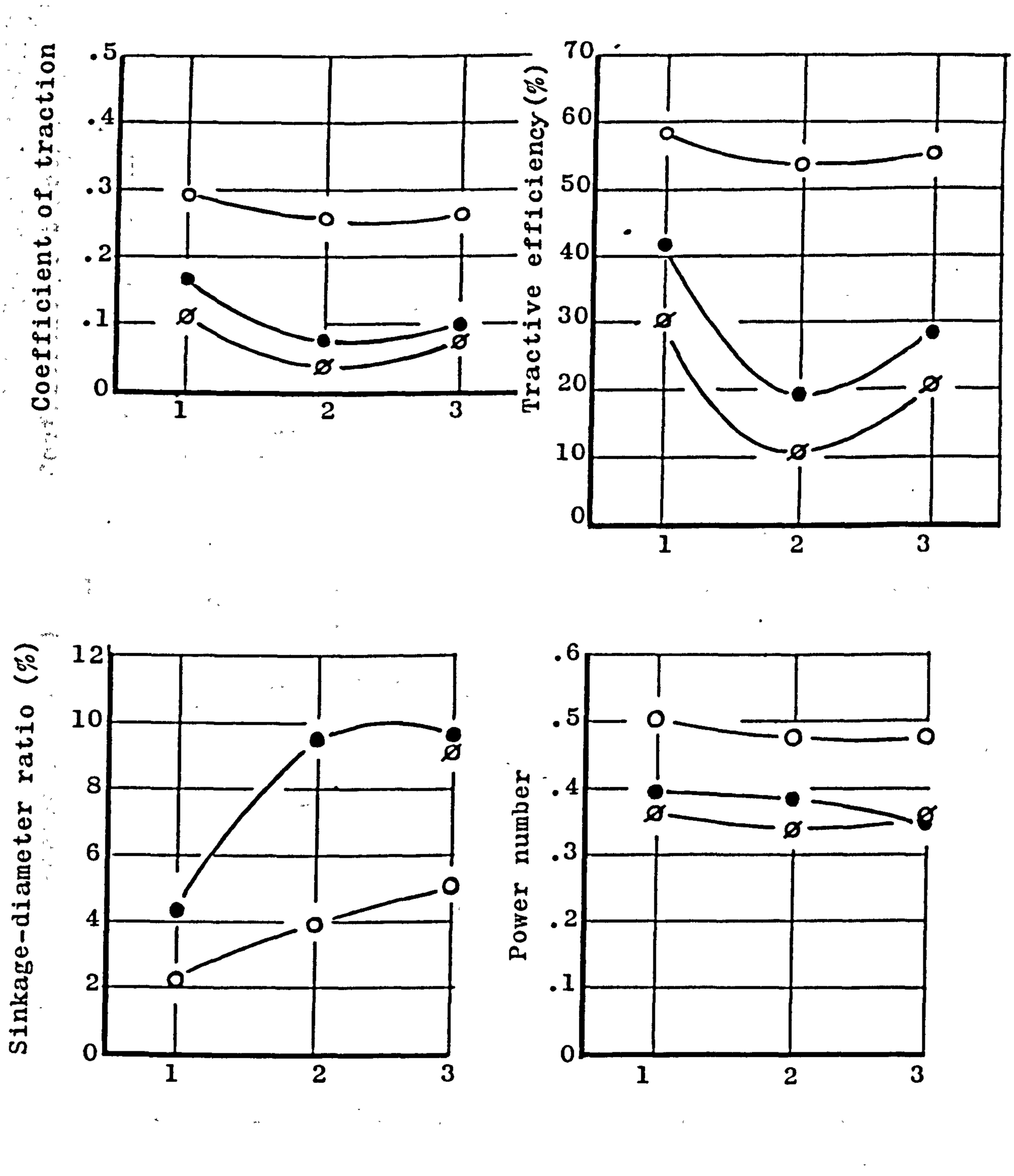

Fig. 6.11 - Traction performance of a 6.00-16-2PR smooth tyre at 20% slip on medium dense air-dry Leighton Buzzard sand recorded on three consecutive passes

Symbol	Test	W(N)	i.p.(psi)	D_d(%)
O	LB8	864	6.5	61-63
●	LB2	1413	11	62-66
Ø	LB4	2002	14.5	64-66

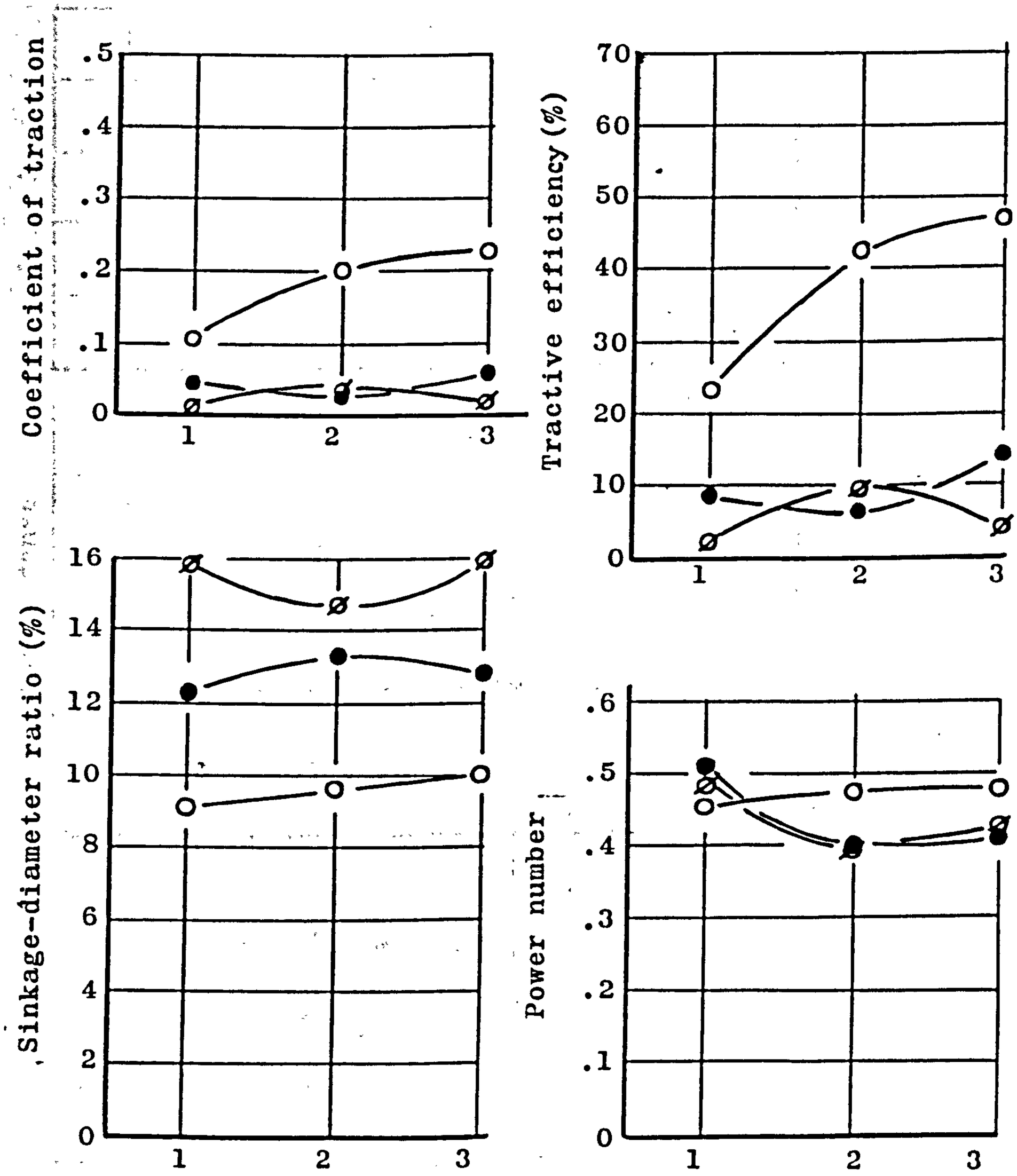

Fig. 6.12 - Traction performance of a 6.00-16-2PR smooth tyre at 20% slip on very loose air-dry Leighton Buzzard sand recorded on three consecutive passes

Symbol	Test	W(N)	i.p.(psi)	D_d(%)
O	LB9	864	6.5	9-12
●	LB3	1413	11	5- 9
Ø	LB6	2002	14.5	10-11

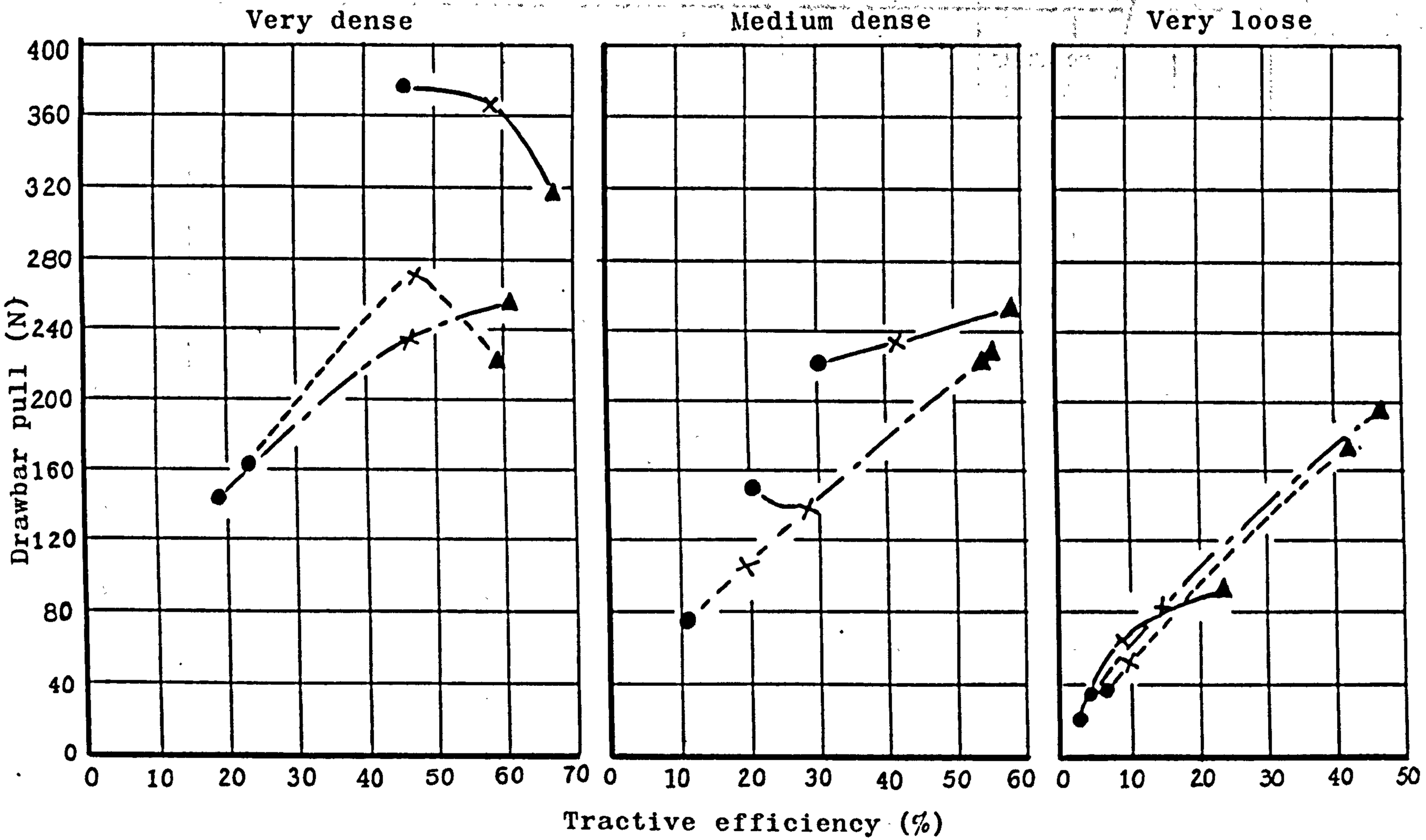

Fig. 6.13 - Drawbar pull versus tractive efficiency from tests on air-dry Leighton Buzzard sand with a 6.00-16-2PR smooth tyre at 20% slip and 30% deflection: (a) Very dense ; (b) Medium dense ; (c) Very loose.

● W=2002 N × W=1413 N ▲ W=864 N

First pass (——) ; Second pass (-----) ; Third pass (— - —)

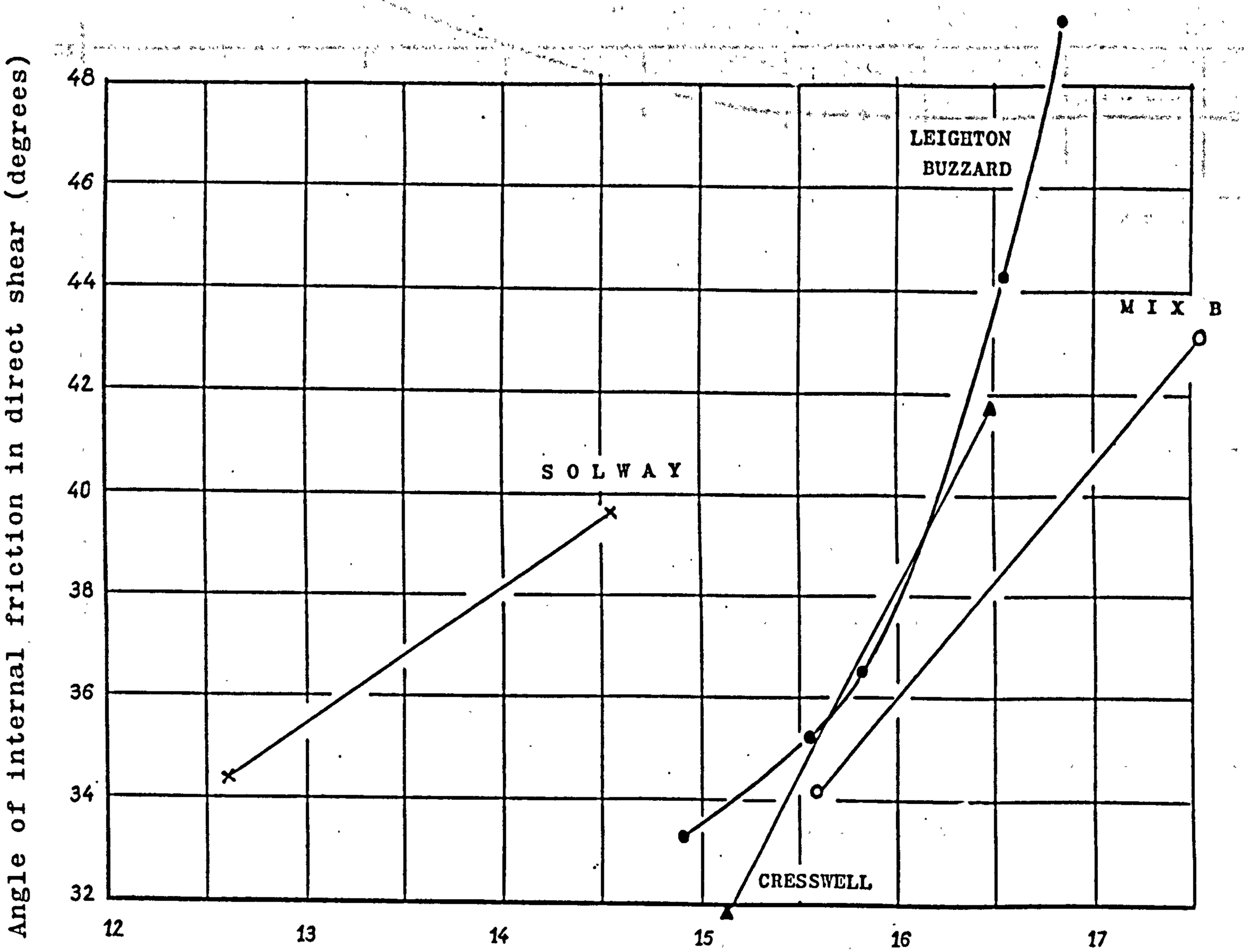

Fig. 7.1 - Relation between angle of friction and bulk density for the sands tested in Newcastle.

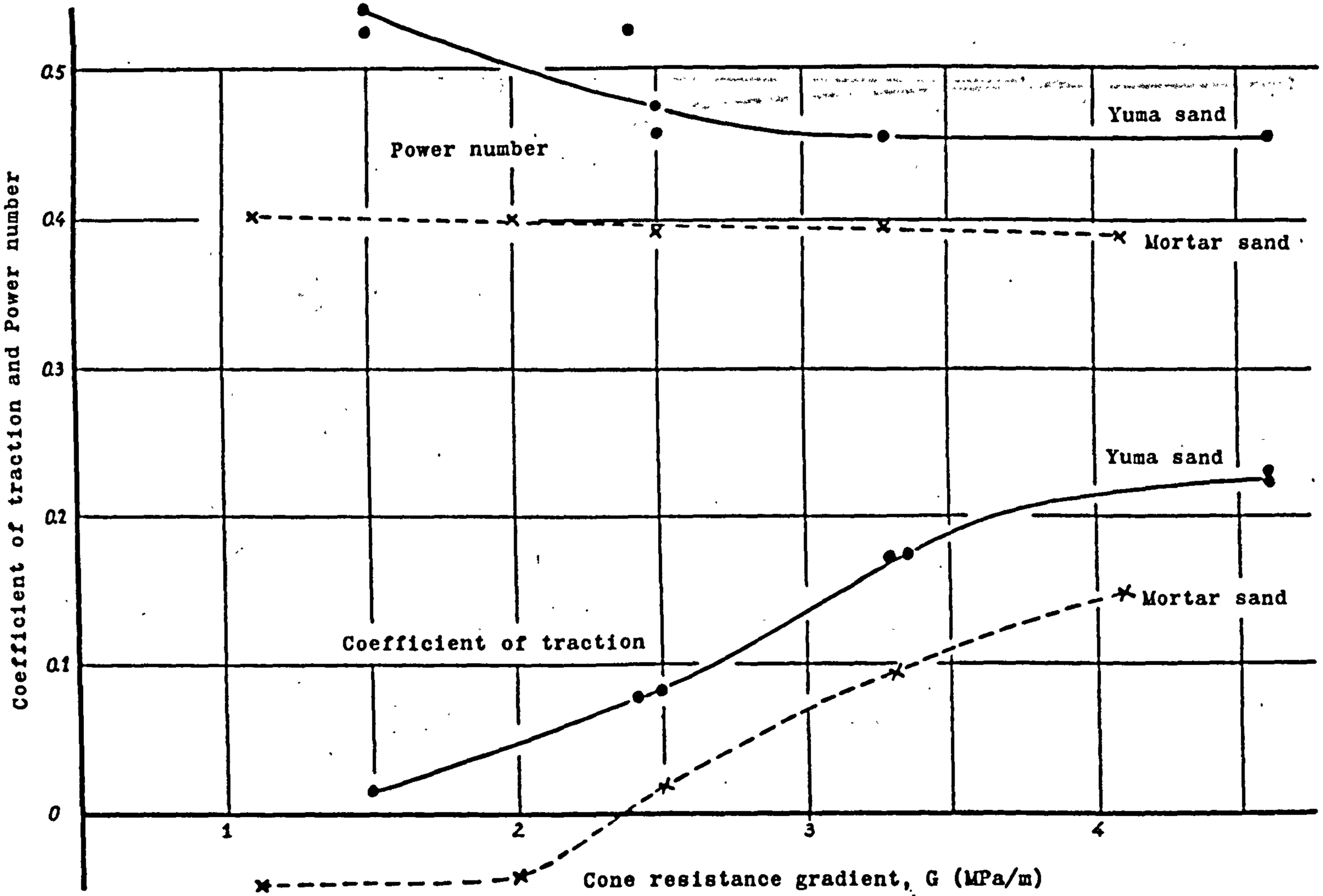

Fig. 7.2 - Coefficient of traction and power number from tests with a 9.00-14-2PR tyre at 20% slip, W=3.9kN, ip=35psi, on Yuma and Mortar sands, plotted against the cone resistance gradient.

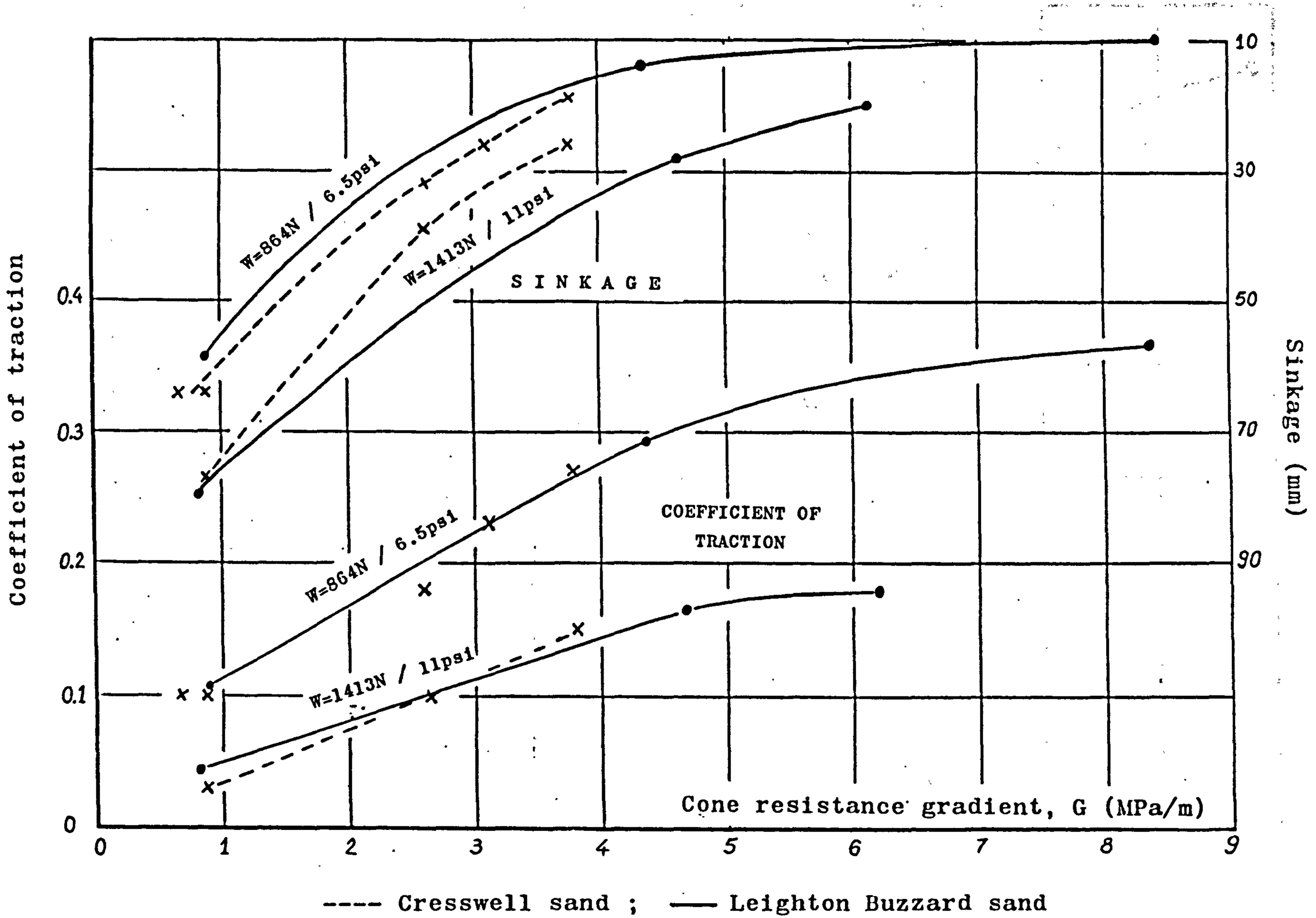

---- Cresswell sand ; —— Leighton Buzzard sand

Fig. 7.3 - Coefficient of traction and sinkage from tests with a 6.00-16-2PR smooth tyre at 20% slip , 30% deflection on hard surface, plotted against the cone resistance gradient.

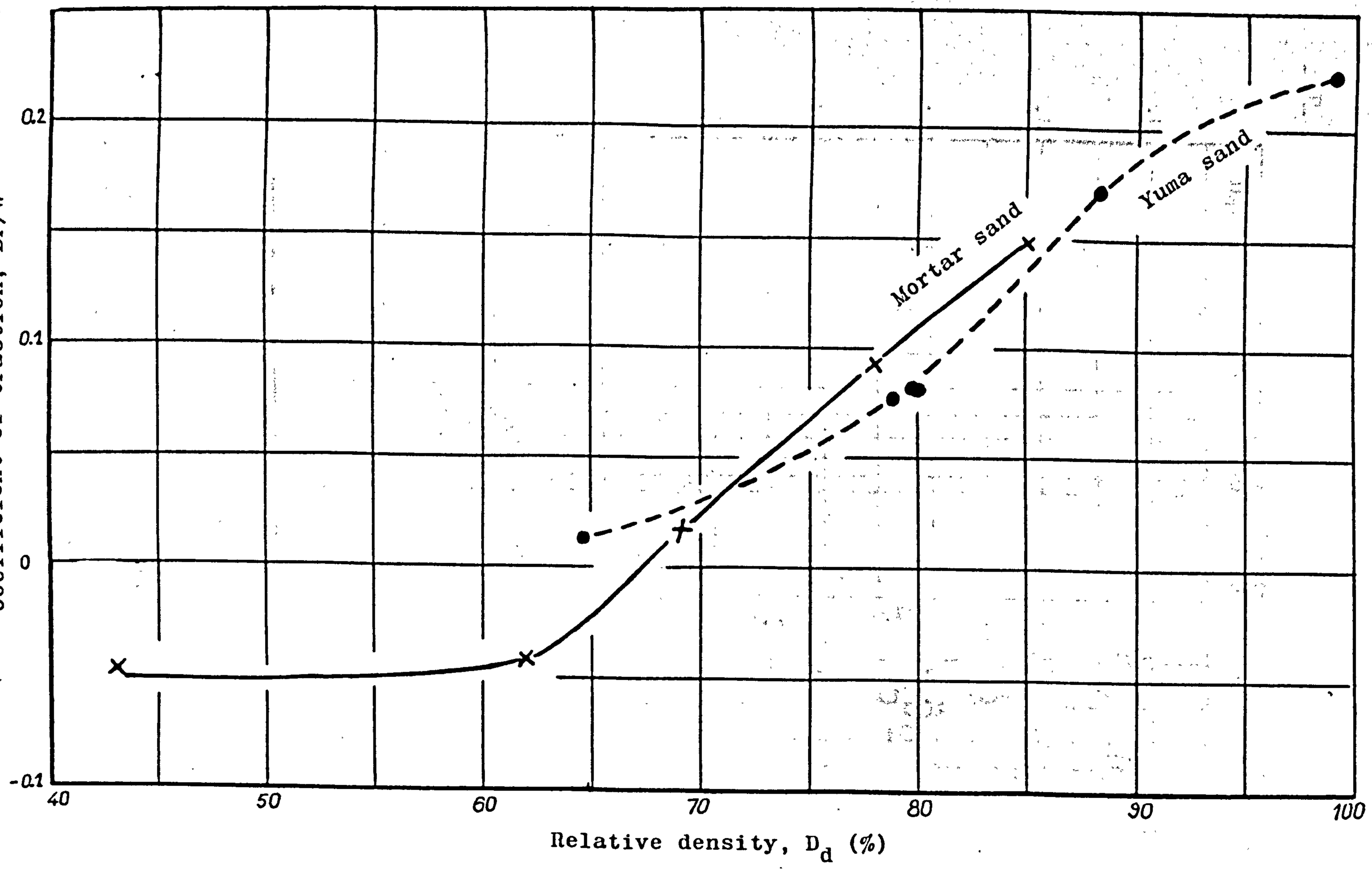

Fig. 7.4 - Coefficient of traction from tests with a 9.00-14-2PR tyre at 20% slip, W=3.9kN, ip=35psi, on Yuma and Mortar sands, plotted against the soil relative density.

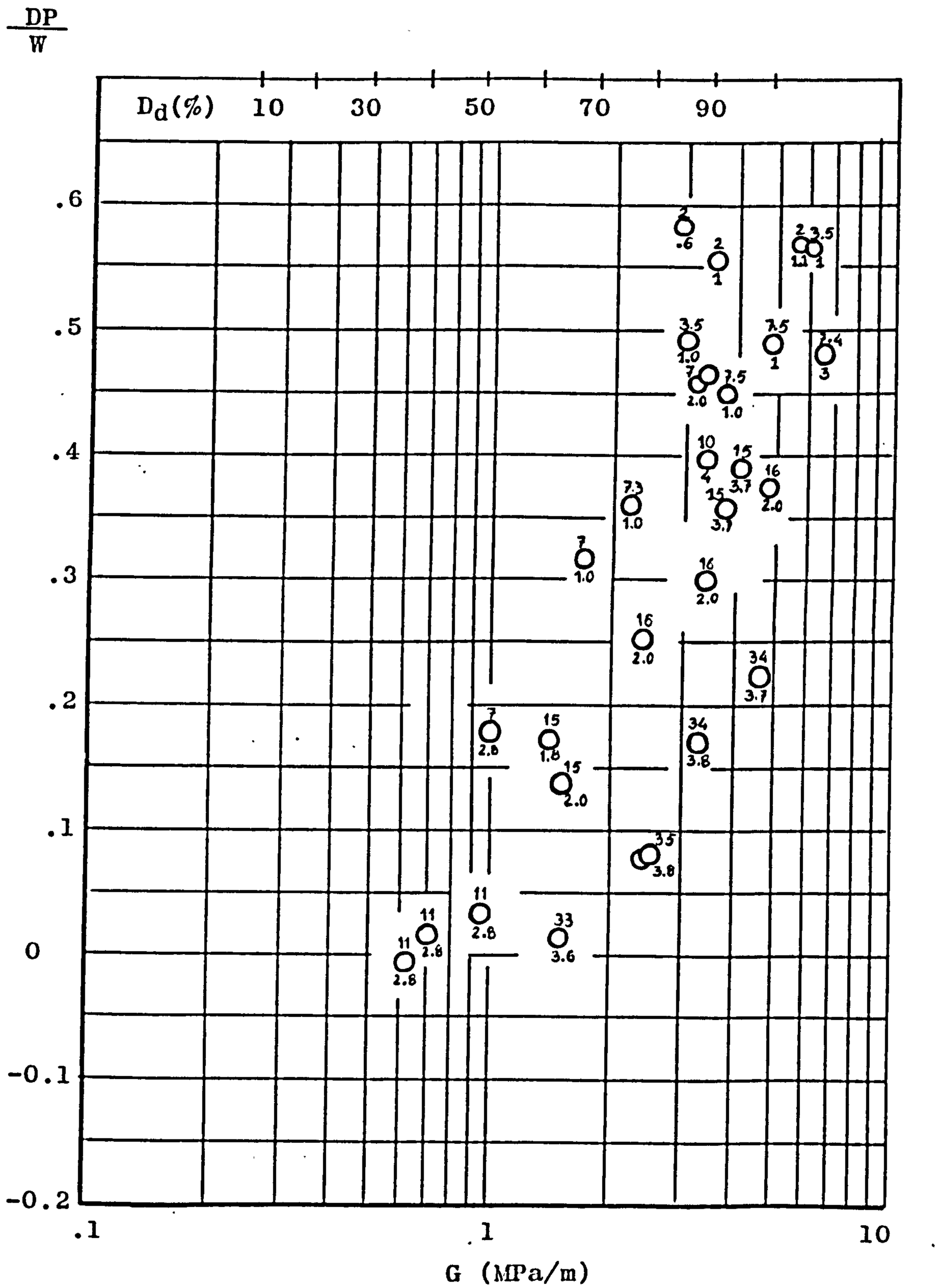

Fig. 7.5 - Results of tests with a 9.00-14-2PR tyre on Yuma sand versus cone resistance gradient, G. Slip=20%. Data from Turnage (1972b).

symbols $\underset{W\ (kN)}{\overset{i.p.(psi)}{O}}$

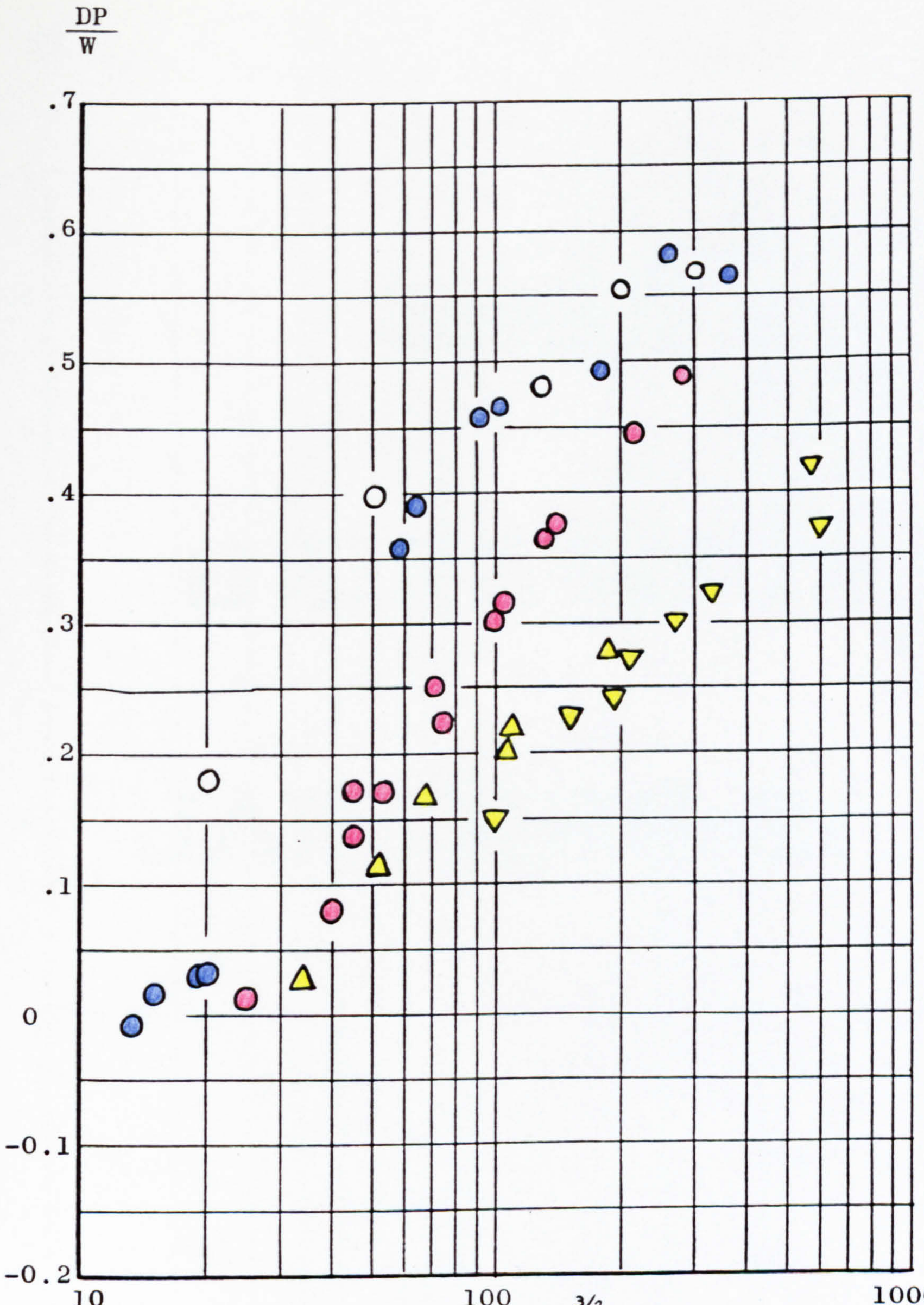

○ - δ/h=35% ; ● - δ/h=25% ; ● - δ/h=15% ; △ - rigid wheel b=15cm d=71cm ; ▽ - rigid wheel b=31cm , d=71cm.

Fig. 7.6 - Results of tests with a 9.00-14-2PR tyre and two rigid wheels plotted against the number $G(bd)^{3/2}/W$. Data from Turnage (1972b).

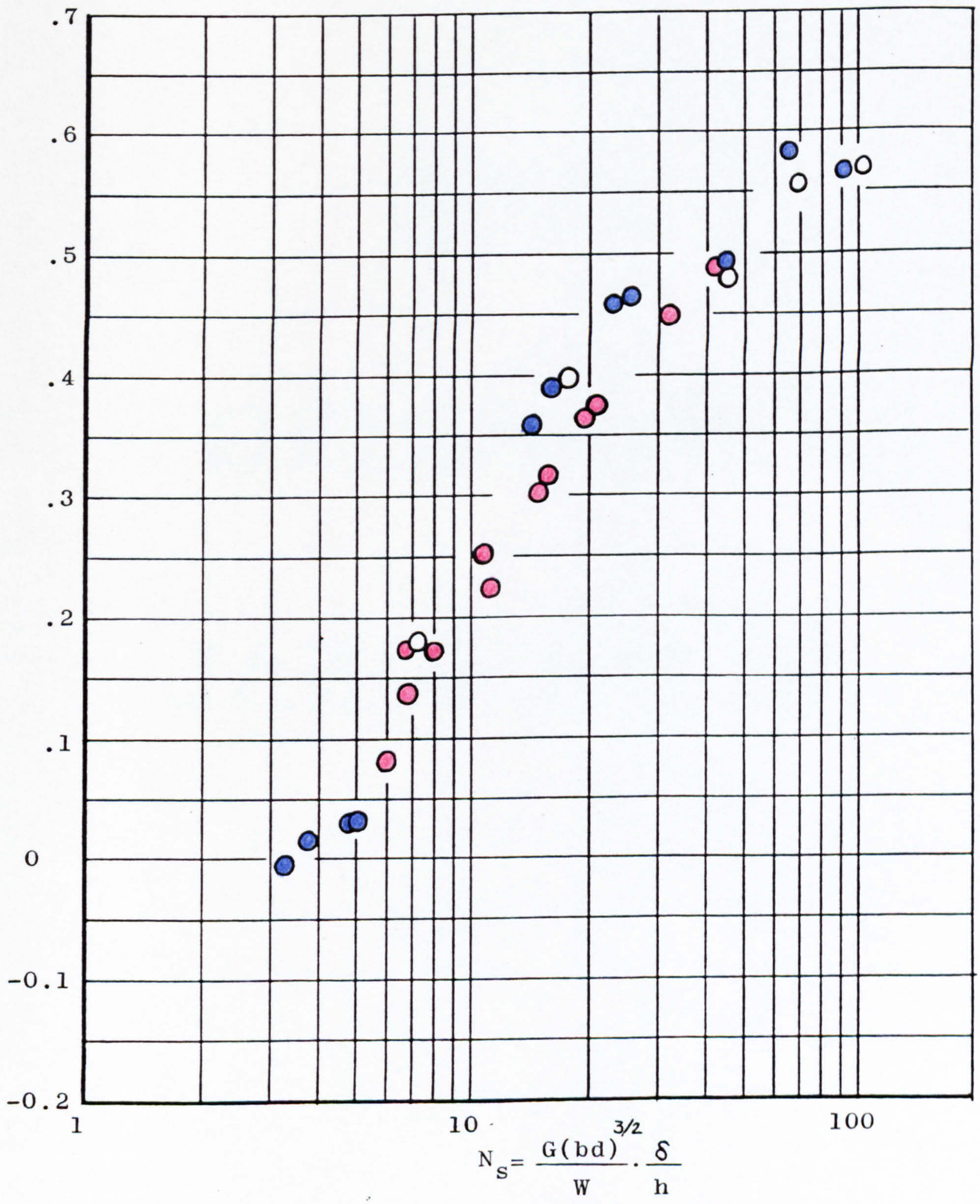

Fig. 7.7 - Results of tests with a 9.00-14-2PR tyre on Yuma sand plotted against the W.E.S. sand number N_s. Data from Turnage (1972b).

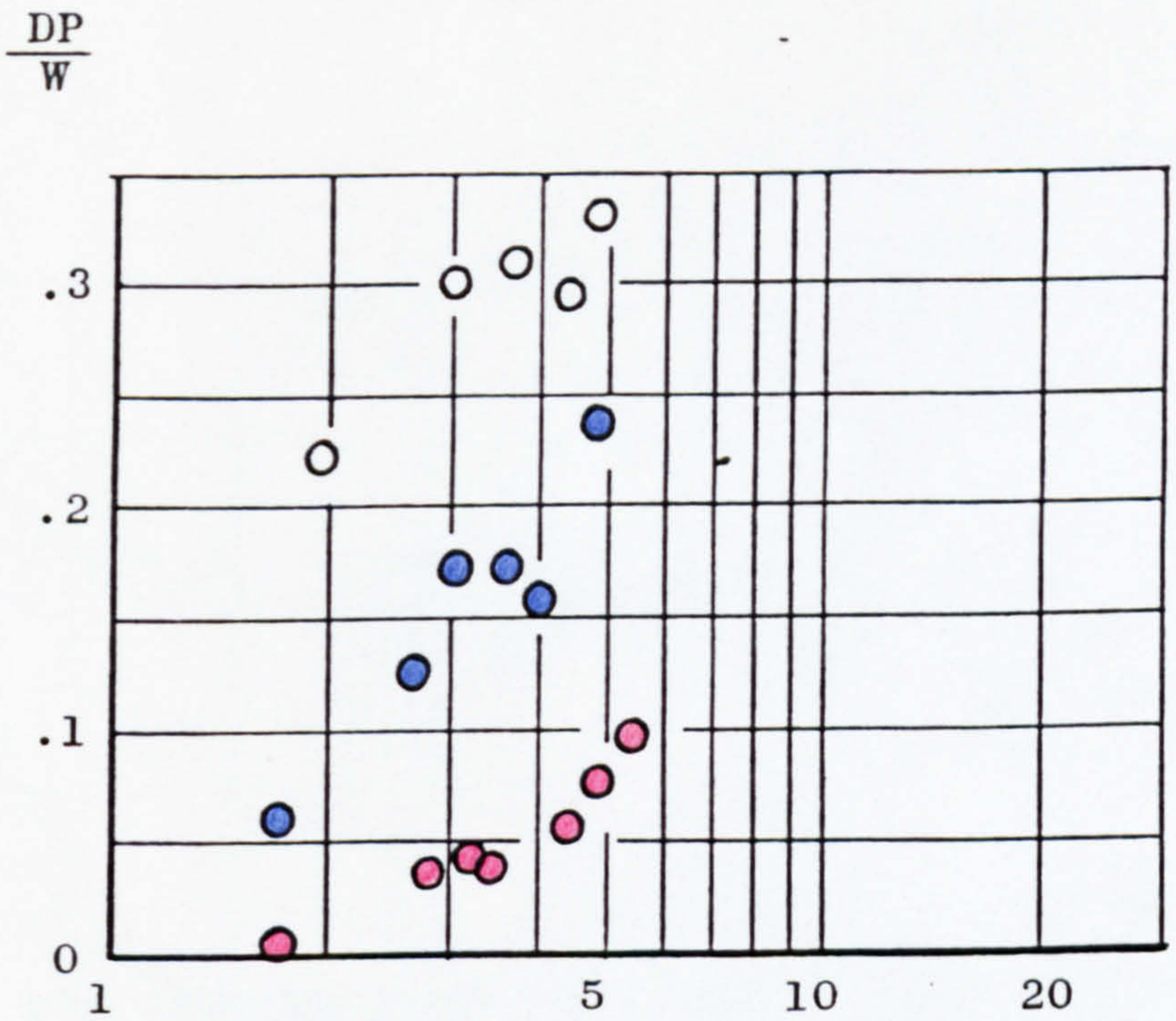

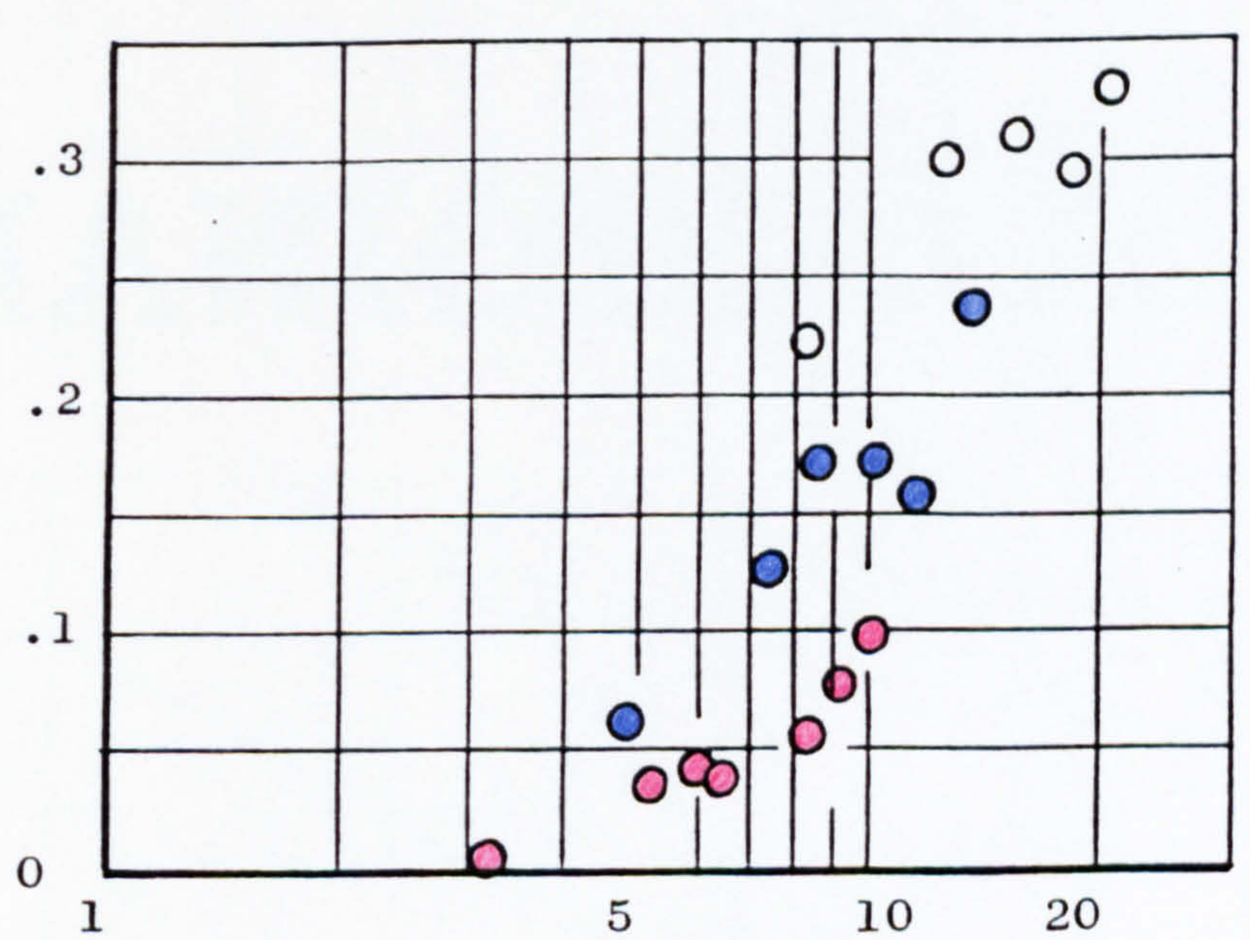

Fig. 7.8 - Results of tests with a 11.00-20-12PR tyre on Yuma sand at constant vertical load W=13.35kN and 20% slip plotted (a) versus cone resistance gradient, G, and (b) versus the W.E.S. sand number N_s. Data from Turnage (1972b).

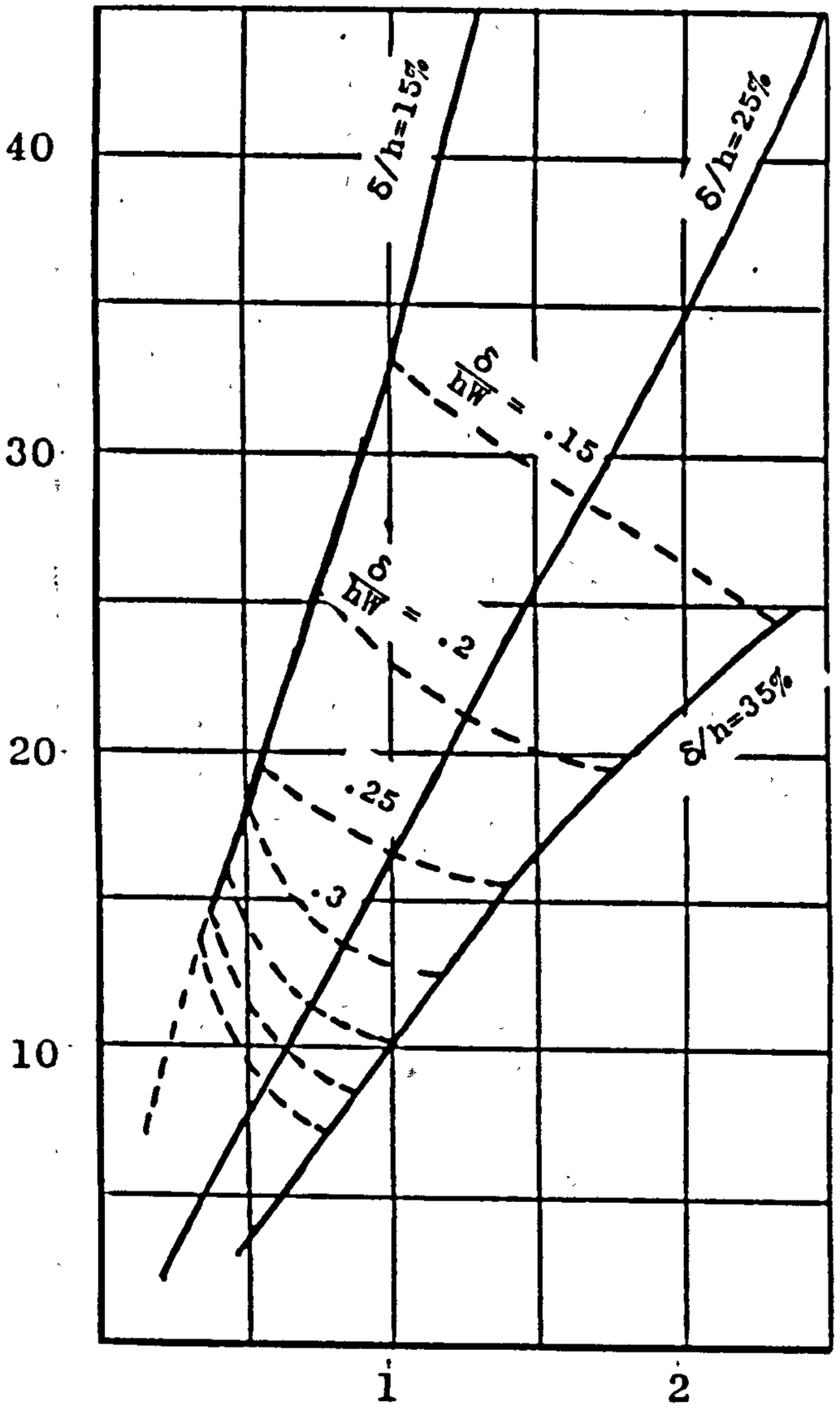

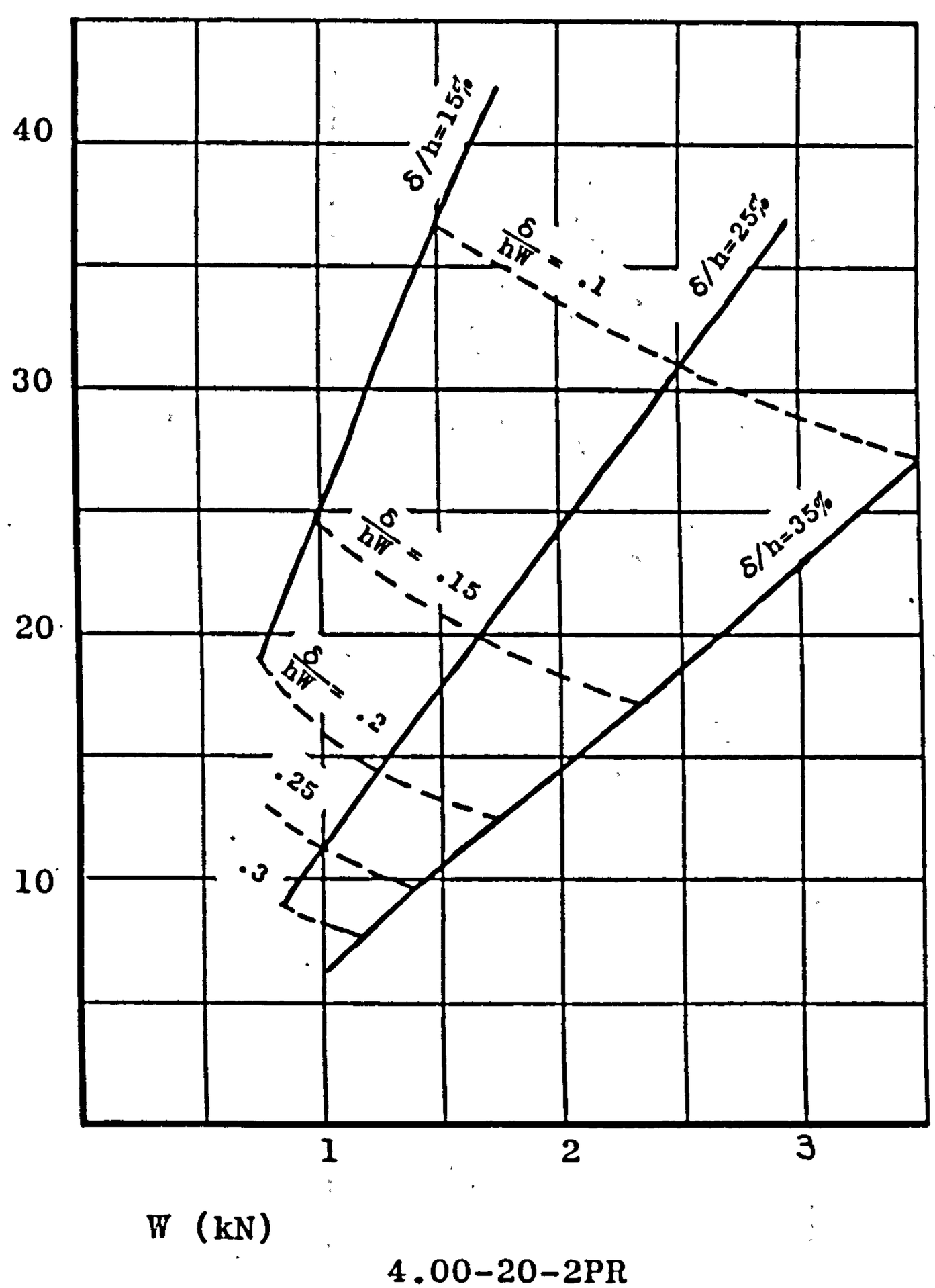

Fig. 7.9 - Load-pressure diagrams for the 4.00-7 and 4.00-20 tyres.

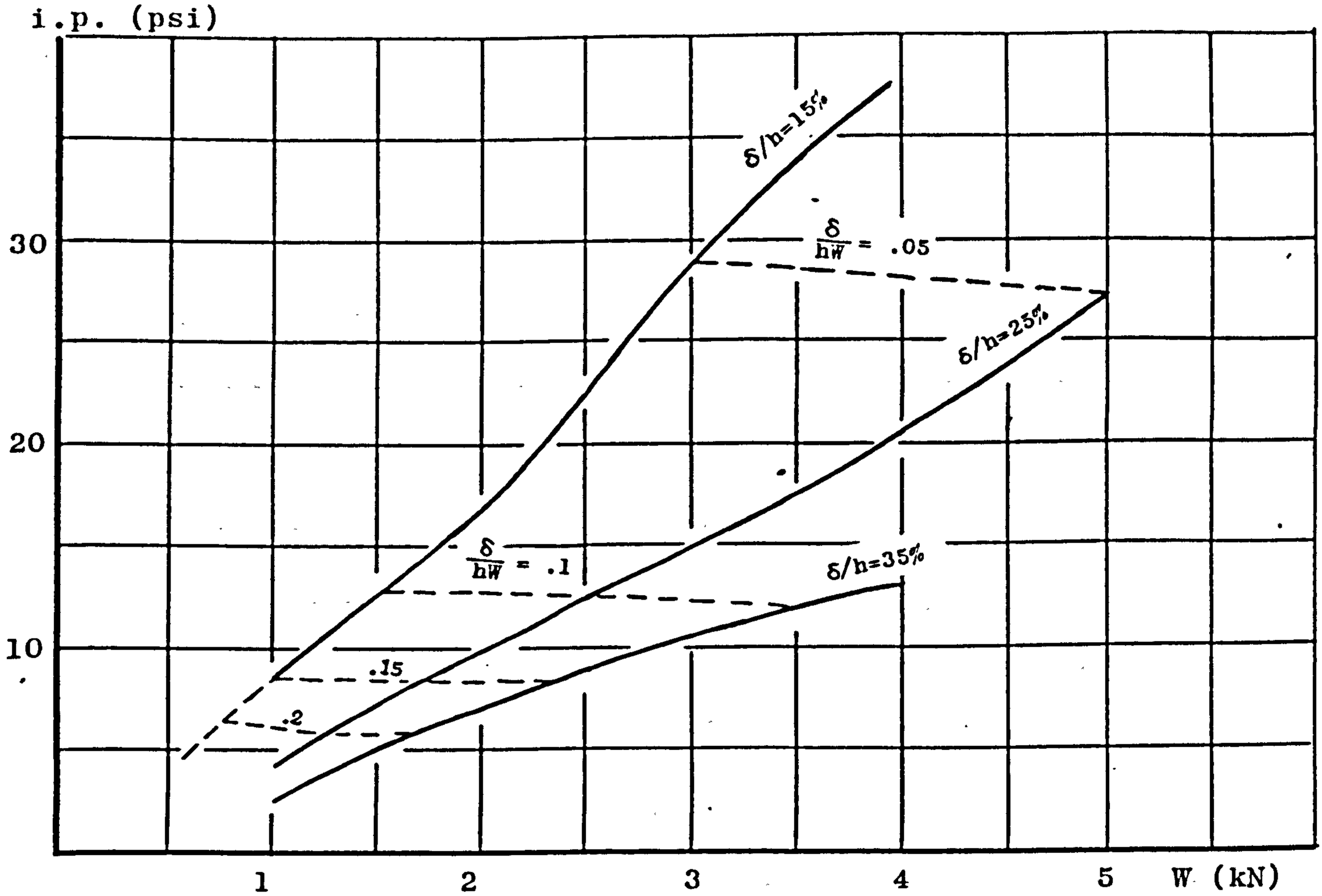

Tyre : 6.00-16-2PR

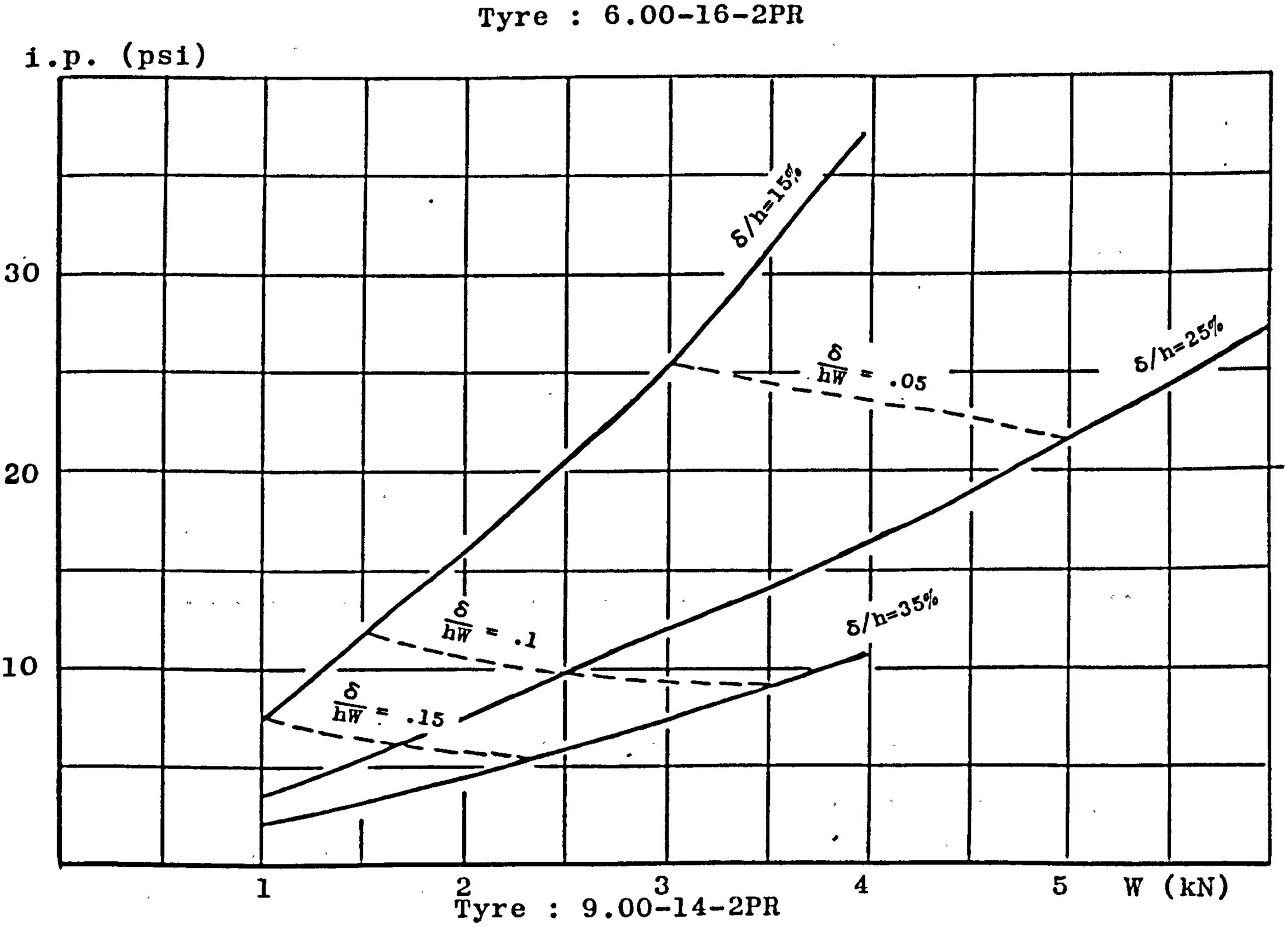

Tyre : 9.00-14-2PR

Fig. 7.10 - Load-pressure diagrams for the 6.00-16 and 9.00-14 tyres

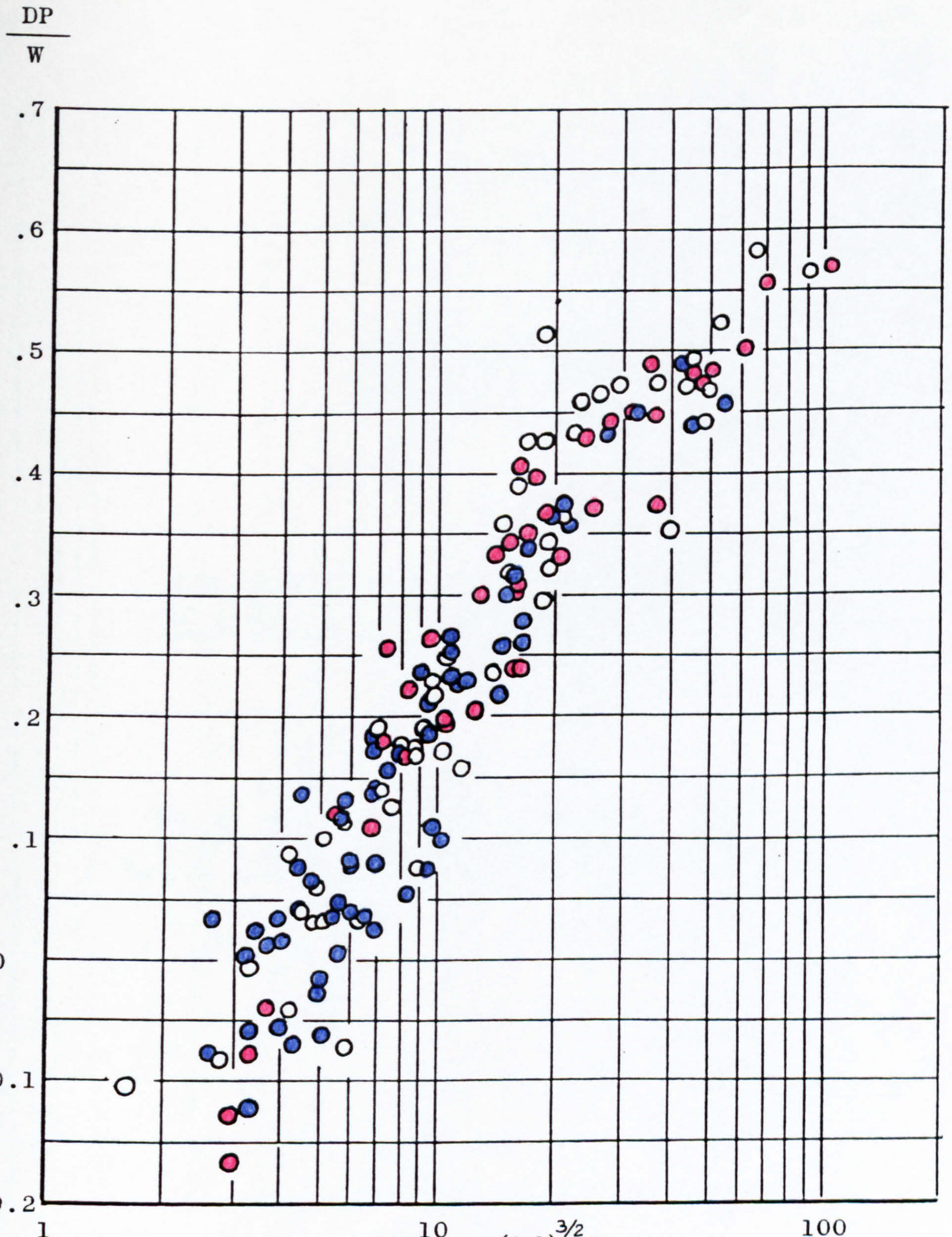

○ - δ/h =35% ; ● - δ/h =25% ; ● - δ/h =15%

Fig. 7.11 - Results of tests with 10 different tyres at 20% slip done by W.E.S. on Yuma sand plotted against the original W.E.S. sand number N_s . Data from Turnage (1972b).

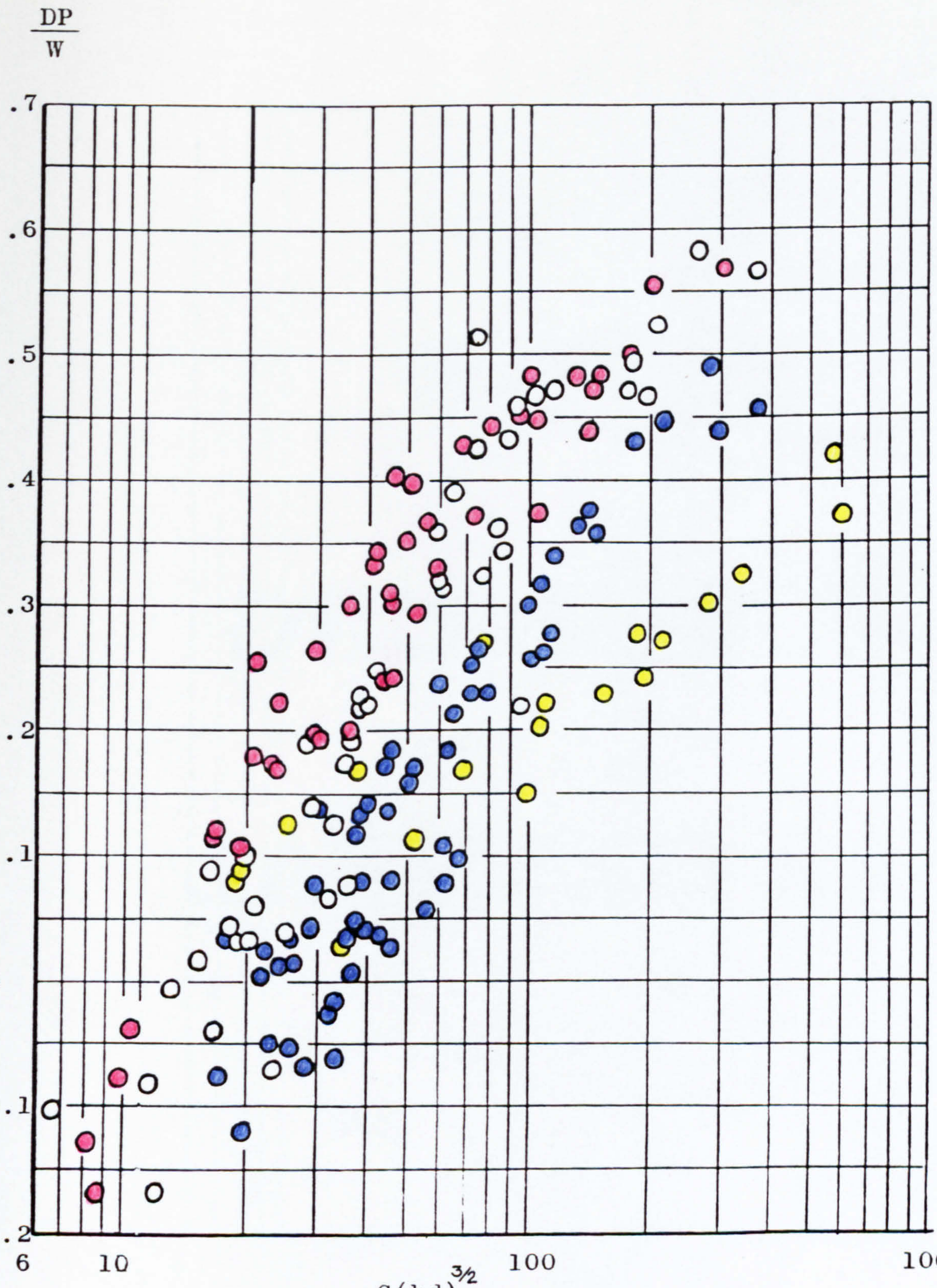

● - δ/h=35% ; ○ - δ/h=25% ; ● - δ/h=15% ; ○ - Rigid wheels

Fig. 7.12 - Results of tests with 10 different tyres and 3 rigid wheels done by W.E.S. on Yuma sand plotted against the sand number $G(bd)^{3/2}/W$. Data from Turnage 1972b.

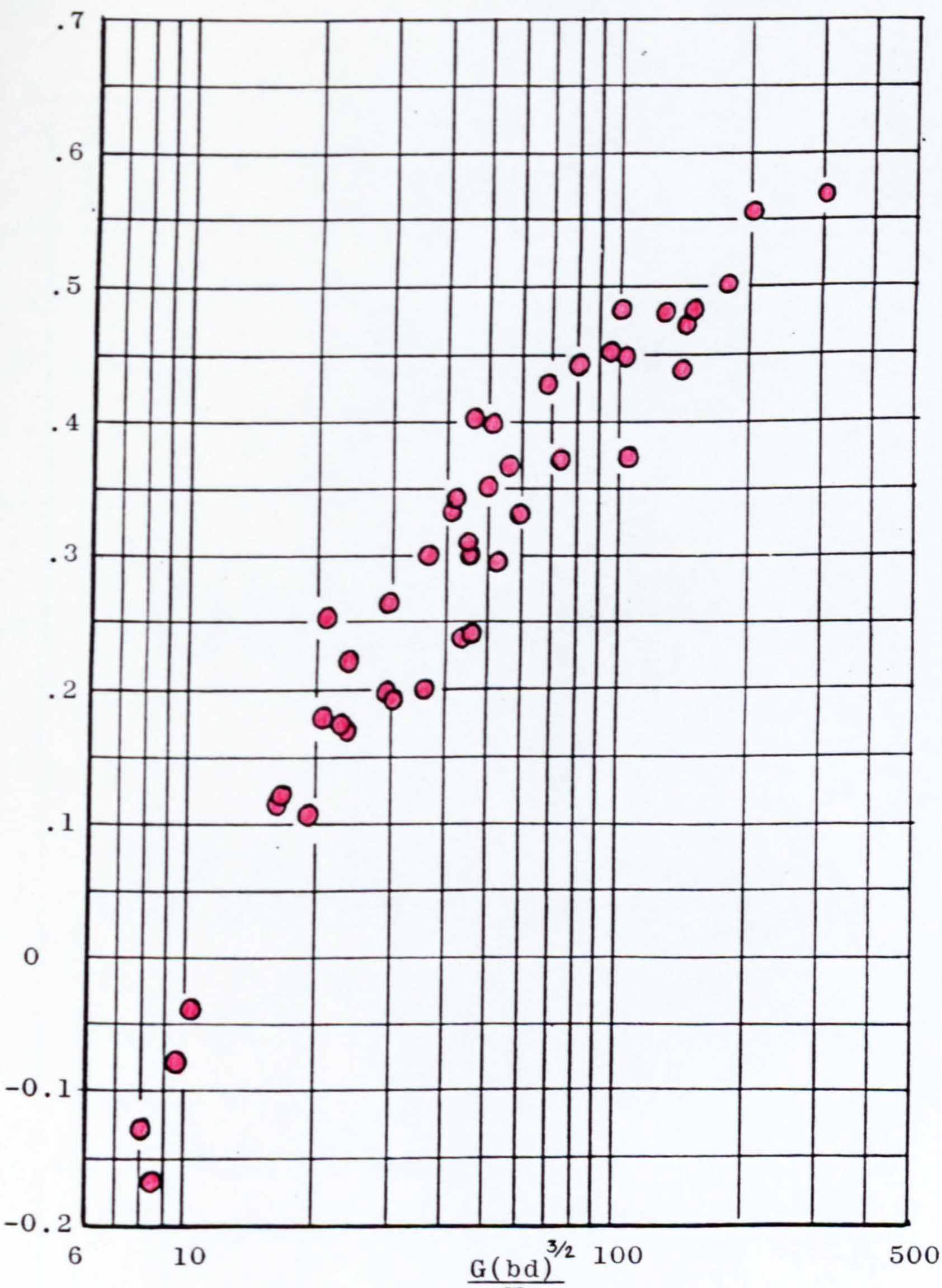

Fig. 7.13 - Results of tests with 10 different tyres at 35% deflection done by W.E.S. on Yuma sand plotted against the number $G(bd)^{3/2}/W$. Data from Turnage (1972b).

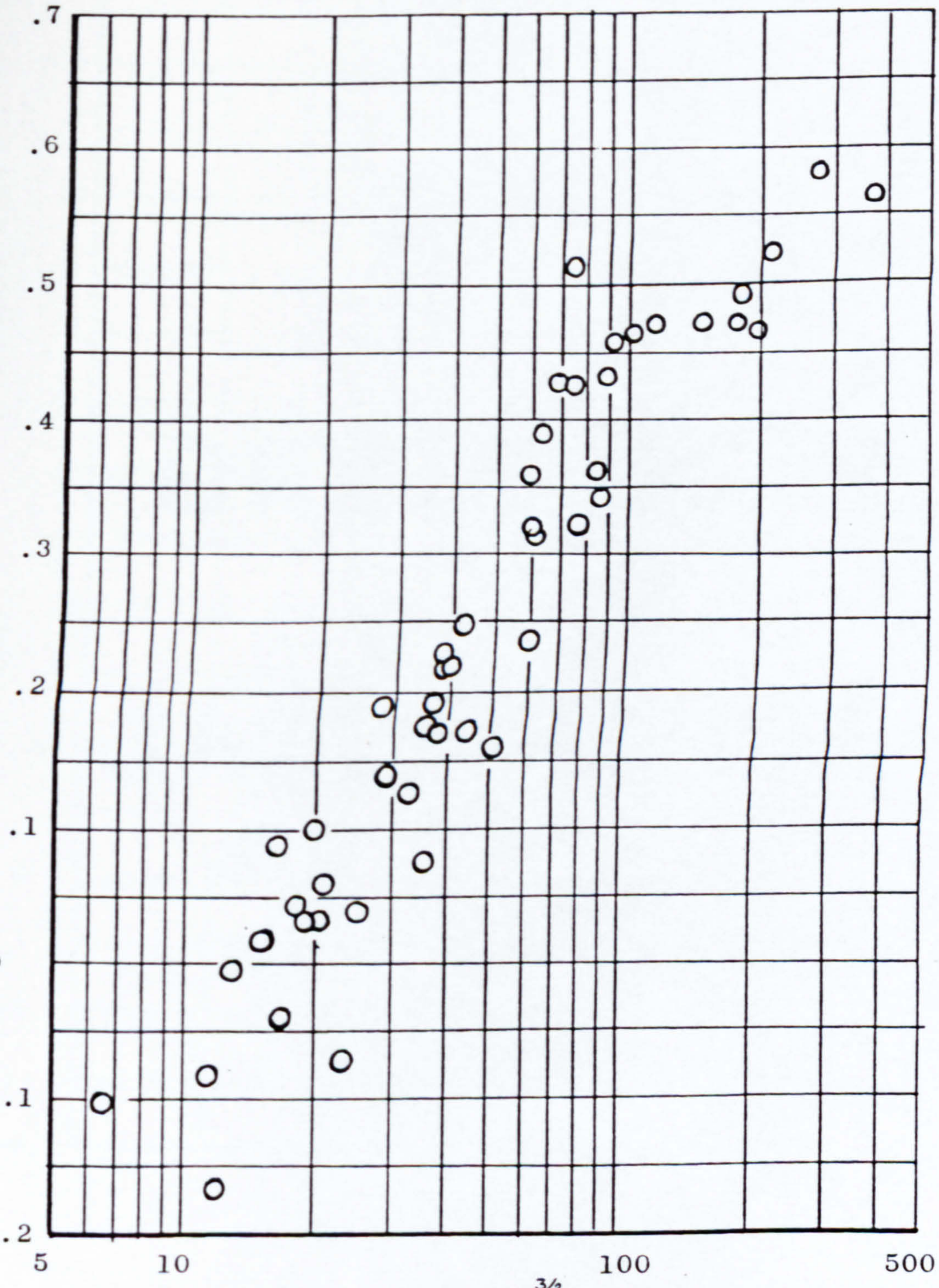

Fig. 7.14 - Results of tests with 10 different tyres at 25% deflection done by W.E.S. on Yuma sand plotted against the number $G(bd)^{3/2}/W$. Data from Turnage (1972b).

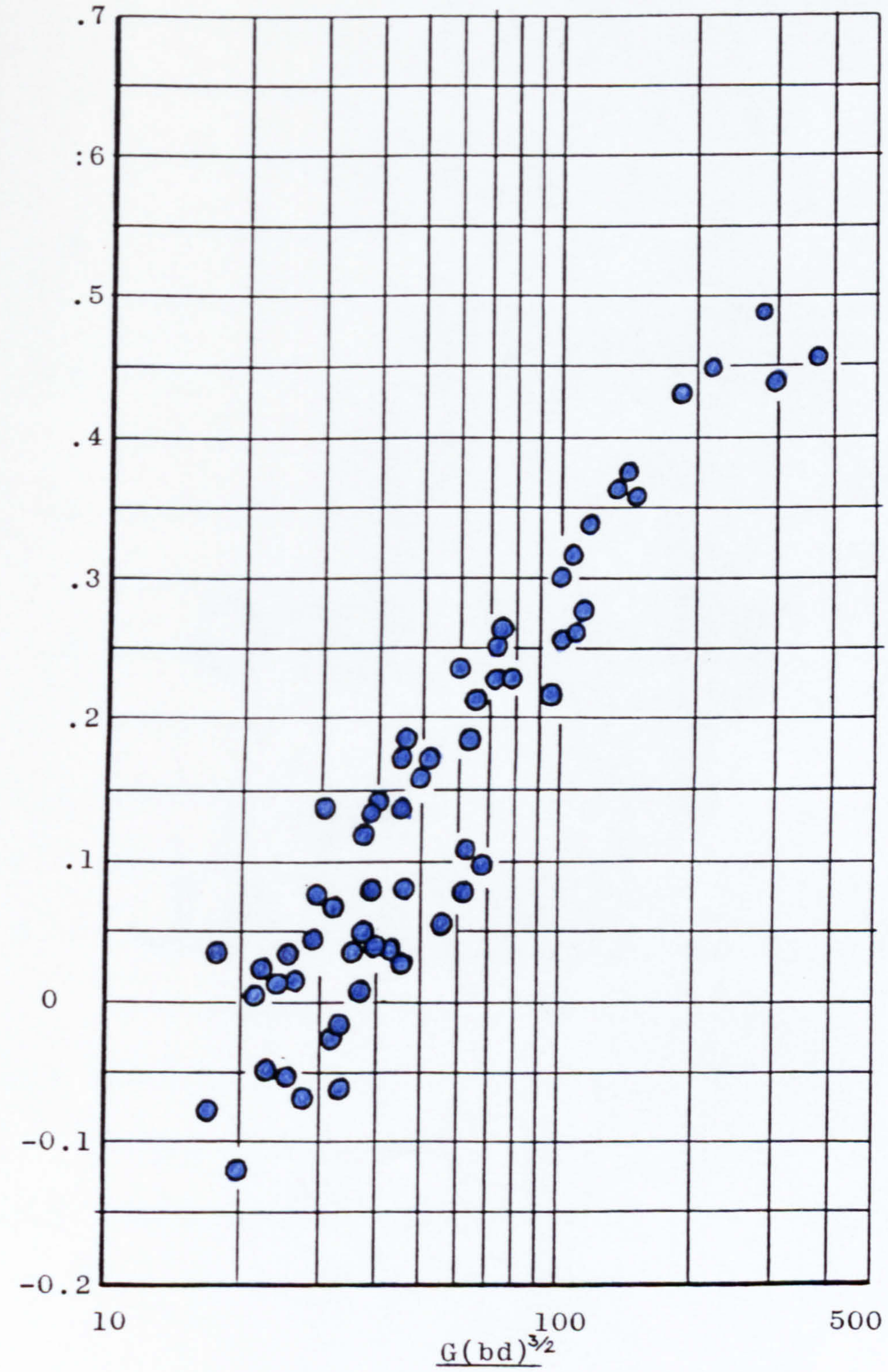

Fig. 7.15 - Results of tests with 10 different tyres at 15% deflection on Yuma sand plotted against the number $G(bd)^{3/2}/W$. Data from Turnage (1972b).

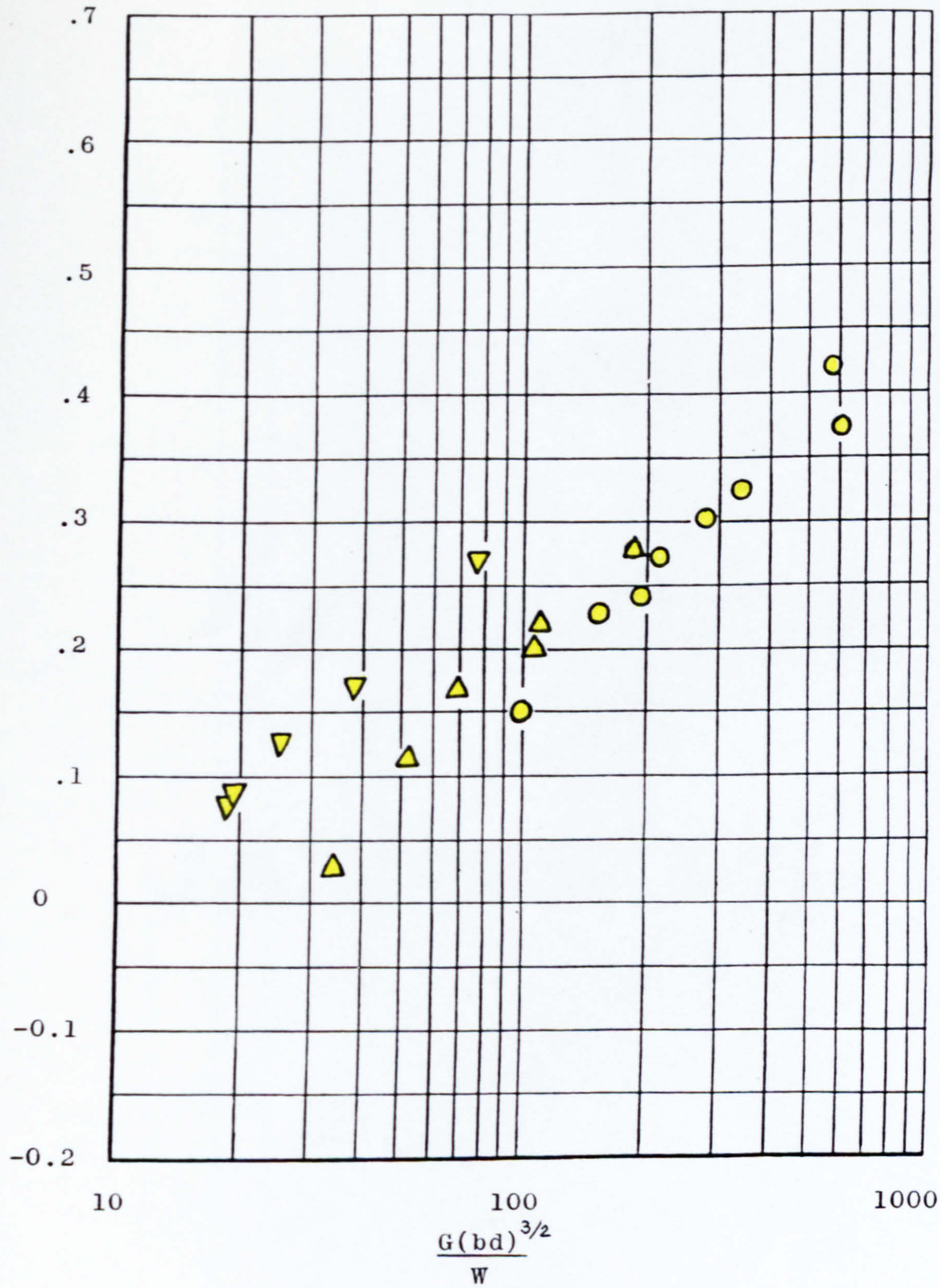

▽ - b=7.6cm , d=71cm ; △ - b=15cm , d=71cm ; ○ - b=31cm , d=71cm

Fig. 7.16 - Results of tests with 3 rigid wheels done by W.E.S. on Yuma sand plotted against the number $G(bd)^{3/2}/W$. Data from Turnage (1972b).

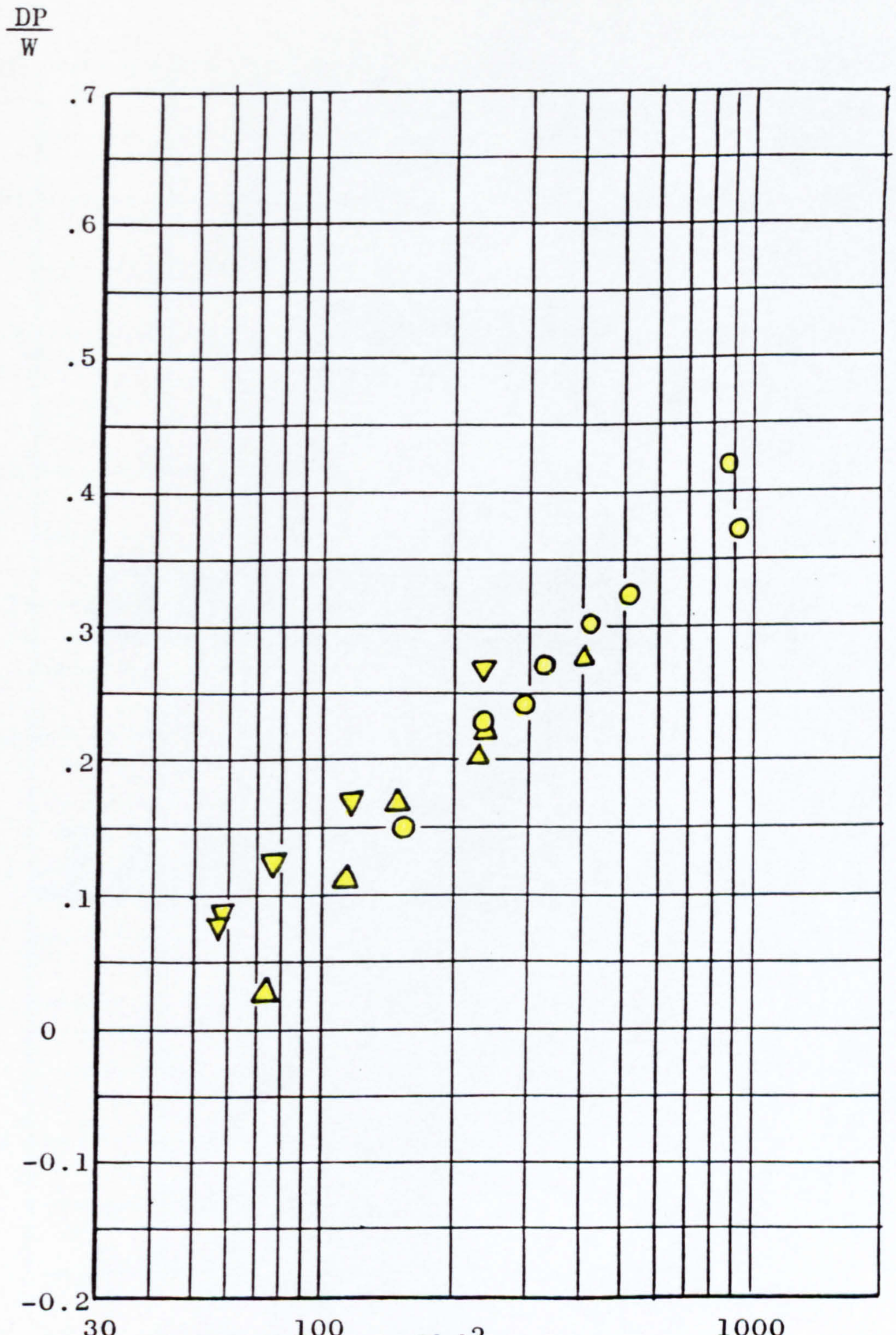

▽ - b=7.6cm , d=71cm ; △ - b=15cm , d=71cm ; ○ - b=31cm, d=71cm

Fig. 7.17 - Results of tests with 3 rigid wheels done by W.E.S. on Yuma sand plotted against the number Gbd^2/W. Data from Turnage (1972b).

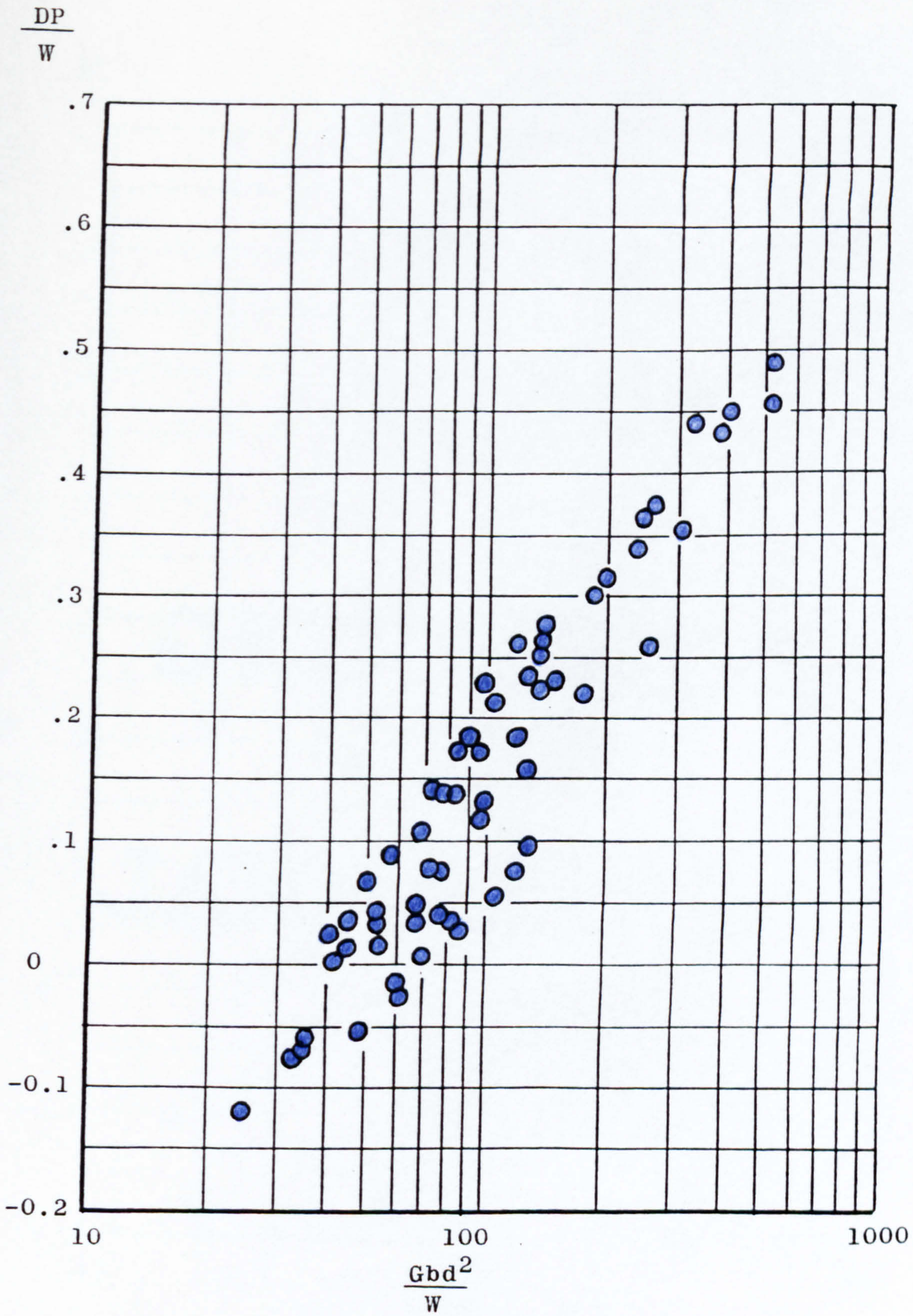

Fig. 7.18 - Results of tests with 10 different tyres at 15% deflection done by W.E.S. on Yuma sand, plotted against the number Gbd^2/W . Data from Turnage (1972b).

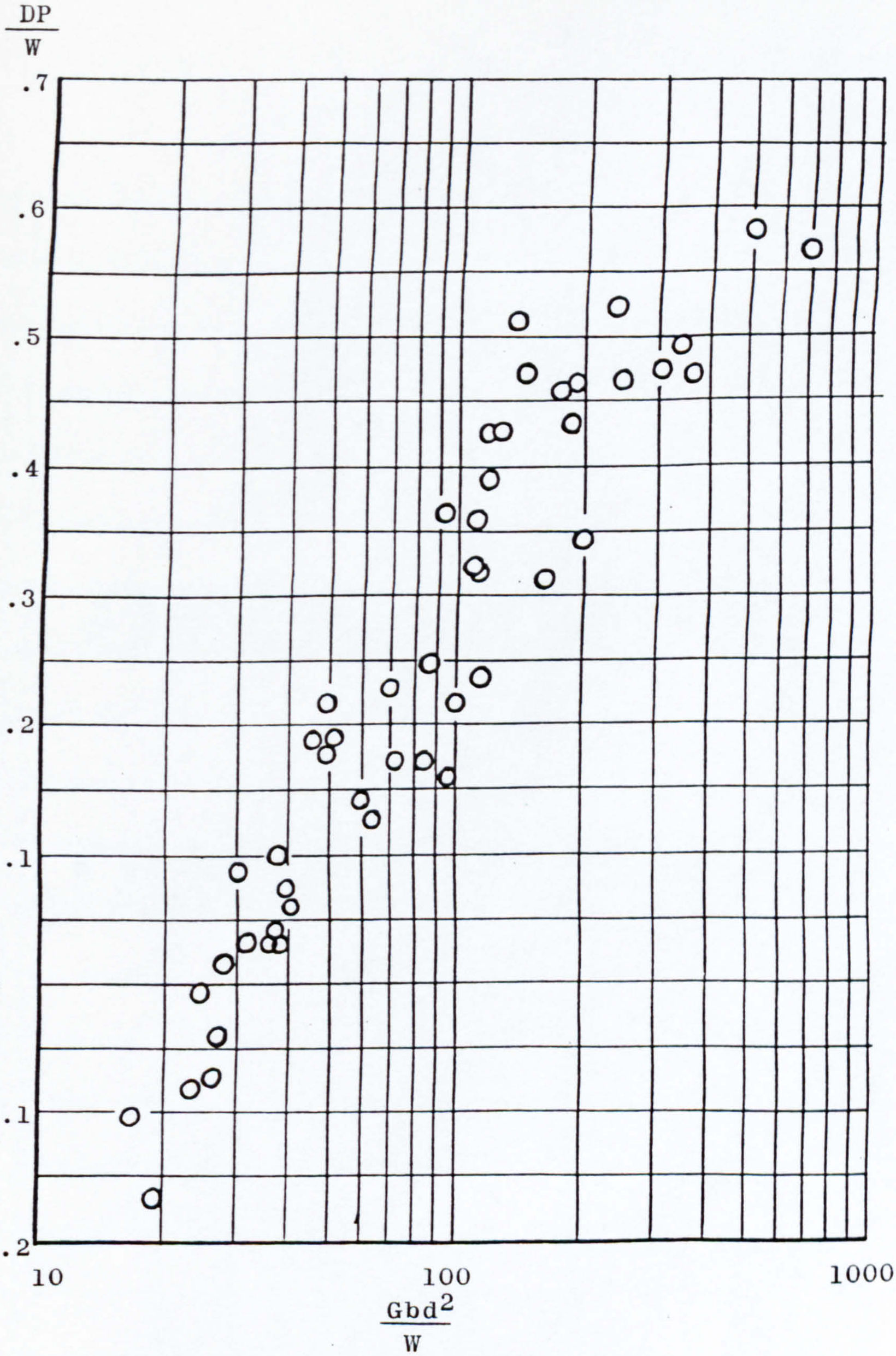

Fig. 7.19 - Results of tests with 10 different tyres at 25% deflection done by W.E.S. on Yuma sand, plotted against the number Gbd^2/W . Data from Turnage (1972b).

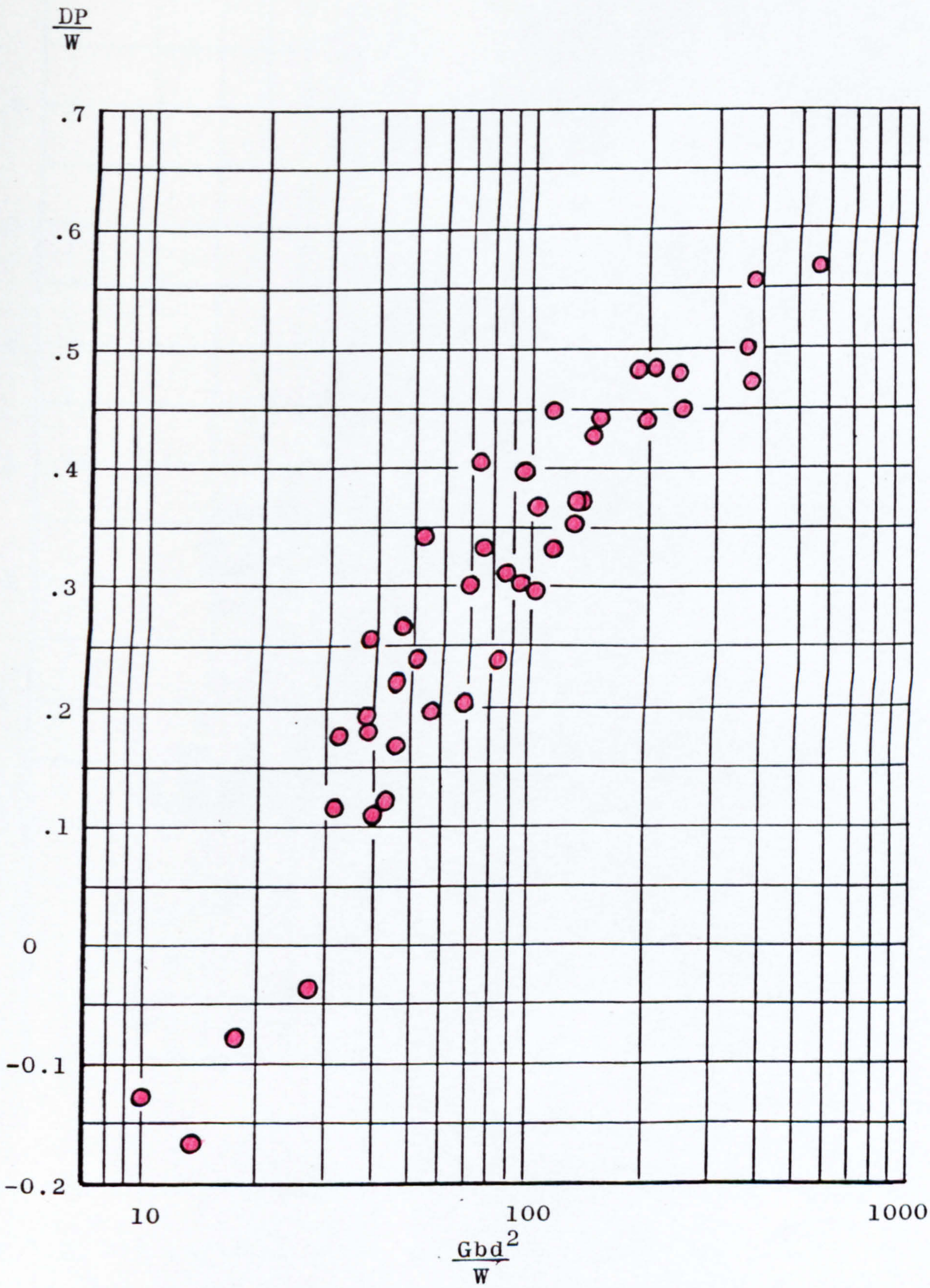

Fig. 7.20 - Results of tests with 10 different tyres at $\delta/h=35\%$ deflection done by W.E.S. on Yuma sand, plotted against the number Gbd^2/W.

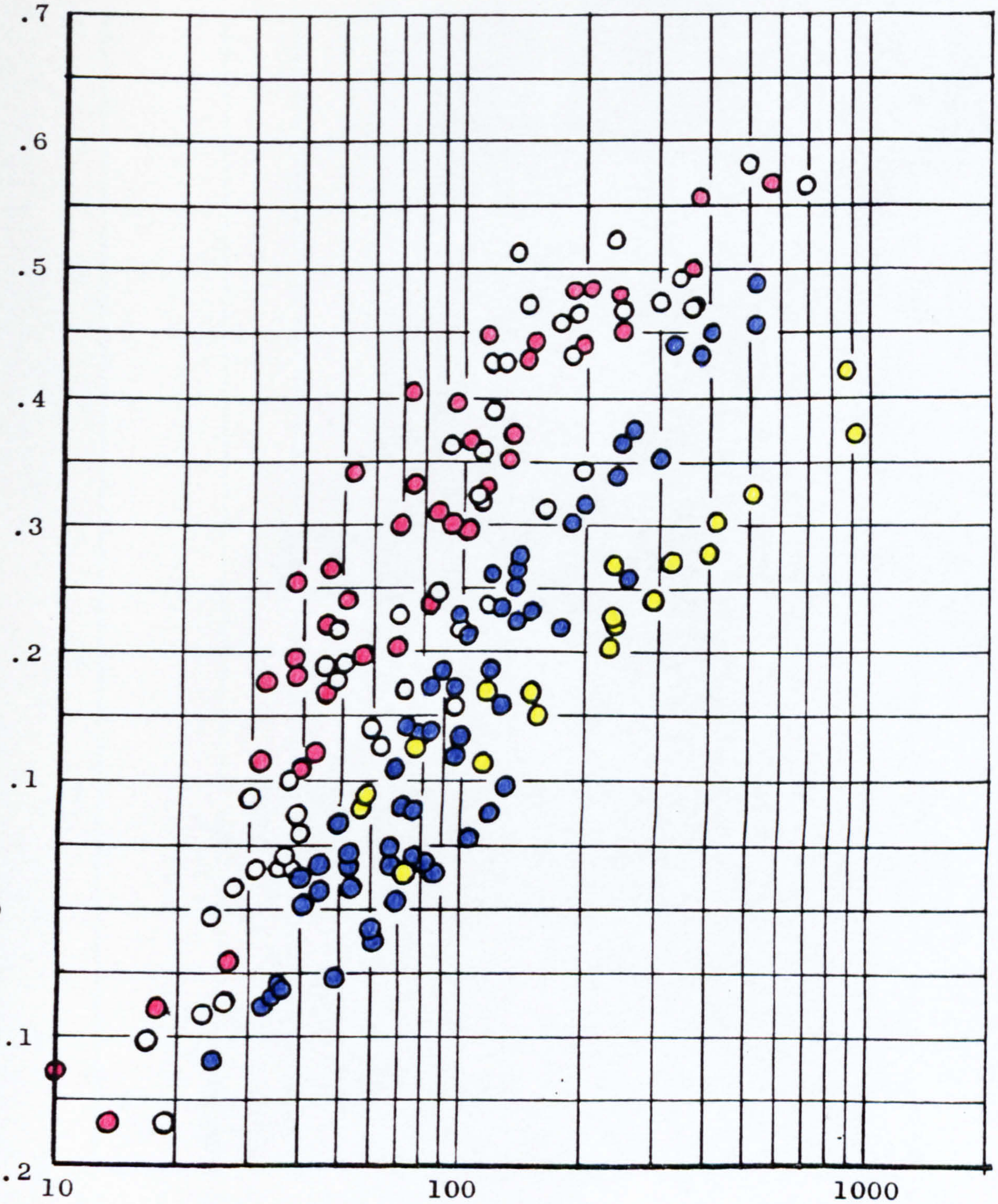

● - δ/h = 35% ; ○ - δ/h = 25% ; ● - δ/h = 15% ; ○ - Rigid wheels

Fig.7.21 - Results of tests with 10 different tyres and 3 rigid wheels done by W.E.S. on Yuma sand plotted against the sand number Gbd^2/W. Data from Turnage (1972b).

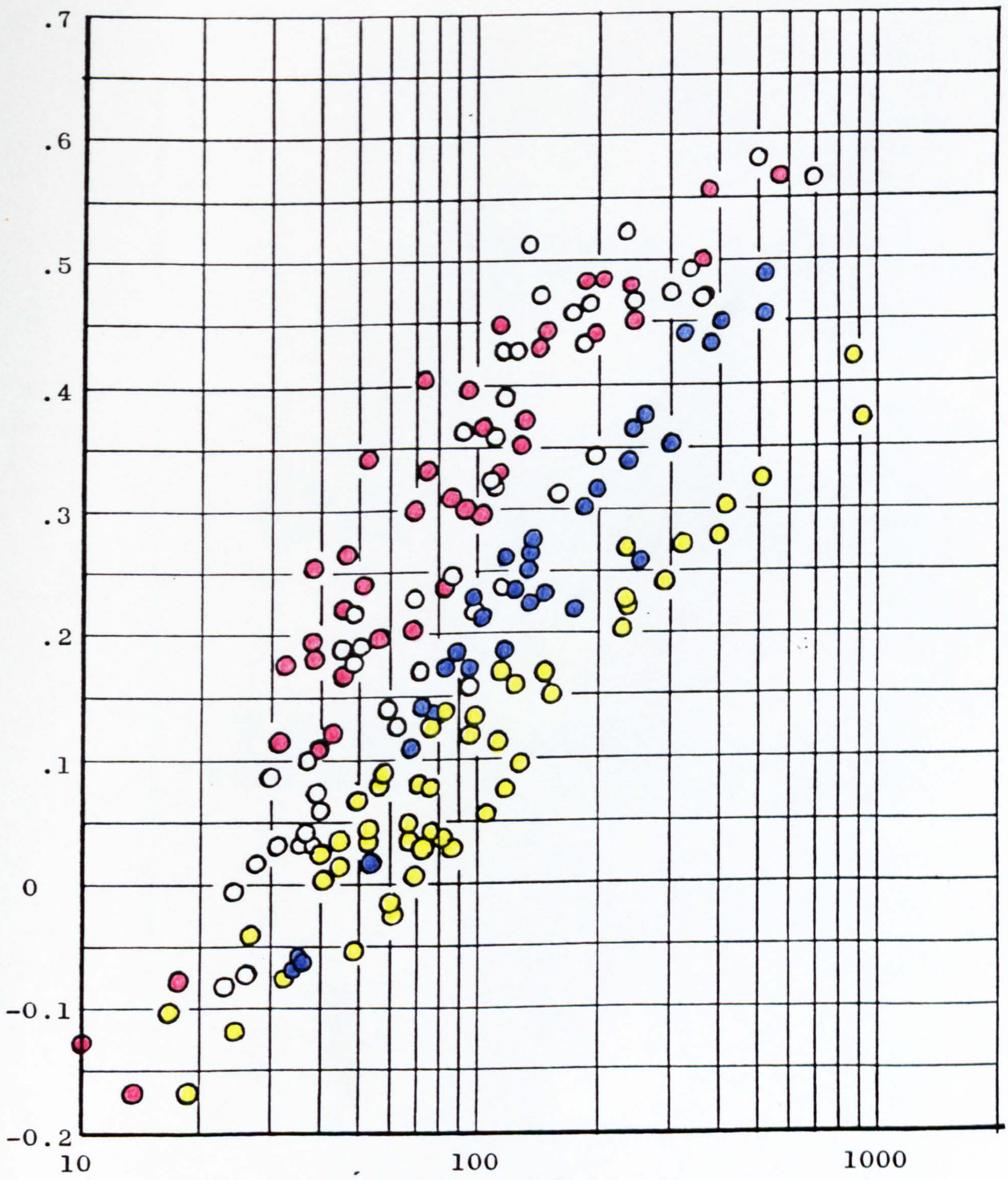

● - δ/h = 35% ; ○ - δ/h = 25% ; ● - δ/h = 15% ; ○ - Rigid wheels and highly inflated tyres.

Fig. 7.22 - Results of tests with 10 different tyres and 3 rigid wheels done by W.E.S. on Yuma sand plotted against the sand number Gbd^2/W. Data from Turnage 1972b.

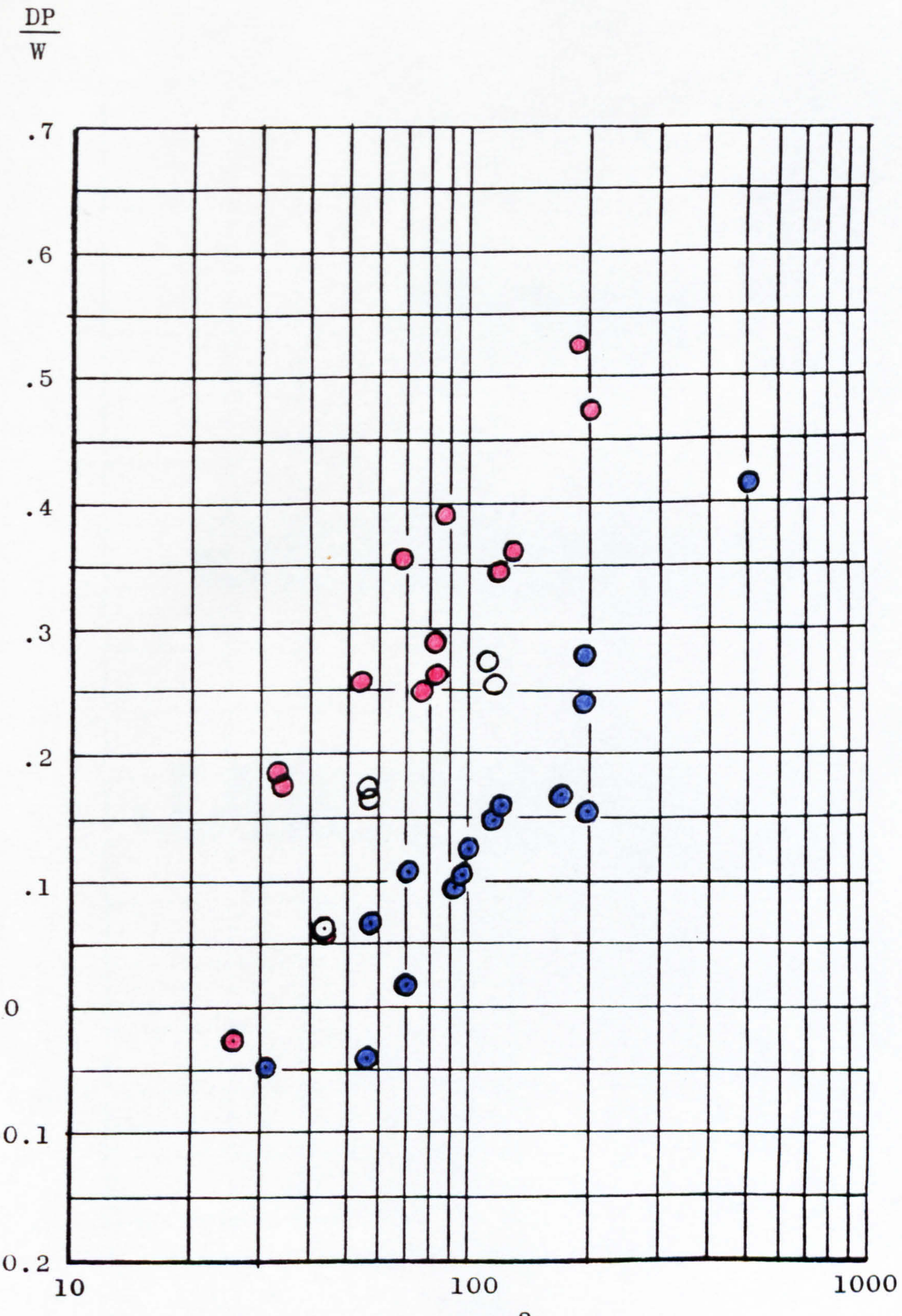

● - δ/h = 35% ; ○ - δ/h = 25% ; ● - δ/h = 15%

Fig. 7.23 - Results of tests with 7 different tyres done by W.E.S. on Mortar sand plotted against the sand number Gbd^2/W. Data from Turnage 1972b.

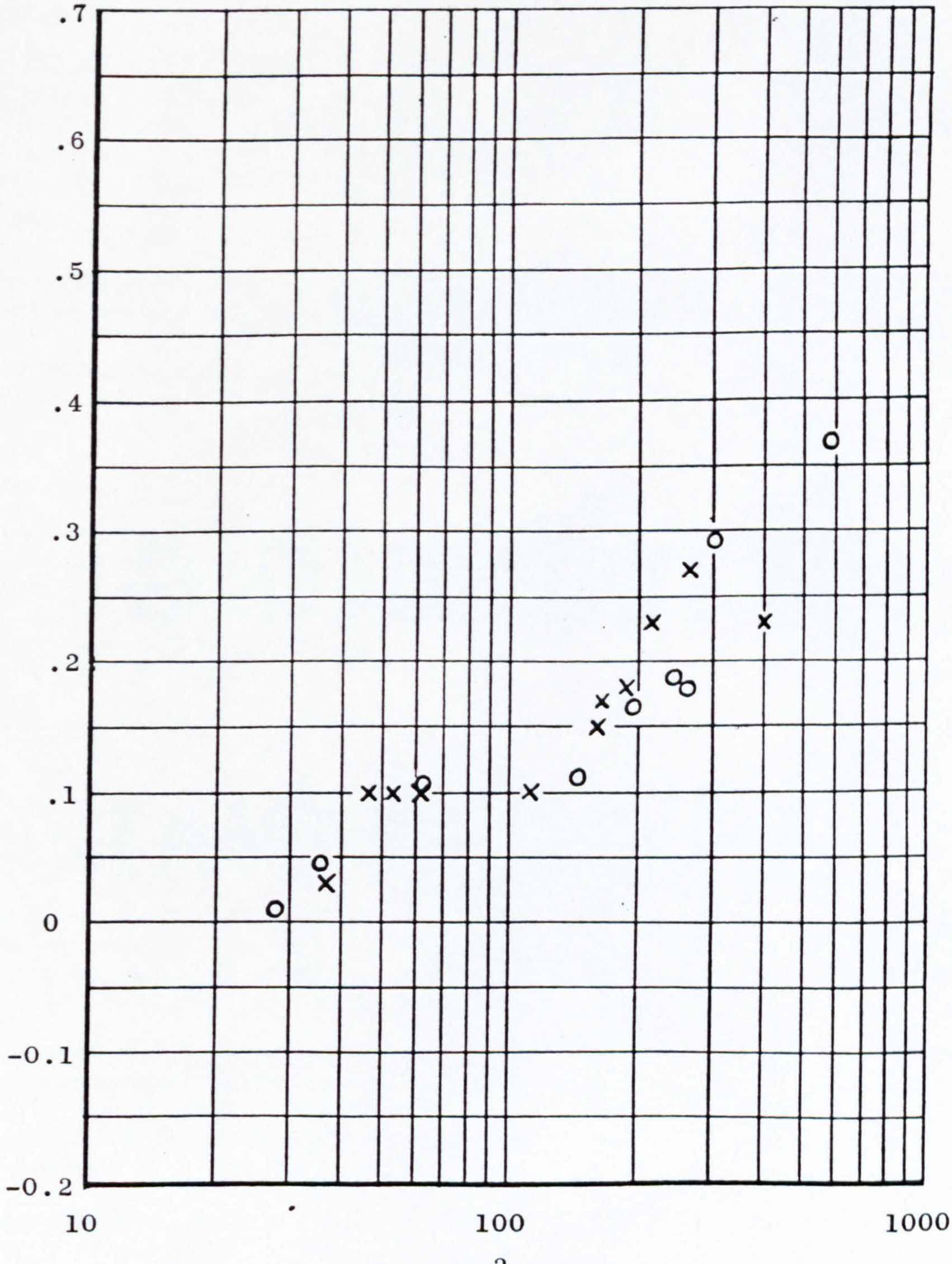

× - Cresswell sand o - Leighton Buzzard sand

Fig. 7.24 - Results of the wheel tests performed in Newcastle plotted against the sand number Gbd^2/W . Tyre deflection on hard surface = 30%.

ROWE - HORNE STRESS DILATANCY THEORY

Rowe (1962) studied regular packings of a cohesionless mass of spheres in axially symmetric triaxial compression.

Figure A.1.1a and b shows a typical result, where σ_1 and $\sigma_2 = \sigma_3$ are principal effective stresses and ε_v and ε_a are respectively the volumetric and axial strains, which are function of the principal strains as follows:

$$\varepsilon_v = \varepsilon_1 + \varepsilon_2 + \varepsilon_3 = \varepsilon_1 + 2\varepsilon_3$$

$$\varepsilon_a = \varepsilon_1$$

The sample is compacting from 0 to A at a decreasing rate and dilating from then onwards, with a maximum dilating rate at C and a zero dilating rate at B.

Rowe (1962) was particularly concerned with the ratio

$$\frac{\sigma_1/\sigma_3}{1 - \frac{d\varepsilon_v}{d\varepsilon_a}}$$

called the energy ratio and representing the ratio of work done per unit of volume on the assembly, by the major principal stress, to the work done on the minor principal stress by the assembly during an increment of expansion.

The result of Rowe's finding are resumed in equation A1 which forms the basis of his stress-dilatancy theory:

$$\frac{\sigma_1}{\sigma_3\left(1 - \frac{d\varepsilon_v}{d\varepsilon_a}\right)} = \tan^2 (45 + \tfrac{1}{2} \phi_\mu) \qquad (A1)$$

ϕ_μ being the so called angle of interparticle friction, i.e. the true angle of friction between the mineral surfaces of the soil particles.

In the process of obtaining equation A1 the following postulate was put forward without further proof: "the ratio of the energy dissipated, as friction, by the soil during an increment of expansion, and the work done per unit of volume on the assembly by the major principal stress is a minimum".

This brought equation A1 to experimental confirmation which was done first in a random mass of irregular particles and then in dry sands and silts. The results showed clearly that equation A1 could not cover the entire sample deformation. As shown in Fig. A.1.1c it was only satisfied for a test of dense sample and only up to the peak of stress ratio.

As a consequence a more general equation was put forward:

$$\frac{\sigma_1}{\sigma_3\left(1 - \frac{d\varepsilon_v}{d\varepsilon_a}\right)} = \tan^2 (45 + \tfrac{1}{2} \phi_f) \qquad (A2)$$

where ϕ_f is the so called effective angle of internal friction.

For a dense sample up to the peak of stress $\phi_f = \phi_\mu$, increasing afterwards to the critical state when $\phi_f = \phi_{cv}$.

At the critical state the sample is straining at constant volume ($d\varepsilon_v = 0$) which means that equation A2 becomes

$$\frac{\sigma_1}{\sigma_3} = \tan^2 (45 + \tfrac{1}{2} \phi_{cv}) , \qquad (A3)$$

or in more recognizable form $\tau = \sigma \tan \phi_{cv}$, the Mohr-Coulomb yield criterion for sand. Attempts have been made to relate ϕ_{cv} and ϕ_μ; among other the theoretical relationship by Horne (1969) seems to have good experimental support. It shows a reasonably constant value $\phi_{cv} - \phi_\mu = 7$ degrees for values of $\phi_\mu = 10$ to 30 degrees.

The general equation A2 may be regarded as a stress-strain law for the case of loading paths on the Hvorslev side of the critical state wall, in the same way as Cam-clay flow rule and Roscoe and Burland flow rule are examples of stress-strain relationships for loading paths on the Roscoe side of the critical state wall. The particular significance of equation A2 lies on being based on a fundamental property such as the true angle of friction between the surfaces of grains.

Equation A1 was also confirmed by Horne (Part 1 - 1965) again after the minimum energy postulate has been accepted.

More recently, De Josselin De Jong (1976) showed the validity of Rowe-Horne's stress dilatancy theory based on reasons other than the principle of minimum energy. He applied the rules of friction to the forces on the separation surface of a triaxial specimen subjected to axi-symmetric compression.

The study of the strain ratio $\frac{d\varepsilon_v}{d\varepsilon_a}$ was taken by Horne (Part II - 1965) which developed a theory based on a random anisotropic packing of spheres undergoing triaxial compression. He found that at the peak of stress ratio, point C in Fig. A1.1a, the maximum theoretical value for $d\varepsilon_3/d\varepsilon_1$, which is found if the sample is in a very dense packing and tested at a very low cell pressure, is -1.

Since $\varepsilon_v = \varepsilon_1 + 2\varepsilon_3$

$$\therefore \quad \frac{d\varepsilon_v}{d\varepsilon_1} = \frac{d\varepsilon_v}{d\varepsilon_a} = 1 + 2 \frac{d\varepsilon_3}{d\varepsilon_1}$$

and therefore in the above conditions

$$\frac{d\varepsilon_v}{d\varepsilon_a} = -1 \quad \text{or} \quad 1 - \frac{d\varepsilon_v}{d\varepsilon_a} = 2 \qquad (A4)$$

Experimental results in various granular materials agreed reasonably well with the theoretical value of 2, showing a slight influence of particle shape but only for extreme variations as between glass spheres (1.92) and crushed glass (1.78).

Substituting the above result into equation A1 it yields the theoretical upper limit for stress ratio:

$$\frac{\sigma_1}{\sigma_3} = 2 \tan^2 (45 + \tfrac{1}{2} \phi_\mu) \qquad (A5)$$

which was also accepted by Rowe (1969) as ruling the peak of stress ratio for dense samples when tested at low cell pressure.

Apart from the values of ϕ_μ computed from the results of triaxial compression using equation A1, there have been attempts to measure it directly by sliding one grain, a few or a large number of soil particles against a flat block of the same material, or sliding grain against grain or flat block against flat block. An extensive account of measured values of the angle of interparticle friction ϕ_μ using these direct techniques is given by Procter and Barton (1974) for different materials and different surface conditions, like dry or water-saturated. Values found for quartz are: dry, 6 degrees, by two authors, and 17.4 degrees, by one author; saturated, an average value of 25 degrees from results by five authors. Since these values do not cover a wide range of geometry and roughness of the contact surfaces on which the true friction angle is measured, they must not be considered as universal values to be used for any quartz granular material.

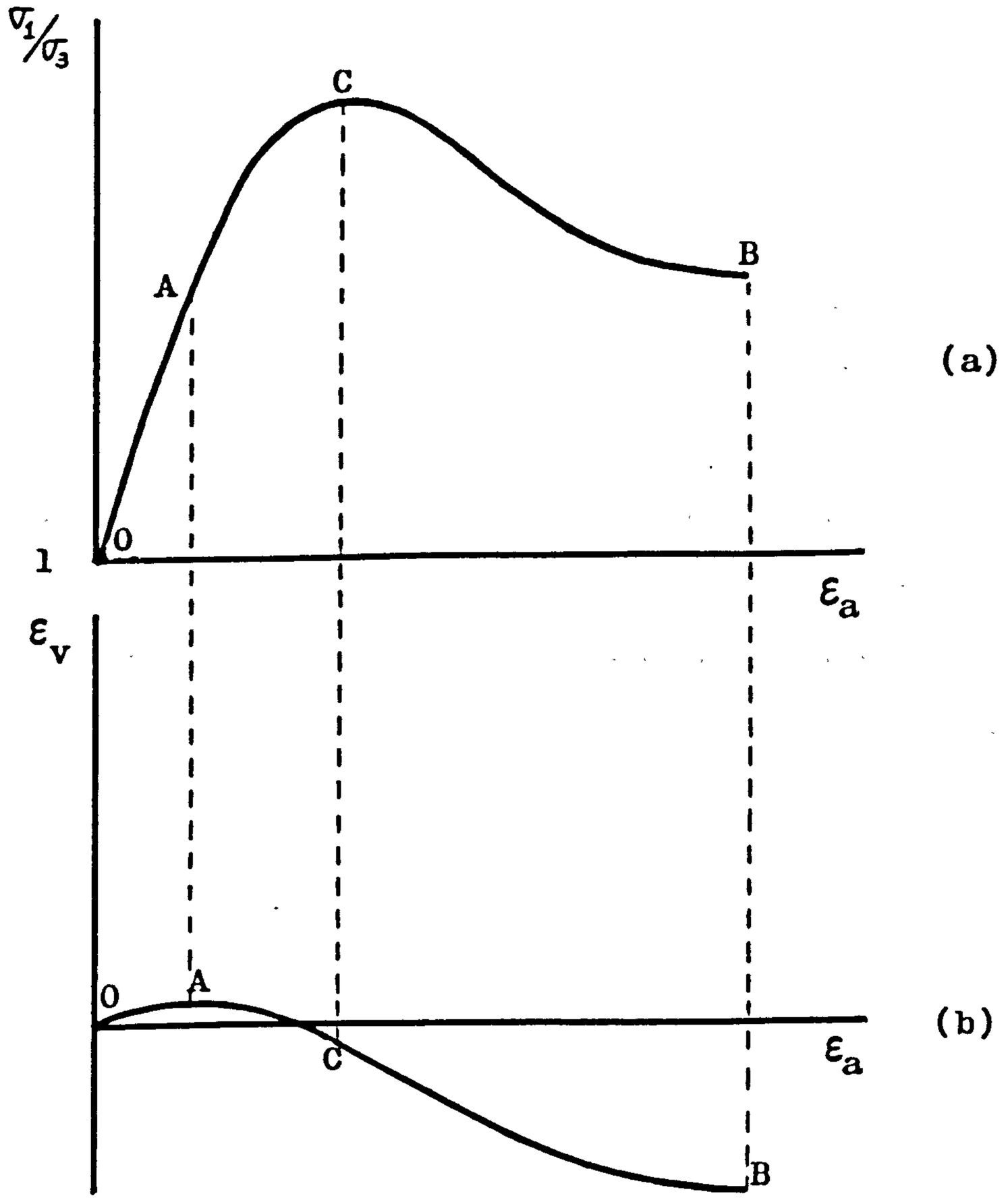

Fig. A.1.1 - (a) and (b): a typical result for a drained triaxial compression test of dense sand. (c): a typical result of stress ratio versus dilatancy rate for a specimen of dense sand according to Horne (1965).

APPENDIX 2

TYRE DEFLECTION

It was suggested in section 7.4, that the factor δ/h, representing empirically the effect of tyre pressure on traction, should be replaced by δ/d. To investigate this proposition, data from Fig. 7.22 was replotted in Fig. A.2.1, showing that there is equally a separation of the results according to the values of δ/d, therefore supporting the claim. Doing so, not only the irrelevant dimension h is eliminated from the correlation, but above all deflection is expressed as a percentage of a clearly defined tyre dimension d.

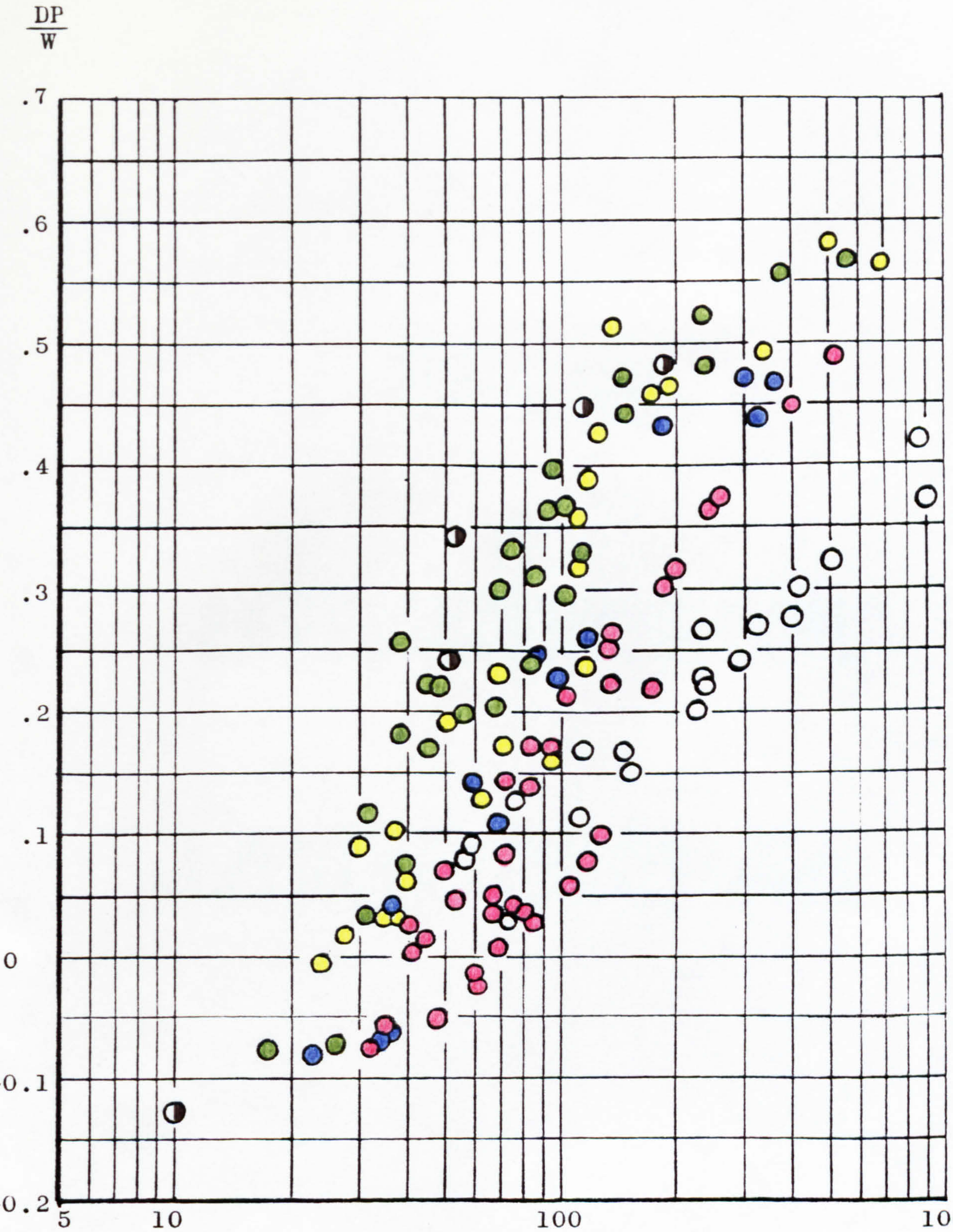

○- δ/d=0 ; ●- δ/d=3.0 to 3.5% ; ●- δ/d=4.5 to 5.0%

●- δ/d=5.5 to 6.0% ; ●- δ/d=7.5 to 8.0% ; ◑- δ/d=10.5 to 11%

Fig. A.2.1 - Results of tests with 7 different tyres and 3 rigid wheels done by W.E.S. on Yuma sand plotted against the sand number Gbd^2/W showing separation according to the values of δ/d. Data from Turnage (1972b).